Soils and Rocks Volume 35, N. 2 2012

ISSN 1980-9743

Soils and Rocks

Soils and Rocks

An International Journal of Geotechnical and Geoenvironmental Engineering

Volume 35, N. 2
May-August 2012

Soils and Rocks is an International Journal of Geotechnical and Geoenvironmental Engineering published by

ABMS - Brazilian Association for Soil Mechanics and Geotechnical Engineering
Av. Prof. Almeida Prado, 532, – Prédio 11 – Térreo
Cidade Universitária, 05508-901 São Paulo, SP
Brazil

SPG – Portuguese Geotechnical Society
LNEC, Avenida do Brasil, 101
1700-066 Lisboa
Portugal

Issue Date: *September 2012*

Issue: *350 copies and 2150 online-distributed copies*

Manuscript Submission: *For review criteria and manuscript submission information, see Instructions for Authors at the end.*

Disclaimer: The opinions and statements published in this journal are solely the author's and not necessarily reflect the views or opinions of the publishers (ABMS and SPG). The publishers do not accept any liability arising in any way from the opinions, statements and use of the information presented.

Copyright: Authors and ABMS-Brazilian Society of Soil Mechanics and Geotechnical Engineering

SOILS and ROCKS

An International Journal of Geotechnical and Geoenvironmental Engineering

Editor André Pacheco de Assis - University of Brasilia, Brazil

Co-editor Manuel Matos Fernandes - University of Porto, Portugal

Executive Board

Márcio Muniz de Farias
University of Brasilia, Brazil

João Maranha
LNEC, Portugal

Fernando Schnaid
Federal Univ. Rio Grande do Sul, Brazil

Jorge Almeida e Sousa
University of Coimbra, Portugal

Associate Editors

H. Einstein
MIT, USA

John A. Hudson
Imperial College, UK

Kenji Ishihara
University of Tokyo, Japan

Michele Jamiolkowski
Studio Geotecnico Italiano, Italy

Willy A. Lacerda
COPPE/UFRJ, Brazil

E. Maranha das Neves
Lisbon Technical University, Portugal

Nielen van der Merve
University of Pretoria, South Africa

Paul Marinos
NTUA, Greece

James K. Mitchell
Virginia Tech., USA

Lars Persson
SGU, Sweden

Harry G. Poulos
University of Sidney, Australia

Niek Rengers
ITC, The Netherlands

Fumio Tatsuoka
Tokyo University of Science, Japan

Luiz González de Vallejo
UCM, Spain

Editorial Board Members

Claudio P. Amaral
Pontifical Catholic University, Brazil

Roberto F. Azevedo
Federal University of Viçosa, Brazil

Nick Barton
Consultant, Norway

Richard J. Bathurst
Royal Military College of Canada

Frederick Baynes
Baynes Geologic Ltd., Australia

Pierre Bérest
LCPC, France

Omar Y. Bitar
IPT, Brazil

Helmut Bock
Q+S Consult, Germany

Laura Caldeira
LNEC, Portugal

Tarcisio Celestino
University of São Paulo-SC, Brazil

António S. Cardoso
University of Porto, Portugal

Chris Clayton
University of Surrey, UK

António G. Coelho
Consultant, Portugal

Nilo C. Consoli
Federal Univ. Rio Grande do Sul, Brazil

António G. Correia
University of Minho, Portugal

Rui M. Correia
LNEC, Portugal

Roberto Q. Coutinho
Federal Univ. of Pernambuco, Brazil

António P. Cunha
LNEC, Portugal

R. Jonathan Fannin
University of British Columbia, Canada

Sérgio A.B. Fontoura
Pontifical Catholic University, Brazil

Roger Frank
LCPC, France

Maria H.B.O. Frascá
IPT, Brazil

Carlos D. Gama
Lisbon Technical University, Portugal

Vinod Garga
University of Ottawa, Canada

Nuno Grossmann
LNEC, Portugal

Richard J. Jardine
Imperial College, UK

Milton Kanji
University of São Paulo, Brazil

Peter Kaiser
Laurentian University, Canada

Luís L. Lemos
University of Coimbra, Portugal

José V. Lemos
LNEC, Portugal

Serge Leroueil
University of Laval, Canada

Robert Mair
University of Cambridge, UK

Mario Manassero
Politécnico di Torino, Italy

He Manchao
CUMT, China

João Marcelino
LNEC, Portugal

António C. Mineiro
New University of Lisbon, Portugal

Teruo Nakai
Nagoya Inst. Technology, Japan

Claudio Olalla
CEDEX, Spain

Antonio M.S. Oliveira
University of Guarulhos, Brazil

Ennio M. Palmeira
University of Brasilia, Brazil

José D. Rodrigues
Consultant, Portugal

R. Kerry Rowe
Queen's University, Canada

Rodrigo Salgado
University of Purdue, USA

Sandro S. Sandroni
Consultant, Brazil

Luís R. Sousa
University of Porto, Portugal

Fabio Taioli
University of São Paulo, Brazil

Luis Valenzuela
Consultant, Chile

Ricardo Vedovello
São Paulo Geological Institute, Brazil

Andrew Whittle
MIT, USA

Jorge G. Zornberg
University of Texas/Austin, USA

Lázaro V. Zuquette
University of São Paulo, Brazil

Soils and Rocks publishes papers in English in the broad fields of Geotechnical Engineering, Engineering Geology and Geo-environmental Engineering. The Journal is published in April, August and December. Subscription price is US$ 90.00 per year. The journal, with the name “Solos e Rochas”, was first published in 1978 by the Graduate School of Engineering, Federal University of Rio de Janeiro (COPPE-UFRJ). In 1980 it became the official magazine of the Brazilian Association for Soil Mechanics and Geotechnical Engineering (ABMS), acquiring the national character that had been the intention of its founders. In 1986 it also became the official Journal of the Brazilian Association for Engineering Geology and the Environment (ABGE) and in 1999 became the Latin American Geotechnical Journal, following the support of Latin-American representatives gathered for the Pan-American Conference of Guadalajara (1996). In 2007 the journal acquired the status of an international journal under the name of Soils and Rocks, published by the Brazilian Association for Soil Mechanics and Geotechnical Engineering (ABMS), Brazilian Association for Engineering Geology and the Environment (ABGE) and Portuguese Geotechnical Society (SPG). In 2010, ABGE decided to publish its own journal and left the partnership.

Soils and Rocks

1978,	1 (1, 2)
1979,	1 (3), 2 (1,2)
1980-1983,	3-6 (1, 2, 3)
1984,	7 (single number)
1985-1987,	8-10 (1, 2, 3)
1988-1990,	11-13 (single number)
1991-1992,	14-15 (1, 2)
1993,	16 (1, 2, 3, 4)
1994-2010,	17-33 (1, 2, 3)
2011,	34 (1, 2, 3, 4)
2012,	**35 (1, 2,**

ISSN 1980-9743 CDU 624.131.1

ISSN 1980-9743

SOILS and ROCKS

An International Journal of Geotechnical and Geoenvironmental Engineering

Publication of

ABMS - Brazilian Association for Soil Mechanics and Geotechnical Engineering

SPG - Portuguese Geotechnical Society

Volume 35, N. 2, May-August 2012

Table of Contents

Victor de Mello Lecture

The Victor de Mello Lecture was established in 2008 by the Brazilian Association for Soil Mechanics and Geotechnical Engineering (ABMS), the Brazilian Association for Engineering Geology and the Environment (ABGE) and the Portuguese Geotechnical Society (SPG) to celebrate the life and professional contributions of Prof. Victor de Mello. Prof. de Mello was a consultant and academic for over 5 decades and made important contributions to the advance of geotechnical engineering. Each year a worldwide acknowledged geotechnical expert is invited to deliver this special lecture. It is a privilege to have Dr. Harry G. Poulos (Coffey Geotechnics, Australia) delivering the second edition of the Victor de Mello Lecture. Dr. Poulos and Prof. de Mello were close friends for decades and in his lecture he reviews the contributions of the late Victor de Mello to foundation engineering and highlights the insights that he provided in a number of key areas.

Prof. MICHELE JAMIOLKOWSKI began his professional career in 1969 at the Department of Geotechnical Engineering, University of Torino, Italy, where currently he is Professor Emeritus. Since 1964 he has been President of the Studio Geotecnico Italiano. He has gathered many awards, among them: de Beer Award (Belgium Geotechnics Association, 1994-1998); the Karl Terzaghi Award and the Ralph B. Peck Lecture Award (American Association of Civil Engineering, ASCE); and the Italian Award "Saviour of the Art". He was also President of the International Association of Soil Mechanics and Geotechnical Engineering (1994-1997) and President of the International Committee for Safeguarding the Leaning Tower of Pisa (1990-2001). He is member of several organisations and academies, including Honourable International Member of the Japanese Geotechnical Association, and member of the Group of Consultants for the European Bank involved in reconstruction and development for the new nuclear power plant installations in Chernobyl, Ukraine. Professor Jamiolkowski will deliver the 53rd Rankine Lecture organized by the British Geotechnical Association

Role of Geophysical Testing in Geotechnical Site Characterization

M. Jamiolkowski

Abstract. The lecture attempts to highlight the insights late Victor De Mello provided on some key areas. Considering the increasing role of the geophysical methods in the geotechnical site characterization, the writer focuses on the use of in-hole geophysical methods when assessing, both in field and in laboratory, the parameters depicting the soil state and its stiffness at small strain. With this aim the writer draws the attention to seismic transversal (S) and longitudinal (P) body waves generated both in field, during in-hole tests, and in laboratory using piezocristals. Within this framework the following issues are discussed:
- Stiffness at very small strain as obtainable from the S and P velocities.
- Difference between fully from near to saturated soils from the measured P-wave velocity.
- Evaluation of undisturbed samples quality based on the comparison of S-waves velocities measured in field and in laboratory respectively.
- Evaluation of porosity and void ratio from measured P and S waves velocity.
- S-wave based evaluation of the coarse grained soils susceptibility to cyclic liquefaction.
Keywords: seismic body waves, stiffness, fully and near to saturated state, porosity, liquefaction.

A Friend's Legacy

"Try to know yourself and your preferences. Listen, observe, investigate: choose your love and love your choice." (Victor de Mello).

And indeed this was Victor de Mello, certainly no ordinary man nor just an engineer.

Both personally and professionally Victor personified excellence, with a deep set of values and an amazing ability to stay connected with those he knew. And I am so proud for being one of his "brothers of blood" as he used to call Harry Poulos, John Burland and myself.

Victor was my mentor and my role-model and has certainly impacted my professional life. I have hugely benefitted from our many inspiring conversations. Occasionally he was a severe critic but his analyses have always been constructive encouraging my quality work and, however firm in his resolution, always explaining the nature of his disagreement.

It is fascinating to look into Victor De Mello's background, to his philosophical spirit and his working methods. He combined the engineer rigor with a solid passion for life. His interests ranged widely: engineering sciences, geology, philosophy and ethics, flowers, conversation, travel, literature, music, writing, art, women, food, wines and so forth.

He was also a prolific correspondent and Victor's wise thoughts and advices, always unconditionally given on so many occasions, will remain with me.

He used to say "*We professionals beg less rapid novelties, more renewed reviewing of what is already there"* and this is where I want to start from. In this paper I will attempt to continue the lively, sometimes conflictual, channel of communication Victor and I have been carrying on for ages on issues related to the geotechnical site characterization and on the key requisites for a safe and cost-effective design, in which area Victor de Mello made notable contributions.

1. Introduction

Considering the growing importance of the geophysical methods [Stokoe (2011)] for the geotechnical site characterization, this paper focuses on the in-hole techniques, such as cross-hole (CH) and down-hole (DH) tests which, if properly instrumented and performed, can provide reliable values for compression (V_p) and shear (V_s) waves velocity.

M. Jamiolkowski, Emeritus Professor, Technical University of Turin, Turin, Italy, e-mail: m.jamiolkowski@studiogeotecnico.it.

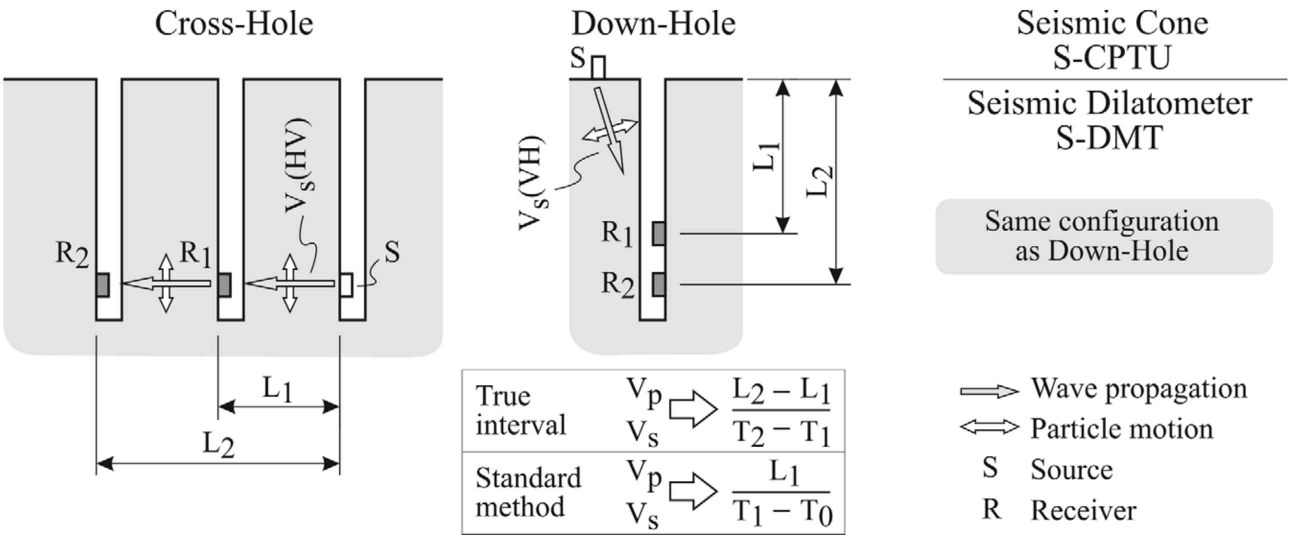

Figure 1 - In-hole geophysical tests.

When it is only requested the knowledge of V_s, reference will also be made to seismic cone penetration tests (S-CPTU) and to seismic Marchetti's dilatometer (S-DMT), equipped to provide a reliable measure of V_s in DH-mode. The main features of CH and DH tests are shown in Fig. 1, while Fig. 2 highlights the seismic waves that can be propagated *in situ*, during CH and DH tests, and in laboratory by means of bender elements (BE).

The generated seismic waves are classified according to the propagation direction (first capital letter) and to the polarization plane (second capital letter).

Figure 2 shows also the soil stiffness at very small shear strain ($10^{-6} \leq \gamma \leq 10^{-5}$), see Rahtje *et al.* (2004) and Cox (2006), that can be computed from the seismic waves velocity, being: G_0 = shear modulus at very small strain, M_0 = constrained modulus at very small strain and ρ_t = bulk soil mass density.

The following aspects, relative to the use of in-hole measured seismic body wave velocities in geotechnical design, are discussed:

1. Stiffness at very small strain: $G_0 = f\,(V_s)$ and $M_0 = \mathrm{f}(V_p)$ (Applicable to V_p propagated through dry soils or at least having $S_r < 90\%$).
2. Distinction between fully saturated and near to saturated soils $\rightarrow$ f (V_p).
3. Assessment of undisturbed samples quality $\rightarrow$ f [V_s (Field) *vs.* V_s (Lab.)].
4. Evaluation of *in situ* void ratio e_0 by means of Foti *et al.* (2002) approach f (V_p and V_s).
5. Susceptibility of coarse grained saturated soil to cyclic liquefaction $\rightarrow$ f (V_s).

The above topics are only loosely interconnected, thus each subject matter is detailed in a specific section with dedicated closing remarks.

2. Stiffness at Very Small Strain and its Anisotropy

The use of seismic waves velocity allows to evaluate, *in situ* and in laboratory, the shear modulus $G_0 = \rho_t V_s^2$ and the constrained modulus $M_0 = \rho_t V_p^2$.

G_0 is representative of the very initial portion of the soil stress-strain curve (Fig. 3), which, upon loading is linear and in unloading state exhibits a recoverable strain, including a minor amount of the delayed viscous component.

The linear portion of the stress-strain curve is delimited by the linear threshold strain γ_t^ℓ [Lo Presti (1991), Jardine (1992), Ishihara (1996), Hight & Leroueil (2003)].

The γ_t^ℓ for non rocky-like materials usually ranges between 10^{-5} and 10^{-4}, see Fig. 4a which reports also the volumetric threshold shear strain (γ_t^v), see [Dobry *et al.* (1982) and Vucetic (1994)]. The γ_t^v corresponds to the point where a soil element, subject to constant mean effective stress (p'), under the action of shear stress increase, during

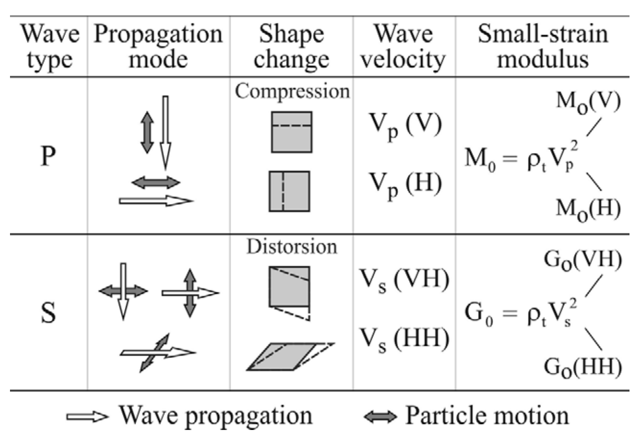

Figure 2 - Compression (P) and shear (S) waves generated *in situ* and in laboratory tests.

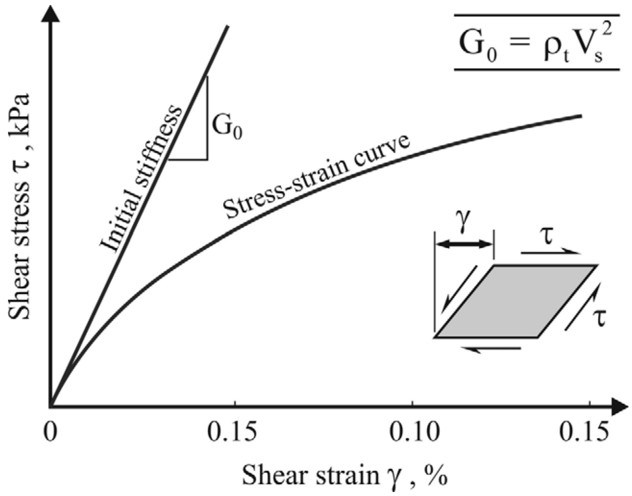

Figure 3 - Small strain shear modulus from seismic tests.

drained loading starts exhibiting plastic strain, whereas, under undrained loading a pore pressure excess is generated.

It can be therefore assumed that G_0 represents the initial tangent shear stiffness of a given geomaterial applicable to both static and dynamic problems, with possibly minor differences due to the strain rate effects involved in two different loadings modes, see Fig. 4b.

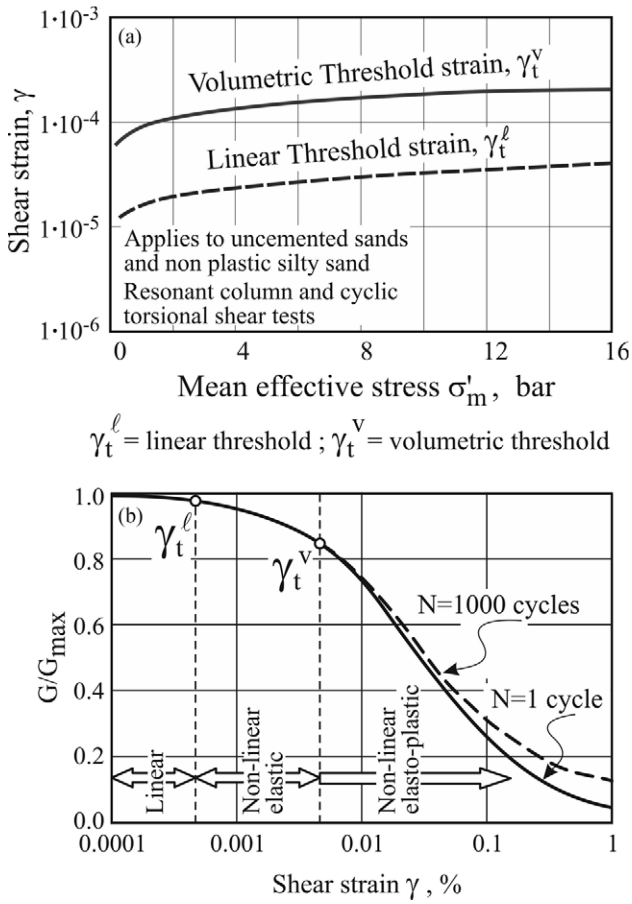

Figure 4 - (a) Small strain shear modulus from seismic tests, Darendelli (1991). (b) Normalized shear modulus degradation curve, Menq (2003).

This figure, after Menq (2003), reports an example of the normalized shear modulus [$G/G_0 = \text{f.}(\gamma \geq \gamma_t^\ell)$] degradation curve as function of the shear strain γ, pointing out the difference between monotonic and cyclic loadings.

As such, G_0 plays a role in the numerical analyses involving complex constitutive soil models, allowing separating elastic from total strains.

Another important function of G_0(F) measured in the field is to allow for the correction of the laboratory determined modulus degradation curve $G(\gamma)$ for disturbance effect. The procedure, see Fig. 5, is based on the available field and laboratory extensive data base, proposed by Ishihara (1996) and makes reference to the following empirical formula:

$$G(\gamma)_{\text{Field}} = C_r \frac{G_0(\text{Field})}{G_0(\text{Lab})} G(\gamma)_{\text{Lab}} \tag{1}$$

being G_0(F) = shear modulus at very small strain ($\gamma \leq \gamma_t^\ell$) from *in situ* seismic tests, G_0(L) = shear modulus at very small strain ($\gamma \leq \gamma_t^\ell$) measured in laboratory, G(L) = shear modulus measured in laboratory at the given value of $\gamma \geq \gamma_t^\ell$, G(F) = corrected field value corresponding to the same value of γ likewise G(L) and C_r = correction factor depending on the sample quality and type.

In his work, Ishihara (1996) provides C_r values as function of the strain level for different kinds of sampling techniques including reconstituted specimens.

In a given soil G_0 and M_0 are controlled by the effective ambient stresses and by the current value of void ratio, reflecting the state of the material.

With reference to the seismic waves propagation and to their computed moduli, the following empirical relations, experimentally validated, [Roesler (1979), Lewis (1990), Lee & Stokoe (1986), Weston (1996)], allow exploring how the current soil state affects V_s, hence G_0 and V_p, thus M_0 respectively:

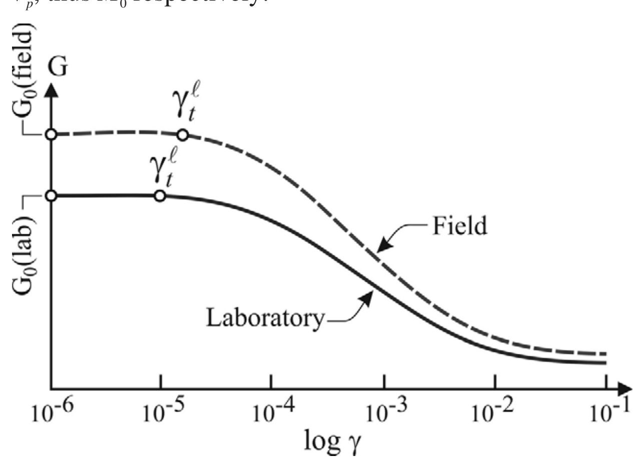

Figure 5 - Ideal field *vs.* laboratory shear modulus degradation curve, after Ishihara (1996).

$$V_s = C_s[(\sigma'_a)^{na}(\sigma'_b)^{nb}(p_a)^{-(na+nb)}]\sqrt{F(e)} \quad (2.1)$$

$$G_0 = C_G F(e)\,[(\sigma'_a)^{2na}(\sigma'_b)^{2nb}(p_a)^{-2(na+nb)}] \quad (2.2)$$

$$V_p = C_p[(\sigma'_a)^{na}(\sigma'_b)^{nb}(p_a)^{-(na+nb)}]\sqrt{F(e)} \quad (3.1)$$

$$M_0 = C_M F(e)[(\sigma' a)^{2na}(\sigma'_b)^{2nb}(p_a)^{-2(na+nb)}] \quad (3.2)$$

being C_s, C_p, C_G, C_M = experimental material constant, *na*, *nb* = experimental stress exponent, F(e) = experimental void ratio function, p_a = reference stress = 98.1 kPa, σ'_a = effective stress in the direction of wave propagation and σ'_b = effective stress on polarization plane. Note: In case of V_s, $na \neq nb$, while for V_p, $na = nb$.

The above formulae consent to estimate, for a given soil, the V_s and G_0 as well as the V_p and M_0 values at different stress levels and densities, once the material constants and the void ratio function have been established, see Lee & Stokoe (1986), Lo Presti (1991a), Ishihara (1996), Bellotti *et al.* (1996), Weston (1996), Hoque & Tatsuoka (1998), Fioravante (2000), Kuwano & Jardine (2002).

In the everyday practice, G_0 and M_0 are considered as isotropic elastic body stiffness making simpler also to assess the Young E_0 and bulk B_0 modulus assuming the value of Poisson coefficient of the soil skeleton ν'_0. With this respect it is worth mentioning that, as confirmed by laboratory tests, ν'_0 at strain level not exceeding the linear threshold, ranges between 0.15 and 0.25, typically exhibiting a trend to decrease with increasing the confining stresses [Hoque (1996), Weston (1996)].

However, the lesson learnt from the propagation of seismic waves *in situ* and in laboratory [Lee & Stokoe (1986), Lee (1993), Bellotti *et al.* (1996), Fioravante (2000), Kuwano & Jardine (2002), Giretti *et al.* (2012)] has demonstrated that in the presence of the level-ground the soil behavior, at very small strain ($\gamma \leq \gamma_t^{\ell}$), can be better approximated by the cross-anisotropic (= transversally isotropic) linear elastic half-space, with the vertical axis (*z*) of symmetry and the horizontal plane (*xy*) of isotropy [Love (1927)]. The relationship, broadly describing the stress-strain behavior of such body, requires determining five independent elastic material constants, see the stiffness matrix in Fig. 6.

For the plane body waves generated on the vertical (*xz*) or horizontal (*yx*) planes, White (1965) derived three equations expressing the velocities in terms of five independent material constants of the cross-anisotropic half-space, see Stokoe *et al.* (1991) and Lee (1993).

The difference in velocities of V_p and V_s propagating on *zx* and *xy* or *yx* planes, coinciding with the principal stresses directions respectively, reflect the material *initial anisotropy.*

$$\boxed{[\sigma'] = [C][\varepsilon]}$$

Where [C] = Stiffness matrix (according to Love, 1959)

$$[C] = \begin{bmatrix} C_{11} & C_{12} & C_{13} & 0 & 0 & 0 \\ C_{12} & C_{11} & C_{13} & 0 & 0 & 0 \\ C_{13} & C_{13} & C_{33} & 0 & 0 & 0 \\ 0 & 0 & 0 & C_{44} & 0 & 0 \\ 0 & 0 & 0 & 0 & C_{44} & 0 \\ 0 & 0 & 0 & 0 & 0 & C_{66} \end{bmatrix}$$

C_{11} = M(H) on the isotropic plane

$\left.\begin{array}{l} C_{33} = \text{M(V)} \\ C_{44} = \text{G(VH)} \end{array}\right\}$ in plane of the symmetry axis

C_{66} = G(HH) on the isotropic plane

C_{13} = fifth indipendent parameter

C_{12} = M(H) - 2G(HH) dependent parameter

Figure 6 - Stress-strain relationship and stiffness matrix of the cross-anisotropic elastic halfspace, Love (1959).

Dealing with the initial elastic anisotropy ($\gamma \leq \gamma_t^{\ell}$) of the non rocky-like geomaterials, two components of different phenomenological nature should be distinguished:

- *Fabric* or *structural* anisotropy exhibited by the soil under isotropic state of stress.
- *Stress induced* anisotropy disclosed even by a soil with isotropic fabric when subject to anisotropic stress state.

Referring to the level ground, *i.e.* geostatic stress state, the stress induced anisotropy is governed by the magnitude of earth pressure coefficient at rest K_0, hence by the soil depositional and post-depositional history.

The initial anisotropy can be quantified in the field measuring, during CH tests, V_s(HH) on the isotropy plane and V_s(VH) along the symmetry axis plane.

The same measurements have been carried out at the copper mine tailings at Zelazny Most (Poland) site yielding initial anisotropy values in terms of *Vs*(HH)/V_s(VH) ratio ranging between 0.92 and 1.12.

Unfortunately, the five independent constants of the cross-anisotropic geomaterials cannot be determined *in situ*. Four of them: G_0(HH), G_0(VH), M_0(H) and M_0(V) can be assessed from the corresponding shear and compression waves measurable in CH tests.

However, for M_0 values, to ensure that the V_p propagation is entirely controlled by the soil skeleton compressibility, such approach is limited to materials that are either dry or with a satisfactorily low degree of saturation[1].

1 See also Fig. 8

In these circumstances, the basic studies for cross-anisotropic materials have been mostly carried out in laboratory, testing mainly on reconstituted soil specimens. Three different methodologies have been employed so far:

- Using exclusively the static stress-strain laboratory probing [Hoque (1996), Hoque & Tatsuoka (1998)], however requiring a simplified assumption to assess the fifth independent cross-anisotropy body parameter.
- As above, combining the results of static probing, with the dynamic measurements of seismic waves velocity using bender elements. This methodology has allowed Kuwano & Jardine (2002) to determine all the five independent material constants.
- Using solely seismic waves generated in large calibration chambers [Lee (1985), Lee & Stokoe (1986), Stokoe *et al.* (1991), Bellotti *et al.* (1996), Giretti *et al.* (2012)], as well as in triaxial apparatuses, see Fioravante (2000), all the above five independent material parameters can be determined.

In these tests, usually carried out under biaxial confinement, it can be determined the fifth independent material parameter, even though generating, in the anisotropy plane, the V_p and V_s waves at the angle Θ with respect to the axis of symmetry (*z*). Lee (1985) and Lee & Stokoe (1986) have pointed out that the propagation of planar waves in *zx* and *zy* planes, and not along the principal stress directions, uncouples the *velocity surface* (= the front of the wave normal) from the overlapping *wave surface* (energy ray path). On the other hand, as observed by Stokoe *et al.* 1991 and Lee 1993, for dry silica sands the resulting discrepancy is sufficiently small and leads to minor corrections of the measured ray velocity to obtain the phase velocity.

In the following are given some examples of seismic tests carried out in a large calibration chamber housing specimen 1.2 m in diameter and 1.5 m in height and instrumented with miniature geophones, see Fig. 7. The adopted geophones arrangement allows the generation, under biaxial confinement, of *P* and *S* waves in three orthogonal principal stress directions *xyz* in Fig. 7 as well as of the oblique waves *P*(Θ), *S*(Θ) inclined at an angle of 45° as regard the axis of symmetry (*z*), with the oblique shear waves *S*(45°) polarized in a vertical plane.

Details of the tests experimental setup can be found in Lo Presti & O'Neill (1991) and Bellotti *et al.* (1996). In the second work, it is also illustrated the trial and error computation procedure used to estimate, with the aid of *P*(45° V) and *S*(45° V), the fifth independent parameter C_{13} of the stiffness matrix of Fig. 6.

Hereafter are summarized some examples of seismic tests results performed in CC on dry pluvially deposited TS-Ticino river (Bellotti *et al.* 1996) and KS-Calcareous Kenya beach (Giretti *et al.* (2012) sands; the same test sands were employed by Fioravante (2000) to investigate, in a triaxial apparatus, the elastic anisotropy. The test sands characteristic are depicted in Table 1.

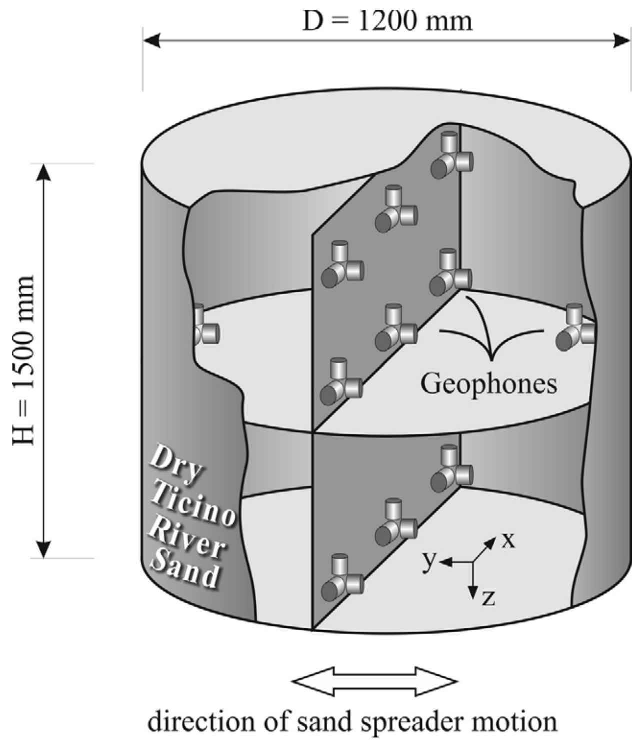

Figure 7 - ISMGEO calibration chamber with geophones to measure the body waves velocity.

Table 1 - Test sands properties.

	Ticino river	Kenya beach
G_S	2.681	2.783
d_{50}	0.55	0.13
C_u	1.69	1.85
e_{min}	0.578	1.282
e_{max}	0.927	1.776
φ'_{cv}	33°	40°
	Siliceous	Carbonatic

Tables 2 and 3 show the moduli ratio G_0(HH)/G_0(VH) and M_0(H)/M_0(V) as obtained from CC seismic tests in dry TS and KS.

More details respectively for TS and KS, can be found in the works by Bellotti *et al.* (1996) and Giretti *et al.* (2012).

To sum up, the seismic waves velocity measurement, *in situ* and in laboratory, plays a central role in the evaluation of the soil stiffness at very small strain and of its anisotropy.

The main issues significant to the engineering applications are:

- G_0 corresponding to the initial tangent shear modulus for both static and dynamic loading.
- Knowing G_0, elastic and plastic strains can be separated.

Table 2 - Dry Ticino river siliceous sand elastic anisotropy.

Medium dense	σ'_h/σ'_v	G_{hh}/G_{vh}	M_h/M_v	E_h/E_v	Stress range σ'_v (kPa)
D_R = 41%	0.5	0.96	0.83	0.81	50 to 300
	1.0	1.20	1.20	1.22	50 to 300
	1.5	1.25	1.55	1.52	50 to 300
	2.0	1.44	1.88	1.86	50 to 300

Very dense	σ'_h/σ'_v	G_{hh}/G_{vh}	M_h/M_v	Stress range σ'_v (kPa)
D_R = 88%	0.5	1.13	1.05	50 to 300
	1.0	1.15	1.31	50 to 300
	1.5	1.25	1.40	50 to 300

Siliceous river sand, G_s = 2.681, e_{max} = 0.927, e_{min} = 0.578, C_u = 1.69, φ'_{cv} = 33°, F(e) = $e^{-1.3}$.

Table 3 - Dry oolithic calcareous Kenya beach sand elastic anisotropy.

Medium dense	σ'_h/σ'_v	G_{hh}/g_{vh}	M_h/M_v	E_h/E_v	Stress range σ'_v (kPa)
D_R = 35%	0.5	0.93	0.78	0.79	50 to 500
	1.0	1.12	1.27	1.24	50 to 500
	2.0	1.26	2.05	1.92	25 to 250

Very dense	σ'_h/σ'_v	G_{hh}/G_{vh}	M_h/M_v	E_h/E_v	Stress range σ'_v (kPa)
D_R = 88%	0.5	1.09	0.94	0.98	50 to 500
	1.0	1.24	1.27	1.29	50 to 500
	1.5	1.28	2.08	1.93	25 to 250

- G_0 inferred from V_s measured in the field offers the possibility to correct the laboratory *G vs.* γ degradation curves accounting for disturbance effects.
- The generation of *S*(HH) and *S*(VH) waves in field and in laboratory consent to estimate the material initial anisotropy.
- Although so far limited to laboratory testing on reconstituted specimens, the generation of seismic waves, alone or in combination with static probing, carried out in the triaxial apparatus consent to study the basic behavior of the elastic cross-anisotropic geomaterials.

3. Fully Saturated *vs.* Near-To-Saturated Soils

In the last two decades many laboratory and field experiments have proved that the compression wave propagation is an extremely sensitive tool to distinguish fully from near to saturated soils: [Ishihara *et al.* (1998); Kokusho (2000); Tsukamoto *et al.* (2001); Ishihara *et al.* (2004); Nakazawa *et al.* (2004); Ishihara *et al.* (2004), Valle Molina (2006)]. The compression wave propagation can be used both in the field via in-hole geophysical methods and in the triaxial cell instrumented by means of BE tests, *e.g.*: Fioravante (2000); Tsukamoto *et al.* (2001); Kuwano & Jardine (2002); Valle Molina (2006), Valle Molina & Stokoe (2012).

Figures 8 and 9 show the results of laboratory experiments aimed at exploring the dependence of V_p on the saturation degree. The results confirm the extreme sensitivity of the *P*-wave velocity to even small deviations from the full saturation, occurring when V_p exceeds 1450 to 1500 m/s, and correspond to the compression wave in water velocity.

Figure 10 presents the result of CH tests carried out from the sea bottom of the Venice Lagoon as part of the site characterization for the Mose barriers project [Jamiolkowski *et al.* (2009)] aimed at safeguarding this unique city

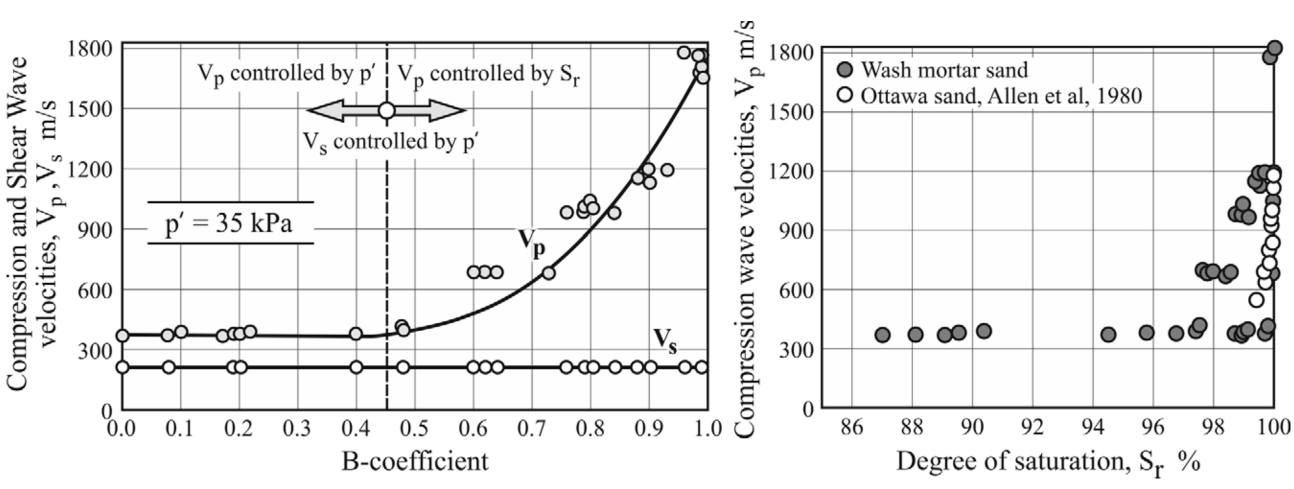

Figure 8 - P-waves and S-waves dependence on saturation degree, Valle-Molina (2006).

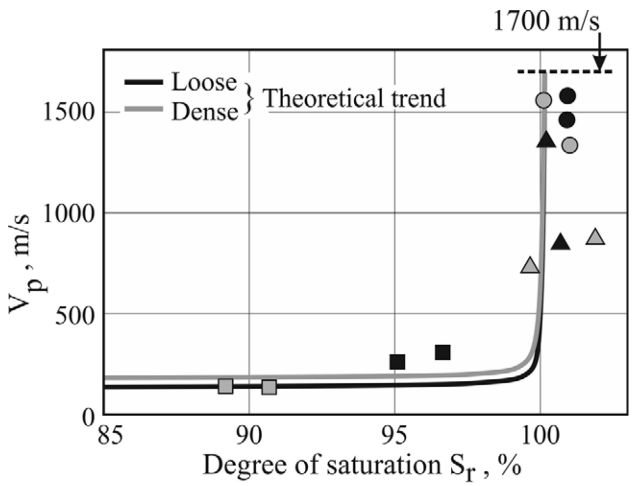

	D_R %	Saturation method	S_r %
■	90.2-93.5	Atmosphere	89.2-90.7
□ (grey)	15.3-25.9	Atmosphere	95.1-96.7
▲	96.7-97.7	Vacuum	100
△ (grey)	25.4-29.9	Vacuum	100
●	96.2-99.7	Vacuum+CO_2	100
○ (grey)	24.6-31.2	Vacuum+CO_2	100

Figure 9 - Compression wave velocity *vs.* saturation degree, Takahashi *et al.* (2001).

from high tides. This figure shows V_p(H) as well as V_s(HV) and V_s(HH) resulting from CH tests, together with the relevant lagoon soil profile.

The V_p profile highlights the presence, below the sea bottom, of an unsaturated soil zone, ≈ 12 m thick, due to marsh gas.

The capacity of V_p to detect the presence in the subsoil of near to saturated spots, plays a crucial role in evaluating the susceptibility of coarse grained soils to cyclic and monotonic liquefaction during undrained loading [Ishihara *et al.* (1998); Grozic *et al.* (1999, 2000); Ishihara *et al.* (2004), Lee *et al.* (2005)]. Figure 11 displays the cyclic resistance ratio (CRR) obtained from undrained triaxial tests of the near to saturated Toyoura sand, normalized with respect to the CRR of the same sand at full saturation, see Ishihara *et al.* (1998) and Tsukamoto *et al.* (2001).

The V_p capability to map the saturation surface position in the subsoil, finds many important applications in the engineered constructions experiencing complex hydraulic regime, variable in time and space.

A typical example is the second world largest copper tailings storage disposal, whose peculiar features can be inferred from Fig. 12. At this Polish site, in Zelazny Most, since 1993 CH tests are being carried out periodically on the pond beaches, to map the position of the saturation line in the tailings, [Jamiolkowski *et al.* (2010)]. Figure 13 shows the location of 9 CH tests performed during the 2011 campaign.

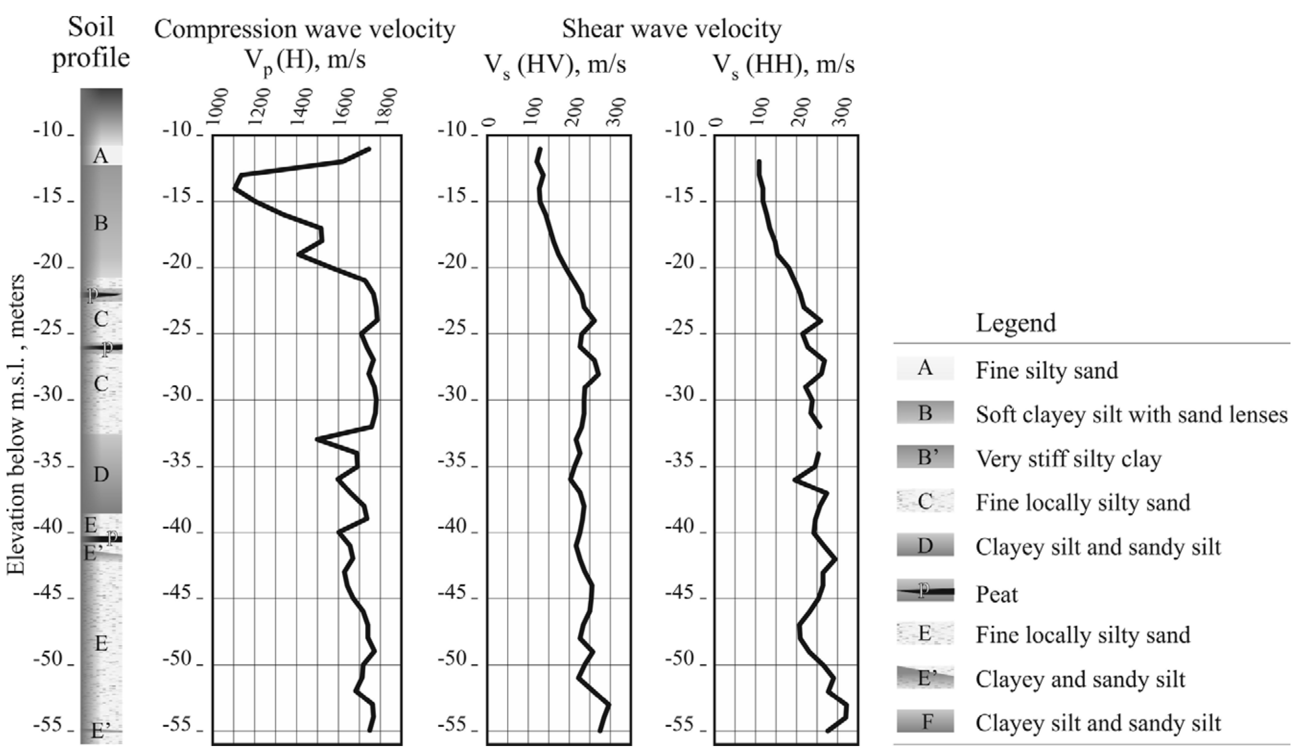

Figure 10 - Venice Lagoon, Chioggia inlet- Cross-hole test results.

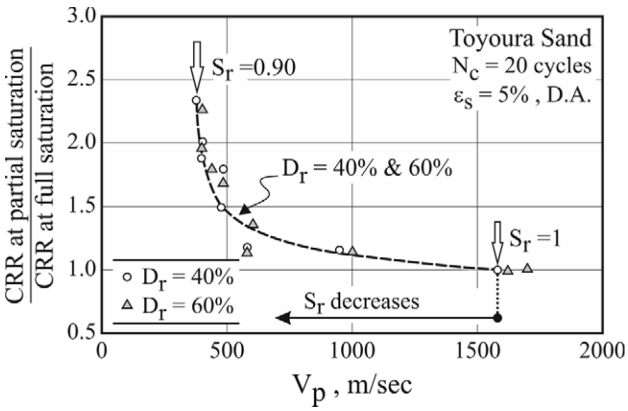

Figure 11 - Cyclic resistance ratio dependence on saturation degree Ishihara *et al.* (1998), Tsukamoto *et al.* (2001).

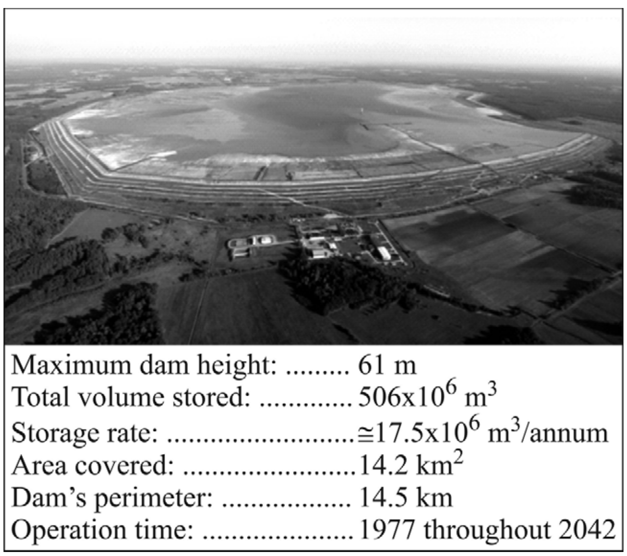

Figure 12 - Zelazny Most (Poland), copper tailings disposal: aerial view.

Figures 14 through 16 display the depth position of the saturation line in the tailings, as determined based on the V_p measured in CH tests at variable distance from dam crest for cross-sections in correspondence of the West, North and East dams respectively. As the figures show, the measured V_p value, allows recognizing the presence of saturated tailings at a depth below which V_p remains greater than 1450 to 1500 m/s. Moreover, the profiles of V_p *vs.* depth show also the presence, in the tailings, of the perched water horizons. See Figs. 15 and 16 where the perched water horizons are labeled with the symbol P_H.

From the above one can deduce that:

- The measured V_p is an extremely sensitive tool to distinguish *in situ* and in laboratory fully ($S_r \cong 100\%$) from near to saturated ($90\% \le S_r < 100\%$) state; see Fig. 9 after Tsukamoto *et al.* (2001) and the recent work by Valle Molina & Stokoe (2012).

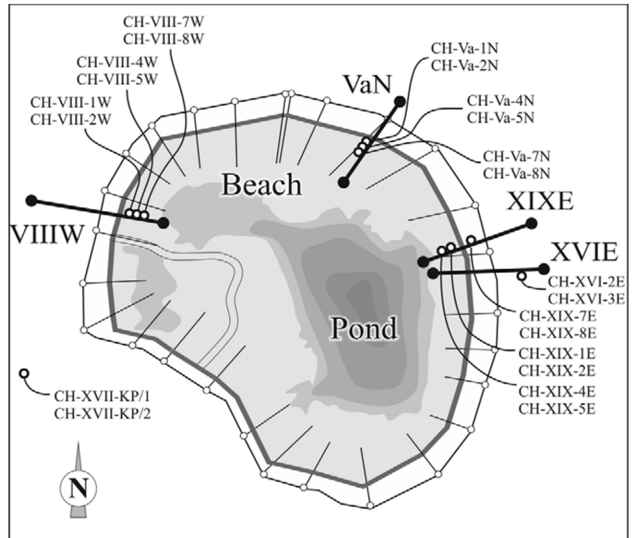

Dam	Section	Crest elev. (m)	CH n°	Distance from dam crest (m)
W	VIII	171.0	CH-VII-1W/2W	40.6
		170.5	CH-VII-4W/5W	132
		169.9	CH-VII-7W/8W	217
N	Va	171.1	CH-Va-1N/2N	40
		170.8	CH-Va-4N/5N	120
		170.4	CH-Va-7N/8N	200
E	XIX	165.1	CH-XIX-7E/8E	-147*
		170.2	CH-XIX-1E/2E	95
		169.8	CH-XIX-4E/5E	195

(*) Beyond the first dam crest.

Figure 13 - Zelazny Most: Cross-hole tests location.

- This V_p feature represents a simple and reliable tool to map the distribution of fully and nearly to saturated soil deposits *in situ*.

- In the last decade there have been many attempts to correlate Skempton's (1954) pore pressure coefficient B measured in laboratory against the velocity of the compression wave, [Kokusho (2000), Tsukamoto *et al.* (2001), Takahashi *et al.* (2006), Valle Molina & Stokoe (2012)].

4. Quality Assessment of Undisturbed Samples

In case of homogeneous low permeability clays, quality undisturbed samples can be evaluated in laboratory measuring the sample suction p_s immediately after its retrieval from the ground, [Skempton (1961), Chandler *et al.* (2011)]. This approach is quite complex, see Chandler *et al.* (2011) and time consuming thus not routinely employed. Moreover, it is restricted to homogeneous fine grained soils able to preserve high suction after zeroing of the total *in situ* stress as results of sample retrieval.

This prompts to develop some easier semi-empirical criteria to assess undisturbed samples quality.

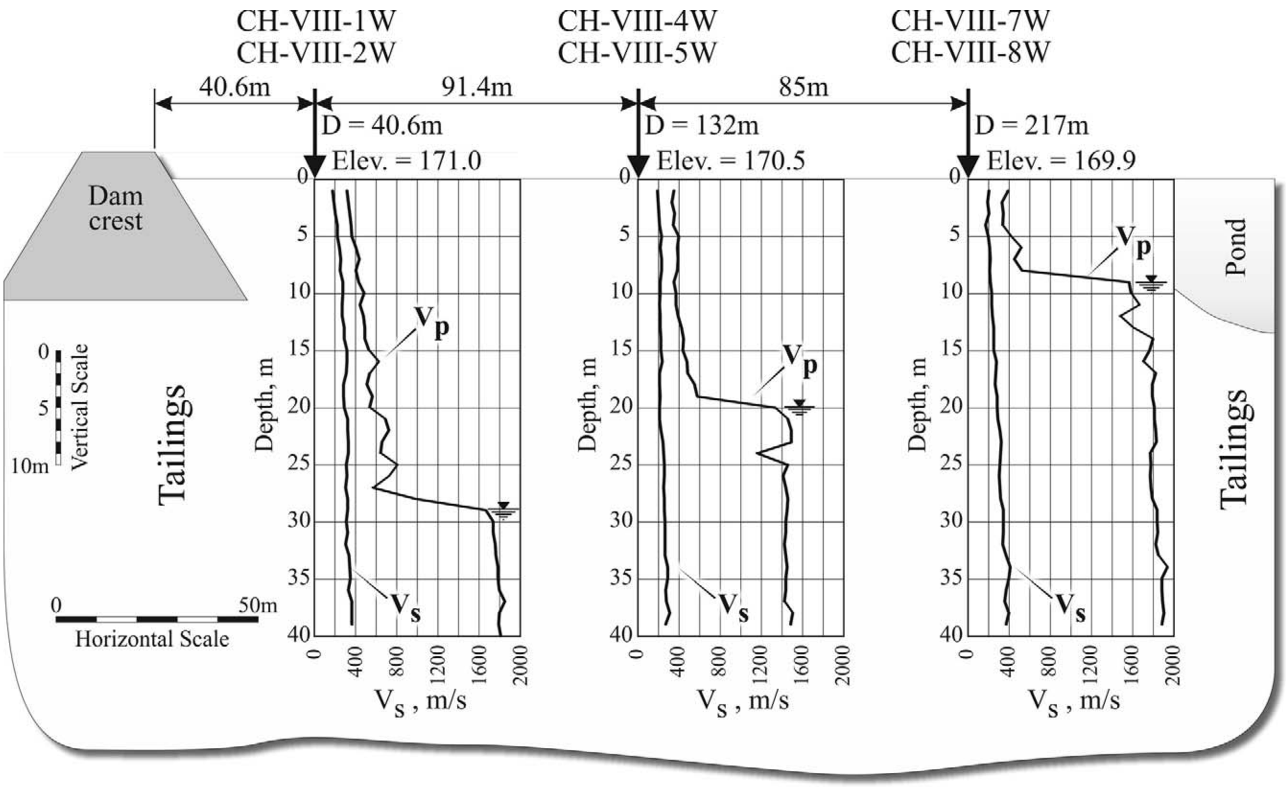

Figure 14 - West dam, cross-hole tests results

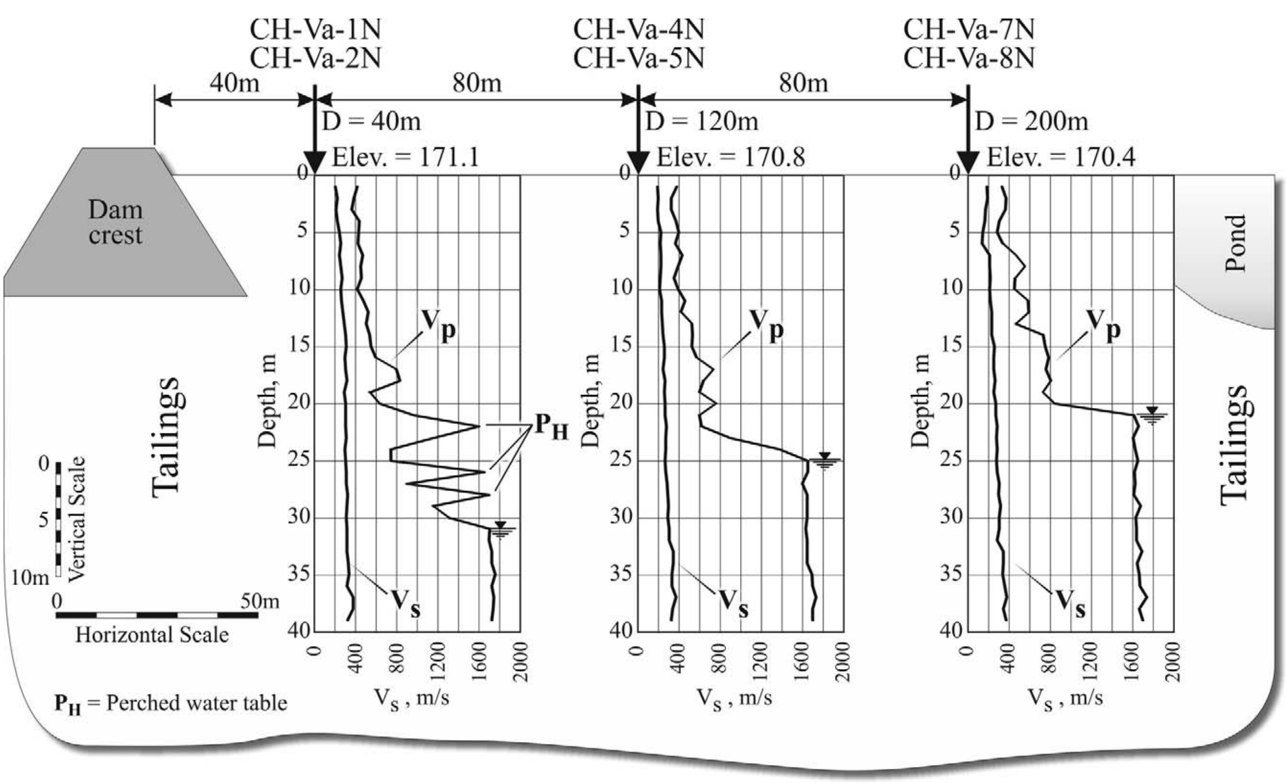

Figure 15 - North dam, cross-hole tests results.

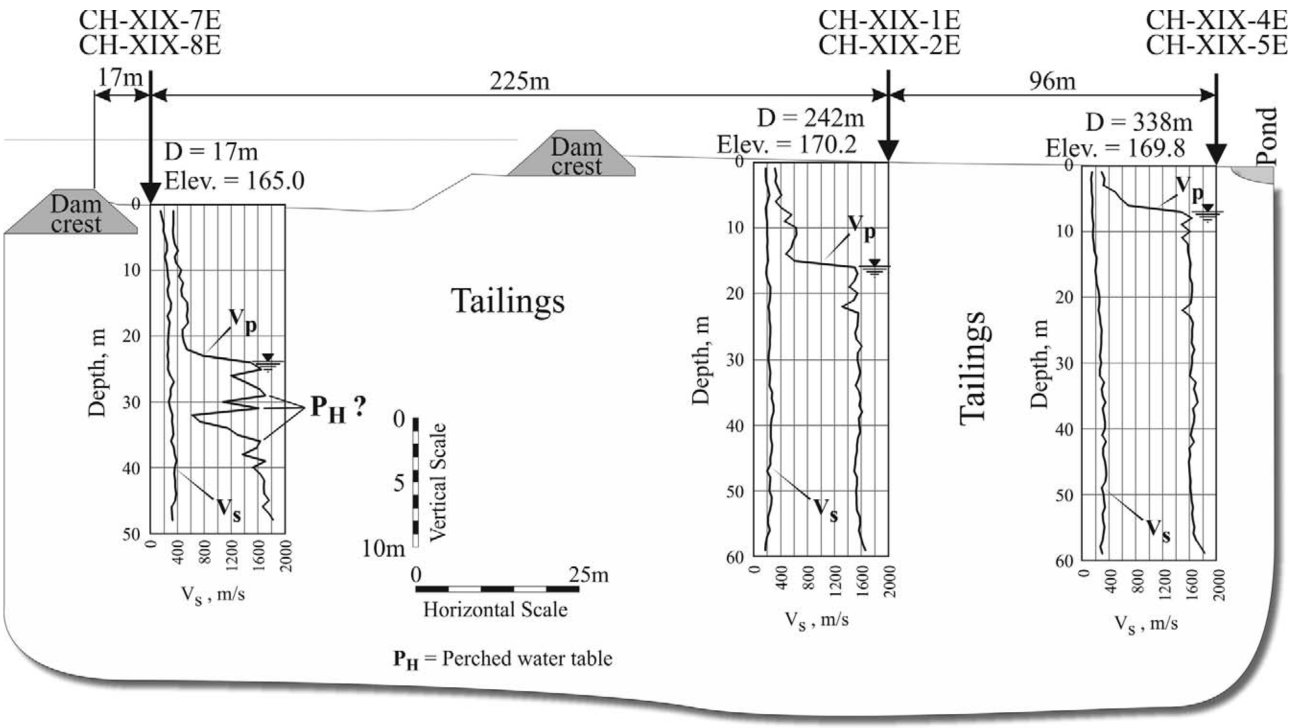

Figure 16 - East dam, cross-hole tests results.

With this respect, a widely used criterion has been proposed by Lunne *et al.* (1997; 2006) for fine grained soils in terms of $\Delta e/e_0$ ratio, being:

- Δe = reduction of the void ratio during one dimensional recompression of undisturbed specimen to *in situ* vertical effective stress σ'_{v0} existing at a depth from which the sample were retrieved.
- e_0 = *in situ* void ratio.

The other criterion, applicable to both coarse and fine grained soils [Sasitharan *et al.* (1994); Landon *et al.* (2007) De Groot *et al.* (2011); Fioravante *et al.* 2012)] is based on the comparison of normalized shear wave velocity V_{s1}(L) measured on laboratory specimens with that measured in the field V_{s1}(F) by means of one of the methods recalled in Fig. 1.

The values of V_{s1}(F) and V_{s1}(L) are computed by means of the formula 4, a somehow simplified version than Eq. 2.1, considering that the separate values of exponents na and nb are difficult to measure and therefore rarely available:

$$V_{s1}(\mathrm{L}) = V_s\left(\frac{2p_a}{\sigma'_{v0}+\sigma'_{h0}}\right) \tag{4}$$

where V_s(F) = shear wave velocity measured in the field at the same depth the sample has been retrieved, V_s(L) = shear wave velocity measured in laboratory on the specimen reconsolidated to the best estimate of the *in situ* geostatic stresses at the same depth the sample has been retrieved, p_a = reference stress = 98.1 kPa, σ'_a = effective stress in the wave propagation direction, σ'_b = effective stress on the plane of the wave polarization, *ns* = stress exponent na+nb, pertinent to V_{s1}(F), σ'_{v0} = effective vertical stress at the sampling depth, σ'_{h0} = effective horizontal stress at the sampling depth, ns = stress exponent na+nb, pertinent to V_{s1}(L).

The closer V_{s1}(L)/V_{s1}(F) ratio is to unity, the better the quality of undisturbed sample.

This ratio can also be used to estimate the mechanical characteristics of the specimens reconstituted in laboratory that the soil, in undisturbed state, should have *in situ*.

Overall, exponents np and ns, the former pertinent to V_p, vary within a relatively narrow range (0.22 to 0.25) in case of fine grained soils and uniform sands but tend to increase in coarse gravelly sand and sandy gravel as the uniformity C_u coefficient increases [Weston (1996)], see Fig. 17. This figure adapted after the quoted work by Weston, with the support of some writer's data, gives the stress exponents n_S and n_G from V_S and G_0 respectively determined experimentally in laboratory tests on the reconstituted specimens.

The quality evaluation of three examples based on V_{S1}(L)/V_{S1}(F) ratio is hereafter presented.

The *first* example deals with undisturbed samples of sandy gravel 600 mm in height (H_s) and 300 mm in diameter (D_s) retrieved on the Sicilian shore of Messina Strait by means of the freezing technique [Fioravante *et al.* (2012)], see Fig. 18.

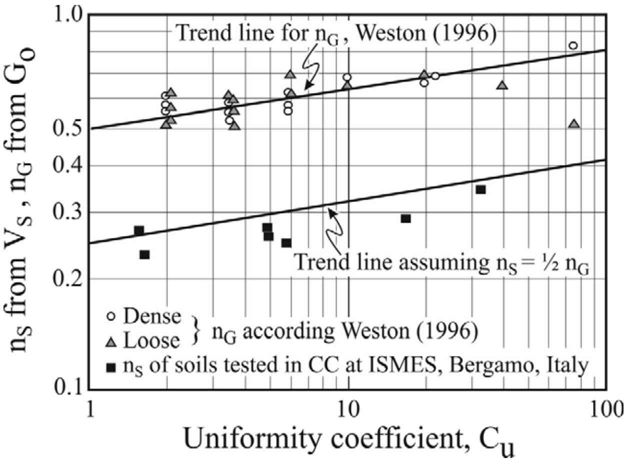

Figure 17 - Stress exponent n_s from V_s and n_G from G_0, adapted after Weston (1996).

Figure 19 shows the comparison between V_{S1}(F) measured during CH test and V_{S1}(L) obtained from bender element (BE) tests.

Due to the large dimensions of the gravelly particles ($63 \leq d_{max}$ 100 mm; $3 \leq d_{50} \leq 16$ mm; $10 \leq C_u \leq 35$), to measure the reliable values of V_s the propagation seismic waves through laboratory specimens, need to fulfill the ASTM D 2845 (1997a) requirements, see also: Sanchez-Salinero *et al.* (1986), Viggiani & Atkinson (1995), Brignoli *et al.* (1996), Jovicic *et al.* (1996), Pennington (2001), Arroyo & Greening (2002) and Maqbool *et al.* (2004).

In the examined case, the characteristics of the generated shear waves during BE tests were as follows:

- Wave mean length: λ_m = 25 mm; applied frequency: f = 10 kHz; H_s/D_s = 2.0; D_s/λ_m = 12.0; λ_m/d_{50} = 2.5; H_s/λ_m = 24.0.
- The above values fulfill the ASTM recommendations, with the exception of λ_m/d_{50} ratio which should be ≥ 3.0.

The *second* example refers to undisturbed samples of fine to medium sand retrieved by means of freezing, see Fig. 20 at the Tyrrhenian shore close to Gioia Tauro, in Southern Italy.

Table 4 reports the values of V_{s1}(L)/V_{s1}(F) ratio as obtained for the tested undisturbed samples. Again in this case, V_s(L) has been measured by means of BE tests while V_{s1}(F) was obtained from CH test whose results[2].

The resulting values of V_{s1}-ratio, probably except for the one from a 24.5 m depth, confirm the tested samples high quality.

The *third* example deals with the undisturbed sampling of very uniform stiff to hard OC clay, see Fig. 21, retrieved at the Porto Empedocle site on the Eastern Sicilian Coast. In this case, besides using the available V_{s1} ratio, the quality of undisturbed samples has been evaluated from suction measured by means of Ridley & Burland (1993) transducer, carried out soon after the samples retrieval, see Chandler *et al.* (2010) and also referring to the Lunne *et al.* (1997, 2007) criterion based on the ratio of $\Delta e/e_0$ measured in oedometer tests.

Table 5 shows the comparison for a number of Porto Empedocle clay samples between V_{s1}(L)/V_{s1}(F) and $\Delta e/e_0$ ratios together with the ratio of p_s/p'_0, being: p_s = measured suction in the sample, p'_0 = the best estimate for mean *in situ* effective stress at the sampling depth. In the case in hand, all the three used approaches indicate the excellent quality of tested samples.

The information collected by De Groot et (2011) supports the idea that both ratios, V_{s1}(L)/V_{s1}(F) and $\Delta e/e_0$, as shown in Fig. 22 are useful and complementary tools when evaluating undisturbed samples quality.

Basically, based on the above the following comments apply:

- V_{s1}(F) reflects *in situ* soil state, fabric, aging and particles bonding.
- V_{s1}(L) has to be assessed on specimens reconsolidated to the best estimate of *in situ* geostatic stresses.

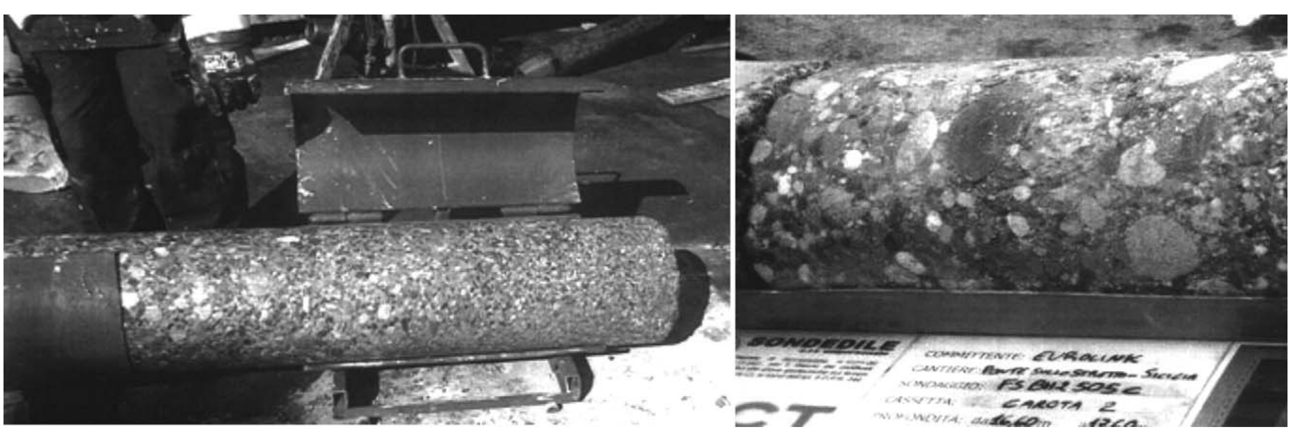

Figure 18 - Messina Strait sandy gravel, undisturbed sample.

2 See Fig. 25.

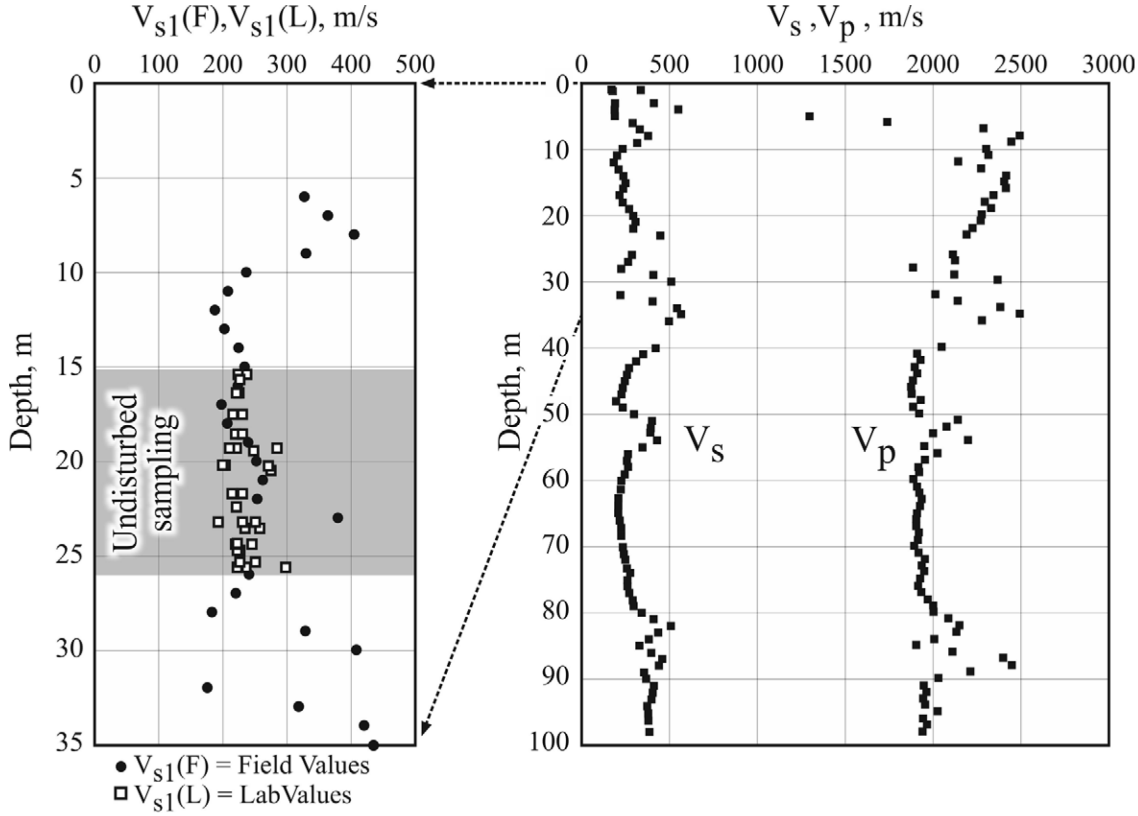

Depth	15	16	17	18	19	20	21	22	26
$\frac{V_{s1}(L)}{V_{s1}(F)}$	1.03	1.08	1.17	1.14	1.00	0.87	0.94	0.94	1.01

Figure 19 - Messina Strait- V_{s1}(F) from cross-hole test *vs.* V_{s1}(L) from bender element tests.

Figure 20 - Gioia Tauro, fine to medium sand, undisturbed sample.

- The main uncertainty in determining V_{s1}(L) is linked to an appropriate selection of the laboratory horizontal consolidation stress.
- The closer V_{s1}(L)/V_{s1}(F) is to one, the better the quality of the specimen tested in laboratory.
- Unlike other methods for the assessment of undisturbed samples quality (*e.g.* suction measurements or the comparison of the void ratio reduction after the specimen 1-D

Table 4 - Gioia Tauro-V_{s1}(F) from cross-hole test *vs.* V_{s1}(L) from bender element tests.

Depth (m)	V_{s1}(F) (m/s)	V_{s1}(L)* (m/s)	V_{s1}(L)/ V_{s1}(F)
24.5	315	227	0.72
28.6	274	222	0.81
30.2	245	230	0.94
31.0	265	227	0.87

(*)BE tests on undisturbed samples obtained by *in situ* freezing.

Table 5 - Porto Empedocle OC clay – Multiple approach to sample quality assessment.

Depth (m)	$\Delta e/e_0$	V_{s1}(L)/ V_{s1}(F)	p'_s/p'_0
28.6	0.0093	0.984	0.983
31.3	0.0069	0.983	1.078
31.2	0.0059	0.973	1.082
49.8	0.0112	0.984	0.852
53.1	0.0032	0.972	0.938
56.1	0.0052	0.992	0.991

Figure 21 - Porto Empedocle, very stiff to hard clay, undisturbed sample.

recompression to the *in situ* effective overburden stresses), the V_{s1}(L)/V_{s1}(F) ratio can be used in both fine and coarse grained geomaterials.

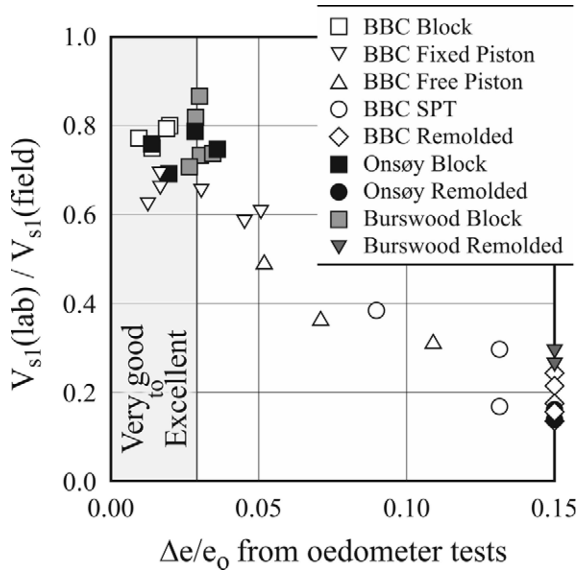

Figure 22 - Undisturbed clay sample quality assessment-Field *vs.* laboratory criterion, DeGroot *et al.* (2011).

5. Evaluation of *In Situ* Void Ratio

The geomaterials *in situ* porosity n_0 and void ration e_0 are important state parameters, crucial for a thorough site characterization when working out many geotechnical boundary value problems.

The assessment of n_0 or e_0, while routinely determined via laboratory tests on undisturbed samples of fine grained soils, results by far more complex and expensive when dealing with coarse grained soils in which undisturbed sampling [(Yoshimi *et al.* (1978), Hofmann (1997), Yoshimi (2000), Huang *et al.* (2008)] is still far to become a common practice.

To overcome this restraint, several empirical correlations have been proposed based on various penetration tests [Schmertmann (1978), Skempton (1986), Cubrinovski & Ishihara (1999), Jamiolkowski *et al.* (2001)] and *in situ* relative density (D_R), which, in combination with laboratory determined maximum (e_{max}) and minimum (e_{min}) void ratio allow estimating, in first approximation, the e_0.

In this circumstance, the researchers and practitioners attention was drawn by Foti *et al.* (2002) work who, within the frame of Biot (1956) linear theory of poroelasticity, has developed a procedure to compute *in situ* e_0 or n_0 via inversion of the seismic waves V_p and V_s measured in the in-hole geophysical tests.

The formula by Foti *et al.* (2002), applicable to *fully saturated* soils only is reported here below:

$$n = \frac{\rho_s - \sqrt{\rho_s^2 - \dfrac{4(\rho_s - \rho_f)B_f}{V_p^2 - 2\left(\dfrac{1-\nu_s}{1-2\nu_s}\right)V_s^2}}}{2(\rho_s - \rho_f)} \tag{5}$$

where ρ_s = soil particles mass density, ρ_f = pore fluid mass density, B_f = bulk modulus of pore fluid, ν_s = Poisson ratio of soil skeleton.

Since its publication this formula has been calibrated against laboratory tests results carried out on good quality undisturbed samples of fine grained geomaterials [Foti & Lancellotta (2004), Arroyo *et al.* (2007), (Jamiolkowski *et al.* (2009)], yielding, overall, satisfactory results.

In the following are compared, and when appropriate commented, three examples of void ratio e_0 computed from seismic waves velocity measured in CH tests and those obtained in laboratory on high quality undisturbed samples.

The *first* examples, see Fig. 23, compares n_0 values measured in laboratory on high quality undisturbed samples of soft lightly OC Pisa clay with those computed from V_p and V_s.

The *second* example in Fig. 24, compares the e_0 measured in laboratory on the undisturbed samples of sandy gravel retrieved by means of freezing, at Messina Strait and those computed from the V_p and V_s measured in the CH test located nearby the in-hole from which the frozen samples have been retrieved. The e_0 computed values on average result to be 10 to 15 percent lower than those determined in laboratory (Fioravante *et al.* 2012). The reasons for this difference can be attributed to a combination of the following factors: uncertainties involved in the accuracy of measured

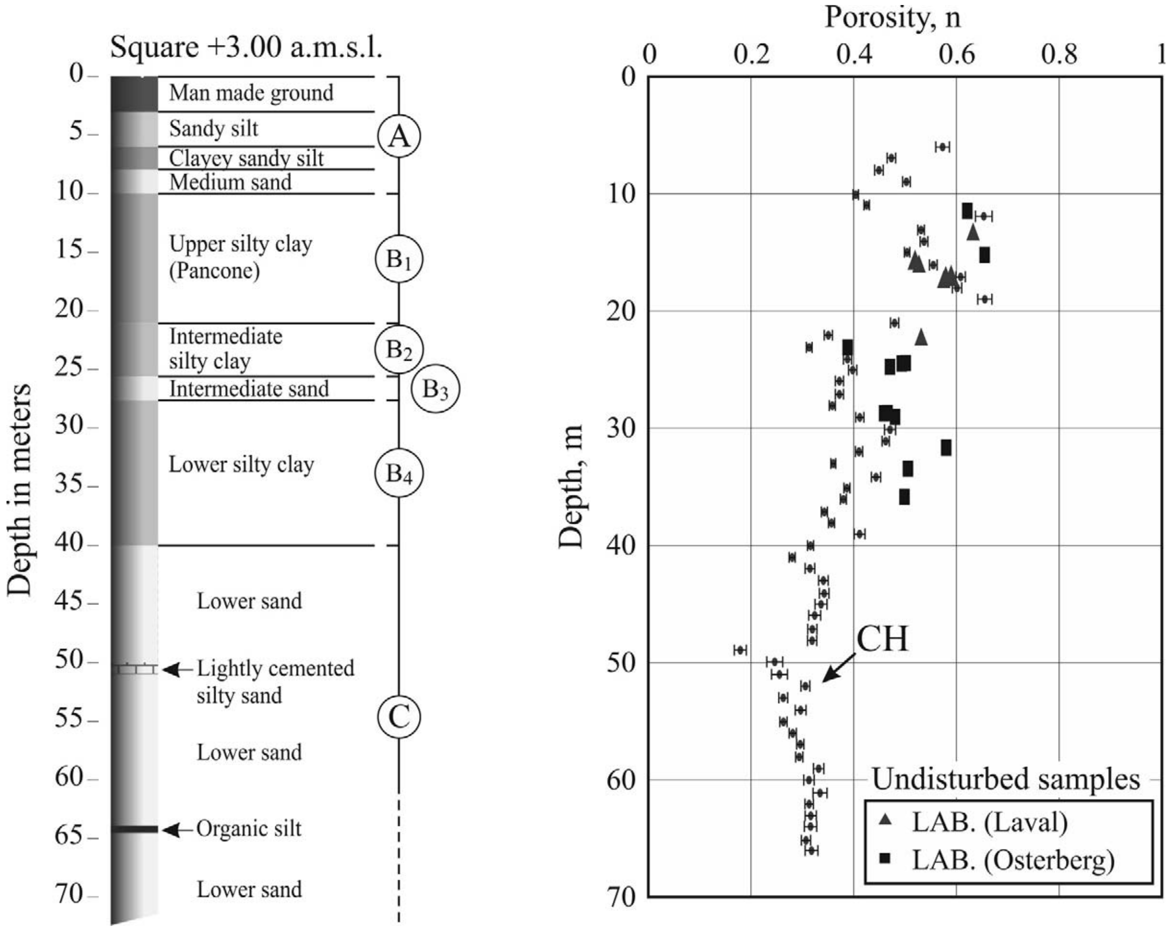

Figure 23 - Pisa clay- Porosity from V_p and V_s *vs.* laboratory determined values.

V_p and V_s; the large disparity between the volume of the undisturbed specimen tested in laboratory and the volume of soils involved in waves propagation during CH testing associated with the spatial variability of the sandy gravel deposit in question.

The *third* examples in Fig. 25, displays the comparison between e_0 measured in laboratory on undisturbed frozen samples of fine to medium sand retrieved at Gioa Tauro site, with those computed from the V_p and V_s measured in the CH test located in the vicinity of the sampling in-hole. In this case, the agreement between e_0 values measured and computed is satisfactory.

However, as to the reliability of the *in situ* void ratio, as computed from V_p and V_s measured in the state of the art CH tests, not all the experimental evidences, collected so far by the writer, have yielded satisfactory comparisons with the laboratory determined e_0. Figure 26 reports the extreme case of a very stiff to hard homogeneous marine Pliocene clay at Porto Empedocle site where the e_0 computed from V_p and V_s significantly underestimates the laboratory measured values by almost a constant offset of about 30 to 50 percent of the laboratory values.

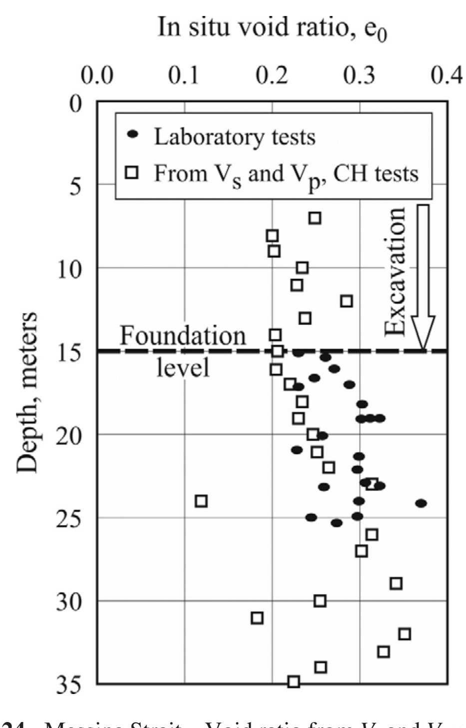

Figure 24 - Messina Strait – Void ratio from V_p and V_s *vs.* laboratory determined values.

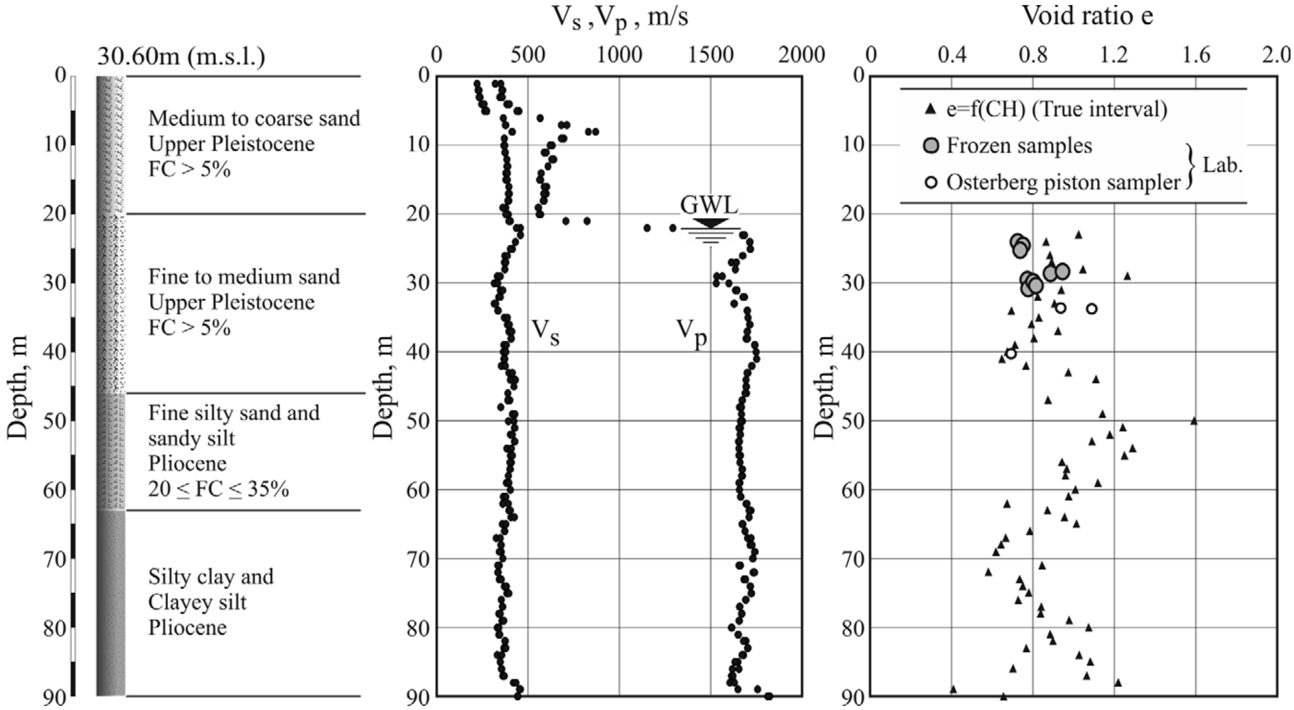

Figure 25 - Gioia Tauro – Void ratio from V_p and V_s *vs.* laboratory determined values.

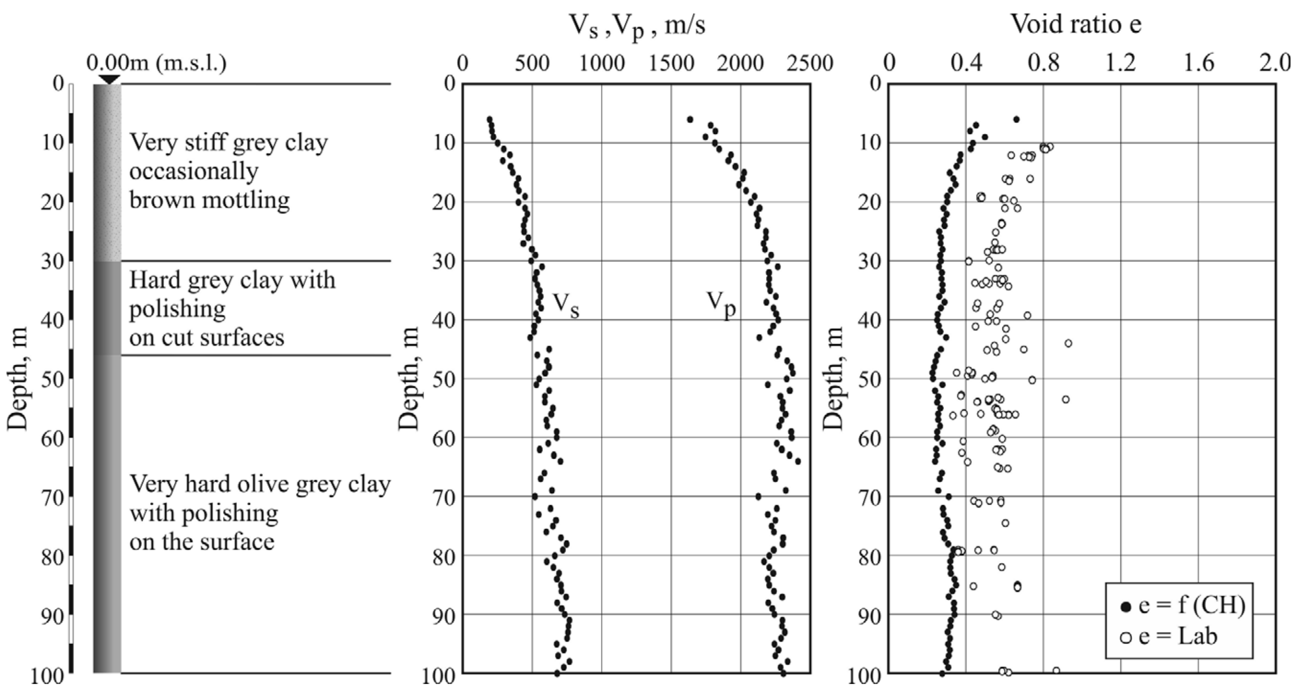

Figure 26 - Porto Empedocle – Void ratio from V_p and V_s *vs.* laboratory determined values.

A few similar examples have raised the issue of the accuracy and reliability of *in situ* void ratio computed from V_p and V_s. This subject has been addressed by Foti (2003) who has investigated the error propagation of the measured seismic waves velocities in the porosity computed by means of Foti *et al.* (2002) formula.

As it can be expected, dealing with an inverse problem, the reliability of the computed e_0 or n_0 is very sensitive to the accuracy of the measured key input parameters, V_p and, to a less extent, V_s.

Figure 27 exemplifies how, on the measured seismic waves velocity, in the range of V_p and V_s characteristic for

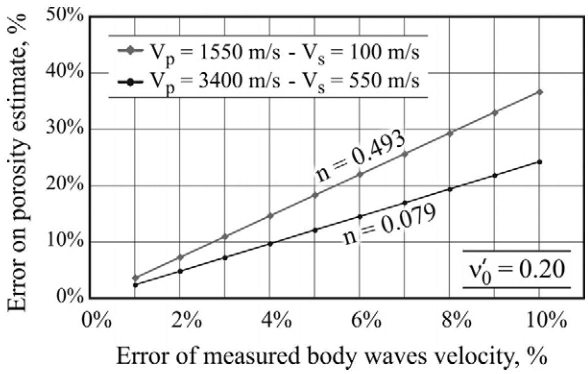

Figure 27 - Error propagation in computing porosity from V_p and V_s as per Foti (2003).

non rock like geomaterials, the error affects the computed porosity. It can be observed that within the range of the considered V_p and V_s, the error on the measured seismic wave velocity amplifies, by three times that of the computed porosity.

Moreover, Lai & Crempien (2012), investigating the stability of the inversion procedure to compute the porosity after the formula by Foti *et al.* (2002), have pointed out that there are combinations of V_p, V_s and pair with the soil skeleton Poisson ratio ν'_0 can be solved only in terms of complex numbers.

However, within the range of CH tests data base covered by the Author ($100 \leq V_s = 550$ m/s; $1500 \leq V_p = 3500$ m/s) in combination with $0.15 \leq \nu'_0 \leq 0.25$, the use of Foti *et al.* (2002) formula has, so far, yielded a solution in terms of real numbers.

This holds also for the data reported in Fig. 26, where the Foti's formula, although well posed, has yielded results conflicting with the comprehensive and reliable set of e_0 values determined in laboratory [Chandler *et al.* (2011)].

The evidence that the error on measured seismic waves velocity for the range of V_p and V_s considered in Fig. 27, amplifies by three times the error on the computed n_0, has triggered the attempt to explore the intrinsic variability of V_p and V_s measured during 9 state-of-the-art CH tests recently carried out at the Zelazny Most site copper tailings, mentioned in Section 3 of this paper.

The following testing program has therefore been set up:

- In each CHT, at 1 m intervals, the seismic waves (V_p and V_s) velocity measurements have been repeated 10 times and the obtained values stored.
- In each in-hole a survey of the deviation from the verticality and of its azimuth has been carried in both in down-hole and up-hole modes repeating all the measurements three times at depth intervals of 3 m.

The bulk of the collected data will be used for the statistical and probabilistic evaluation of how the combination of the two independent variables, *time* and *distance,* affect the accuracy of measured V_p and V_s in the high quality CH tests.

The following preliminary information arising from the above tests can, currently, be anticipated:

- Figures 28 and 29, besides two CH tests results, report the standard deviation values of V_p and V_s measured ev-

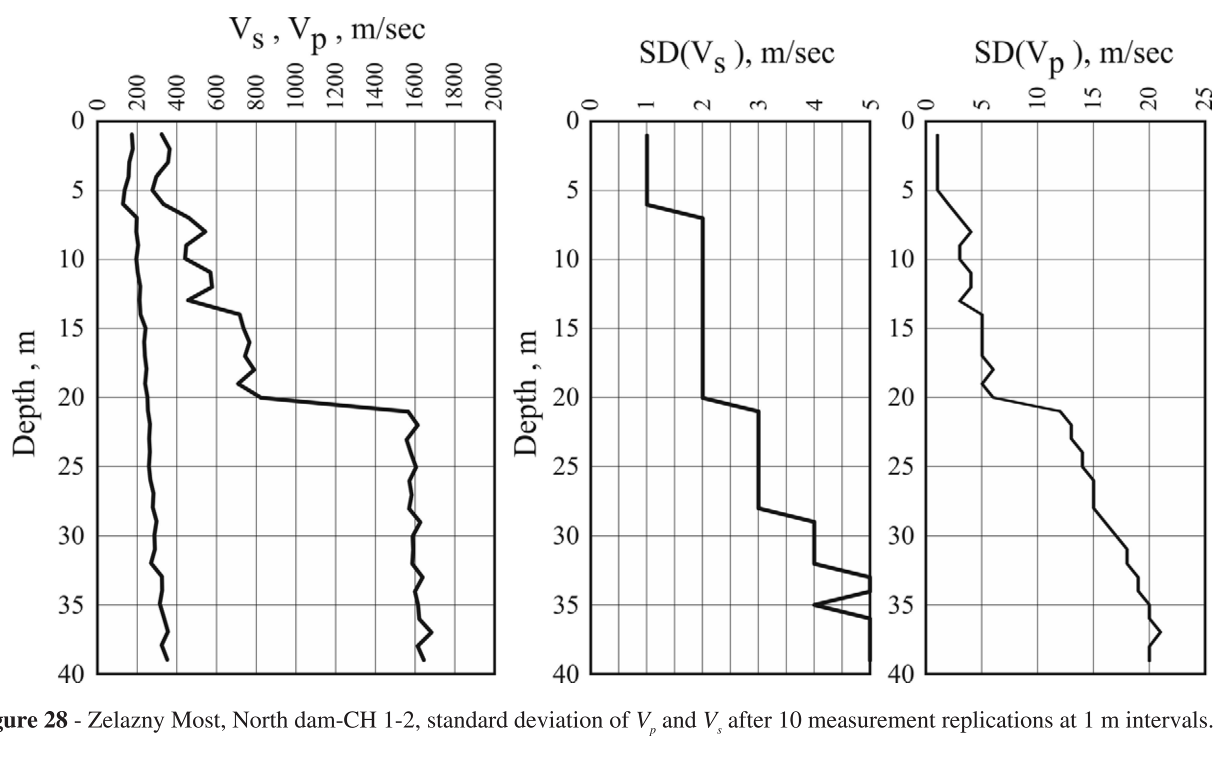

Figure 28 - Zelazny Most, North dam-CH 1-2, standard deviation of V_p and V_s after 10 measurement replications at 1 m intervals.

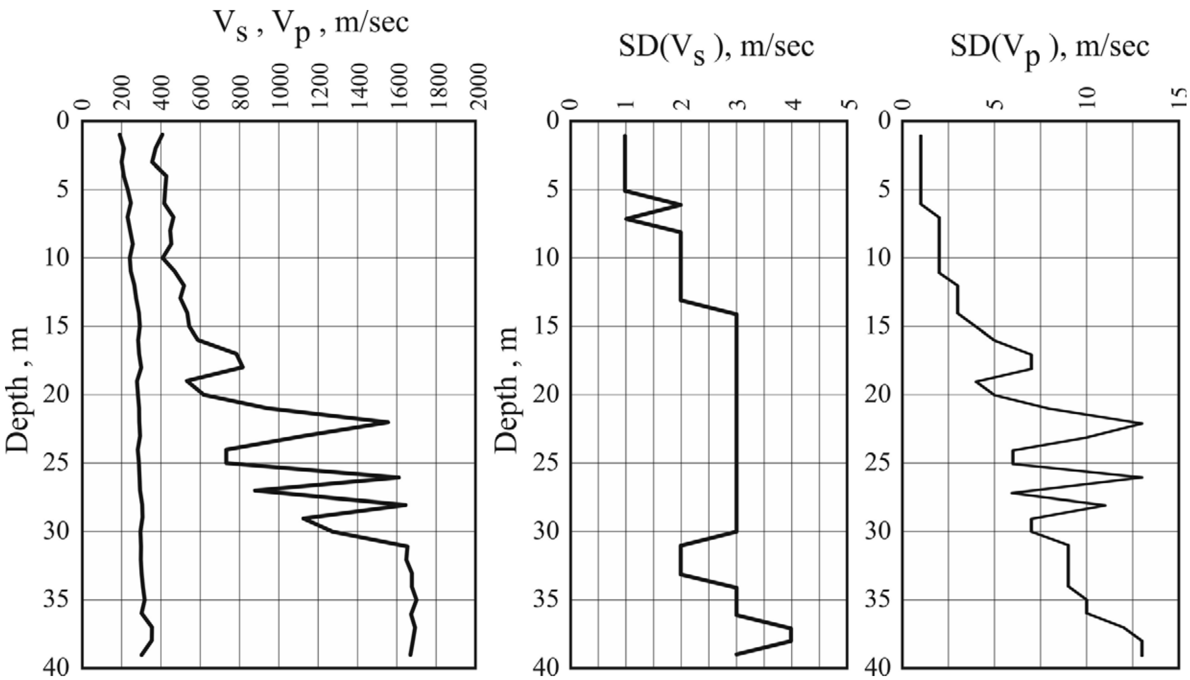

Figure 29 - Zelazny Most, North dam-CN 7-8, standard deviation of V_p and V_s after 10 measurement replications at 1 m intervals.

ery 1 m, computed from the data gathered after the tenfold replications of the waves propagation.

- Figure 30 exemplifies how the variables uncertainties, *travel time* and *travel distance*, individually considered, affect the standard deviation and covariance of the measured V_p.

Figure 30 highlights the important evidence that, at least in the examined case, the uncertainty linked to the variable *travel distance* has a more significant impact than the *travel time* on the measured seismic waves velocity in CH tests reliability.

Thanks to its solid theoretical background, the formula by Foti *et al.* (2002) allows assessing e_0 and n_0 with the consistency most demanding engineering applications require, remarking that the hardware and software employed in CH and DH tests will be improved.

This work by Foti *et al.* (2002), offers a valid opportunity to estimate the porosity and the void ratio *in situ* of fully saturated soils from seismic body waves velocity measured in the field. However, when using this formula, which is yet to be validated, the following points should be considered:

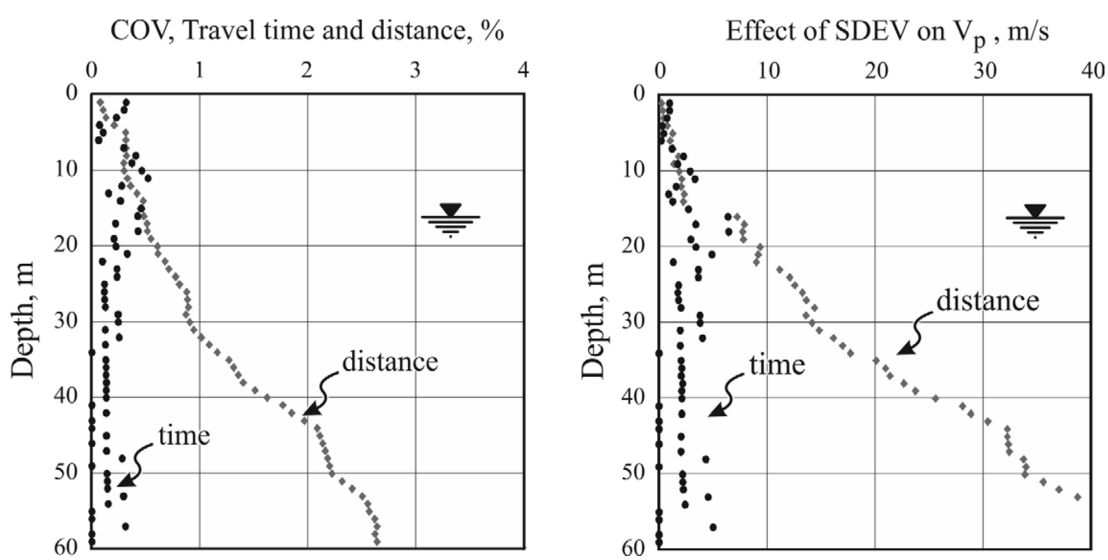

Figure 30 - Zelazny Most, P-waves arrival time and travel distance – Uncertainties involved.

- Dealing with the solution of an inverse problem, the computed value of porosity or void ratio is significantly affected by the accuracy and reliability of the measured seismic waves velocity. The above is especially relevant as regard the compression wave [Foti (2003)].
- However, the above issue, crucial when dealing with liquefaction and flow failure problems, becomes less significant in other engineering applications for which Foti *et al.* (2002) procedure, represents a step forward compared with the empirical correlations reliability between D_R and penetration tests results, used in common practice.
- A properly arranged and interpreted CH test is the most suitable mean to obtain independent, accurate V_p and V_s measurements to be used as input in the Foti *et al.* (2002) formula.
- As to Poisson coefficient ν_0 to be adopted when computing the porosity or the void ratio from V_p and V_s, it should be considered that the strains associated with the propagation of seismic waves is of the order of 10^{-6} at the best up 10^{-5}. At this strain level, the results of the large data base collected from the drained triaxial and plain strain tests with internal strains measurement, suggest values of ν_0 in the range between 0.15 and 0.25.
- The porosity and the void ratio computed using Foti *et al.* (2002) procedure, can be further enhanced if the uncertainties involved in assessing the picking arrival time and travel distance of V_p and V_s are accounted for.

6. Susceptibility of Coarse Grained Soils to Liquefaction

Since the pioneering work by Andrus & Stokoe (2000), the empirical approach to assess the susceptibility of sandy soils to cyclic liquefaction, based on the V_s measured in field, has been used in parallel with more conventional methods based on penetration tests results (SPT, CPTU, DMT). Figure 31 shows the correlation of V_{s1} *vs.* the cyclic stress ratio (CSR) valid for an earthquake of $M_W = 7.5$ magnitude based on the analysis of the collected case records at locations where the cyclic liquefaction has been observed.

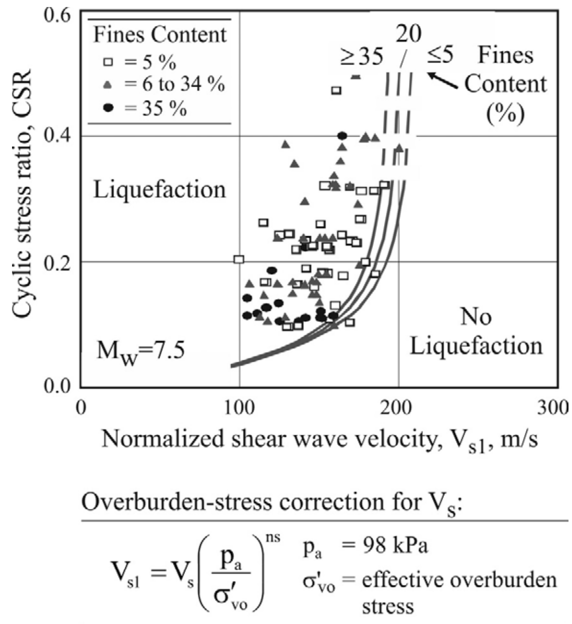

Figure 31 - V_s-based liquefaction susceptibility, Andrus & Stokoe (2000).

A comprehensive discussion and enhancement of the V_s procedure to estimate to what extent the coarse grained soil deposit is prone to liquefaction can be found in the book by Idriss & Boulanger (2008), who, in their discussion, raise the issue, already pointed out by Liu & Mitchell (2006), that V_s exhibits a lower sensitivity to variation of D_R *in situ* if compared to penetration tests.

The writer, referring to a large data base of more than 650 CPT DMT and seismic tests carried out in CC's on a variety of pluvially deposited dry sands, has attempted to explore the V_{s1} response to D_R changes as compared to those

Table 6 - V_s-sensitivity to D_R changes.

Calcareous oolithic Kenya sand				Siliceous Ticino sand			
D_R	p' (kPa)	V_s (m/s)		D_R	p' (kPa)	V_s (m/s)	
35%	100	175	$C_s = 238$	41%	100	119	$C_s = 90$
	200	212	$n_s = 0.27$		200	141	$n_s = 0.235$
	300	237	$d = 1.30$		300	155	$d = 1.30$
88%	100	230	$C_s = 275$	88%	100	191	$C_s = 110$
	200	278	$n_s = 0.25$		200	226	$n_s = 0.236$
	300	310	$d = 1.30$		300	247	$d = 1.30$
$V_s(D_R = 88\%)/ V_s(D_R = 35\%) = 1.31$				$V_s(D_R = 88\%)/ V_s(D_R = 41\%) = 1.60$			

$$V_s = C_s \left(\frac{p'}{p_a}\right)^{ns} \cdot \sqrt{F(e)} \qquad F(e) = e^{-d}$$

Table 7 - CPT and DMT sensitivity to D_R changes.

	CPT			DMT	
D_R	p' (kPa)	q_c (m/s)	D_R	p' (kPa)	K_D (-)
30%	100	6.0	30%	100	1.77
	200	8.3		200	1.57
	300	10.0		300	1.45
60%	100	14.3	60%	100	3.52
	200	20.0		200	3.10
	300	24.0		300	2.89
$\frac{q_c(D_R = 60\%)}{q_c(D_R = 30\%)} = 2.4$			$\frac{K_D(D_R = 60\%)}{K_D(D_R = 30\%)} = 2.0$		

of CPT cone resistance q_c and of the Marchetti's DMT lateral stress index K_D. The results for the crushable calcareous oolithic Kenya sand [Fioravante (2001)] and for the siliceous Ticino river sand [Bellotti *et al.* (1996), Jamiolkowski *et al.* (2001)] are shown in Tables 6 and 7.

Comparing the results reported in Table 6 with those in Table 7 it can be confirmed the minor sensitivity of V_{s1} to D_R changes with respect to those of q_c and K_D. It is worthy to recall the readers' attention, that this difference is even more pronounced if the different range of D_R considered in the compilation of Tables 6 and 7 is accounted for. The brief mention to V_s used to assess the susceptibility of sandy soils to cyclic liquefaction allows the following comments:

The CC tests results on two dry sands confirm the lower capability of shear waves to respond to D_R changes if compared to the CPT-q_c and the DMT-K_D. This happens despite V_s, similarly to q_c and K_D, is function of *in situ* void ratio and effective stresses. Moreover, differently from all the penetration tests, since V_s measurements are less invasive than penetration tests, are more prone to be affected by some depositional and post-depositional phenomena as aging, cementation and cyclic pre-straining.

In the light of the above, the use of V_s should continue to evaluate the liquefaction potential, although subject to further laboratory and field validations. The current state of such method development offers the advantage of an easy application in gravelly soils where the feasibility and reliability of the approaches based on penetration tests, in many circumstances, appear questionable.

References

Andrus, R.D. & Stokoe, K.H. (2000) Liquefaction resistance of soils from shear-wave velocity. J. Geotechnical & Geoenvironmental Eng., ASCE, v. 126:11, p. 1015-1025.

Arroyo, M. & Greening, P.D. (2002) Phase and amplitude responses associated with the measurement of shear-wave velocity in sand by bender elements: Discussion. Canadian Geotechnical J., v. 39:2, p. 483-484.

Arroyo, M.; Ferreira C. & Sukolrat J. (2007) Dynamic measurements and porosity in saturated triaxial specimens. Ling, H.I.; Callisto, L.; Leshchinsky, D. & Koseki, J. (eds) Soil Stress-Strain Behavior: Measurement Modeling and Analysis. Springer, A.A. Dordrecht, The Netherland, p. 537-546.

ASTM (2008) D2845-08 Standard Test Method for Laboratory Determination of Pulse Velocities and Ultrasonic Elastic Constants of Rock, Conshohochen, PA, USA, 14 pp.

Bellotti, R.; Jamiolkowski, M.; Lo Presti, D.C.F. & O'Neill, D.A. (1996) Anisotropy of small strain stiffness in Ticino sand. Gèotechnique, v. 46:1, p. 115-131.

Biot, M.A. (1956) Theory of propagation of elastic waves in a fluid-saturated porous solid. Part 1. Low frequency range. The Journal of the Acoustical Society of America, v. 28:2, p. 168-178.

Brignoli, *e.g.*M.; Fretti, C.; Jamiolkowski, M.; Pedroni, S. & Stokoe, K.H. (1996) Stiffness of gravelly soils to small strains. Proc. XIV Int. Conf. on Soil Mechanics and Foundation Engineering, Hamburg, v.1, pp. 37-40.

Chandler, R.J.; Jamiolkowski, M.; Faiella, D.; Ridley, A.M. & Rocchi, G. (2011) Suction measurements on undisturbed samples of heavily overconsolidated clays. Proc. XXIV Convegno Nazionale di Geotecnica, Napoli, v. 1, pp. 361-374.

Cox, B.R. (2006), Development of a Direct Test Method for Dynamically Assessing the Liquefaction Resistance of Soils *In Situ*. PhD Dissertation, Texas University, Austin.

Cubrinovski, M. & Ishihara, K. (1999) Empirical correlation between SPT N-value and relative density for sandy soils. Soils and Foundations, v. 39:5, p. 61-71.

De Groot, D.J.; Lunne T. & Tjelta T.J. (2011) Recommended best practice for geotechnical site characterisation of cohesive offshore sediments. Gourvenec & White, (eds) Frontiers in offshore Geotechnics II. Perth Western Australia. Taylor and Francis Group, London, pp. 33-57.

Darendelli, M.B. (1991) Development of a new family of normalized modulus reduction and material damping curves. PhD Dissertation, University of Texas, Austin.

Dobry, R.; Ladd, R.S.; Yokel, F.Y.; Chung, R.M. & Powell, D. (1982) Prediction of pore water pressure buildup and liquefaction of sands during earthquakes. Building Science Series 138, National Bureau of Standards, U.S. Dept of Commerce, Washington, D.C., 168 pp.

Fioravante, V. (2000) Anisotropy of small strain stiffness of Ticino and Kenya sand from seismic wave propagation measured in triaxial testing. Soils and Foundations, v. 40:4, p. 129-142.

Fioravante, V.; Giretti, D.; Jamiolkowski, M. & Rocchi, G.F. (2012) Triaxial tests on undisturbed samples of gravelly soils from the Sicilian shore of Messina strait. Accepted for publication in the Bulletin of Earthquake Engineering.

Foti, S.; Lai, C.G. & Lancellotta, R. (2002) Porosity of fluid-saturated porous media from measured seismic wave velocities. Gèotechnique, v. 52:5, p. 359-373.

Foti, S (2003) Personal communication.

Foti, S. & Lancellotta, R. (2004) Soil porosity from seismic velocities. Technical note. Gèotechnique, v. 54:8, p. 551-554.

Giretti, D.; Fioravante, V.; Jamiolkowski, M.; & Lopresti, D.C.F. (2012) Elastic stiffness anisotropy of Kenya carbonatic sand. Paper in preparation.

Grozic, J.L.H.; Robertson, P.K. & Morgenstern, N.R. (1999) The behavior of loose gassy sand. Canadian Geotechnical J., v. 36:3, p. 482-492.

Grozic, J.L.H.; Robertson, P.K. & Morgenstern, N.R. (2000) Cyclic liquefaction of loose gassy sand. Canadian Geotechnical J., v. 37:4, p. 843-856.

Hight, D.W. & Leroueil, S. (2003) Characterization of soils for engineering purposes. Proc. Int. Workshop on Characterisation & Engineering Properties of Natural Soils, Balkema, Singapore, p. 255-360.

Hofmann, B.A. (1997) *In situ* ground freezing to obtain undisturbed samples of loose sand for liquefaction assessment. PhD Dissertation, University of Alberta.

Hoque, H. (1996) Elastic deformation of sands in triaxial tests. Doctor of Engineering Dissertation, The University of Tokyo.

Hoque, E. & Tatsuoka, F. (1998) Anisotropy in the elastic deformation of material. Soils and Foundations, v. 38:1, p. 163-179.

Huang, A.B.; Tai, Y.Y.; Lee, W.F. & Ishihara, K. (2008) Sampling and field characterization of the silty sand in Central and Southern Taiwan. Proc. 3rd International Conference on Geotecnical and Geophysical Site Characterization, Taipei, Taylor & Francis Group, London, pp. 1457-1463.

Idriss, I.M. & Boulanger, R.W. (2008) Soil liquefaction during earthquakes. Earthquake Engineering Research Institute, MNO-12, Oakland.

Ishihara, K. (1996) Soil Behaviour in Earthquake Geotechnics. Clarendon Press, Oxford, UK, 350 pp.

Ishihara, K.; Huang, Y. & Tsuchiya, H. (1998) Liquefaction Resistance of Nearly Saturated Sand as Correlated with Longitudinal Wave Velocity in Poromechanics: A Tribute to Maurice A. Biot. Balkema, Rotterdam, The Netherland, p. 583-586.

Ishihara, K.; Tsukamoto, Y. & Kamada, K. (2004) Undrained behaviour of near-saturated sand in cyclic and monotonic loading. Proc. International Conference on Cyclic Behaviour of Soils and Liquefaction Phenomena, Bochum, p. 27-40.

Jardine, R.J. (1992) Some observations on the kinematic nature of soil stiffness. Soils and Foundations, v. 32:2, p. 111-124.

Jamiolkowski, M.; Lo Presti, D.C.F. & Manassero, M. (2001) Evaluation of relative density and shear strength of sands from CPT and DMT Soil Behaviour and soft ground construction. ASCE GSP no. 119, p. 201-238.

Jamiolkowski, M.; Ricceri, G. & Simonini, P. (2009) Great Project Lectures: Safeguarding Venice from high tides: site characterization & geotechnical problems. Proc. XVII ICSMGE, Alexandria, v. 4, p. 3209-3227.

Jamiolkowski, M.; Carrier, W.D.; Chandler, R.J.; Hoeg, K.; Swierczynski, W. & Wolski, W. (2010) The geotechnical problems of the second world largest copper tailings pond at Zelazny Most, Poland. Dr. Za-Chieh Moh Distinguished Lecture. Keynote Speech I, VII Southeast Asian Geotechnical Conf. Taipei, v. 2, pp. 12-27.

Jovicic, V.; Coop, M.R. & Simic, M. (1996) Objective criteria for determining G_(max) from bender element tests. Geotechnique, v. 46:2, p. 357-362.

Kokusho, T. (2000) Correlation of pore-pressure B-value with P-wave velocity and Poisson's ratio for imperfectly saturated sand or gravel. Soils and Foundations, v. 40:4, p. 95-102.

Kuwano, R. & Jardine, R. (2002) On the applicability of cross-anisotropic elasticity to granular materials at very small strains. Gèotechnique, v. 52:10, p. 727-749.

Lai, C.G. & Crempien de la Carrera, J.G.F. (2012) Stable inversion of measured V_p and V_s to estimate porosity in fluid-saturated soils. Gèotechnique, v. 62:4, p. 359-364.

Landon, M.M.; DeGroot, D.J. & Sheahan, T.C. (2007) Nondestructive sample quality assessment of a soft clay using shear wave velocity J. Geotechnical & Geoenvironmental Eng., ASCE, v. 133:4, p. 424-432.

Lee, N.K.J. (1993) Experimental Study of Body Wave Velocities in Sand Under Anisotropic Conditions. PhD Thesis, University of Texas, Austin.

Lee, S.H. (1985) Investigation of Low-Amplitude Shear Wave Velocity in Anisotropic Material. PhD Thesis, University of Texas, Austin.

Lee, S.H. & Stokoe K.H. (1986) Investigation of low-amplitude shear wave velocity in anisotropic material. Report GR 86-6. University of Texas, Austin.

Lee, S.J.; Cho, G.C. & Santamarina, J.C. (2005) Liquefaction: strength and wave based monitoring. First Japan-US Workshop on Testing Modeling and Simulation in Geomechanics. Boston, 2003, ASCE GSP no. 143, p. 463-474.

Lewis, M.D. (1990) A Laboratory Study of the Effect of Stress State on the Elastic Moduli of Sand. PhD Thesis, University of Texas, Austin.

Liu, N. & Mitchell, J.K. (2006) Influence of non plastic fines on shear wave velocity-based assessment of liquefaction. J. Geotechnical & Geoenvironmental Eng., ASCE, v. 132:8, p. 1091-1097.

Lo Presti, D.C.F. & O'Neill, D.A. (1991) Laboratory investigation on small strain modulus anisotropy in sand. Proc. First International Symposium on Calibration Chamber, ISOCCT1 Potsdam, p. 213-224.

Lo Presti, D.C.F. (1991) Discussion on threshold strain in Soil. Proc. X European Conference on Soil Mechanics and Foundation Engineering, Firenze, v. 4, p. 1282-1283.

Lo Presti, D.C.F. (1991a) Discussion on behaviour of sand at small strain. Proc. X European Conference on Soil

Mechanics and Foundation Engineering, Firenze, v. 4, p. 1229-1230.
Love, A.E.H. (1927) A Treatise on the Mathematical Theory of Elasticity. Cambridge University Press, Cambridge (reprinted by Dover Publication Inc. 1944).
Lunne, T.; Berre, T. & Strandvik, S. (1997) Sample disturbance effects in soft low plastic Norwegian clay. Proc. International Symposium on Recent Developments in Soil and Pavement Mechanics, Rio de Janeiro, p. 81-102.
Lunne, T.; Berre,T.; Andersen, K.H.; Strandvik, S. & Sjursen, M. (2006) Effects of sample disturbance and consolidation procedures on measured shear strength of soft marine Norwegian clays. Canadian Geotechnical J, v. 43:7, p. 726-750.
Menq, F.Y. (2003) Dynamic Properties of Sandy and Gravelly Soils. PhD Dissertation, The University of Texas, Austin.
Maqbooll, S.; Koseki, J. & Sato, T.(2004) Effect of compaction on small strain Young's moduli of gravel by dynamic and static measurements. Bulletin of Earthquake Resistant Structure, Research Centre no. 37, p. 41-50.
Nakazawa, H.; Ishihara, K.; Tsukamoto, Y. & Kamata, T. (2004) Case studies of liquefaction of imperfectly saturated soil deposits. Proc. International Conference on Cyclic Behaviour of Soils and Liquefaction Phenomena, Bochum, p. 295-304.
Pennington, D.S.; Nash, D.F.T. & Lings, M.L. (2001) Horizontally mounted bender elements for measuring anisotropic shear moduli in triaxial clay specimens. ASTM Geotechnical Testing J, v. 24:2, p. 133-144.
Rahtje, E.M.; Chang, W.J.; Stokoe, K.H. & Cox, B.R. (2004) Evaluation of ground strain from *in situ* dynamic testing. 13th World Conf. on Earthquake Engng., Vancouver, paper 3099, 15 p.
Ridley, A.M. & Burland, J.B. (1993) A new instrument for the measurements of soil moisture suction. Gèotechnique, v. 43:2, p. 321-324.
Roesler, S.K. (1979) Anisotropic shear modulus due to stress anisotropy. J. Geotechnical Eng., ASCE, v. 105:GT7, p. 871-880.
Sanchez-Salinero, I.; Roesset, J. & Stokoe, K.H. (1986) Analytical studies of body wave propagation and attenuation. Geotechnical Engineering Report GR86-15, University of Texas, Austin, 348 pp.
Sasitharan, S.; Robertson, P.K. & Sego, D.C. (1994) Sample disturbance from shear wave velocity measurements. Canadian Geotechnical J., v. 31:1, p. 119-124.
Schmertmann, J.H. (1978) Guidelines for Cone Penetration Test Performance and Design. US Dept of Transportation, FHWA, R78-209, Washington, D.C. USA, p. 151.
Skempton, A.W. (1954). The pore pressure coefficients A and B. Geotechnique, v. 4:4, p. 143-147.
Skempton, A.W. (1961) Horizontal stresses in an overconsolidated Eucene clay. Proc. V Int. Conf. on Soil Mechanics and Foundation Engineering, Paris, v. 1, pp. 351-357.
Skempton, AW. (1986) Standard penetration tests procedures and the effects in sands of overburden pressure, relative density, particle size, ageing and overconsolidation. Gèotechnique, v. 36:3, p. 425-447.
Stokoe, K.H.; Lee, J.N.K. & Lee, S.H.H. (1991) Characterization of soil in calibration chambers with seismic waves. Proc. First International Symposium on Calibration Chamber, ISOCCT1, Potsdam, p. 363-376.
Stokoe, K.H. II (2011) Seismic measurements and geotechnical engineering. 47th Terzaghi Distinguished Lecture, presented at Geo-Frontiers 2011, Geo-Institute National Meeting, ASCE, Dallas, March 15, 2011 to be published.
Takahashi, H.; Katazume, M.; Ishibashi, S. & Yamawaki, S. (2006) Evaluating the saturation of model ground by P-wave velocity and modelling of models for a liquefaction study. International Journal of Physical Modelling in Geotechnics, v. 6:1, p. 13-25.
Tsukamoto, Y.; Ishihara, K.; Nakazawa, H.; Kamada, K. & Huang, Y. (2001) Resistance of partly saturated sand to liquefaction with reference to longitudinal and shear wave velocities. Soils and Foundations, v. 42:6, p. 93-104.
Valle Molina, C. (2006) Measurements of V_p and V_s in Dry, Unsaturated and Saturated Sand Specimens with Piezoelectric Transducers. PhD Dissertation, University of Texas, Austin.
Valle Molina, C. & Stokoe, K.H. (2012) Seismic measurements in sand specimens with varying degrees of saturation using piezoelectric transducers. Canadian Geotechnical J., v. 49:6, p. 671-685.
Viggiani, G. & Atkinson, J.H. (1995) Stiffness of fine-grained soil at very small strains. Gèotechnique, v. 45:2, p. 249-265.
Vucetic, M. (1994) Cyclic threshold shear stains in soils. Journal of Geotechnical Engineering, ASCE, v. 120:12, p. 2208-2228.
Yoshimi, Y.; Hatanaka, M. & Oh-Oka, H. (1978) Undisturbed sampling of saturated sands by freezing. Soils and Foundations, v. 18:3, p. 59-73.
Yoshimi, Y. (2000) A Frozen Sample of Sand That Did Not Melt, Proc. of GEOTECH – YEAR 2000. Developments in Geotechnical Engineering. Balasubramaniam, A.S. & Bergado, D.T. (eds) Asian Institute of Technology, Bangkok, v. 1. pp. 293-295.
Weston, T.R. (1996) Effects of Grain Size and Particle Distribution on the Stiffness and Damping of Granular Soils at Small Strains. MS Thesis, University of Texas, Austin.
White, J.E. (1965) Seismic Waves: Radiation, Transmission and Attenuation. McGraw-Hill Book Company, New York.

Articles

Formation of Fine Iron Ore Tailings Deposits

L.M.K. Lima, W.L. Oliveira Filho

Abstract. Deposit formation back analysis of a two-year iron ore slime impoundment managed by the sub-aerial method is performed using two complementary approaches. The first one tries to identify the deposit stratigraphy and its formation history. This is made possible through sorted document review (reports, design documents, personal communication, photos, etc.) and by means of an extensive geotechnical investigation program, including laboratory and field testing. The second approach, considered more quantitative, deals with modeling the sub-aerial deposition method, using a numerical solution for events such as large strain consolidation and desiccation of fine, soft tailings, following filling and waiting periods, according to that disposal technique. For modeling, the computer program CONDES is used with constitutive functions of available material, also using actual slime management data. The numerical model rendered a final deposit height of 8.16 m, very close to the actual height measured in the field, providing the model validation. The analyses suggest that the desiccation process inherent to the sub-aerial method had a minimal effect or did not even occur during the impoundment operation. Other potential disposal schemes were also evaluated and comparisons were made. The study has shown the ability to understand the formation of fine iron ore mining tailing deposits, and how to make use of this tool in projects.
Keywords: fine tailings deposit, back analysis, sub-aerial method, tailings disposal, field investigation, numerical modeling.

1. Introduction

Mining industry is booming these days and in consequence an increasing amount of mine tailings has been generated, requiring increasing containment areas for disposal, since tailings are usually discarded as fluid pulp. Tailings placement depends on its grading. Coarse material is usually disposed close to the containment structure where it can be used as construction material for raising of dikes and dams, and also to function as their foundation. On the other hand, fine tailings are disposed upstream the impoundment, forming a decantation lake and generating a soft, compressible, low density deposit with poor bearing capacity.

Although man-made, fine tailing deposits present a similar behavior to the natural stratus of soft soils, showing, for example, high compressibility and low hydraulic conductivity. This fact potentially allows that the general knowledge of soft soil engineering properties and performance, accumulated over the years by geotechnical engineers, could be used to understand how fine tailings deposits work.

According to Massad (2003), soft soils are sedimentary soils with low shear strength (SPT indices not higher than 4). The clay fraction makes these soils cohesive and very compressible. The behavior of these soils depends, among other things, on the water content, the stress state and mineral characteristics. Additionally, the clay fraction also plays an important role in the characteristics and properties of soft soils, such as compressibility, permeability and shear strength.

The engineering properties of fine tailings are important for settlement analyses and bearing capacity calculations of the deposits. In dredging materials and in soft mine tailings (slimes), large deformations are expected, requiring more sophisticated analyses, such as the ones that use large strain consolidation theories. On the other hand, slope stability analyses are usually performed in terms of total stresses or undrained conditions.

In this paper, different strategies to study the formation of fine iron ore tailings deposits aiming at storage planning and as a foundation substrate for surface rehabilitation (closure) and temporary structures are discussed.

2. Background

2.1. Physical processes and disposal methods

Tailings are commonly produced as fluid pulp, which is transported through channels or pipes and disposed in confined areas (Vick, 1983). During disposal, fine tailings may experience several physical processes: sedimentation, consolidation, desiccation, and desaturation. Sedimentation is relatively fast, and volume change depends on the initial solid content of the pulp. In the consolidation and desiccation phases, significant but deferred settlements of the deposited material may occur. The desiccation phase is divided in two distinct steps: one-dimensional desiccation and three-dimensional desiccation. In the three-dimensional phase, crack opening and propagation occur. Finally, if tailings still lose water, without volume change, the material starts to desaturate. Figure 1 shows the sequence of

Luciana de Morais Kelly Lima, MSc, Pimenta de Ávila Consultoria, Belo Horizonte, MG, Brazil, e-mail: luciana.lima@pimentadeavila.com.br.
Waldyr Lopes de Oliveira Filho, PhD, Associate Professor, Departamento de Engenharia de Minas, Universidade Federal de Ouro Preto, Ouro Preto, MG, Brazil, e-mail: waldyr@em.ufop.br.
Submitted on April 4, 2008; Final Acceptance on August 6, 2012; Discussion open until December 29, 2012.

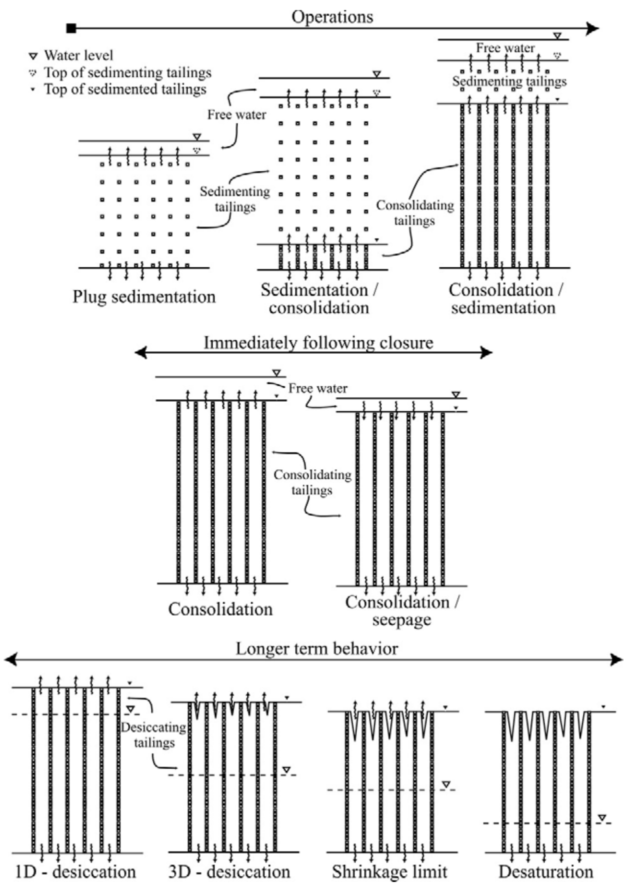

Figure 1 - Physical processes experienced by tailings during and after operational impoundment life-time. (Oliveira-Filho & van Zyl, 2006a).

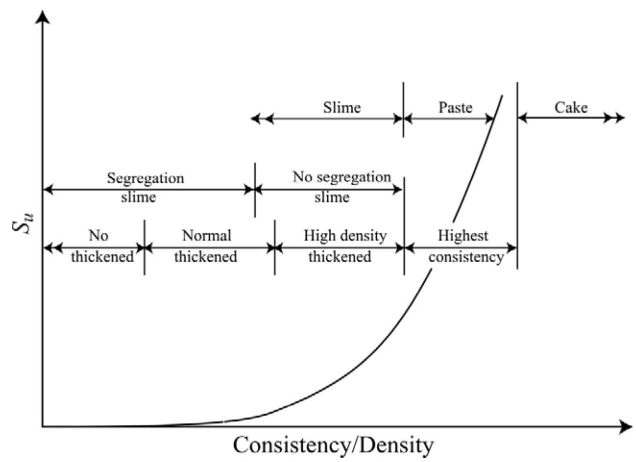

Figure 2 - Shear strength slime versus consistency (ICOLD, 2002).

these phenomena. Almeida (2004) and also Oliveira-Filho & van Zyl (2006a) present a detailed description of all these physical processes.

Alternatively, other tailings disposal schemes have been devised for fine tailings, leading to initial solid content higher than when disposed in the conventional way (Norman & Raforth, 1998; Ulrich *et al.*, 2000). The alternative methods, from lower to higher initial density at the time of disposal, are: sub-aerial disposal, thickened tailings (TTD), and paste. A common characteristic of these alternative methods is their intermittent character of disposal with alternating cycles of filling and waiting periods (no disposal). Figure 2 shows the initial gain in shear strength resulted from the different disposal techniques.

Development of alternative methods of tailings disposal has been mainly related to the search of tailings facilities with: reduced risk and liability, easier permitting in difficult regulatory environments, improved water recovery, faster area rehabilitation, and expanded storage of higher volumes in smaller areas. However, the alternative methods have a relatively higher cost when compared to the conventional methods. Table 1 compares the alternative methods according to important design features.

As it can be seen in Table 1, one or other option will be more cost-effective depending on which aspects are considered more relevant in a particular project.

2.2. Modeling

Fine tailings deposit materials are constituted of silts and/or clays. Depending on their grading, the deposit behavior is a function of these material engineering properties, such as compressibility, hydraulic conductivity and

Table 1 - Comparison of the alternative fine tailings disposal methods.

	Sub-aerial	TTD	Paste
Final density	Intermediate – High	Intermediate – High	High
Segregation	High – Intermediate	Low	None
Superficial water	High – Some	Some – None	None
Rehabilitation	After some time	Almost immediate	Immediate
Permeability	High – Low	Low	Very low
Application	On the surface	On the surface	On the surface and underground
Water consumption	High – Intermediate	Intermediate	Low
Cost	Intermediate – High	High	High

shear strength. Additionally, the disposal method could impair certain degree of heterogeneity to the tailings deposit which may also affect its behavior. Thus, modeling deposit formation is a task that requires caution, experience and clear hypotheses, and scope.

To model discharge of interstitial water in tailing impoundments, Oliveira-Filho & van Zyl (2006a, 2006b) use the computer code CONDES (Yao *et al.*, 2002; Almeida *et al.*, 2005), which models large strain consolidation and desiccation processes. These are two of the main physical processes experienced by tailings upon deposition, regardless the disposal scheme (conventional or alternative). For consolidation analyses, using CONDES, compressibility and permeability relations are expressed, respectively, by

$$e = A(\sigma' + Z)^B \tag{1}$$

$$k = Ce^D \tag{2}$$

where e is the void ratio, k is the saturated hydraulic conductivity, A, B, C, D and Z the model parameters.

Regarding desiccation analyses, additional material functions have to be provided to CONDES, including compressibility and permeability relations, similar to Eqs. 1 and 2, and other functions related to cracking initiation and propagation, and cracking geometry (Abu-Hejleh & Znidarcic, 1996).

CONDES is also used by Oliveira-Filho & Lima (2006) to model the construction of homogeneous, clayey deposits built using the sub-aerial method. In the proposed sub-aerial disposal scheme, cycles of filling and waiting are simulated, modeling physical processes such as consolidation and desiccation. In their analyses, Oliveira-Filho & Lima (2006) do not consider cracking formation, because this is a secondary factor if the focus is on volume change. In addition, one-dimensional desiccation is treated as an extension of the consolidation analyses, using the same compressibility and permeability relations. The main results of the sub-aerial simulation of a two-layer deposit are shown in Figs. 3 and 4. In Fig. 3, physical processes of volume reduction due to self-weight consolidation, as well as desiccation are presented. The former has two steps (filling and waiting stages) and the latter starts at a certain instant of the waiting period. In Fig. 4, the void ratio decrease at the top of the layer due to desiccation can be noted.

Using the same disposal scheme model, Oliveira-Filho & Lima (2006) expand the analyses, repeating the scheme eight times (eight complete cycles of filling and waiting stages or layers). Figure 5 shows the final void ratio profile for each complete cycle or layer.

As it can be seen in Fig. 5, desiccation on every intermediate layer is still noticeable (see void ratio reduction at the top of the layer), but decreasingly less effective. The consequence of this trend is that a lower overall volume reduction is achieved by the disposal scheme. To obtain a better performance in a tailings management, such as the sub-aerial, Oliveira-Filho & Lima (2006) suggest that the waiting cycle should be gradually increased.

2.3. Back analysis

Man-made fine tailings deposit characteristics and behavior depend on a series of factors, including disposal technique, filling history, material properties, climate, and foundation conditions. All these aspects yield changes in the slime initial consistency, according to the physical phenomena of consolidation and desiccation. The slime consistency modifications often lead to a gradual densification and strength development in the deposit. These changes can be monitored during deposit formation (operational life) (Konrad & Acad., 1997; Silva, 2003). Or, when the deposit

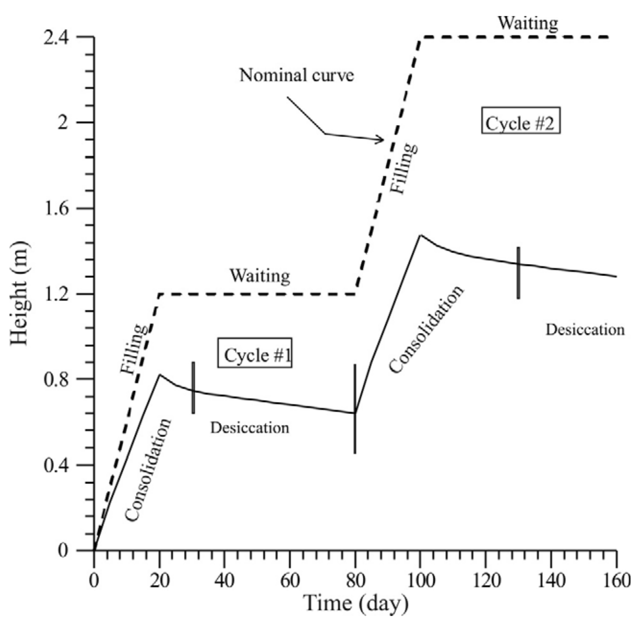

Figure 3 - Sequence of two sub-aerial modeling scheme cycles (nominal and simulation heights), where vertical bars delimit physical processes (Adapted from Oliveira-Filho & Lima, 2006).

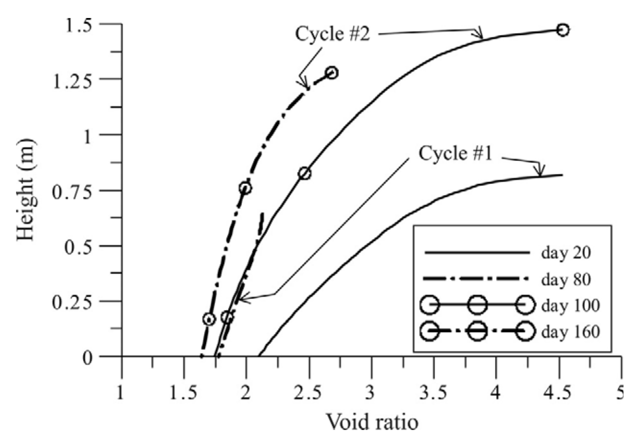

Figure 4 - Sub-aerial modeling results: void ratio profiles at the end of two subsequent filling or waiting cycles (Adapted from Oliveira-Filho & Lima, 2006).

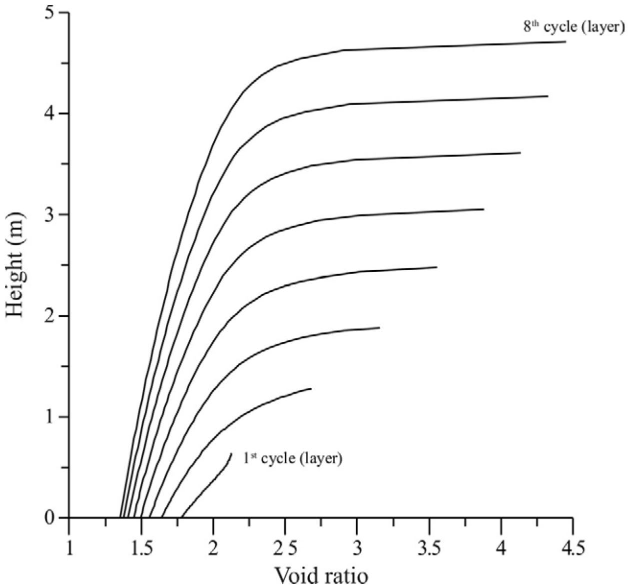

Figure 5 - Void ratio profile at the end of the waiting cycle for an eight-layer deposit (for clearness, filling cycles were omitted; adapted from Oliveira-Filho & Lima, 2006).

is already built, the changes can be assessed by means of a suitable model, combined with site investigations and laboratory tests, in an effort known as back analysis (Lima, 2006). In the first case, *i.e.*, during impoundment operations, monitoring of the slimes can be done by extensive instrumentation programs and sampling. In case of back analysis, experimental work that involves field and laboratory methods is required to determine the deposit stratigraphy and material geotechnical properties. This activity commonly involves geotechnical logging, sampling and also field and laboratory testing (Árabe, 1995; Schnaid, 2000; Oliveira, 2002; Massad, 2003; Spannenberg, 2003; Bedeschi, 2004; Albuquerque Filho, 2004; Mondelli, 2004; and Lima, 2006). Furthermore, in the case of back analysis, history and document researches regarding the deposit play an important role. These data provide information on discharge timeline, amount and kind of disposed material at the site. Certainly, validation of the back analyses should be sought by means of an objective function, which could include data such as actual deposit heights or/and void ratio profiles. With comprehensive information about the deposit, material properties and modeling, the deposit formation can be properly back analyzed. Moreover, the back analysis results could be used in a variety of projects, such as reclamation of closed disposal areas and construction of earthworks on these materials (Wels *et al.*, 1999).

3. Case Study

The previous section sets the basis of a case study presented as follows, where the back analysis of an iron ore slime deposit built by the sub-aerial method is examined. The case explores the engineering judgment to understand the result of a two-year impoundment operation, in order to safely design future temporary and permanent structures on that kind of support (deposit seen as a foundation). In addition, this study provides vital information for mass balance prognoses, supposing that the operation in that deposit would not change. The case study was addressed by developing a suitable model for deposit formation (as explained in item 2.2), combined with site investigations and laboratory tests, production history data, related document reviews, and information obtained from company's staff.

3.1. Deposit history

The slime deposit is located in the Germano dam impoundment that belongs to Samarco Mineração S.A., in the Quadrilátero Ferrífero (Iron Quadrangle), in Mariana, Minas Gerais. From the iron ore processing plant, two kinds of tailings were generated, a coarse (sandy) and a fine (slime).

The Germano tailings were disposed in a conventional way between 1976 and August/2003. Coarse tailings were disposed from the crest of the main dam, forming a beach. They also served as construction material (for raising dikes), after dewatering by gravitational drainage (upstream construction). On the other hand, the slimes were launched from the impoundment upstream, far from the dam crest, forming a sedimentation decant lake, without compromising the safety of the containment structure.

From September/2003, with the increasing of mineral production, and consequently of tailings, the company started a desiccation project for the slime tailings (Pimenta de Ávila Consultoria, 2001). This project aimed to create economic and environmental benefits, such as volume optimization and shortening of the reclamation period.

The desiccation project devised a system of five closed ponding areas (pads or bays). The slimes generated by milling processes were discarded in the padding system through a sole spigot and one structure at a time. This procedure guaranteed an intermittent filling of the slime material in the padding system, allowing drainage and surface drying intervals (waiting stage). Among the padding areas, padding area #4, (Bay 4) shown in Fig. 6, was selected for this case study as the most representative of the sub-aerial method (more regular filling and waiting cycles).

Formation of the deposit in padding area #4, using the sub-aerial method, took place between October/2003 and September/2005. However, the filling and waiting periods started to be recorded only in April/2004 as shown in Fig. 7 (Samarco, 2005).

According to field records (Fig. 7), it is apparent that there were no regular intervals of the filling and waiting phases. For example, in December/2004 and July/2005, no slimes were disposed in the pad area #4, whereas in June/2004, slimes were disposed during the whole month. Throughout the total period, field records indicated 210 days of filling and 333 days of resting.

Figure 6 - Padding area #4 in Germano Impoundment.

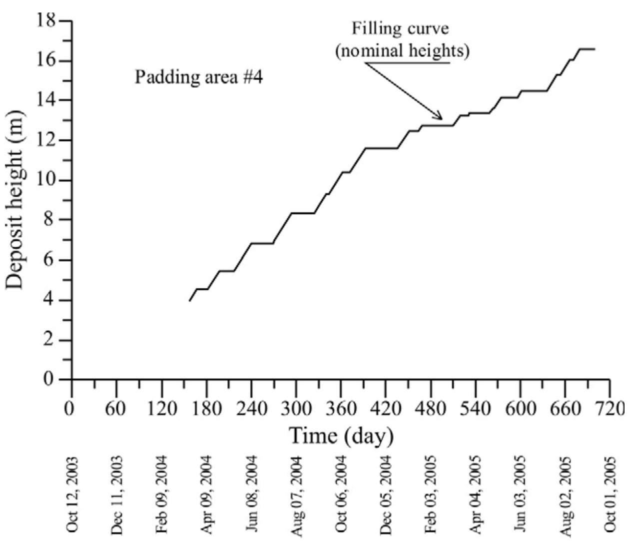

Figure 7 - Filling curve according to dredger records (April 2004 to September 2005).

3.2. Deposit stratigraphy

3.2.1. Investigation program

The investigation program for establishing the deposit stratigraphy consisted of field and laboratory activities. Field investigation took place in the vicinity of the padding area center (El. 905.00 m), and at the crest of the northeast containment wall (El. 907.50 m). Figure 6 shows the approximate investigation locations, represented by black dots.

Field exploration consisted of standard penetration tests (SPT), piezocone tests (CPTU) and undisturbed sampling, performed in phases, and in this order. Two SPT tests were performed for the preliminary evaluation of the deposit stratigraphy. In addition, two piezocone tests provided a better definition of the deposit stratigraphy and classification. Then, thirteen undisturbed samples collected from the deposit at different depths at the crest location allowed a texture calibration of piezocone results for that tailing management (Lima, 2006).

Laboratory tests were performed at the geotechnical laboratory of the Viçosa Federal University (Viçosa, 2006) with those thirteen undisturbed samples collected at the crest location (dike). This testing program was intended to obtain basic characterization of the material that underlies the dike. These characterization tests included construction material of the dike, dike material contaminated by the deposit material and, at depth, the deposit material itself.

3.2.2. SPT tests

SPT tests were performed by a local contractor, following the ABNT standards (Regulations: NBR 6484/2001 and NBR 7250/1982). Figure 8 shows the position of two SPT tests in a schematic cross section, one at the center of the impoundment and the other at the dike (crest).

The profile at the center of the impoundment presents low SPT indices (N_{SPT}) from surface down to 10 m depth (ranging from 0 to 4). These numbers indicate the existence of materials with low to medium shear strength. In general, clayey and silty soils with N_{SPT} lower than 5 are soft and compressible (Schnaid, 2000). Similar values are also typical of loose sands and sandy silts. These results can be extrapolated to the whole deposit layer assuming horizontal homogeneity of the deposited material. This hypothesis is possible since the material was disposed by hydraulic means, with relatively high solid content, and therefore with no possibility of segregation (Vick, 1983).

On the other hand, higher N_{SPT} values were observed in the first meters of the dike profile. These results can be explained by the presence of compacted sandy tailings used in the dike construction. The presence of this type of material at the site and the information that the end dump method was used for dike construction suggest that the dike stratigraphy consists of near surface material with high shear strength, probably the compacted sand tailings, then

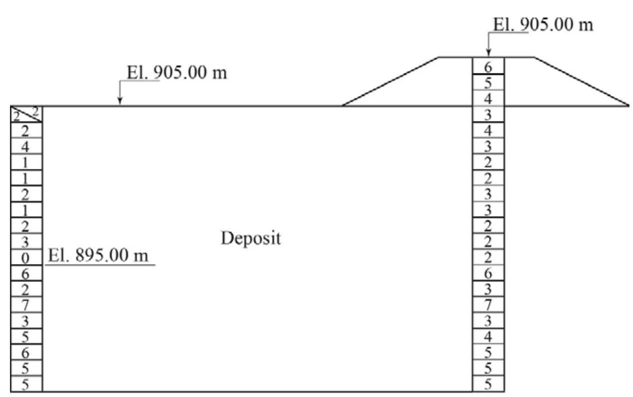

Figure 8 - Position of SPT tests in a schematic cross section, one at the central area and the other at the dike crest (numbers in boxes are N_{SPT}).

no-compacted sandy tailings that sunk displacing the deposit material and eventually mixing with it, and finally the deposit material.

In the two soundings, sampling was unsuccessful at several depths, mainly under the water table. Few samples collected through the SPT sampler allowed strata description as sandy or clayey silt material, deposited in thin layers (centimeter to decimeter thicknesses) as shown in Fig. 9.

3.2.3. Piezocone tests

The piezocone tests were performed, one at the center of the impoundment area and the other at the dike location. Piezocone testing followed MB 3406 (Soil – in situ Piezocone penetration) and ASTM 3441 (Standard test method for deep, quasi-static, cone and friction-cone penetration test of soil). Pore water pressure measurements were performed using a porous element made of bronze, positioned at the cone base (u_2 position).

The cone test results corresponding to the dike location served as basis for texture calibration of the material deposited at the padding area #4. Lima (2006) interpreted these CPTU results using well-known classification charts (Robertson & Campanella, 1983; Senneset *et al.*, 1989; Robertson, 1991). Lima (2006) compared these results with the basic characterization of the samples collected using Shelby samplers at the dike location. Then, Lima (2006) concluded that the better agreement was obtained using the classification by Senneset *et al.* (1989). This classification relates pore pressure coefficient, B_q, (Eq. 3) with corrected tip stress, q_T. In equation 3, u_2 represents the pore water pressure measured at the cone shoulder, u_0 the hydrostatic pressure and σ_{vo} the *in situ* total vertical stress.

$$B_q = \frac{u_2 - u_0}{q_T - \sigma_{V_0}} \quad (3)$$

Figure 9 - SPT sampler with material collected in the soundings: top – clayey silt, middle – clayey and sandy silt in sequence, bottom – sandy silt.

CPTU results at the center of the impoundment are shown in Fig. 10. The profile shows, in general, a soil with low values of corrected tip stress (q_T) and excess of dynamic pore water pressure (u_2). The presence of excess of dynamic pore water pressure is normally related to deposits with mainly fine texture and low hydraulic conductivity (Schnaid, 2000). The existence of these strata within the deposit can also be identified through pore water pressure coefficient (B_q) also shown in Fig. 10.

The interpreted stratigraphy of the deposit according to Senneset *et al.* (1989) is presented in Fig. 11. The inter-

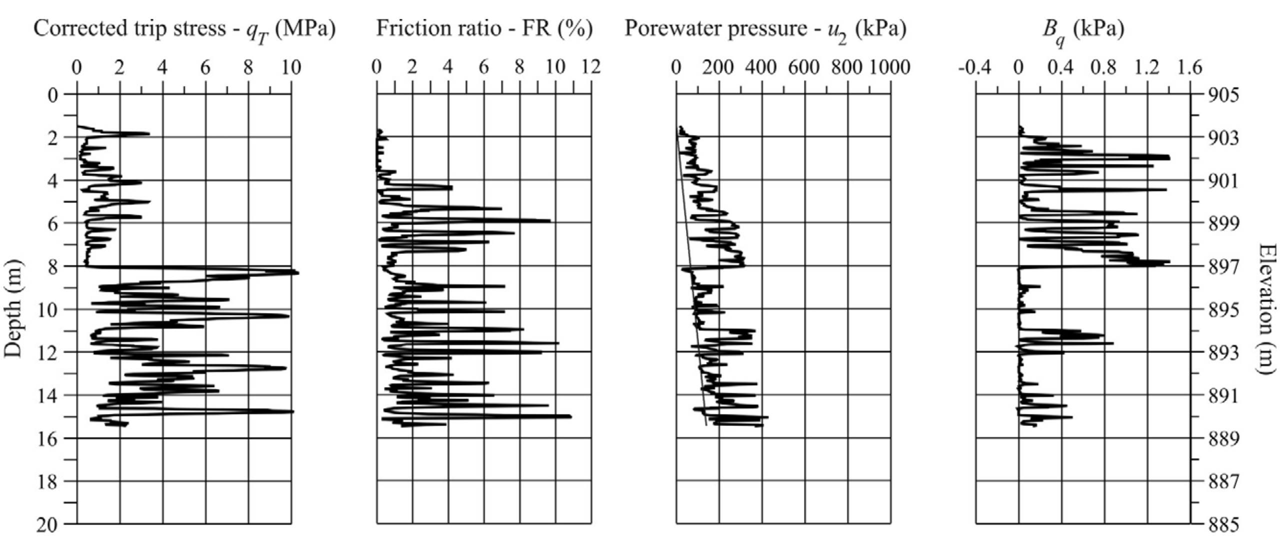

Figure 10 - Piezocone data.

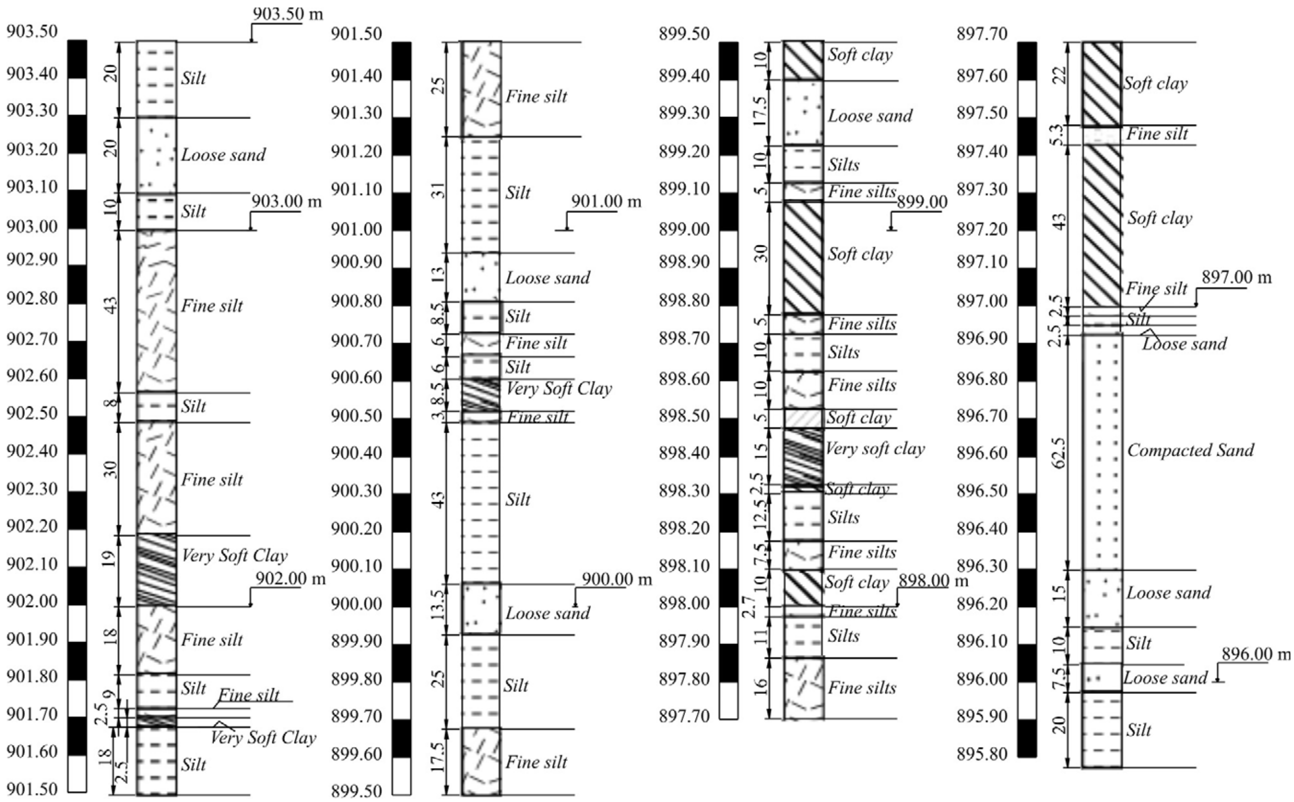

Figure 11 - Deposit stratigraphy interpreted from CPTU data according to Senneset *et al.* (1989).

preted deposit profile is heterogeneous, with uniform strata ranging from sand to soft clays, and layer thicknesses ranging from centimeters to decimeters. Below elevation 897 m there is a significant change in the stratigraphy, which may correspond to the top of the deposit soil foundation. According to the impoundment records, the deposit foundation also consisted of tailing material from previous tailing management in the Germano reservoir (see item 3.1). From this analysis it was concluded that the deposit depth at the center of the impoundment was approximately 8.0 m.

4. Discussion of the Deposit Formation

4.1. Qualitative model

As it appears in Fig. 11, material heterogeneity in the deposit is significant, showing that disposed materials were not only clayey silt slimes, as it was supposed in previous works (Pimenta de Avila Consultoria, 2001; Silva, 2003; Almeida, 2004). The texture sequence of the deposit materials reflects a typical pattern of hydraulic deposition and a particular mode of management. In that respect, the gradual change in the material texture ranging from sand to clay is apparent.

Regarding tailings management, data history indicate that the tailings deposit in padding area #4 originated from dredging operations on a decant pond also in the Germano impoundment. This decant pond served as residence for slimes (to increase solid content) before their relocation into the desiccation pads (item 3.1). Figure 12 shows a schematic diagram of the dredger operation, which typically started at slime level and continued in depth, finding different strata in a vertical profile. When moving the dredger, the operation was repeated, and a similar layering sequence was found. The dredged material was pumped

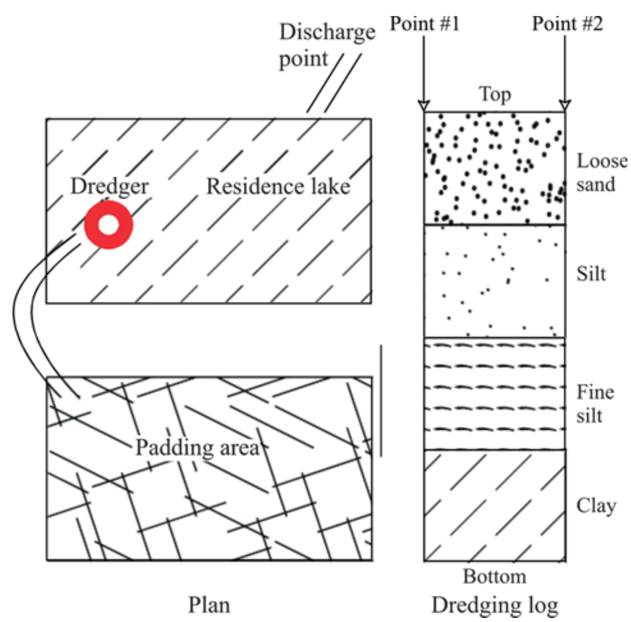

Figure 12 - Dredging operation scheme.

and disposed in the padding structures and the resultant profile had a reversed sequence of the one existing in the residence (decant) lake.

A good example of the above discussion is the profile shown in Fig. 11, between elevations 900.00 m and 899.00 m. In this profile the gradual change of material texture from sand to clay in two contiguous sequences is apparent.

4.2. Numerical model

4.2.1. Input and premises

Back analysis of the deposit formation was simulated using the CONDES software and the disposal scheme as explained in item 2.2 (modeling construction of homogeneous, clayey deposits built using the sub-aerial method) with all its premises and simplifications (*e.g.* no cracking formation). For numerical modeling purpose, it was decided not to use the actual filling curve (Fig. 7), but an averaged one with regular intervals of filling and waiting phases and the same final height of solids (H_s = 3.00 m) or total filling time (276 days). This modeling decision was made in order to simplify the model supposing that it should not affect the analysis. Thus, 23 time intervals of filling and waiting phases of 12 and 18 days, respectively, were adopted. The whole operation lasted 690 days. This last number was established according to the site records (Samarco, 2005) and personal inquiries with Samarco's staff (the extrapolation for the first days without records).

Concerning the deposit material, it was assumed to be homogenous at first approximation, despite this assumption was not supported by the deposit stratigraphy based on field investigations (Fig. 11). The reason for that is the inability of CONDES to model heterogeneous medium and also because similar constitutive relationships (especially compressibility) for all fine tailings which form that depositor an averaged response are expected. Thus, compressibility and permeability relationships for consolidation and desiccation analyses were the same as those obtained by Silva (2003) and Almeida (2004) and presented in Table 2. These authors performed experiments with slimes provided

Table 2 - Input data for analyses.

Input Data		
Constitutive properties	A (kPa^{-1})	2.5438
	B	-0.1920
	C (m/day)	9.45×10^{-5}
	D	4.2370
	Z (kPa)	0.0495
Unit weight of water (kN/m^3)		9.81
Specific gravity of solids		3.89
Minimum void ratio		1.05
Evaporation rate (m/day)		0.002

by Samarco, the former, a field test, and the latter, a series of hydraulic consolidation tests (HCT). Those experiments gave them confidence on the material properties. For this reason it is assumed that these material properties are adequate for the case study presented in this paper.

4.2.2. Analysis results

Modeling results are shown in Figs. 13 and 14 in terms of deposit height versus time and void ratio profile at different times, respectively. Figure 14 shows that the simulated final height of the deposit (H_f) reached 8.16 m after 690 days, which is very close to the measured height in the field (8,0 m, item 3.2.3). This fact can be used to validate the analyses.

Also in Fig. 13, the results show that settlements due to consolidation and desiccation during a cycle were gradually larger. On the contrary, the settlement rates show smaller values as time progresses. This demonstrates that as new layers are superposed, they cause additional settlements (consolidation) in the lower ones due to self-weight. On the other hand, the inferior layers become stiffer (lower void ratio), decreasing settlement rate as cycles succeed.

Focusing on the desiccation process, which is supposed to happen during the waiting period, the analyses show in Fig. 14 that this phenomenon occurs increasingly late as more layers are added to the deposit. Furthermore, in this case, its occurrence could be questioned from the 2nd cycle on, as there is no void ratio reduction on top of the profile during the waiting period, except in the first cycle.

The modeling procedure mentioned before was adequate to make an estimate of the deposit height close to the actual stratified system, despite it has been assumed a homogeneous profile (clayey silt material). This can be explained by probably similar compressibility relationships of the different textures found in the deposit profile. Another aspect that might have contributed to the quality of the back analysis modeling is the fact that flow process of consolidation dominates the whole period of the deposit formation (no desiccation). This validates the hypothesis of averaging the filling curve. Still regarding consolidation, the time to complete the self-weight consolidation of each layer was enough during the filling and waiting stages. It does not matter if the material was sandy or clayey silt.

4.2.3. Other considerations about slime management and design

The foregoing results of slime management (sub-aerial model and actual data) could be compared with other potential management strategies. In case of a conventional disposal scheme, *i.e.* continuous disposal during 276 days, and considering consolidation as the only physical process, using the same filling rate (0,06 m/day) and height of solids, CONDES analyses would result in a final deposit height of 8.20 m after 690 days as shown in Fig. 15. It is practically the same height measured in the field or the one

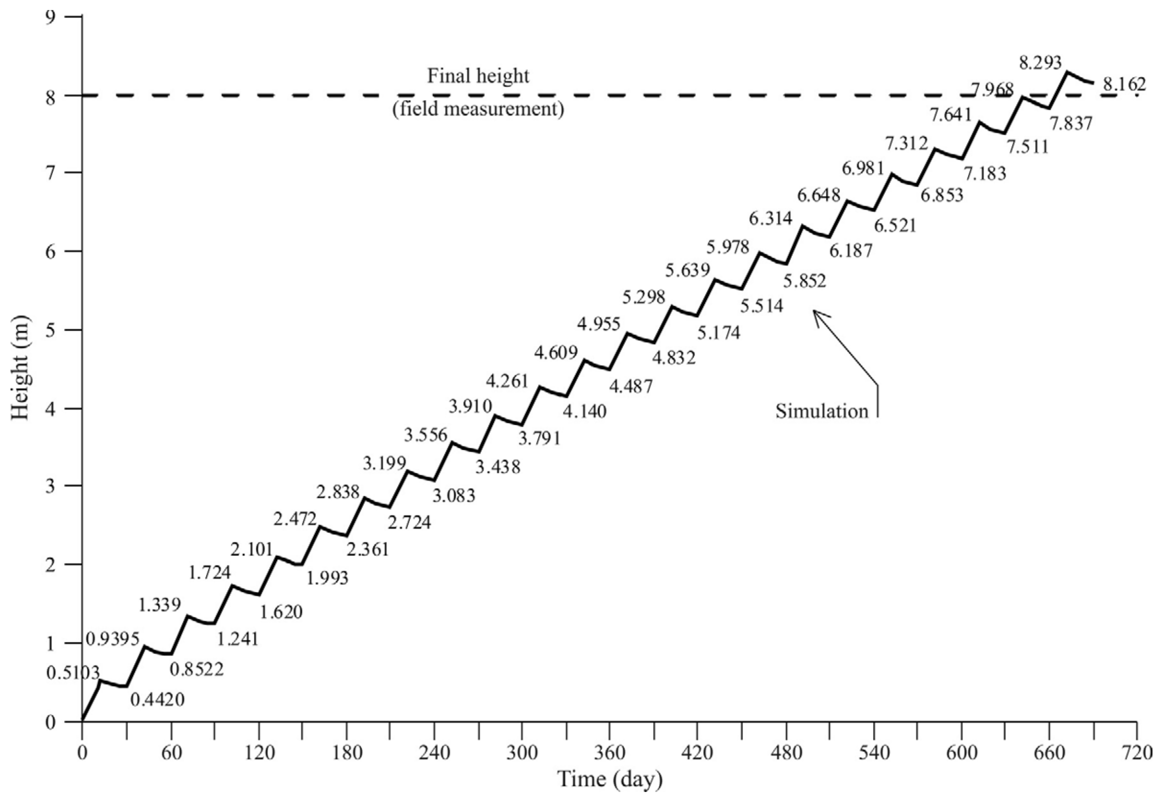

Figure 13 - Deposit height modeling (23 cycles).

obtained in the sub-aerial model analysis. The only drawback in the conventional disposal option would be the requirement of a higher containment structure during the filling operation, because the maximum deposit height would reach 10.22 m. One way to overcome this disadvantage would be to slow down the filling rate (*e.g.* a filling rate that would cover the whole period of 690 days (0.024 m/day). In this case, after 690 days, the deposit height would be 8.22 m, almost the same value obtained above. Figure 15 also shows deposit heights obtained following this second disposal scheme.

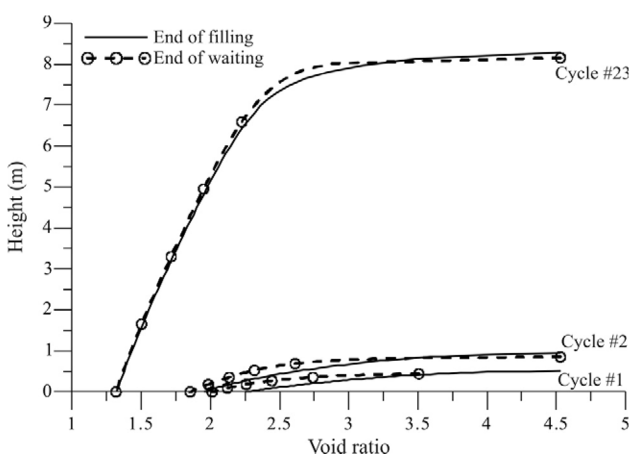

Figure 14 - Void ratio profile progress in the deposit (for clearness, cycles from 3rd through 22nd were omitted).

Another scheme would be to perform the sub-aerial disposal in such a way that thin layers were desiccated to their limit (shrinkage limit), before the placement of new fresh slimes. In this case, a simple model of one-dimensional shrinkage would result in a final deposit height of 6.15 m. For this evaluation, the following Eq. 4 is used,

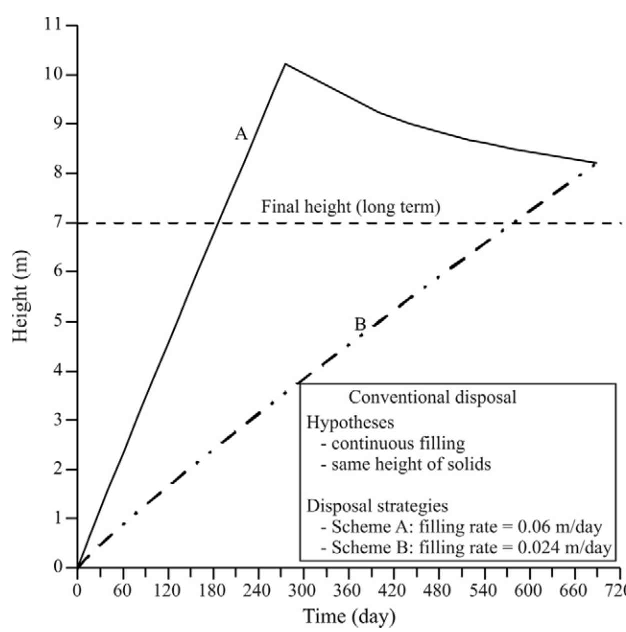

Figure 15 - Conventional disposal models.

where e_{min} corresponds to the void ratio at the shrinkage limit, H_s the height of solids and H_f the final height.

$$H_f = H_s\,(1 + e_{min}) \quad (4)$$

The final height obtained with this desiccation scheme would result in a deposit height even lower than the long term value of the conventional model (7.00 m) shown in Fig. 15. However, this scheme would probably require a period of time longer than the 690 days considered in this analysis (Oliveira-Filho & Lima, 2006).

4.2.4. Final discussion of the deposit modeling

Figure 16 shows a comparison of all results obtained by modeling and the actual deposit height. It is apparent that in the desiccation case, the slime management efficiency would be the maximum, although at a high cost of a longer waiting time (not shown). It is also interesting to note in this study, that the sub-aerial management scheme (actual or modeled with average cycles of filling and waiting) did not result in more efficiency as far as the storage capacity than the conventional disposal method (scheme A or B in Fig. 15).

5. Summary and Conclusions

The ability to understand formation of fine mining tailing deposits is demonstrated with a case study from experimental investigation and numerical analyses. A two-year iron ore slime impoundment built by the sub-aerial method is back analyzed. The analyses were based on a suitable model combined with site investigations and laboratory testing to determine deposit stratigraphy and material geotechnical properties. Field investigation data show that the slime deposit was not homogenous, but composed of stratified layers of tailings, ranging from loose sands to silty clays. Considering a deposit formed only by silt clay slimes, a numerical model was developed with the CONDES computer program (large strain consolidation and desiccation analysis software) using available material functions and slime management data. The analyses resulted in a deposit final height of 8.16 m, which is close to the actual height measured in the field. The result was used to validate the model. The analyses suggested that the desiccation process inherent to the sub-aerial method had a minimal effect or did not even occur. This fact indicates that sub-aerial strategy was not successful in this project and that the same results might have been achieved using a conventional disposal management. Other potential disposal schemes were also evaluated and comparisons made. It is suggested that this case study serve as a model for back analyses of other fine tailing deposits, in which consolidation and desiccation are the major processes involved. Finally, the role of proper site investigation to fulfill the study goal is recognized, especially with a series of piezocone tests to establish the deposit stratigraphy.

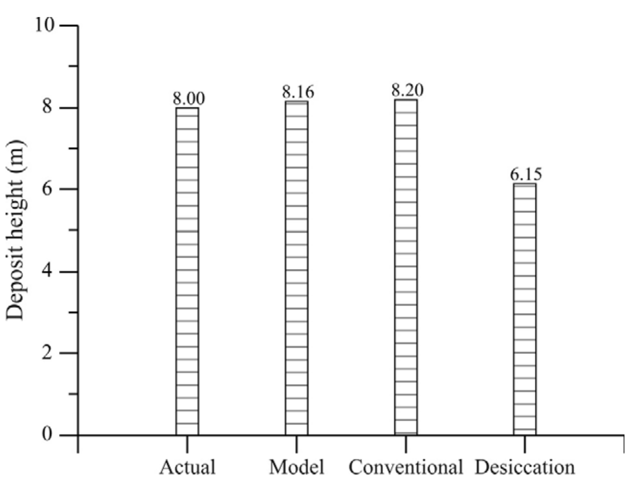

Figure 16 - Comparison of final deposit height according to different disposal strategies.

Acknowledgments

The authors would like to thank Samarco Mineração S.A. for the permission to publish the results of this research and also to thank Fundação Gorceix and FAPEMIG for their financial support.

The authors also would like to thank Prof. Znidarcic, from University of Colorado, for his comments on the contents of this paper.

References

Abu-Hejleh, A.N. (1993) Desiccation Theory for Soft Soils. Ph.D. Thesis, University of Colorado, Boulder.

Abu-Hejleh, A.N. & Znidarcic, D. (1995) Desiccation theory for soft cohesive soils. Journal of Geotechnical Engineering, ASCE, v. 121:6, p. 493-502.

Albuquerque Filho, L.H. (2004) Iron Ore Tailings Dams Analysis using Piezocone Testing. MSc. Dissertation, Civil Engineering Department, Federal University of Ouro Preto, Ouro Preto, 194 pp. (in Portuguese).

Almeida, F.E. (2004) Numerical Analysis of Desiccation of Iron Ore Tailings. MSc. Dissertation, Civil Engineering Department, Federal University of Ouro Preto, Ouro Preto (in Portuguese).

Árabe, L.C.G. (1995) Use of In Situ Testing for Geotechnical Properties Evaluation in Clay Deposits and Residual Soils. DSc. Thesis, Civil Engineering Department, Pontifical University Catholic of Rio de Janeiro, Rio de Janeiro, 346 pp. (in Portuguese).

Bedeschi, M.V.R. (2004) Settlements in Compacted Fills Built on Soft Soil Deposits with Vertical Drains in Barra da Tijuca. MSc. Dissertation, Civil Engineering Department, Federal University of Rio de Janeiro, Rio de Janeiro, 172 pp. (in Portuguese).

ICOLD (2002) International Commission on Large Dams, Comitê Brasileiro de Barragens – CBDB, Belo Horizonte, CD-ROM.

Konrad, J.M. & Ayad, R. (1997) An idealized framework for the analysis of cohesive soils undergoing desiccation. Canadian Geotechnical Journal, v. 34:6, p. 477-488.

Lima, L.M.K. (2006) Back Analysis of Formation of a Fine Mining Tailings Deposit Built by Sub-aerial Method. MSc. Dissertation, Civil Engineering Department, Federal University of Ouro Preto, Ouro Preto, 140 pp. (in Portuguese).

Massad, F. (2003) Earthworks: Basic Course on Geotechnics, 1st ed. Oficina de Textos Press, São Paulo (in Portuguese).

Mondelli, G. (2004) Geoenvironmental Investigation in Landfills using Piezocone. MSc. Dissertation, Civil Engineering Department, Polytechnic School of São Paulo, São Paulo, 246 pp. (in Portuguese).

Norman, D.K. & Raforth, R.L. (1998) Innovations and trends in reclamation of metal mine tailings in Washington. Washington Geology, v. 26:2/3, p. 29-42.

Oliveira-Filho, W.L. & Lima, L.M.K. (2006) Numerical algorithm for modeling formation of a mine fine tailings deposit. Proc. Cilamce'2006, Belém (in Portuguese).

Oliveira, J.T.R. (2002) Influence of Sample Quality in the Stress – Deformation – Strength Behavior of Soft Clays. DSc Thesis, Civil Engineering Department, Federal University of Rio de Janeiro, Rio de Janeiro, 264 pp. (in Portuguese).

Oliveira-Filho, W.L. & van Zyl, D. (2006a) Modeling discharge of interstitial water from tailings following deposition – Part 1. Soils and Rocks, v. 29:2, p. 199-209.

Pimenta de Ávila Consultoria (2001) Review Report on Main Management Plan for Mining Tailings at Germano Facility. Samarco Mineração S.A. Technical Report, Marina, 10 pp. (in Portuguese).

Penna, D.C.R. & Oliveira-Filho, W.L. (2007) Shear Strength gain of fine ore tailings due to desiccation. Proc. VI Brazilian Symposium on Unsaturated Soils, 2007, Salvador (in Portuguese).

Robertson, P.K. (1991) Soil classification using the cone penetration test: Reply. Canadian Geotechnical Journal, v. 28:1, p. 176-178.

Robertson, P.K. & Campanella, R.G. (1983) Interpretation of cone penetration tests. Part I: sand. Canadian Geotechnical Journal, v. 20:4, p. 718-733.

Samarco (2005) Technical Note. Samarco Mineração S.A., Mariana, MG (in Portuguese).

Schnaid, F. (2000) Field Tests and their Applications in Foundation Engineering, 1st ed. Oficina de Textos Press, São Paulo (in Portuguese).

Senneset, K.; Sanven, R. & Janbu, N. (1989) Evaluation of Soil Parameters from Piezocone Tests. Transportation Research Record, Washington, D.C., pp. 24-37.

Spannenberg, M.G. (2003) Geotechnical Characterization of a Soft Clay Deposit. MSc. Dissertation Civil, Engineering Department, Pontifical University Catholic of Rio de Janeiro, Rio de Janeiro, 162 pp (in Portuguese).

Silva, D.R. (2003) Desiccation Studies of Iron Ore Tailings at a Test Area. MSc. Dissertation, Civil Engineering Department, Federal University of Ouro Preto, Ouro Preto, 144 pp (in Portuguese).

Ulrich, B.; East, D.R. & Gorman, J. (2000) Sub-aerial tailings deposition – Design, construction and operation for facility closure and reclamation. Proc. Tailings and Mine Waste'00, Balkema, Rotterdam, pp. 29-37.

Vick, S.G. (1983) Planning, Design and Analysis of Tailings Dams. John Wiley and Sons, Inc., New York, 369 pp.

Viçosa (2006) Testing Partial Report. Federal University of Viçosa, Viçosa (in Portuguese).

Wels, C.; Robertson, A.; Mac G. & Jakubick, A.T. (1999) A Review of Dry Cover Placement On Extremely Weak, Compressible Tailings. Proc. Sudbury'99 - Mining and the Environment II; Conference held September 13-15, Sudbury.

Yao, D.T.C.; Oliveira-Filho, W.L.; Cai, X.C. & Znidarcic, D. (2002) Numerical solution for consolidation and desiccation of soft soils. Int. J. Num. & Anal. Meths. In Geomechanics, London, v. 26:2, p. 139-161.

In-Situ Tests and Numerical Simulation about the Effect of Annulus Thickness on the Resin Mixture for Fully Grouted Resin Bolt

A. Zingano, S. Peng, J. Koppe, J.F. Costa

Abstract. The main purpose of this paper is to study the effect of annulus thickness on the quality of resin mixture for fully grouted resin bolt. Pullout and mixture tests were made in underground coal mines for the following arrangements: (a) 29 mm borehole diameter, and 19 mm roof bolt diameter with steel wire around the roof bolt; (b) 29 mm borehole diameter, and 19 mm roof bolt diameter with no wire around the roof bolt; and (c) 24 mm borehole diameter, and 19 mm roof bolt diameter with no wire around the roof bolt. The mixture test in steel pipe showed that the best resin mixture is for the 24 mm borehole diameter. The arrangement (b) produced big voids around the bolt. But for the 24 mm hole, arrangement (c), the mixture showed the best results. This was corroborated with the pullout tests results where there was a difference in grout stiffness: in the 24 mm borehole diameter is was about 10 times higher than in the 29 mm borehole diameter. On the other hand, as far as the cohesive strength is concerned, the difference is not significant. Numerical models were built to simulate the pullout tests, and also to simulate the roof support at an intersection. Convergence at two underground intersections, consisting of an immediate roof with laminated sandstone, was monitored to evaluate the performance of the roof supports, using the 29 and 24 mm diameter boreholes (*i.e.* arrangements 'a' and 'b'). The readings showed that the 24 mm borehole diameter resulted in a slightly smaller convergence.

Keywords: glove finger, roof support, numerical modeling, coal underground mining,

1. Introduction

Roof support designs require information about the thickness and quality of each roof rock layer, the entry dimensions, and the properties of the bolt and resin.

In terms of bolt anchor, there are two types of roof support in underground coal mining,: (i) point anchor bolt, and (ii) fully grouted bolt. The point anchor bolt works as a support for the weak strata, which is anchored on the immediate strong layer above, and a pre-tension might be applied to push the weak layers against the strong layer to close separations. On the other hand, the function of the fully grouted roof bolt is to reinforce the roof by building a strong beam within the bolted area. In the beam building concept, the immediate roof is reinforced by restraining the vertical displacements of roof layers using the fully grouted roof bolts (Peng, 2008).

In a fully grouted roof bolt, the void space between the bolt and the wall of the borehole must be completely filled by grout to obtain the maximum performance of the bolt/grout/rock reinforcement system.

The anchorage mechanism of a fully grouted roof bolt is the cohesive and shear resistance at the interface between the grout and host rock. When this contact is weak, the roof bolt can debond and result in premature failure.

One of the causes for the weakening of the contact shear resistance is called "the gloving or glove fingering" (Peng, 2007; Pastars & MacGregor, 2005; Zingano *et al.*, 2007). It primarily occurs due to operational problems, when the plastic film of the grout cartridge is not completely shred by the rotation of the bolt during installation. It can also occur if there is over drilling.

In addition, the gloving effect can be caused by mixture problems due to a large annulus thickness, between the rock bolt and borehole wall. If this space is too big, the grout mixture wouldnt be as effective because the bolt cannot provide a good mixture for such a large amount of resin.

The main result of the gloving effect is the reduced contact area between the grout and host rock, or between the grout and bolt. This reduces the strength of the contacts which reflects on the stiffness or cohesive strength of the grout/rock or grout/bolt interfaces.

Operational problems like over drilling can be solved by training the roof bolter crew and ensuring that the right equipment is used. However, one question remains: What is the maximum (or minimum) thickness of the space between the bolt and borehole wall to get the best grout mixture?

There are some alternative solutions to increase the efficiency of the grout mixture, which are: (i) to put a steel

Andre Zingano, Associated Professor, Universidade Federal do Rio Grande do Sul, Porto Alegre, RS, Brazil, e-mail: andrezin@ufrgs.br.
Syd Peng, Full Professor, West Virginia University, Charles E. Lawall Chair of Mining Engineering, Morgantown, WV, EUA, e-mail: syd.peng@mail.wvu.edu.
Jair Koppe, Full Professor, Universidade Federal do Rio Grande do Sul, Porto Alegre, RS, Brazil, e-mail: jkoppe@ufrgs.br.
João Felipe Costa, Associated Professor, Universidade Federal do Rio Grande do Sul Porto Alegre, RS, Brazil.
Submitted on April 13, 2010; Final Acceptance on August 6, 2012; Discussion open until December 29, 2012.

wire around the bolt; (ii) make some corrugations on the bolt; (iii) modify the bolt head so that the rotation of the bolt is not centered to enhance mixing, and (iv) to reduce the annulus thickness between the bolt and borehole wall.

The coal mine, which one is mining the Barro Branco (white mud) seam, the immediate roof is a laminated sandstone layer with a 3 m thickness in average, and above are found a siltstone and a massive sandstone layers more than 10 m thick. The floor is massive sandstone, too. The coal seam is 1.8 m thick on average (Fig. 1).

The usual roof support for intersections is built by 2.2 m long fully grouted roof bolt with 19 mm diameter, and the borehole diameter is 29 mm. The bolt spacing is 1 m at intersections. The roof bolt in the entries and crosscuts is 1.5 m long, and 1.2 m row spacing.

There are some installation problems for the long roof bolt in an entry (or intersection) 1.8 m height. The bolt has to be installed in two parts that are connected using a coupled connection. This connection has a diameter of 25 mm, and needs drilling at the larger borehole diameter. It causes slower bolt installation and lower advance rates of the mining face. A steel wire is put around the roof bolt to increase the grout mixture efficiency.

The problems described above were the motivation for this study, which goal is to increase the beam building efficiency by enhancing the resin mixture. The investigation also examined the possibility of reducing the bolt length so it could be installed without using coupled bolts

The purpose of this paper is to study the correlation of the grout properties (grout stiffness and strength) related to the annulus thickness between the bolt and the borehole wall.

The methodologies applied to reach this purpose are:

- Test the mixture efficiency of the grout for different borehole diameters and bolt specifications;
- Conduct pullout tests with the same specifications from the mixture tests, and determine the grout properties (stiffness and cohesive strength);
- Construct numerical models to simulate the pullout tests using the grout properties;
- Design roof supports for intersections in a room-and-pillar underground coal mining, considering the new specifications for borehole and roof bolt;
- Monitor the convergence at the center of the intersection for the new roof support design, and compare it to the convergence of the actual roof support applied;
- Construct and calibrate numerical models for the new and actual roof supports.

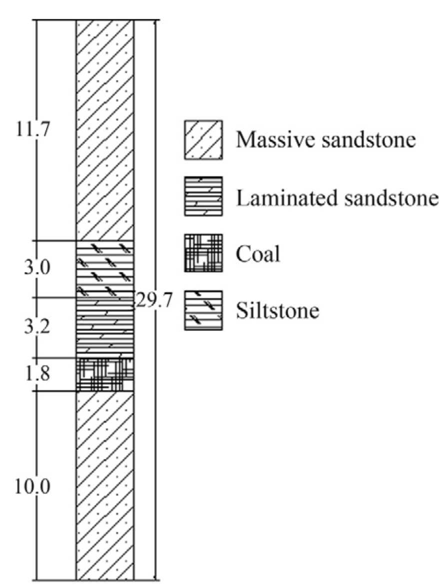

Figure 1 - Geology for Barro Branco Seam at MEL Mine.

2. Grout Mixture Test

The main goal of these tests is to check the mixture quality of the grout for different borehole diameter and bolt specifications. Table 1 shows the specifications for each mixture test.

The tests were conducted in steel pipes with the same internal diameters specified in Table 1, and the same diameters used in underground applications. Three tests were conducted, one for each specification below. The steel pipes were placed vertically to simulate actual bolt installations and the top end was closed to simulate the back of the borehole.

The roof bolt was a dowel GG50 from Gerdau Steel Co., with grooving around the bolt to facilitate the mixture of the resin in the hole (or steel pipe).

The grout is formulated by the company itself in a small grout cartridge manufacture facility. A cross-section of the resin cartridge is shown in Fig. 2a. The amount of required resin was calculated and placed in the pipe to guarantee that voids were caused only by mixture problems. It was observed that a small amount of resin return from the pipe occurred during mixture operation in the 29 mm diameter pipe, which is normal.

After three hours curing time, the pipes were cut and opened to examine the quality of the grout mixture. Figure 2b shows the results of the grout mixture tests for the three specifications (Table 1).

It can be clearly observed that the best grout mixture was in the 24 mm (0.94 in.) diameter pipe. There are no

Table 1 - Borehole and roof bolt specifications for grout mixture tests.

Borehole diameter (mm)	Bolt diameter (mm)	Difference* (mm)	Steel wire
29	19	5.0	Yes
29	19	5.0	No
24	19	2.5	No

*The difference refers to the distance between bolt and borehole wall.

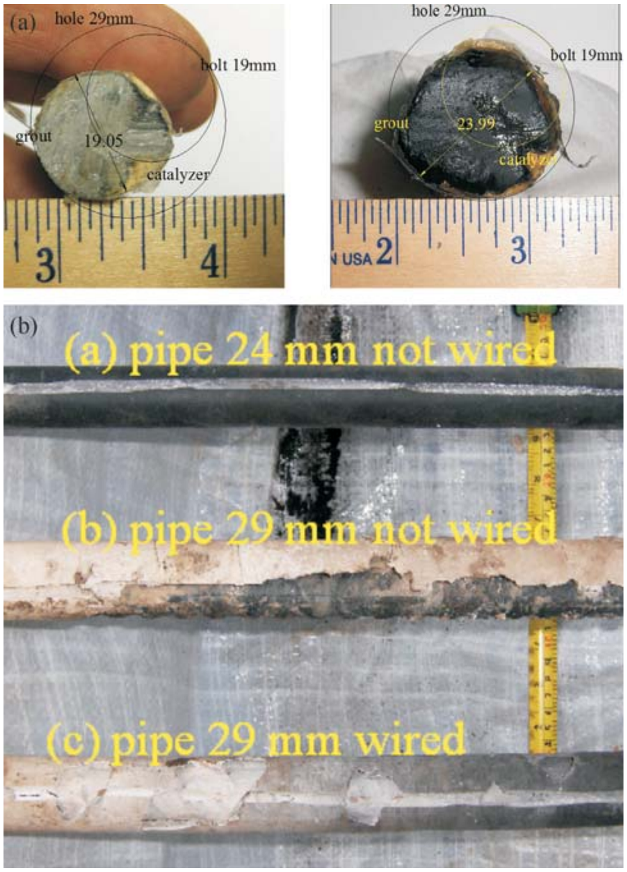

Figure 2 - (a) picture of the cross-section of a resin cartridge, and (b) results for grout mixture tests.

void spaces, and the gray color, which indicates complete mixing of the resin, is more uniform than in the others two tests (29 mm diameter pipe). On the other hand, the tests with the 29 mm diameter pipe contained large voids, and the color was not uniform. The results indicate that the mixture is better for the test bolt with steel wire than the bolt without steel wire.

Therefore, the space between bolt and borehole wall can have a large influence on the efficiency of the grout mixture and the elimination of gloving effects. In this case, the 2.5 mm difference (between bolt and hole wall) was deemed appropriate to obtain a good grout mixture.

The next step is to verify the quality of the contact resin/rock in terms of grout properties using pullout tests, which can be used to calculate the grout stiffness and grout cohesion strength at interface resin/rock.

3. Bolt Pullout Test

The intent of the bolt pullout test is to determine the mechanical parameters of the grout (grout stiffness and grout strength cohesion). The pullout tests were conducted underground in the immediate roof, using the same bolt and borehole specifications described in Table 1, but the bolt length is reduced to 30 cm (1 ft). Figure 3 shows the apparatus for the pullout test.

The chart in Fig. 4 shows the pullout tests results for each borehole and bolt specification. In the pullout test, the grout stiffness is the inclination of the force/displacement

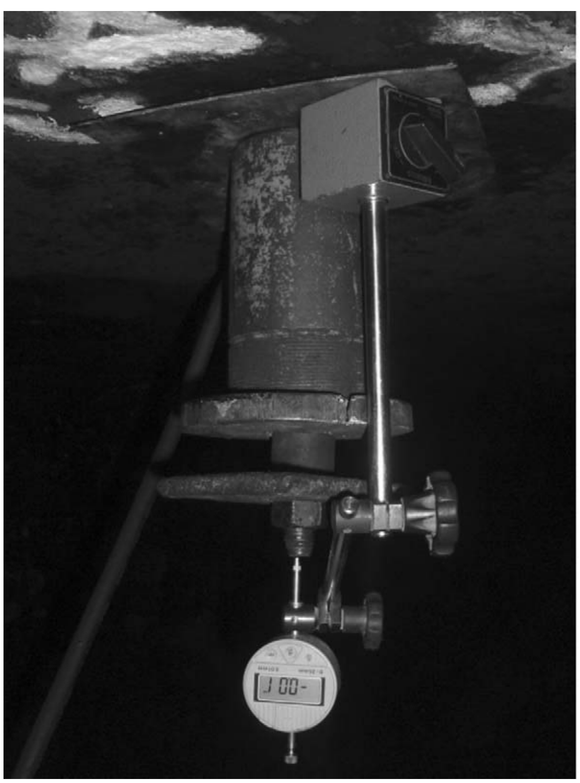

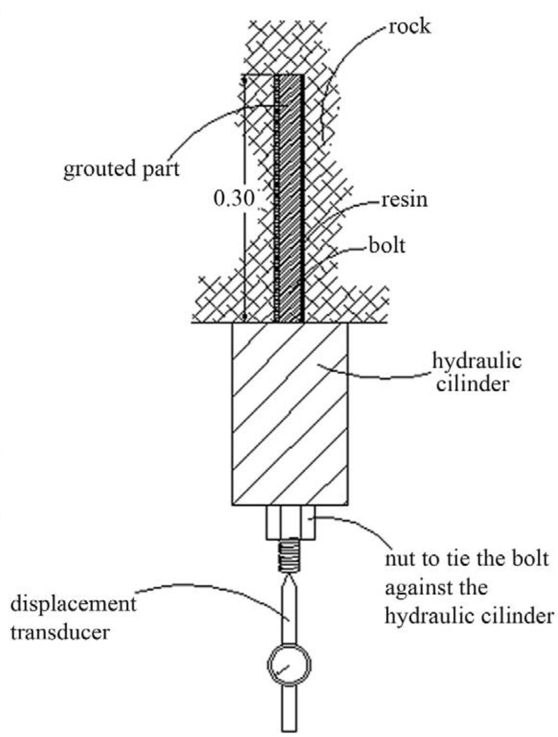

Figure 3 - Apparatus for pullout test.

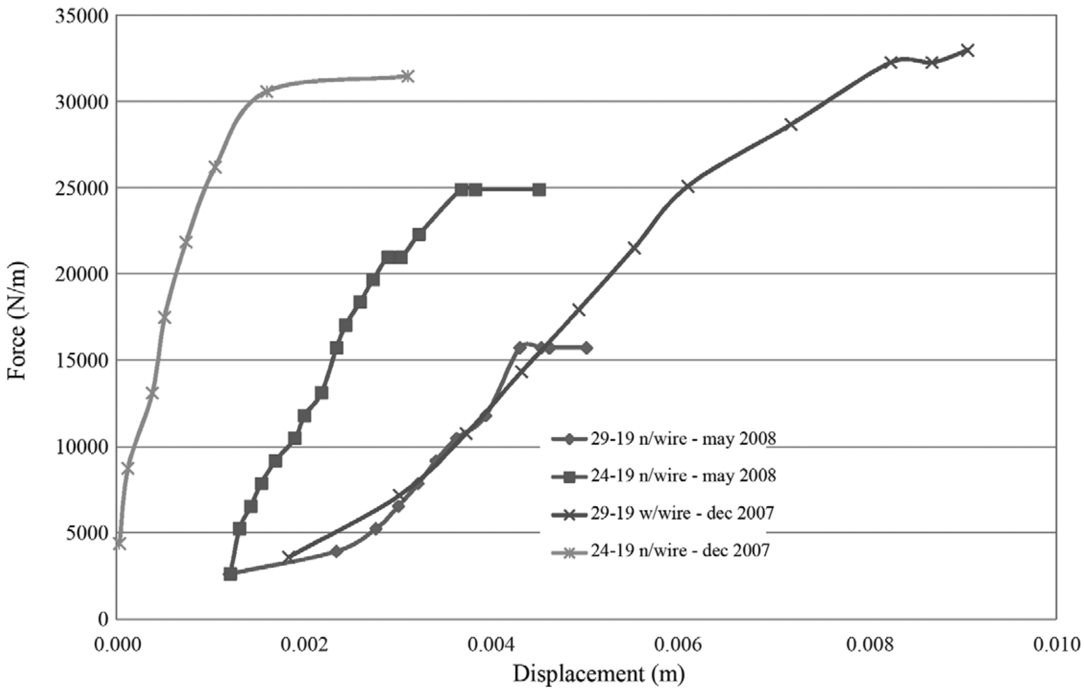

Figure 4 - Force/displacement for pullout tests.

curve (the unit is N/m/m), and the cohesive strength is the maximum force read in the test (the unit is N/m).

The grout stiffness for the test in a 24 mm borehole diameter is higher than the tests in a 29 mm borehole diameter, regardless of whether a steel wire is installed around the bolt or not. It is also possible to see that the grout stiffness is quite similar for the bolts with and with no steel wire around the bolt in a 29 mm diameter borehole. However, the cohesive strength is twice as much for bolts with steel wire around them. Table 2 shows the pullout tests results.

Numerical models were developed to simulate the pullout tests that were made in the field. The bolt and borehole specifications were considered in these models, and the models were also adjusted to grout stiffness and cohesive strength determined from the field tests. The numerical models were built using FLAC-2D version 5.0 of Itasca Inc., in which the models geometry is a rock block (laminated sandstone), and the rock bolt with the same specifications detailed in Table 1.

The results of the models suited the field tests very well, confirming the mechanical parameters of the grout for each test. Figure 5 shows the charts that compare the numerical models on pullout test simulations with the pullout tests made in the field.

The results from the numerical simulations were applied to the roof support numerical models at the entries intersection.

4. Roof Support Design

One of the challenges to underground coal mining is the roof support design for the entries intersections. The intersection dimensions (diagonals) are difficult to control due to the lack of mining operator control and pillar corners sloughed due to stress concentration. In this case, the diagonal dimensions can vary from 9 to 11 meters, instead of 8.6 m.

The roof support for the intersections consists of 2.2 m long roof bolts, while the entry height is about 1.8 m.

Table 2 - Results of the pullout tests.

Borehole diameter (mm)	Bolt diameter (mm)	Diff.* (mm)	Steel wire	Grout Stiffness (N/m/m)	Cohesive Stiffness (N/m)
29	19	5.0	Yes	3.95×10^6	3.2×10^4
29	19	5.0	No	3.60×10^6	1.6×10^4
24	19	2.5	No	6.78×10^6	2.5×10^4
24	19	2.5	No	2.37×10^7	3.1×10^4

*The difference refers to the distance between bolt and borehole wall.

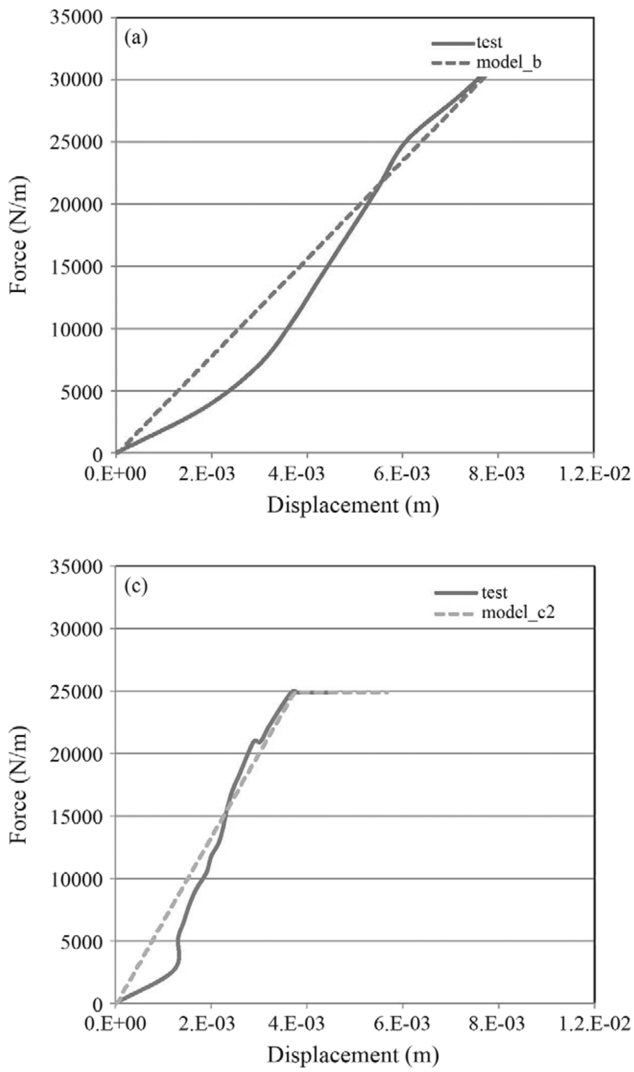

Figure 5 - Results of the numerical simulation for pullout tests compared to the field tests. (a) Borehole 29 mm and bolt with steel wire; (b) Borehole 29 mm and bolt with no steel wire; (c) and (d) Borehole 24 mm and bolt with no steel wire.

Bolt lengths longer than entry heights make roof bolt installation very difficult and impacts productivity negatively. Therefore, the challenge is to determine if a roof bolt length less than 1.8 m would provide adequate and safe support.

The new support design was taken into account using the empirical methods proposed to Unal (1983) and Bieniawski (1989), where the length of the roof bolt is calculated based on the load height in the immediate roof. For intersection roof support the diagonal dimensions must also be considered.

Considering the RMR (rock mass rating) for laminated sandstone (Table 3), and the maximum diagonal dimension (11 m), the support spacing was determined for roof bolts with 19 mm diameter and 1.8 m long. For this roof bolt dimension, the bolt spacing was estimated at 0.85m in the diagonal direction, which resulted in a safety

Table 3 - Material properties.

Rock	RMR	Young's Modulus (Pa)	Poisson's ratio	Internal friction angle (degree)	Cohesion (Pa)
Laminated sandstone	65	2.99E+10	0.17	35	8.00E+06
Massive sandstone	80	2.99E+10	0.17	20	5.00E+06
Siltstone	50	9.90E+09	0.25	15	1.80E+06
Coal	55	4.00E+09	0.25	15	1.40E+06

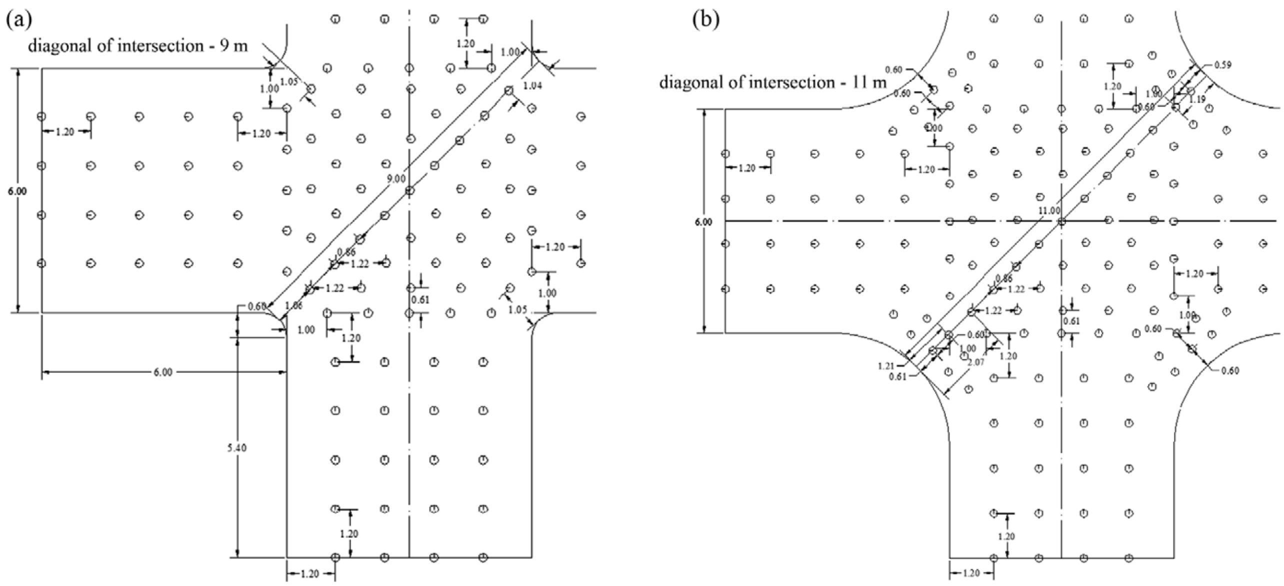

Figure 6 - New roof support design for intersection, considering 1.8 m long roof bolt for diagonal (a) 9 m, and (b) 11 m.

factor of 1.7. Considering the grout mixture and pullout tests, the borehole was designed for a 24 mm diameter. Figure 6 shows the configurations of roof support design for intersection diagonals of 9 and 11 m.

A monitored intersection test was established with instruments to evaluate the roof convergence with the intention of determining whether the new roof support design would eliminate separation above the roof bolt support horizon. For comparison purposes , another intersection was instrumented and evaluated, which utilized the traditional support systems so the convergence between two roof support designs could be compared.

Figure 7 shows the readings of the convergence at the center of the intersection for the two monitored intersections, which the anchor depths in the roof of the instruments are 1.5 m (5 ft), 3.0 m (9.8 ft), and 4.5 m (14.7 ft). The charts shows that both intersections reached equilibrium, and there werent any problems with roof stability.

It can be observed that the extensometer anchor 4.5 m above the roof has more convergence than the other two extensometers for both roof support designs. This happens because the extensometers are anchored in the siltstone layer (Fig. 1). The two anchor depths (1.5 and 3.0 m) are in the laminated sandstone layer.

The charts show different roof convergences, in which the current roof support gets less convergence than the new roof support design, and it also reached equilibrium in shorter time. There are two hypotheses for this behavior: (i) the beam built by the used roof support is stronger than the new one because the roof bolt is longer (2.2 m), or (ii) the time elapsed between the intersections excavation date and the beginning of monitoring were different for both.

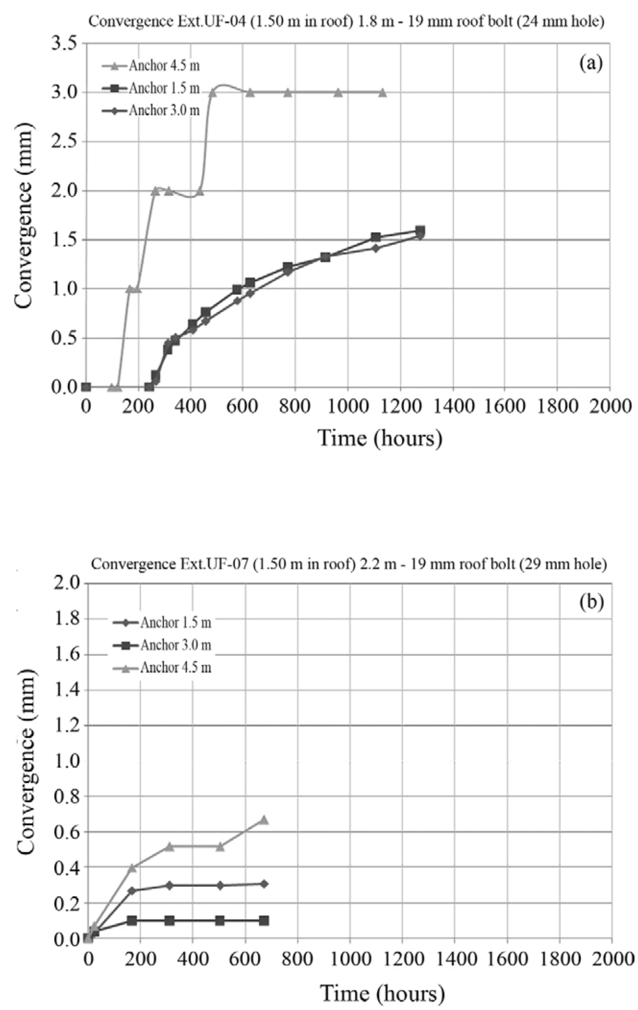

Figure 7 - Roof convergence for (a) new roof support design, and (b) old roof support design.

Numerical models were built to check which of these hypotheses is more reasonable. These models were 3-D models of an entry intersection.

These models were built using the design geometries of the entries and intersections, which were 6 m wide and 1.8 m high. The geology and material properties are based on Fig. 1 and Table 3, respectively. The initial stress field considered that the horizontal and vertical stresses are the main stresses with a stress rate of one, and the depth of the coal seam is 150 m.

Table 4 shows the vertical displacement of the immediate roof, and 1.5 m (5 ft) into the roof, which is the same depth of the extensometer anchors of the monitored intersections. Figure 9 shows the vertical roof displacements for the roof with no installed support.

The vertical displacements at the immediate roof at the intersections center are 6.42 mm (0.25 in.) and 6.80 mm (0.27 in.) for new and traditional roof support, respectively. The new roof support design had less vertical displacement than the traditional roof support, but the difference is minimal. Therefore, the difference that was observed in the field monitoring was most likely caused by the second hypothesis; the time differences between the installed instrumentation and subsequent development.

It must be emphasized that the difference between the in-situ monitoring and numerical modeling convergence happens because the in-situ convergence measuring does not suffer the deformation and the roof sagging right after the excavation of the intersection.

Table 5 shows the maximum stress that the grout and bolt are subjected to for the three roof support specifications (Table 1). The larger grout stress is observed when the resin annulus is smaller, as expected.

The grout stress for the 1.8 m (6 ft) long bolt is almost double than that of the 2.2 m (7 ft) long bolt, because the amount of bolt for 1.8 m (6 ft) bolt is less than for the 2.2 m (7 ft) bolts, and the annulus thickness of grout is also smaller (2.5 mm *vs.* 5 mm). Also, the bolt stress is much higher than in the 2.2 m bolts. However, no yield was observed in any of the examined bolts.

5. Conclusions

The objective of this work was to verify the influence of the annulus thickness between the bolt and borehole wall on the grout mixture and the effect of gloving; and also its influence on the grout properties and roof support quality.

The grout mixture and pullout tests showed that a smaller annulus thickness provided a better grout mixture and no gloving effects were observed. In this case study a 2.5 mm annulus thickness appeared to be enough to eliminate any adverse effects of gloving.

Operations staff should be warned that bolt installations can be adversely impacted by over drilling or when continuing to rotate the drilling steel after the adequate length has been achieved.

Therefore, the roof support efficiency in underground coal mining must take into account the quality of roof bolting installation operations, and also the quality of grout mixture.

Simple tests, like grout mixture and pullout tests can provide important information for roof support design and roof bolting operation installation controls.

The mining company is changing to the new roof support design, which will increase the bolting operation productivity, even with the number of additional bolts required in the intersections In the same way, the cost of the roof bolting operation will be reduced due to reductions in bolt borehole and bolt lengths and reduced resin usage. Additional savings will be achieved by eliminating the steel wire and the additional manufacturing required for coupled bolts.

Table 4 - Vertical roof displacement for the three roof support specifications.

Borehole and Bolt diameter (mm)	Bolt length (m)	Immediate roof (mm)	1.5 m in the roof (mm)
29-19	2.2	6.79	4.91
29-19 wired	2.2	6.80	4.91
24-19	1.8	6.42	4.89
No Bolt	-	6.82	4.91

Table 5 - Grout stress and bolt stress for the three roof support specifications.

Borehole and Bolt diameter (mm)	Bolt length (m)	Max. Grout stress (Pa)	Max. Bolt stress (Pa)
29-19	2.2	1.72×10^5	6.09×10^6
29-19 wired	2.2	2.13×10^5	7.52×10^6
24-19	1.8	4.06×10^5	2.22×10^7

Acknowledgements

The authors would like to thank Cia. Carbonífera Metropolitana for partnering for this study; permitting and assisting with all the field tests in its facilities. The authors also would like to recognize the important partnership between the Mining Industry and Universities to continue to develop knowledge about ground control in coal mining to make the mines safer.

References

Bieniawski, Z.T. (1989) Engineering Rock mass Classification, Jonh Wiley and Sons, New York, 251 pp.

ITASCA Consulting Group (2002) FLAC-2D version 5.0, User's Manual.

Pastars, D. & MacGregor, S. (2005) Determination of load transfer characteristics of glove resin bolts from laboratory and in-situ field testing. Proc. 24th Int. Conf. on Ground Control in Mining, Syd Peng, Sr. Ed., West Virginia University, Morgantown, pp. 329-337.

Peng, S.S. (2007) Ground Control Failure – A Pictorial View of Case Studies. Syd Peng (ed), Morgantown Printer Inc., Morgantown, 330 pp.

Unal, E. (1983) Design Guidelines and Roof Control Standards for Coal Mine Roofs. Ph.D. Thesis, Pennsylvania State University, Uneversity Park, 355 pp.

Zingano, A.C.; Morsy, K.M.; Peng, S.S. & Kallu, R.R. (2007) Comparison among the conventional fully-grouted bolt, combination bolt, and one-step bolt using numerical modeling. Proc. 26th Int. Conf. on Ground Control in Min., Syd Peng (ed), West Virginia University, Morgantown, pp. 257-263.

Using DMT to Determine Overconsolidation Ratio (OCR) in Compacted Fills

A.C.G. Queiroz, J.C. Carvalho, R.C. Guimarães

Abstract. Quality of compacted fills is essential to the proper functioning of a structure as a whole. Currently, quality control is achieved by testing to determine the deviation of moisture content of recently compacted soil in relation to optimum moisture and degree of compaction reached. Based on the results, deformability, permeability and strength related characteristics are inferred. However, data obtained by using this technique do not always reflect actual behavior of soil, and are only applicable during the construction phase. More elaborate field tests are generally used only when problems are detected at completed landfills, but such tests may also be of great value during execution, since they provide soil geotechnical parameters, thus enabling control based on behavior rather than just physical properties. This study examined the application of correlations developed by several authors for estimating OCR by DMT in compacted fills. The results showed that dilatometer testing (DMT) is a potential tool for control of compaction and should be further studied, particularly in relation to the effects of suction on DMT results.

Keywords: DMT, compacted fills, OCR, suction, correlations, control of compaction.

1. Introduction

In earth dams and road works the quality of compaction of fills is essential for proper performance. In most cases, technological control of compaction is carried out layer by layer, based on moisture and degree of compaction. However, this technique is only applicable during construction and the data obtained do not always reflect soil behavior.

When problems are detected in finished landfills, or those still under construction, but quite high, possible causes may be investigated by bore holes, bell holes or field trials. Although rarely used, these tests may also be useful during construction in order to have compaction control based on the material's behavior. However, few reports cover in-situ investigation of the behavior of compacted fills for validating correlations between results from these tests and geotechnical parameters obtained in laboratories.

Of the field testing methods, DMT may be a good option for examining the behavior of landfills since it is relatively simple to do and provides estimates for soil geomechanical parameters used to predict the behavior of fills such as earth dams.

The parameter selected for this study was the overconsolidation ratio (OCR), based on the belief that it can represent the behavior of compacted soil, while also being directly related to compaction control parameters. Furthermore, in earthworks such as fills used for dams or highway embankments, an important feature is the soil's elastic regime, hence the importance of estimating OCR in these cases.

2. Uses of DMT For Estimating Overconsolidation Ratio (OCR)

The ratio between maximum effective vertical stress experienced by the soil and the current effective vertical stress is called the preconsolidation ratio (PCR) or overconsolidation ratio (OCR). In the case of compacted soils this is obviously a pseudo preconsolidation ratio, since it reflects only the effects of compaction rather than the effect of actual consolidation as such.

Marchetti (1980) observed a certain similarity between the profiles of horizontal strain index K_D and OCR. Based on data from a non-cemented clay, he proposed Eq. 1, valid for soils in which $0.2 < I_D < 2$, and I_D is material index.

$$\mathrm{OCR} = (0.5K_D)^{1.56} \quad (1)$$

Marchetti & Crapps (1981) reviewed the original approach to develop Eqs. 2, 3 and 4.

$$I_D < 1.2 \quad \mathrm{OCR} = (0.5K_D)^{1.56} \quad (2)$$

$$I_D > 2.0 \quad \mathrm{OCR} = (0.67K_D)^{1.91} \quad (3)$$

$$1{,}2 < I_D < 2.0 \quad \mathrm{OCR} = (mK_D)^{n} \quad (4)$$

where

$$m = 0.5 + 0.17P \quad (5)$$

Angela Custódia Guimarães Queiroz, M.Sc, Doctoral student with the Geotechnical Graduate Program, Universidade de Brasília, Brasília, DF, Brazil, e-mail: eng_angela@yahoo.com.br.
José Camapum de Carvalho, PhD, Professor, Geotechnical Graduate Program, Universidade de Brasília, Brasília, DF, Brazil, e-mail: camapum@unb.br.
Renato Cabral Guimarães, PhD, Professor, Universidade Estadual de Goiás, and engineer with FURNAS Centrais Elétricas S.A., Aparecida de Goiânia, GO, Brazil, e-mail: renatocg@furnas.com.br.
Submitted on November 18, 2010; Final Acceptance on August 6, 2012; Discussion open until December 29, 2012.

$$n = 1.56 + 0.35P \quad (6)$$

$$P = \frac{I_D - 1.2}{0.8} \quad (7)$$

Eq. 8 is a suggestion from Lacasse & Lunne (1988) to estimate OCR, and is valid for OCR >1.25.

$$\text{OCR} = 0.225 K_D^m \quad (8)$$

where m = 1.35-1.67, lower value corresponds to high- and higher to low-plasticity soils.

Lunne *et al.*(1989) posed OCR estimates considering age of clay (Eqs. 9 and 10).

$$\text{OCR} = 0.3 K_D^{1.17} \text{ for } S_u / \sigma'_{v_0} \leq 0.8 \text{ (young clays)} \quad (9)$$

$$\text{OCR} = 2.7 K_D^{1.17} \text{ for } S_u / \sigma'_{v_0} > 0.8 \text{ (aged clays)} \quad (10)$$

It is noteworthy that the proposals outlined above for determining the OCR were originally created to be applied to clay soils. However, this study used due to the lack of equations for the compacted soils, thereby aiming to evaluate if these adequariam well or need adjustment.

3. Materials and Methods

To conduct the study was selected an area on the left shoulder of the João Leite dam in the municipality of Goiânia (GO), approximately 6.5 km from the state capital. The extensive experimental campaign involved three DMT-type boreholes and digging a pit for removal of deformed and undeformed samples in order to carry out several laboratory tests, such as consolidation, triaxial, and determining the water retention characteristic curve using the filter paper technique. Figure 1 shows plant location of the tests.

This clayish fill was made up from homogeneous residual soils that were plastic (liquid limit over 40%, clay fraction over 20% by weight, obtained with the use of dispersant), not very active, and showed low permeability ($k < 10^{-8}$ m/s) when compacted. Compaction was executed with energy equivalent to Normal Proctor.

The methodology used for laboratory testing followed specifications set by the Brazilian Technical Standards Association (ABNT), the American Society for Testing and Materials, and Furnas Soil Laboratory procedures. Our DMT procedure followed the *Flat Dilatometer Manual* and ASTM D 6635 recommendations.

4. Estimated Overconsolidation Ratio (OCR)

OCR was calculated using correlations proposed by Marchetti (1980), Marchetti & Crapps (1981), Lacasse & Lunne (1988), Lunne *et al.* (1989) for young clays, and laboratory test results (consolidation and k_0 type triaxial). Figure 2 and Table 1 show the findings.

A review of the OCR values obtained with the correlations suggested for dilatometer testing shows that they overestimated this parameter. The equation developed by Lunne *et al.* (1989) is the one that comes closest to laboratory findings, however, the latter were also higher than expected.

Obtaining this parameter in the laboratory consists of just determining the pre-consolidation stress, and for this study this was done using the compressibility curves of the consolidation and K_D triaxial testing type, since geoestatic

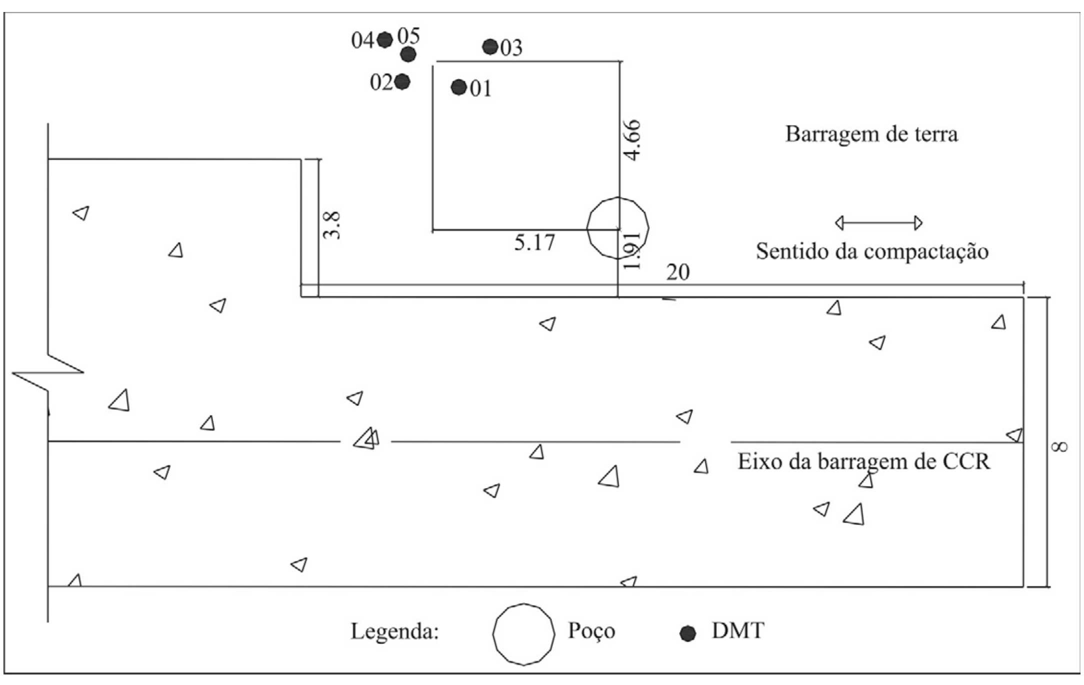

Figure 1 - Plant location of the tests.

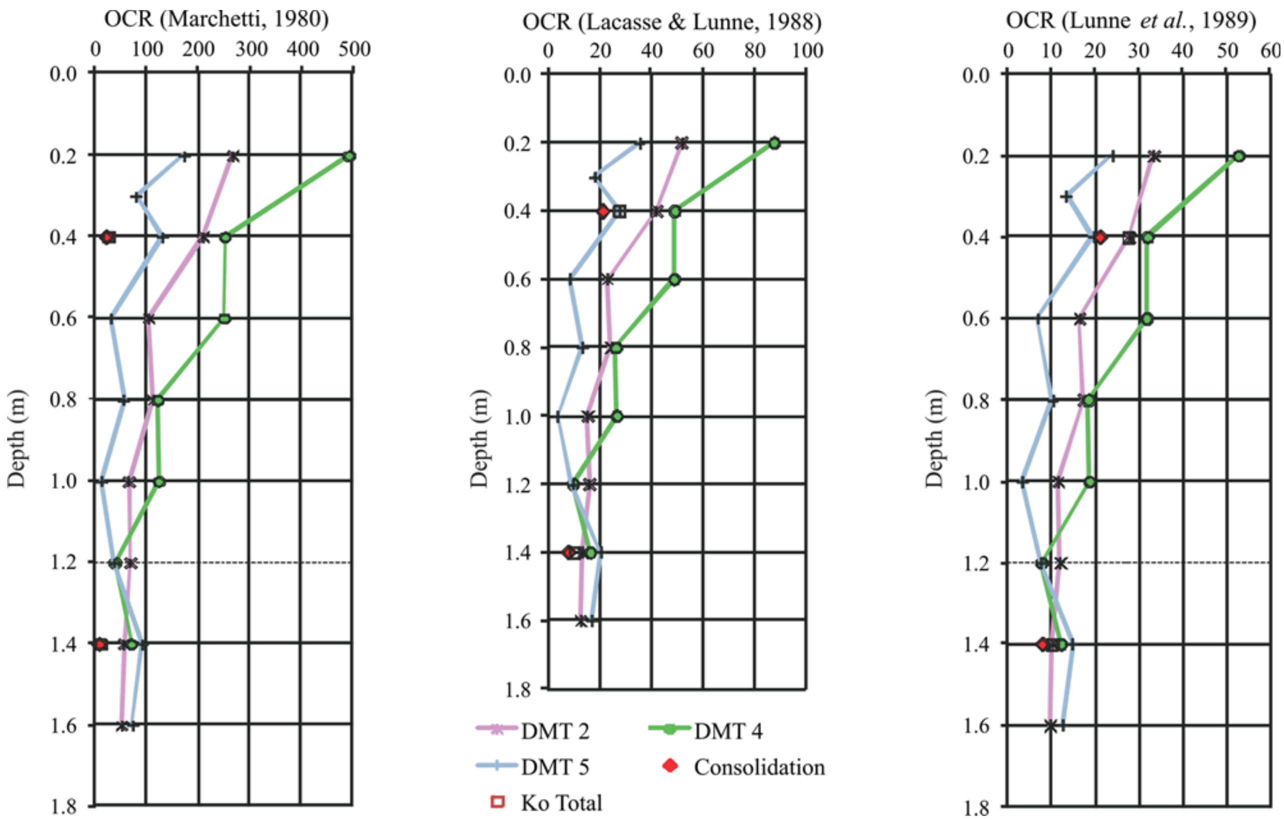

Figure 2 - OCR calculated from oedometric compression testing and DMT.

stress is just calculated. This calculation does not take into account the effects of suction acting on the material and may lead to significant errors in results. Another aspect to be noted is preconsolidation as a result of compaction is affected by aspects such as roller weight, leg shape and size or tire pressure, depending on the situation, and compaction moisture.

Correlations proposed for OCR are based on the dilatometric ratio K_D, which uses a calculated geostatic stress value and excludes suction effects.

Table 1 - OCR calculated using method proposed by Marchetti & Crapps (1981).

Depth (m)	OCR		
	DMT 2	DMT 4	DMT 5
0.2	14856.5	8671.0	5937.8
0.4	756.0	1026.3	598.9
0.6	322.2	250.3	1087.8
0.8	354.2	388.8	164.4
1.0	180.9	396.9	44.3
1.2	192.6	94.6	37.1
1.4	149.4	198.7	271.7
1.6	136.7	-	72.9

Since both laboratory findings and values obtained from correlation proved to be high, and neither took into account suction effects, an analysis including this parameter was conducted to evaluate any effect it might have on results. However, this analysis was only applied to type k_0 triaxial tests and the method proposed by Lunne *et al.* (1989), due to their results being apparently providing a better fit than expected.

Figure 3 shows characteristic curves to water retention related suction matrica a function of moisture obtained for the studied soil.

For the results of the k_0 test, the predetermined consolidation stress was maintained and suction added to geo-

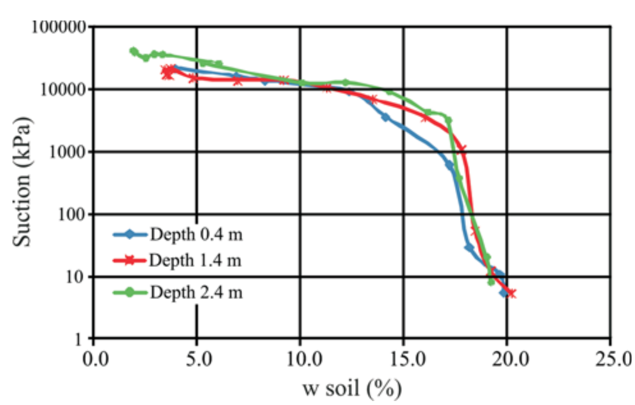

Figure 3 - Characteristic curves as a function of moisture.

static stress, so geostatic stress was then the sum of suction stress and calculated geostatic stress. These suction values were found as follows: with experimentally determined moisture contents corresponding to the depth in question, suction was obtained by reading on the appropriate characteristic curves.

For the results obtained using the method proposed by Lunne *et al.* (1989) K_D values were recalculated using geostatic stress with suction effect. Having obtained these values, new OCRs were determined, as shown in Fig. 4, together with the new laboratory OCRs.

The results obtained considering the suction effect on geostatic stress and consequently on OCR, were substantially better than previous ones. However, the values found up to 0.80 m depth show some scatter. This dispersion may be due to unevenness in compression itself, since for the compressed fill involved has really a pseudo OCR, *i.e.* a state of pre-consolidation induced by compaction which may vary slightly from point to point. The dispersion shown may also be caused by variations in moisture and therefore in suction across testing points. This hypothesis was verified as described below.

An average of the OCR values obtained for the three tests (DMT 2, 4 and 5) was calculated and the values found were almost identical to those for DMT test 2 (Fig. 4). The mean OCR results obtained were matched with the correlation of Lunne *et al.* (1989) for each point in the three tests, and with known p_0, effective vertical stress (σ'_{vo}) was determined. From this amount it was removed the portion of vertical stress due to own weight, thus leaving suction. The following is an outline of the verification:

$$\overline{\text{OCR}} = \text{OCR}_n = 0.3 \cdot k_d^{1.17} = \left[0.3 \cdot \left(\frac{P_0}{\sigma'_{v_0}} \right)^{1.17} \right]_n \therefore \qquad (11)$$

$$\sigma'_{v_0} = \sigma'_{VPP} + S$$

where σ'_{vpp} = vertical stress due to own weight, or calculated vertical stress and S = suction.

Using the appropriate characteristic curves (representative of depth) and the suctions obtained, the corresponding moistures were found. Figure 5 shows moisture content values determined directly in the laboratory and those found via the characteristic curve, and also deviations between them.

Figure 5 shows that the moisture values found using the characteristic curve are very close to the laboratory values, with a maximum deviation of 1.45%. This means that OCR estimated by DMT does reflect the material's properties. Note also that the results are more scattered in the range up to 0.8 m depth, as are the OCR results, which confirms the initial hypothesis that OCR variation is mainly due to moisture variations.

Since the moisture results obtained using characteristic curve were satisfactory, the same methodology was applied to obtain the degree of saturation, but this time using

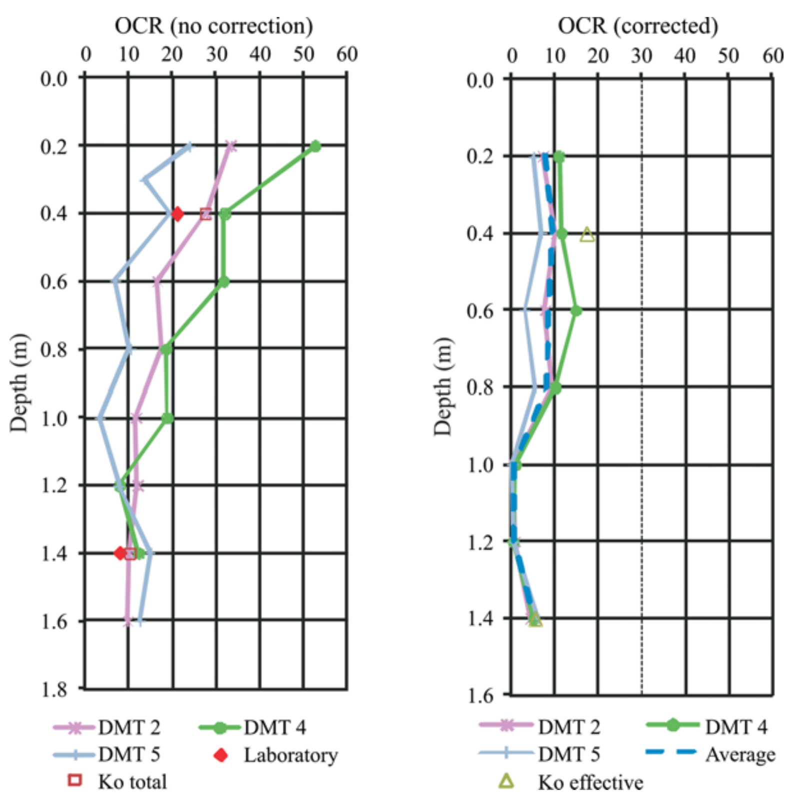

Figure 4 - OCR values calculated with and without the effect of suction.

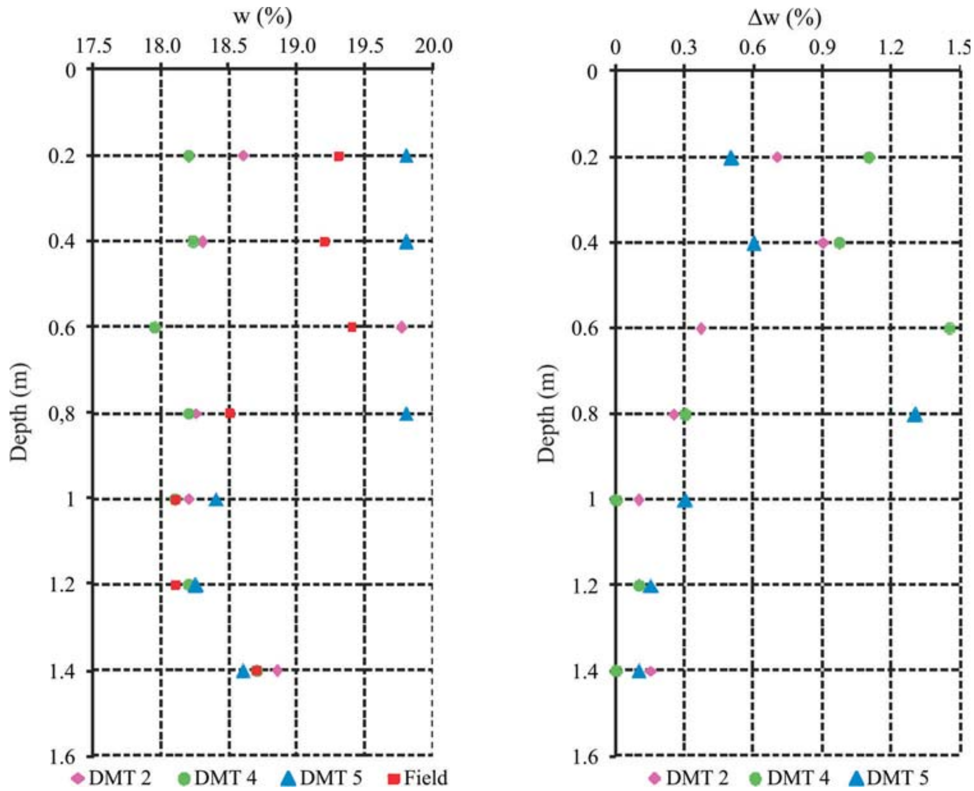

Figure 5 - Moisture values obtained in the laboratory and those found using the characteristic curve, and deviations of moisture (in module)

the characteristic curves depending on the degree of saturation. The main aim of this procedure was to determine the void ratio and therefore specific dry weight and degree of compaction.

Knowing the degree of saturation, four different void index profiles were determined for each test point, thus for each profile using moisture values obtained in different ways. The first used the moisture values found from characteristic curves (e_{cc}), the second the average of the latter ($e_{cc\ average}$), the third laboratory values ($e_{bellhole}$) and the fourth, the average of the latter ($e_{bellhole\ average}$). This artifice was used in an attempt to find the values showing the best fit with those calculated conventionally. Figure 6 shows the average of the results obtained.

Void ratios determined using the degree of saturation obtained from the characteristic curve and those calculated conventionally show a good fit down to 0.80 m depth, *i.e.* in the range where the curve used corresponded to the level altimetry 710,400 m. From this point, indices determined using the new method diverged considerably from those found by the conventional method. This was due to problems in determining void ratios during the filter paper test for this depth, leading to unrepresentative results for the soil studied.

Void ratios found for different soil moisture conditions were not greatly different, but the profile using moisture obtained from the characteristic curve proved to be a better option. Therefore the determination of this parameter would be based on the DMT results and the characteristic curves. However, the void ratio determination also requires the real specific weight of grains, but a correlation between this and the dilatometer test could be studied subsequently in order to optimize the process.

Having determined void ratio, and having obtained maximum dry density for the material studied, dry density and degree of compaction (DC) was calculated. Figure 7 shows the values obtained for degree of compaction.

The values of the degree of compaction wee consistent and agree with each other and with those obtained in the laboratory up to 0.80 m depth. What happens after that is due to problems in executing the filter paper test, as explained above. The behavior obtained was as expected, since the degree of compaction reflected the void ratio. Generally, however, it was found that using DMT to determine the degree of compaction may be a good alternative, since errors found up to 0.80 m depth were less than 1%, as shown in Table 2. Equation 11 was used to define percentage error.

$$\text{Error}\,(\%) = \frac{\text{DMT} - \text{Laboratory}}{\text{Laboratory}} \times 100 \qquad (12)$$

Strength and deformability parameters being known, compaction control based soil-behavior may be executed. However, the usual practice for this control is based on dry density and therefore the degree of soil compaction, since

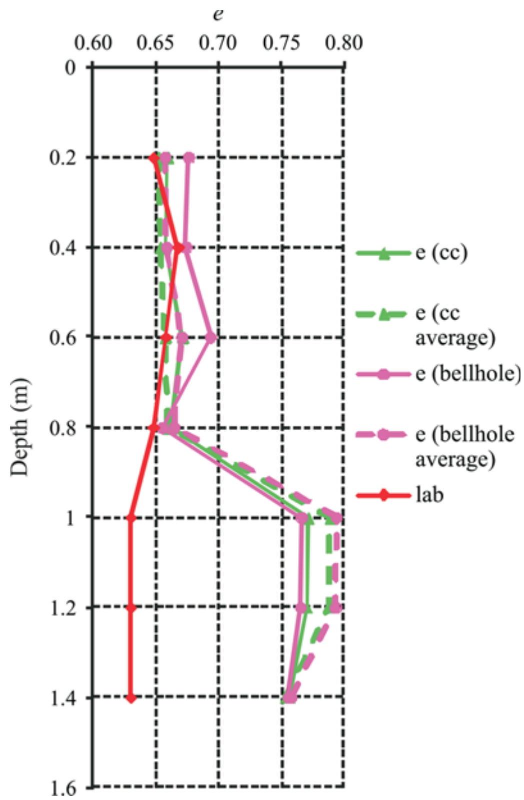

Figure 6 - Void ratios obtained for different soil moisture conditions.

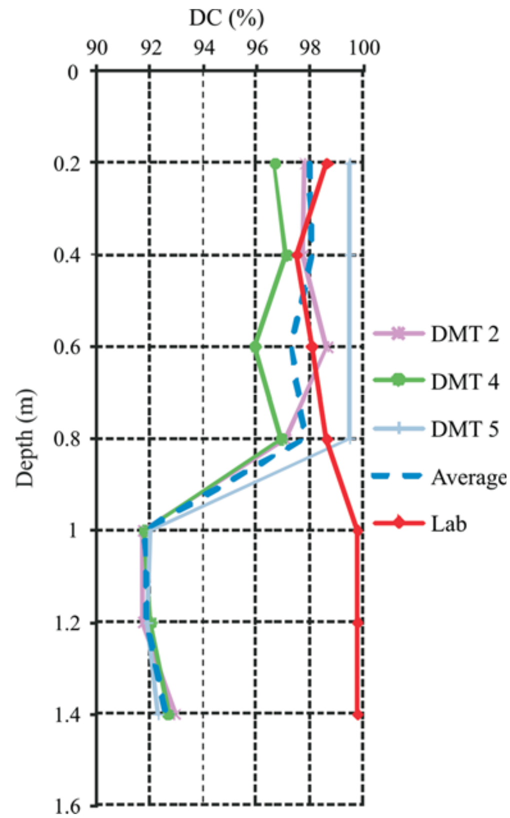

Figure 7 - Degree of compaction.

this means that liberation of the compacted layer is executed in accordance with predetermined limits, and does not require more accurate analysis. This control procedure does not faithfully represent fill properties and behavior. Therefore, there is a crucial need for a method that will control compaction by providing both geotechnical parameters and determining the degree of compaction, which is what the dilatometer test may do.

An important point to consider is that inserting the dilatometric flat in soil leads to compaction of the area around the membrane, and along with reduced void ratio, moisture tends to migrate (Camapum de Carvalho, 1985). Both of which contribute to boost suction. Together with the reduction of void ratio and moisture content there is an increase in the degree of saturation, causing suction to vary. However, there is no way of a priori indication whether it will increase or decrease irrespective of the soil and the characteristic curve shape itself.

Therefore, although the results shown point to the possibility of using the dilatometer test in compacted soils, it is essential to appraise the effect of dilatometer penetration on densification and water migration in different types of compacted soil. Another need is to have well-defined characteristic curves, knowing point-to-point void ratio and moisture content, thus enabling more precise definition of e.pF *vs.* degree of saturation curves proposed by Camapum de Carvalho & Leroueil (2004).

Table 2 - Percentage error – laboratory degree of compaction values and average using DMT.

Depth (m)	Error (%)
0.2	-0.7
0.4	0.6
0.6	-0.8
0.8	-0.8
1.0	-8.0
1.2	-7.9
1.4	-7.2

5. Conclusions

OCR estimates made using the dilatometer test proved superior to those found by laboratory testing. However, laboratory results were also high. Therefore an accurate analysis was performed considering the effects of suction on this parameter, obtained by both the k_0 type triaxial and the proposal of Lunne *et al.* (1989), which produced much more consistent values, thus highlighting the importance of suction when evaluating the mechanical behavior of compacted solids.

However, the results still showed some dispersion, and another aspect emerged on attempting to explain this:

moisture variations were causing dispersion of OCR values and based on the latter, by a retrospective analysis combined with characteristic curves, the soil's void ratios may be determined and hence its degree of compaction.

Dilatometer testing, together with the plotting of characteristic curves representing the loan area used, could provide a good means of controlling compaction of fills for dams, based on soil behavior. Using this technique for highway fills would be somewhat more complicated, since borrow areas move frequently and an excessive flow of tests could be generated.

Control of landfill compaction must be combined with rational use of borrow area, since soil alteration profile strongly affects mechanical and hydraulic behavior.

A point to note is that our comments herein are based solely on testing in just one location. Further research on different types of soil and compaction is needed to develop methodology applicable to compacted soils in general.

References

ASTM (2001) Standard Test Method for Performing the Flat Plate Dilatometer, D 6635-01. West Conshohocken, Pensilvânia, USA, 15 pp.

Camapum de Carvalho, J. (1985) Etude du Comportement Mecanique d'une Marne Compactee. These, nº 9, l'Institut National des Sciences Appliquees de Toulouse, Toulouse, 181 pp.

Camapum de Carvalho, J. & Leroueil, S. (2004) Curva característica de sucção transformada. Solos e Rochas, v. 27:3, p. 231-242.

Lacasse, S. & Lunne, T. (1988). Calibration of Dilatometer Correlations, Proc. ISOPT-1, Orlando, Florida, v. 1, pp. 539-548.

Lunne, T.; Lacasse, S. & Rad, N.S. (1989) SPT, CPT, pressuremeter testing and recent developments on in situ testing of soils. General Report Session. 12th International Conference of Soil Mechanics Foundation Engineering, Rio de Janeiro, pp. 2339-2404.

Marchetti, S. & Crapps, D.K. (1981) Flat Dilatometer Manual. International Report of GPE Inc., Gainesville, Florida.

Marchetti, S. (1980) In Situ Tests by Flat Dilatometer. Journal of Geotechnical Engineering, ASCE, v. 106:GT3, p. 299-321.

Laboratory Research on EPS Blocks Used in Geotechnical Engineering

J.O. Avesani Neto, B.S. Bueno

Abstract. Geosynthetic geofoam has a cellular structure made of expanded polystyrene (EPS) and has been used as a lightweight material for geotechnical use in embankments, bridges seat, base and sub-base of roads pavements and infrastructure protection applications. This paper presents research data on EPS laboratory tests aiming to characterize Brazilian EPS for geotechnical use. The mechanical tests comprised unconfined axial compression (with variation of temperature, specimens dimensions and rates of deformation velocity), interface shear friction (EPS – EPS) and creep under compressive load. A simple loss weight test by mice attack was also conducted in an attempt to quantify the damage in samples of EPS by biological attack. Samples of 10 kg/m^3, 14.5 kg/m^3, 17 kg/m^3, 20 kg/m^3, 30 kg/m^3 and 40 kg/m^3 densities with virgin material and 10 kg/m^3 with recycled material were used. The results have shown that EPS has a great strength in compression and creep solicitation and high interface friction strength despite its very low density, and good geotechnical properties for applications in geotechnical engineering works. In the weight loss test it was found that the mice only attach the material mainly for a specific situation.

Keywords: geofoam, EPS, compression strength, shear friction, creep, mice attack.

1. Introduction

The use of expanded polystyrene (EPS) and extruded polystyrene (XPS) in civil engineering has already a recognized application in buildings due to then high thermal capacity, acoustic insulation and absorption of impacts and settlements. However their use as geosynthetic has only recent applications.

In geotechnical engineering this material, manufactured in prismatic blocks named geofoam, has properties that allow its use in many applications. The low density EPS (approximately 100 times lower than the soil, a result of its manufacturing process) and a relatively high mechanical strength give the EPS geofoam larger applicability in embankments as a lightweight fill – especially in areas with low bearing capacity soils and mainly as a base and sub-base of road pavements and bridge seat (Horvath, 1994, Beinbrech & Hillmann, 1997, Piana, 1997 and Stark *et al.*, 2004), thermal insulation (Horvath, 1995) and compressible inclusion to alleviate pressures on walls and slopes and infrastructure protection (Horvath, 1996, 1997, Murphy 1997 and Ikizler *et al.*, 2008).

In these applications, EPS blocks are submitted in varied solicitations. Thus, it is necessary to study the response of the material when subjected to these solicitations, both mechanical and hydraulically (Stark *et al.*, 2004).

Horvath (1994) studied the behavior of cubic specimens of EPS-geofoam in axial compression and observed a large influence of density on the compressive strength. He proposed a correlation between the modulus of elasticity and the density, and compared different suggestions of correlations from other authors.

Duskov (1997) performed compression tests in two EPS-geofoam samples of 15 kg/m^3 and 20 kg/m^3 densities and cylindrical shape (300 mm height and 150 mm diameter). The EPS strength values (defined for 10% strain) obtained were relatively high, despite the low density of the material. The author also suggested a correlation between the initial modulus of elasticity and the density. The speed of tests also seemed to influence the EPS-geofoam strength. This speed was also investigated by Duskov (1997 who concluded there was an increase in the strength in function of increased velocity. However, this strength increase was not significant.

Stark *et al.* (2004) observed that specimens of cylindrical shape tended to show a lower modulus of elasticity and yield strength value when compared with cubic specimens. They also tested samples of different sizes and the results showed that increasing the sample size there was a significant increase in its modulus of elasticity. However, the results were not conclusive and still require further investigations.

Bueno (2005) conducted compression tests in EPS-geofoam (10 kg/m^3 and 20 kg/m^3) using cylindrical-shape specimens, with height/diameter ratios of 3:1 (h = 150 mm and d = 50 mm). The author concluded that the samples did not reach rupture with the traditional patterns. In such a configuration, the samples showed a lateral instability (buckling), which is evidence that the use of samples

José Orlando Avesani Neto, MSC, Escola de Engenharia de Sao Carlos, Universidade de São Paulo, Av. Trabalhador Sãocarlense 400 São Carlos, SP, Brazil, e-mail: avesani.neto@gmail.com.
Benedito de Souza Bueno, Full Professor, Escola de Engenharia de Sao Carlos, Universidade de São Paulo, Av. Trabalhador Sãocarlense 400 São Carlos, Brazil, e-mail: bsbueno@sc.usp.br.
Submitted on December 20, 2010; Final Acceptance on March 28, 2010; Discussion open until December 29, 2012.

of cylindrical shape can mislead the real compressive strength of the material.

Yeo & Hsuan (2006) performed unconfined axial compression tests at different elevated temperatures. The authors used five temperatures, ranging from 30 °C to 58 °C, with 7 °C intervals, and observed a decrease in strength with increasing temperature and a bi-linear behavior, with a pronounced change of slope at 44 °C.

Hazarika (2006) suggested a constitutive model based on various compression tests of EPS blocks of different shapes – cylindrical and cubic – and dimensions. The author concluded that EPS geofoam applications can be broadly divided into two categories: small-strain and large-strain, in which the desired constitutive (stress-strain-time) properties vary depending on each application.

Sun (1997) performed creep tests in 50 mm cubic samples of 18 kg/m^3 density EPS. The stress levels ranged between 30% and 70% of compressive strength at 5% strain (85 kPa). The author observed that the creep deformation effects were negligible at stress levels up to 30% of compressive strength (at 5% strain).

Duskov (1997) reported creep test results of cylindrical samples of EPS geofoam. He verified that the immediate strain (occurred on the first day) could represent values above 50% of the total strain. The same behavior was observed by Sheeley (2000) with cubic specimens of 50 mm.

According to Horvath (1994), there are two shear modes that are important to EPS blocks. The internal blocks shear, that there is no apparent collapse of the samples and are not frequent, and the shear of interface between blocks (joint), which is an important factor of stability in works with horizontal solicitations.

Sheeley & Negussey (2000) conducted interface shear tests in EPS blocks (EPS – EPS) with no connection and with a barbed connector plate. They observed that barbed connector plates did not cause any increase in the shear strength of EPS – EPS interface and concluded that the difference in the shear strength between different foam densities was only marginal.

Barrett & Valsangkar (2009) performed shear strength tests in EPS geofoam blocks with no connections and connected with barbed connector plates and with polyurethane adhesive. The authors found that the friction coefficient between blocks was consistent with the values reported in the literature and conservative in terms of commonly used design values. Furthermore, they concluded that the barbed connector plates did not provide any additional interface shear strength, but the polyurethane adhesive connector worked very well making the individual blocks act as one large mass.

This paper introduces data on lab tests performed in various EPS blocks with large density variation. The main objective is to compare engineering data of the various EPS bocks according to their density.

2. Laboratory Tests

2.1. Samples

The nominal densities of the EPS blocks used in this research ranged between 10 kg/m^3 and 40 kg/m^3. Prior to the tests, all samples were placed in an acclimatized room with temperature of 23 °C and relative air humidity of 50%, for a period up to 24 h. The densities were then determined in accordance with ASTM (2007). Table 1 summarizes the data obtained. The variations of densities were small, showing a standard deviation (S.D.) smaller than 2.0 with an average value of 1.10 and coefficient of variation (CV(%)) smaller than 5.9% with an average value of 4.60.

2.2. Unconfined axial compression tests

In the axial compression (ASTM, 2000) test all densities showed in Table 1 were used in cubes of 100 mm and 50 mm dimensions. The influence of speed was also verified. The rates of deformation tested were 5 mm/min, 10 mm/min, 15 mm/min, 50 mm/min and 200 mm/min.

The influence of temperature was also checked using axial compression tests when EPS samples were incubated in an environmental chamber for twelve hours. Temperatures in the range of 30 °C to 72 °C with 7 °C intervals (starting from room temperature of 23 °C) were used.

2.3. Joint direct shear tests

It was used the equipment of direct shear testing in soils (ASTM, 1998). EPS samples of 10, 20, 30 and 40 kg/m^3 densities with virgin material and 10 kg/m^3 with recycled material were tested.

Figure 1 shows the main steps of the sample preparation.

Normal stresses of 10 kPa, 20 kPa, 30 kPa, 40 kPa, 50 kPa and 60 kPa were chosen since in most application they can represent field situations.

2.4. Creep in compression tests

The creep in compression tests has been standardized by ASTM (2001) and ASTM (1995).

Table 1 - Densities of tested samples.

Nominal density (kg/m^3)	Measured density (kg/m^3)			S. D.	CV (%)
	Max.	Min.	Aver.		
10 (30% recycled)	15.4	12.0	13.0	0.6	4.4
10	13.1	10.3	11.7	0.7	5.6
14.5	15.5	14.0	14.7	0.4	2.5
17	20.0	16.6	18.8	0.6	3.3
20	25.5	20.7	22.2	1.2	5.3
30	38.6	30.3	33.2	2.0	5.9
40	43.7	38.6	41.0	2.0	5.0

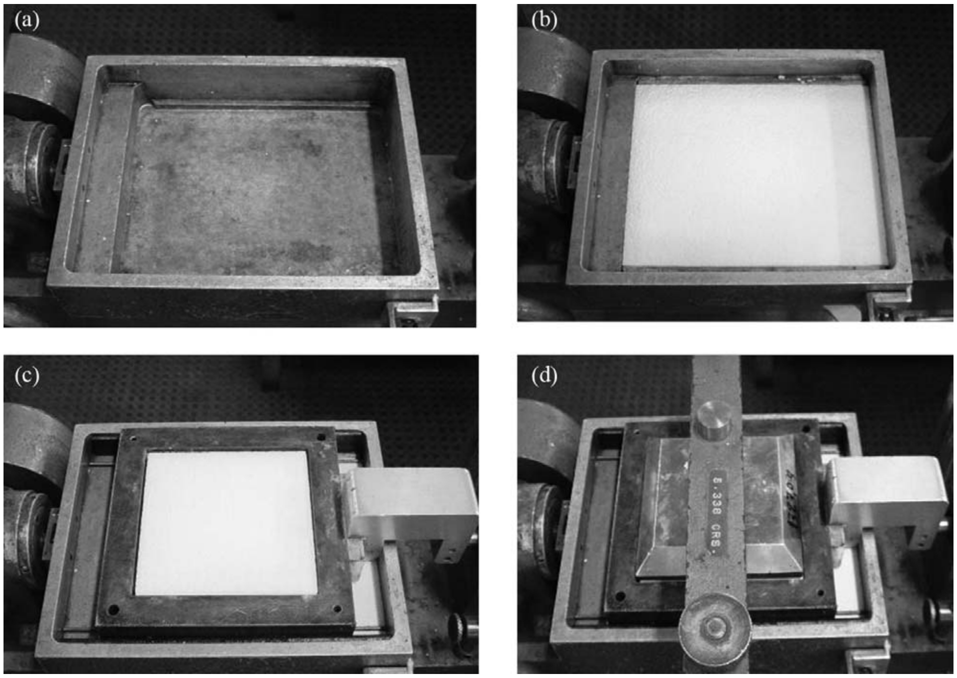

Figure 1 - Steps of sample preparation for direct shear tests of EPS joints: (a) shear box; (b) bottom sample of EPS placed in the box; (c) top block of EPS placed into the shear box; (d) top plate and system to apply the normal load already placed on top of the sample.

The EPS specimens were cubes of 50 mm dimensions. Table 2 presents the densities used and the compression loads applied. Figure 2 shows the test performed.

2.5. Loss weight test by attack of mice

As the EPS material is used in works it may be in contact with animals and various biological agents, not just in construction time but also in its lifetime, it was subjected to a test to evaluate the loss weight of samples with contact with mice.

Figure 3 shows a typical mouse (of *Mus musculus* specie) used as the agent of damage to the EPS samples.

Two control variables that influence mice actions were considered: the presence of food (food and water) and straw for building their nest. The mouse can bite the specimens for feeding itself and extract material for the construction of its nest. There were three groups of tests to determine the worst case in which the individual bites the samples as much as possible: In the first case the mouse is deprived of food and water and forced to nibble on the EPS

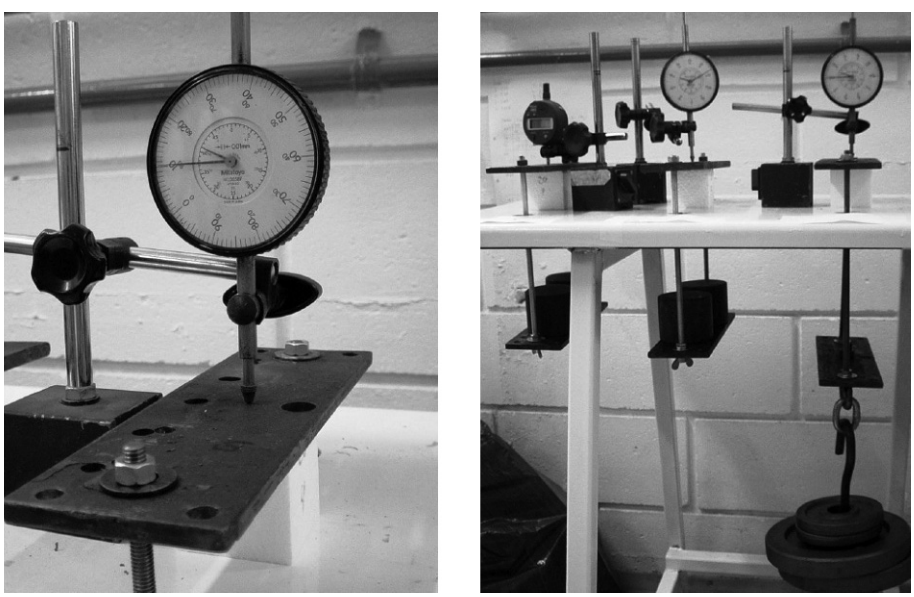

Figure 2 - Creep in compression tests.

Table 2 - Densities and applied loads used in the creep in the compression tests.

Nominal density (kg/m^3)	Average density (kg/m^3)	Normal load applied (kPa)	Normal load applied / stress at 2% deformation (%)
10	11.7	10	30
		20	60
		40	115
		60	170
17	18.8	20	25
		40	50
		60	75
		80	100
20	22.2	20	15
		40	35
		60	50
		80	70
30	33.2	20	10
		40	20
		60	30
		80	40

as it is very hungry; in the second case the mouse can access the food, but the straw is removed (deprivation of straw). It is forced to bite the EPS sample to build its nest. In the third case the mouse is deprived of both straw and food (total deprivation). Figures 4a and 4b show, respectively, an individual with total deprivation and straw deprivation.

The specimens used in the animal attack tests were blocks of 100 mm x 100 mm x 50 mm dimensions and all densities showed in Table 1. The exposure time of all tests was 48 h.

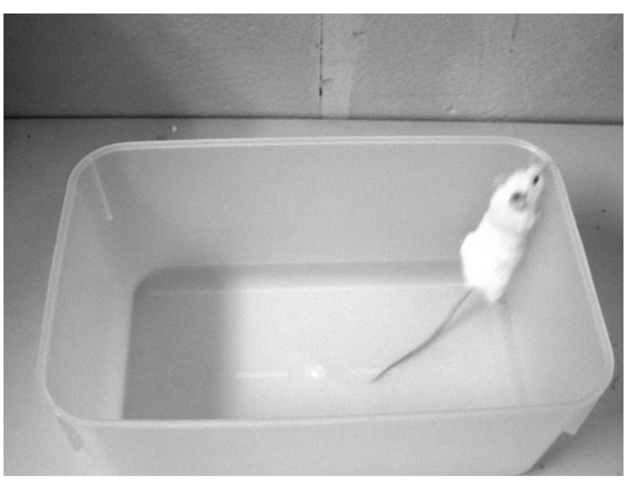

Figure 3 - Mouse used in this research.

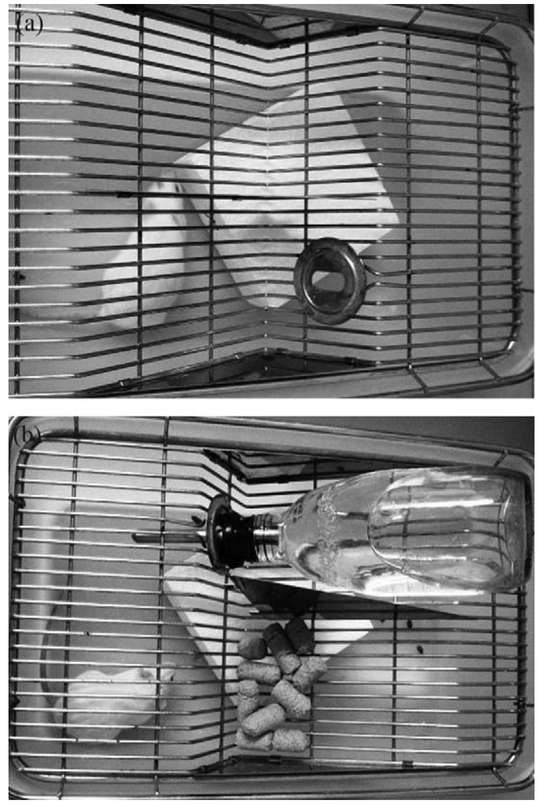

Figure 4 - a) total deprivation; b) straw deprivation.

3. Results

3.1. Unconfined axial compression tests

Figure 5 shows the compression test result of the 30 kg/m^3 density specimen in which the sample was a 100 mm cube.

According to several authors, the compressive strength of the EPS-geofoam is determined at the strain value of 10%. However, the typical behavior of the material, characterized by only one point (compressive strength

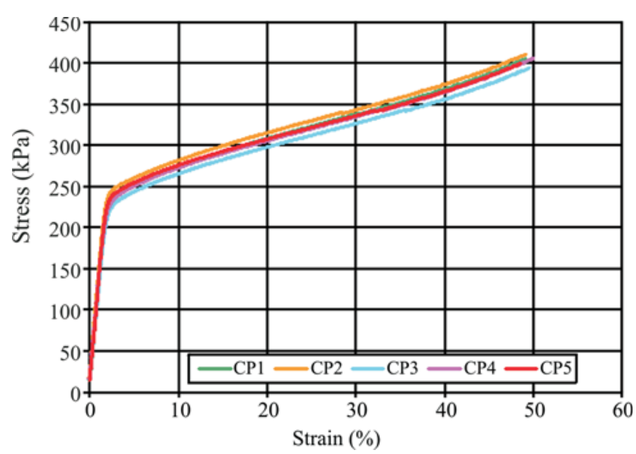

Figure 5 - Compression test result of 30 kg/m^3 EPS-geofoam sample.

at 10% strain), as seen in Figure 5, does not express its behavior adequately. The stress at 10% deformation is a parameter in the second straight-line just above the transition point that is around 2% of deformation.

Therefore, based on Fig. 5 that can be considered a typical stress x strain EPS-geofoam curve there is an elastic region from the beginning of the curve and extending to a value close to 2% of deformation, and a plastic part (over about 2% of deformation). At this stage the material undergoes a hardening behavior. Consequently, in a compression curve of EPS-geofoam one three distinctive points can be observed: (a) a tangent modulus of the elastic phase taken at 1% of deformation; (b) a transition stress adopted as the stress value at 2% of deformation – at this point there is a change in the slope of the curve; (c) a tangent modulus of the hardening stage for a strain above 2% (Fig. 6).

From about 350 compression tests performed, Figs. 7, 8 and 9 show the relationship between tangent modulus of the elastic phase, transition stress and tangent modulus of the hardening phase, respectively, varying with the density of EPS blocks. These figures show a good relationship between density and modulus and stress. Based on these data an EPS curve characterization by three key parameters is proposed, as shown in Fig. 6.

Correlations between the tangent modulus of the elastic phase and the density of EPS blocks were proposed using data from other researchers (van Dorp, 1988; Eriksson & Trank, 1991; Negussey & Sun, 1996; Duskov, 1997; Horvath, 1997; Elragi *et al.*, 2000; and Hazarika, 2006). Figure 10 shows these correlations and compares them with the one of this paper.

The curves obtained by Eriksson & Trank (1991), Duskov (1997) and Avesani Neto (2008) are a nonlinear power function of densities and elastic modulus in low-density cases. All the other curves are expressed as a linear expression. The higher curve of modulus was obtained by Elragi *et al.* (2000), followed by Duskov (1997) and the minor modulus was suggested by Negussey & Sun (1999).

The temperature influence on the compressive strength can be visualized in Fig. 11. The strength value is the average of three tests for each temperature.

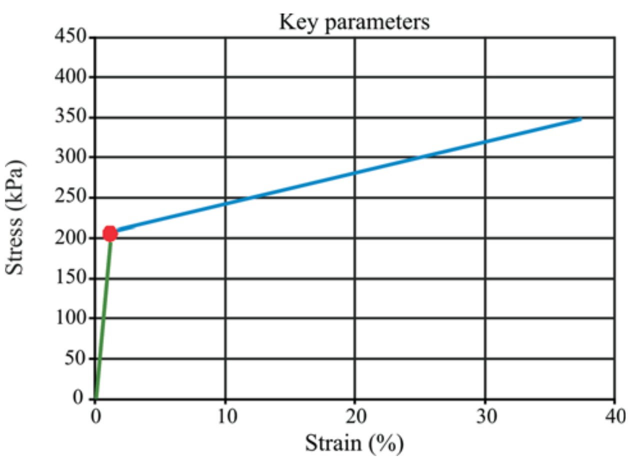

Figure 6 - Three key parameters of compressive behavior.

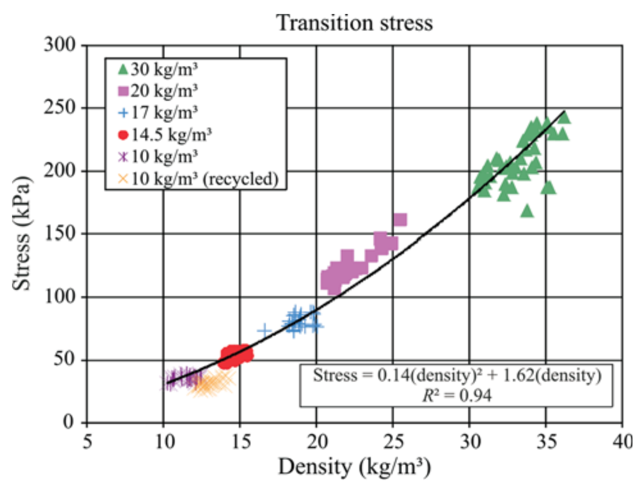

Figure 8 - Transition stress for EPS-geofoam samples.

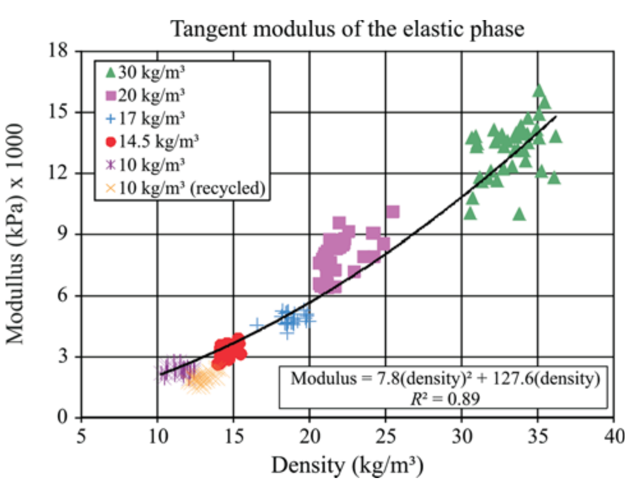

Figure 7 - Tangent modulus of the elastic phase for EPS-geofoam samples.

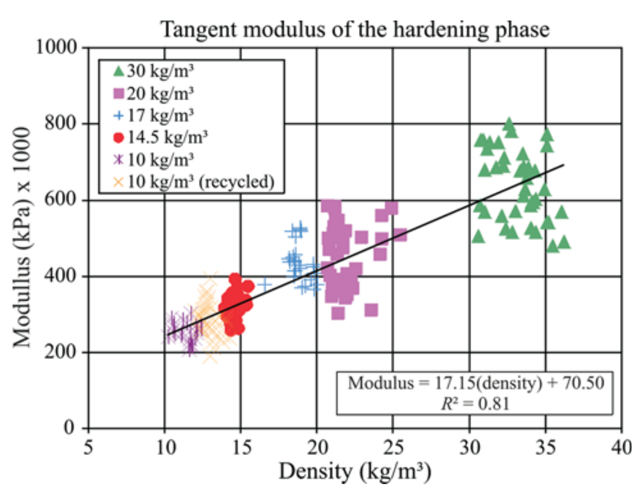

Figure 9 - Tangent modulus of the hardening phase for EPS-geofoam samples.

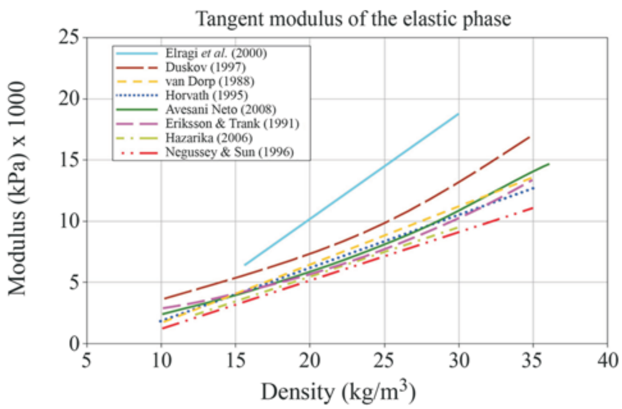

Figure 10 - Different relationships between density and tangent modulus of the elastic phase.

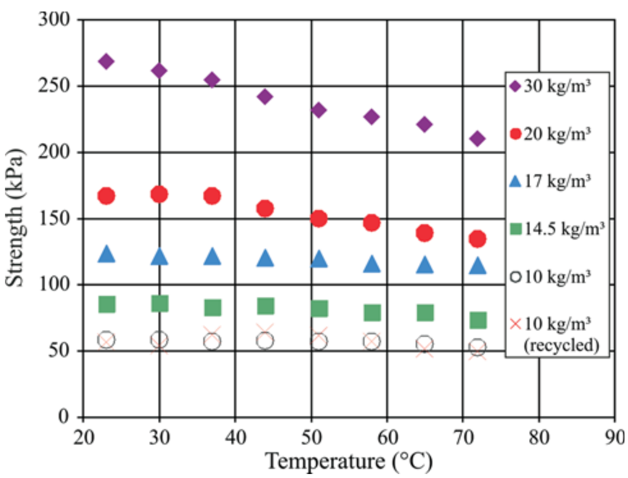

Figure 11 - Compressive strength *vs.* different temperatures.

Figure 11 shows a significant influence of temperature on the compressive strength of EPS-geofoam of higher density values (30 kg/m^3 and 20 kg/m^3) with strength reductions up to 20% for 50 °C changes in temperature. However, the material with lower density is not significantly affected by temperature. This behavior can be explained by the specimen density. Samples with higher density have a smaller amount of voids filled with air and a greater portion of polymer. This polymer portion is more significantly affected by the temperature change than the air in the voids, resulting in a strength reduction with temperature increase. A lower density has a greater amount of voids and a lower portion of polymer; consequently the specimen is less influenced by the temperature change.

Figure 12 shows the relationship between the strength obtained at each tested temperature and at the temperature of reference (in this case 23 °C) only for the densities that showed an appreciable loss of compressive strength (20 kg/m^3 and 30 kg/m^3).

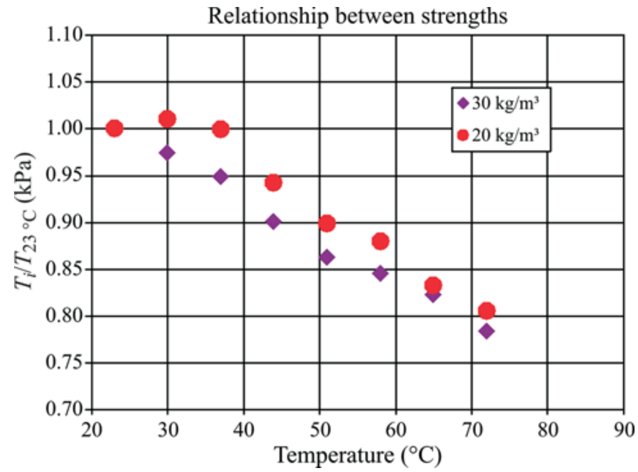

Figure 12 - Temperature influence in the 20 kg/m^3 and 30 kg/m^3 EPS-geofoams.

Figure 12 shows that the strength reduction exceeds 20% for temperatures of 72 °C. There is also a linear trend towards decreasing strength with increasing temperature.

The influence of the test speed and the specimens size was verified in the compressive strength. However, in both cases no significant influence of these variables was found on the EPS-geofoam behavior. Since this influence was less than 5%, the results were not analyzed.

3.2. Joint direct shear tests

The results of the joint direct shear testing in EPS samples of 10 kg/m^3 (with virgin and recycled material), 20 kg/m^3, 30 kg/m^3 and 40 kg/m^3 can be seen in Figs. 13 to 17.

The EPS mechanical behavior in shear tes is similar to the behavior of soil samples, as seen in these Figures. There is a peak value to the shear stress, similar to over-consolidated soils, followed by a reduction of stress due to change in the contact surface area of the blocks for the sample with higher densities (20 kg/m^3, 30 kg/m^3 and 40 kg/m^3). However, for the samples with lower density (10 kg/m^3 vir-

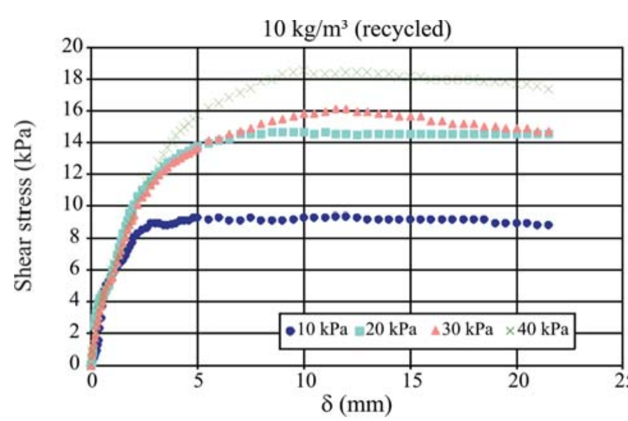

Figure 13 - Data of a direct shear test performed in the 10 kg/m^3 (recycled) EPS sample.

gin and recycled), the behavior is similar to normally consolidated soils, without a peak value.

Two failure envelopes were drawn from the tests data for each material: one with the peak friction angle, which was given the peak stress defined as the maximum shear stress, and another, called here "residual" friction angle, with a value of the shear stress corresponding to a displacement of 15 mm. Figures 18 and 19 show the failures envelopes for peak and residual friction angles for each density sample, respectively.

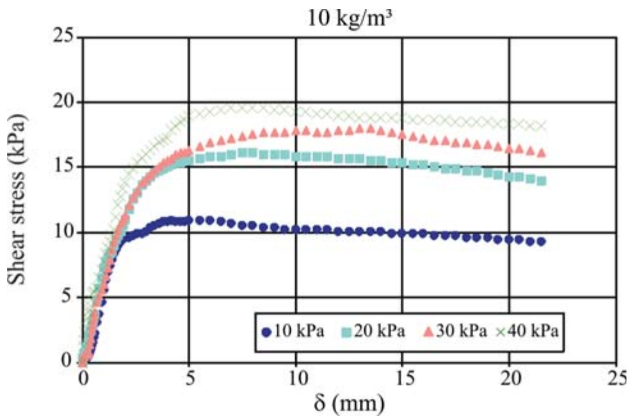

Figure 14 - Data of a direct shear test performed in the 10 kg/m^3 EPS sample.

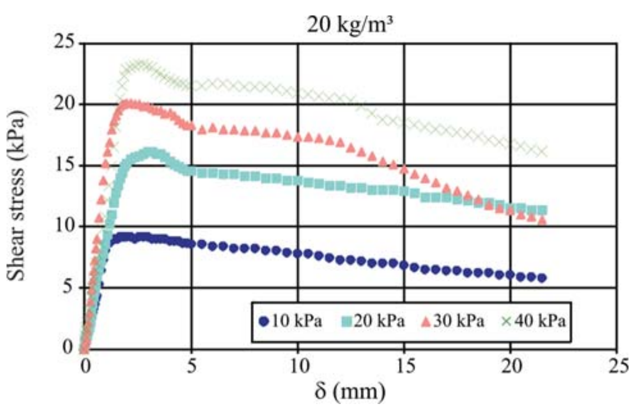

Figure 15 - Data of a direct shear test performed in the 20 kg/m^3

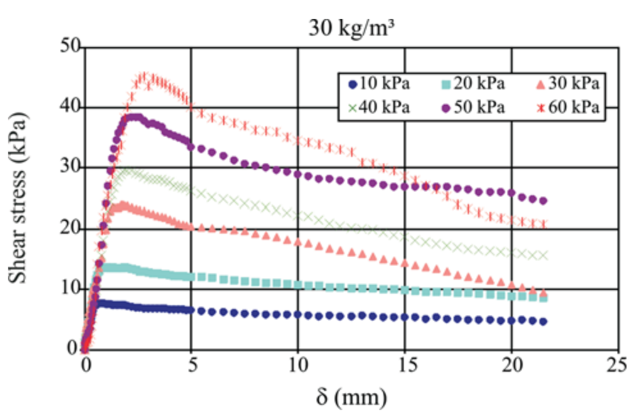

Figure 16 - Data of a direct shear test performed in the 30 kg/m^3 EPS sample.

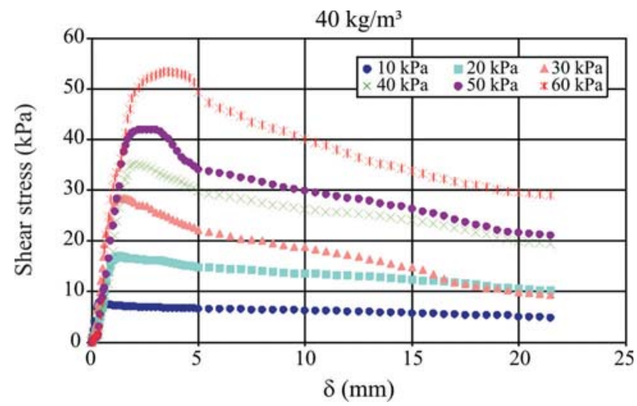

Figure 17 - Data of a direct shear test performed in the 40 kg/m^3 EPS sample.

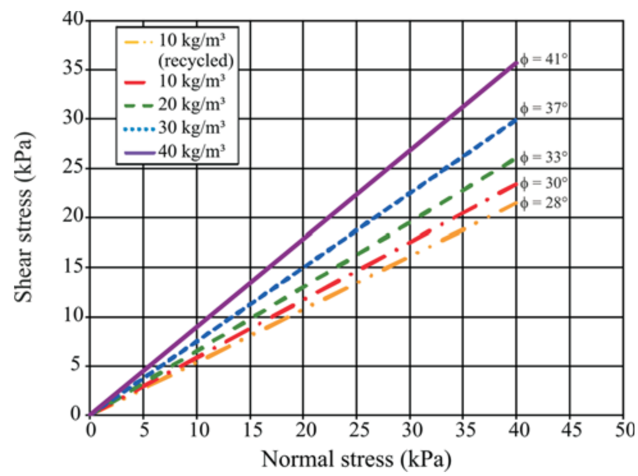

Figure 18 - Failure envelopes of EPS samples at the peak condition.

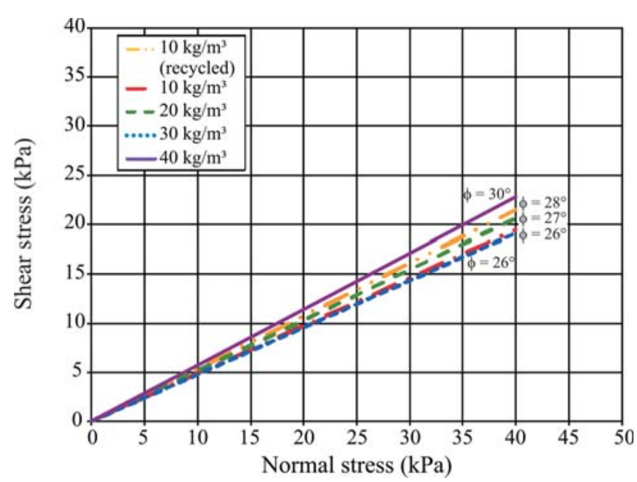

Figure 19 - Failure envelopes of EPS samples at the "residual" condition.

The friction angles obtained for all samples are relatively high for both peak and residual conditions, with values up to 41° (peak) and 30° ("residual"). Comparing the values of the friction angles of samples in each case a visible increase with density at the peak condition is noted. However, for the "residual" condition no significant change in the friction angle was observed with the density increase.

Comparing the results of the friction angles at peak and "residual" conditions, a considerable reduction is observed for samples with higher densities (Table 3).

Table 3 shows a greater reduction in the friction angle in the 30 kg/m^3 sample, lower reduction in the sample of 10 kg/m^3 virgin material, and conservation of the friction angle value in the sample containing recycled material. An explanation for this behavior is due to the contact surface of the material containing recycled EPS (and the sample of 10 kg/m^3 virgin material) which has a higher roughness on the specimens surface that prevent the formation of a lower friction efficiency region between the blocks and maintain the shear stress value at larger displacements.

The results allowed observing there is proportionality between the friction angle and the material density. For higher density values there is an increase in the friction angle at peak condition and reduction at "residual" condition. Thus, it is possible to establish a relationship between the average of friction angle (both for peak and "residual" conditions) with each sample for the average of density. These relationships provided a linear correlation between these two variables.

Figures 20 and 21 display the curves for the peak and "residual" conditions, respectively and the equation of better adjustment.

The figures show the proportionality between the friction angle and density. Although the recycled material has a higher density, it has poor mechanical characteristics if compared with the virgin material.

3.3. Creep in compression tests

The creep in compression tests were performed for a total time of 1000 h (about 42 days). The results of tests with specimens of 10 kg/m^3 (with virgin material), 17 kg/m^3, 20 kg/m^3 and 30 kg/m^3 can be seen in Figures 22 to 25, which indicate the nominal density, the average of measured density (in parentheses), the applied load and the relation between the applied load and the transition stress at 2% deformation.

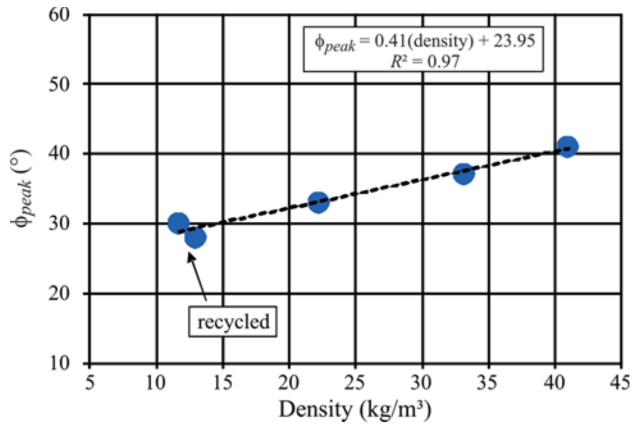

Figure 20 - Relationship between peak friction angle and density.

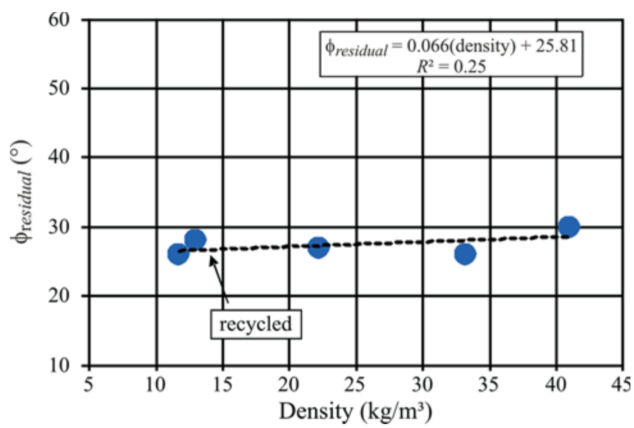

Figure 21 - Relationship between "residual" friction angle and density.

Figures 22 to 25 allowed concluding that the tested EPS material practically does not exhibit creep in compression. However the EPS geofoam has a significant value of initial strain (over 80% of the total strain in all cases) independently of the density and percentage of load applied in relation to the transition stress. A limited creep was observed in the cases whose relation between load applied and

Table 3 - Comparison between data of peak and residual friction angles tests.

Nominal density (kg/m^3)	Average density (kg/m^3)	ϕ at peak (°)	ϕ at 15 mm of displacement (°)	Reduction in function of tanϕ (%)
10 (recycled)	13.0	28	28	0.0
10	11.7	30	26	15.5
20	22.2	33	27	21.5
30	33.2	37	26	35.3
40	41.0	41	30	33.6

transition stress was over than 50%. For values for this ratio below than 50%, the creep is only marginal.

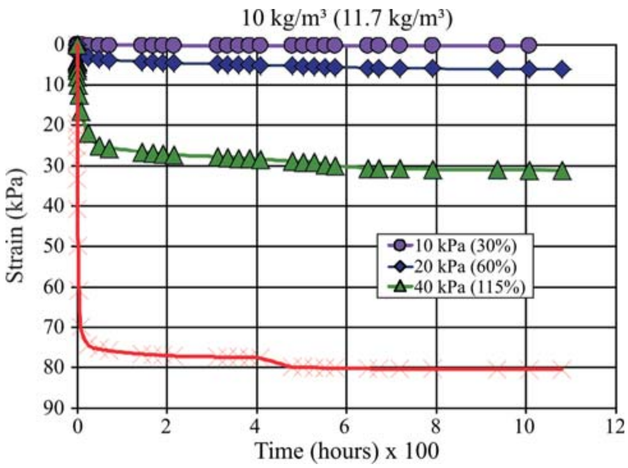

Figure 22 - Results of compression creep tests performed in the 10 kg/m^3 sample.

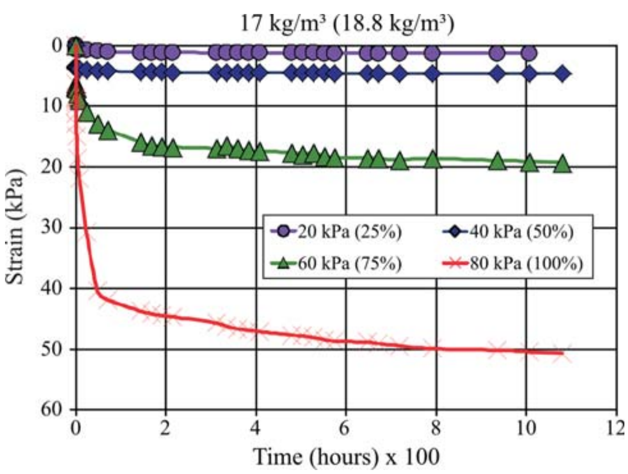

Figure 23 - Results of compression creep tests performed in the 17 kg/m^3 sample.

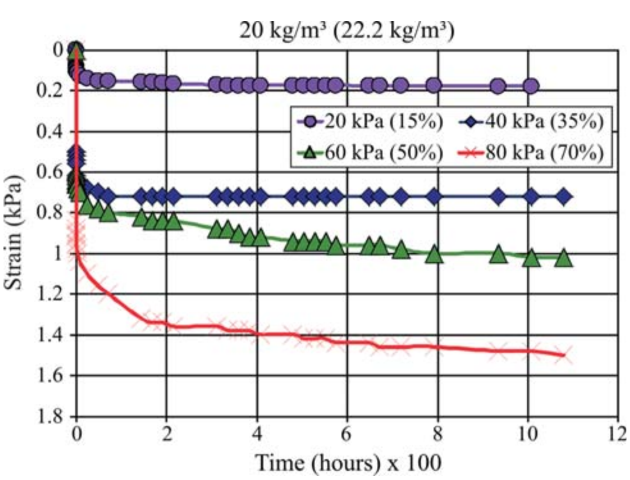

Figure 24 - Results of compression creep tests performed in the 20 kg/m^3 sample.

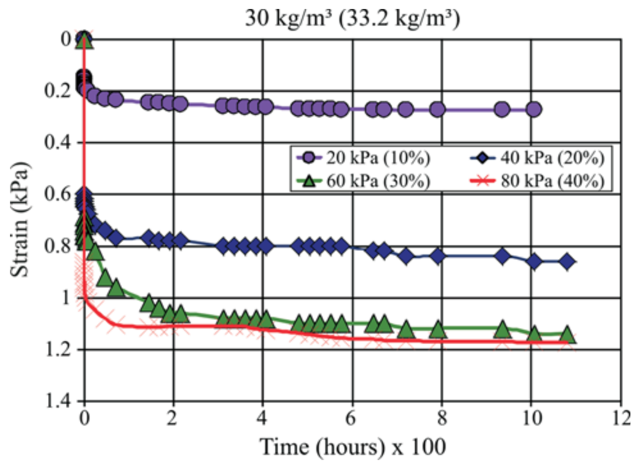

Figure 25 - Results of compression creep tests performed in the 30 kg/m^3 sample.

The creep with a very low value can be explained by the void reduction during the loading. After an initial deformation, the samples exhibit a void decrease, causing strength improvement and reduced specimens creep.

Figure 26 shows the relationship between the recorded strains and the density of all samples for different values of applied load in the same load exposure time (1000 h).

The 10 kg/m^3 sample exhibits a higher strain – almost 10% - for a load of 20 kPa (60% of the transition stress) after 1000 h of loading application. Moreover, the 17 kg/m^3 sample showed greater strain only for a load exceeding 40 kPa (50% of the transition stress). However even for a higher stress value such as 80 kPa, samples of 20 kPa and 30 kg/m^3 showed small strains.

3.4. Loss weight test by mice attack

Table 4 shows the result of loss weight test by mice attack on EPS. This value of weight loss is for a one mouse after 48 h of exposure with specimens.

Table 4 shows there are relatively high values of mass loss only in the case of straw deprivation. For a better view of the data, a chart with these values is shown in Fig. 27.

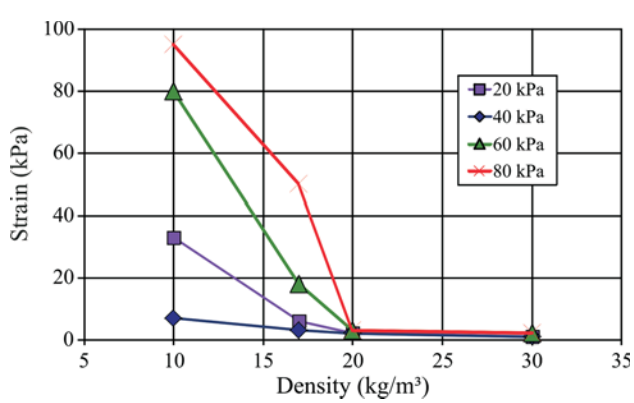

Figure 26 - Relationship between strain and density for each applied load.

Table 4 - Result of loss weight test by mice attack.

Nominal density (kg/m^3)	Total deprivation			Straw deprivation			Food deprivation		
	Initial mass (kg)	Final mass (kg)	Loss (%)	Initial mass (kg)	Final mass (kg)	Loss (%)	Initial mass (kg)	Final mass (kg)	Loss (%)
30	0.016	0.015	9	0.016	0.0095	40	0.017	0.016	5
20	0.012	0.012	4	0.013	0.0070	44	0.012	0.012	1
17	0.0094	0.0089	6	0.0094	0.0076	19	0.0095	0.0094	1
14.5	0.0081	0.0079	3	0.0083	0.0051	38	0.0080	0.0079	1
10	0.0060	0.0057	5	0.0061	0.0047	24	0.0057	0.0056	1
10 (recycled)	0.0070	0.0066	5	0.0072	0.0049	32	0.0068	0.0067	2
		Average	5		Average	33		Average	2

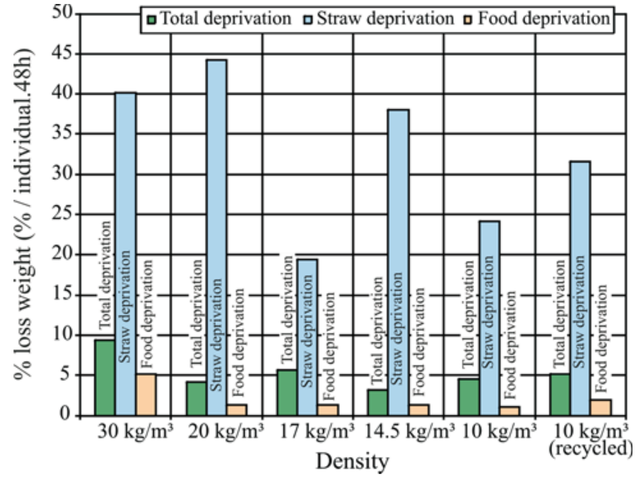

Figure 27 - Result of all loss weight tests by mice attack.

According the Fig. 27, the mass loss was small for two of the case (total and food deprivations) and extremely high in the case of straw deprivation because with the food deprivation the individuals enter in a low activity state to save energy. When there is no lack of food, the animal is in its state of normal activity and attacks the EPS samples to build its nest and generate physical comfort, as seen in Fig. 28. It was observed that there is not a relationship between the samples densities and the mice attack.

It should be considered in this study, for reasons of the available infrastructure for conducting the test, that the individuals were confined with the material, which may have aggravated the attack. However, it is important to observe that the value of mass loss was produced by only one laboratory mouse in a 48 h period. For a colony with larger and more aggressive wild rats and for a long period of time, the mass loss would probably be higher. The approach of this test, therefore, stands out for qualitative analysis of the attack, and not for a precise quantitative research of the mass loss value.

To visually quantify the attack of these animals in the samples, Fig. 28 shows the specimens tested in each case: a virgin specimen (before the test) and the specimens tested under food deprivation, total deprivation, and straw deprivation, respectively from left to right.

Figure 28 shows the elevated attack on the specimen tested under straw deprivation in comparison with the others deprivation. It must be emphasized that were used small size samples in the tests. There are reports that in large blocks – as occurs in real EPS apliccation – the rodents are installed inside them in order to form nests. However, by performing a correct cover of material with the soil in the works, avoiding exposing the EPS, risk of these animals attack the blocks can be reduced.

4. Conclusions

Several mechanical tests such as unconfined axial compression – with temperature variation, direct shear of

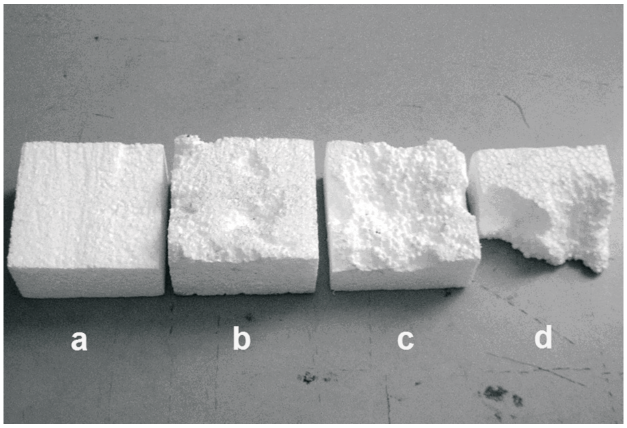

Figure 28 - Tested specimens: a) before the test; b) food deprivation; c) total deprivation; d) straw deprivation.

block joint and creep in compression – were performed in EPS geofoam samples with densities of 10 kg/m^3 (virgin and recycled), 14.5 kg/m^3, 17 kg/m^3, 20 kg/m^3, 30 kg/m^3 and 40 kg/m^3 aiming at their applications in geotechnical engineering. A simple mass loss test by mice attack was also conducted.

The main conclusions of this paper are:

- The current compressive strength definition (at 10% strain) does not express adequately its behavior;
- The material presents a well-defined elastic phase under 2% compression strain;
- The EPS-geofoam compression characterization by three key parameters (tangent modulus of elastic, hardening phases and transition stress) is relatively simple and effective and can be used in subsequent tests;
- The results from compression tests with temperature variation have showed a further influence on the EPS-geofoam strength of samples with densities of 20 kg/m^3 and 30 kg/m^3 with decreases of approximately 15% and 25%, respectively;
- The test speed and specimen size do not significantly affect the compressive strength results;
- The joint direct shear tests showed that the behavior of high-density EPS is similar to that of overconsolidated soils with a peak value of friction angle between 33° and 41°. For the lower-density EPS blocks, the behaviour was similar to normally consolidated soils, with a post-peak friction angle between 28° and 30°;
- The shear strength and consequently the friction angle and the failures envelope are directly proportional to the sample density;
- The reduction in the friction angle values from the peak to post-peak condition was high in EPS samples, reaching up to 30%. This reduction was more expressive at higher densities.
- The initial strain controls the creep in the compression of EPS;
- A limited creep was observed in the cases whose relationship between the applied load and the transition stress was larger than 50%;
- The result of mass loss test by mice attack showed a large loss in the specimen attacked. The most critical attack was recorded under the straw deprivation condition when the animal, in the presence of food, maintains the state of high metabolism and attacks the samples to build its nest and generate physical comfort;
- The values of the mass loss tests illustrate only a qualitative point of view of the phenomenon – proving the assertion of some practical cases – and not a quantitative analysis.

Acknowledgments

The authors would like to acknowledge CAPES (Coordenação de Aperfeiçoamento de Pessoal de Nível Superior) for financing the research of the first author and the Department of Geotechnical Engineering, especially the Laboratory of Geosynthetics, Engineering School of Sao Carlos, University of Sao Paulo (EESC – USP) for the technical support.

References

ASTM (2007) Standard Test Method for Dimensions and Density of Performed Block – Type Thermal Insulation – C 303-10. ASTM International, West Conshohocken, Pennsylvania, USA, 3 pp.

ASTM (2000) Standard Test Method for Compressive Properties of Rigid Cellular Plastics – D 1621-10. ASTM International, West Conshohocken, Pennsylvania, USA, 5 pp.

ASTM (2001) Standard Test Method for Tensile, Compressive and Flexural Creep and Creep – Rupture Plastics – D 2990-09. ASTM International, West Conshohocken, Pennsylvania, USA, 20 pp.

ASTM (1998) Standard test method for direct shear tests of soils under consolidate drained conditions – D 3080/D3080-11. ASTM International, West Conshohocken, Pennsylvania, USA, 9 pp.

ASTM (1995) Standard Test Method for Evaluating the Unconfined Tension Creep Behavior of Geosynthetics – D 5262-07. ASTM International, West Conshohocken, Pennsylvania, USA, 16 pp.

Avesani Neto, J.O. (2008) Characterization of Geotechnical Behavior of EPS through Mechanical and Hydraulic Tests. MSc Dissertation. Engineering School of Sao Carlos, University of Sao Paulo, São Carlos, Brazil, 228 pp. (in Portuguese).

Barrett, J. & Valsangkar, A.J. (2009) Effectiveness of connections in construction. geotextiles and Geomembranes, v. 27:3, p. 211-216.

Beinbrech, G. & Hillmann R. (1997) EPS in road construction – Current situation in Germany. Geotextiles and Geomembranes, v. 15:1, p. 39-57.

Bueno, B.S. (2005) Experimental Evaluation of Mechanical Behavior of EPS samples. Technical Report, Laboratory of Geosynthetic, Department of Geotechnical Engineering, EESC, USP, 34 pp. (in Portuguese).

Duskov, M. (1997) Materials research on EPS20 and EPS15 under representative conditions in pavement structures. Geotextiles and Geomembranes, v. 15:1, p. 147-181.

Elragi, A.; Negussey, D. & Kyanka, G. (2000) Sample size effects on the behavior of EPS Geofoam. Proc. the Soft Ground Technology Conference, ASCE Geotechnical Special Publication, 112. Noordwijkerhout, The Netherlands, pp. 280-291.

Eriksson, L. & Trank, R. (1991) Properties of Expanded Polystyrene, Laboratory Experiments. Swedish Geotechnical Institute, Linköping, Sweden.

Hazarika, H. (2006) Stress-strain modeling of EPS geofoam for large-strain applications. Geotextiles and Geomembranes, v. 24:2, p. 79-90.

Horvath, J.S. (1994) Expanded polystyrene (EPS) geofoam: An introduction to material behaviour. Geotextiles and Geomembranes, v. 13:4, p. 263-280.

Horvath, J.S. (1995) Non-earth subgrade materials and their thermal effects on pavements: An overview. Transportation Research Board, 74th Annual Meeting, Paper No. 95-0069, Washington, 18 pp.

Horvath, J.S. (1996) The compressible inclusion function of EPS geofoam: An overview. Proc. International Symposium on EPS Construction Method, Tokyo, pp. 71-81.

Horvath, J.S. (1997) The compressible inclusion function of EPS geofoam. Geotextiles and Geomembrane, v. 15:1-3, p. 77-120.

Ikizler, S.B.; Aytekin, M. & Nas, E. (2008) Laboratory study of expanded polystyrene (EPS) geofoam used with expansive soils. Geotextiles and Geomembranes, v. 26:2, p. 189-195.

Murphy, G.P. (1997) The influence of geofoam creep on the performance of a compressible inclusion. Geotextiles and Geomembranes, v. 15:1-3, p. 121-131.

Negussey, D. & Sun, M. (1996) Reducing lateral pressure by geofoam (EPS) substitution. Proc. International Symposium on EPS Construction Method. Tokyo, pp. 202-11.

Piana, M. (1997) Construzione di strade, ferrovie ed aeroporti. Piana, M. (Ed.) Isolare le Fundazioni con I'EPS. Be-Ma, Milano, pp. 57-81 (in Italian).

Sheeley, M. (2000) Slope Stabilization Utilizing Geofoam. MSc Dissertation. Syracuse University, New York.

Sheeley, M. & Negussey, D. (2000) An investigation of geofoam interface strength behavior. American Society of Civil Engineers, Geotechnical Special Publication No. 112. Proceedings of the Soft Ground Technology Conference, Noorwijkerhout, The Netherlands.

Stark, T.D.; Arellano, D.; Horvath, J.S. & Leshchinsky, D. (2004) Geofoam applications in the design and construction of highway embankments. NCHRP Document 65 (Project 24-11). TRB of the National Academies, USA.

Sun, M.C. (1997) Engineering Behavior of Geofoam (Expanded Polystyrene) and Lateral Pressure Reduction in Substructures. MSc Dissertation. Syracuse University, New York.

van Dorp, T. (1988) Expanded Polystyrene Foam as Light Fill and Foundation Material in Road Structures. The International Congress on Expanded Polystyrene: Expanded Polystyrene, Milan.

Yeo, S.S. & Hsuan, Y.G. (2006) The compression creep behavior of an expanded polystyrene geofoam. Proc. 8º International Conference on Geosynthetics. Yokohama, v. 4, pp. 1639-1642.

Contribution to the Design of Urban Pavement of Low Volume Traffic Using the Dynamic Cone Penetrometer

H.P. Jordão, A.E.F.L. Lucena, M.B. Chagas Filho, J.K.G. Rodrigues, D.A. Gama

Abstract. The characteristics of the subgrade soil, obtained from laboratory and in situ tests, are of fundamental importance to the design of pavements. The tests carried out in the field, such as CBR in situ, Bredboard and others, represent more significantly the conditions of the soil. The Dynamic Cone Penetrometer (DCP) is an equipment of easy use that has become an alternative to the pavement design. With that kind of equipment it is possible to determine the resistance profile to the penetration of the layers of the compacted soil or in its natural state from the correlations between this test and the CBR *in situ*. This work attemps to adequate a design method for urban pavements of low volume traffic, using the results of the penetration index obtained with the DCP. The results indicate that the DCP presents a high correlation with CBR *in situ* tests for A-2-4 soils, which can be used in pavement design of urban roads of low volume traffic.

Keywords: design of pavements, dynamic cone penetrometer, CBR *in situ*.

1. Introduction

The search for new methods of pavement design aims at greater savings or greater security when compared to traditional methods. Urban roads of low volume traffic must be designed for such request and not the same way as highways, which causes larger amount of pavements.

One of the very first design methods, established by the California Highway Department, in 1939, was based in the CBR (California Bearing Ratio) and until today keeps the same principles. The methods that use as parameters the CBR *in situ* ME-47 (PMSP, 1999) and/or the Plate load Test (ASTM D-1196, 2004), despite of favoring an analyses closer to reality, they become more costly and slower due to the high cost of the equipments and its execution.

An alternative of using a more simple method and of low cost is to use the Dynamic Cone Penetrometer (DCT), and then, its correlation with the CBR *in situ*, which could bring a great economy in the pavement of streets of low volume traffic.

2. Pavement Project

To elaborate a pavement design it is necessary to perform geotechnical studies in the place, which involve studies of the subgrade and of occurrence of materials for pavement that will suit as raw material in the execution of the layers that constitute the pavement.

The aim of studying the subgrade of the roads is the recognition of the soils and of its bearing capacity, for the characterization of its various layers for the effect of the pavement design.

2.1. Determination of the soil capacity *in situ*

Among the several existing methods for determining the soil capacity *in situ*, the Dynamic Cone Penetrometer (DCP) and CBR *in situ* are presented.

2.1.1. Dynamic Cone Penetrometer - DCP

The development of the DCP arouse from the necessity of evaluating, simple and quickly, the subgrade conditions of a certain pavement. The use of this equipment has gained more and more adepts in the last years in a national and international scale, and consequently, the necessity of having the analysis and results that generate more trusty correlations becomes ever increasing (Amaral, 2005).

According to Alves (2002), this test does not require great diggings or perforations, and consequently does not interfere in the traffic of vehicles. This can be characterized as a semi non-destructive test.

The Dynamic Cone Penetrometer (DCP) is an equipment which provides the rate of penetration carried out in non-deformed soils or compacted materials.

The DCP is performed with the help of two people. The length in millimeters that the rod penetrates in the soil, in relation to a determined number of hits, is measured. The results are noted in a pattern spreadsheet where it is indicated the depth versus the number of applied hits. The DCP was designed to penetrate to a middle depth of 800 mm or when rod extension is settled, it can reach a depth of 1.200 mm.

Hugo Pimentel Jordão, MSc, Universidade Federal de Campina Grande, Campina Grande, PB, Brazil, e-mail: hpjordao@yahoo.com.br.
Adriano Elísio de Figueiredo Lopes Lucena, DSc, Professor, Universidade Federal de Campina Grande, Campina Grande, PB, Brazil, e-mail: lucenafb@uol.com.br.
Milton Bezerra das Chagas Filho, DSc, Professor, Universidade Federal de Campina Grande, Campina Grande, PB, Brazil, e-mail: miltoncf@gmail.com.
John Kennedy Guedes Rodrigues, PhD, Professor, Universidade Federal de Campina Grande, Campina Grande, PB, Brazil, e-mail: jkennedy@dec.ufcg.edu.br.
Dennyele Alves Gama, Engenheira Civil, Universidade Federal de Campina Grande, Campina Grande, PB, Brazil, e-mail: dennyelealves@gmail.com.
Submitted on August 17, 2011; Final Acceptance on August 6, 2012; Discussion open until December 29, 2012.

According to Herrick & Jones (2001, apud Guedes, 2008) the measurements of the penetrometer cone can be expressed as the number of hits by millimeter of penetration or as the agerage resistance of the soil by depth of the penetrated soil. This approach does not presume uniformity of the soil, simply generates an average resistance through the depth penetrated by the cone. These average numbers are more informative to soils, which are relatively uniform inside the advance in the depth penetrated in each hit.

It is showed in a graphic the values of the readings obtained from the penetration versus the number of hits. Generally the number of hits is plotted in graphic in the abscissas axis, while the penetration, in the ordered axis (Fig. 1). The DCP curve obtained represents the number of hits to reach a certain depth.

The soil resistance *in situ* is represented by the penetration indexexpressed by:

$$\mathrm{DCP} = \frac{\mathrm{Depth}}{\mathrm{N.\ of\ Hits}} \tag{1}$$

Depending on the type of the material that constitutes the layer of the pavement or its conditions of water content and density, the inclination of the curve changes: when upright, it indicates materials with minor support capacity and when closer to the horizontal, the greater will be its resistance.

2.1.2. CBR in situ

The CBR *in situ* test provides the resistance of the soils, in field, when it is under a certain load. The test method was developed by the United States Army Corps of Engineers (USACE).

The equipment of the CBR *in situ* is composed by a piston of penetration with 4.96 cm of diameter, ring dynamometer with capacity to 4000 kg sensible to 2.5 kg duly calibrated, jack with capacity of 4 tons, capable of providing continuous addition of load, beam of reference with 1 meter of length, comparable watch with dispositive for its fixing in the penetration piston, steel curled discs for overload, divided diametrically in two parts, with 2.268 kg of total weight, with external diameter of 14.92 cm and inner diameter of 5.39 cm and a heavy vehicle or anchor system that provides an reaction equal or superior to 5 tons.

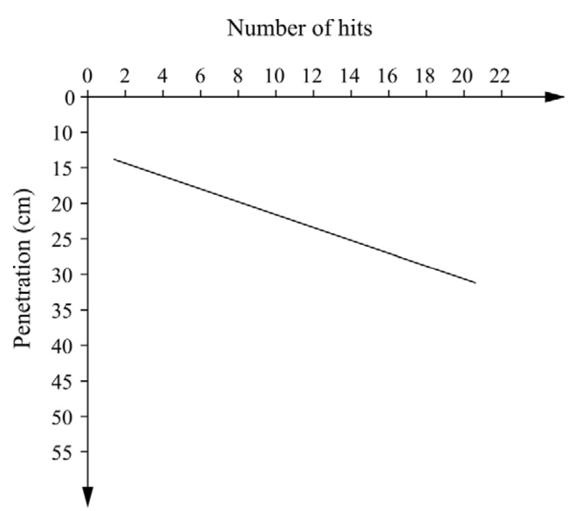

Figure 1 - Graphic of DCP.

According to Yoder (1959, apud Berti, 2005) the test is carried out by similar manner to the laboratory, where the piston of 19.63 cm^2 is forced to press the pavement and compare to the load on the piston with the penetration depth. According to Pattrol (2009), to a test *in situ*, the load reaction is provided by the weight of a loaded truck. The equipment is composed of a mechanic jack, adjusted to the back part of the mobile laboratory, a dynanometric ring, the piston and the connections.

The method of test ME-49/99 - Determination of the Support Index of the Subgrade *in situ*, adopted by the Secretary of Public Roads of the city of São Paulo, determines the support index *in situ* of the various layers of the pavement in its natural state.

According to the standard method, the equipment set (piston, ring and jack) is arranged over the leveled surface, in a way that it stays vertically below of the reaction point of the loaded vehicle. The reference beam is placed leaned by its extremities in two supports equally kept away from the test place, in such a way that the deflectometer rooted in the piston leans in the surface of the beam. Overload discs that are often used in laboratorial CBR loading are placed over the surface around the piston. The load application is initiated with the velocity of 1.27 mm/min, carrying out the readings, calculation of the pressures and graphic representation like the one carried out in the laboratorial test.

2.2. Correlation of results of the CPD with the CBR

The correlations between the DCP and CBR are obtained by the regression analysis of the results. According to Karunaprema & Edirisinghe (2002), these patterns show that there is an inverse relation between the DCP and the CBR for the tested soils. The data can be analysed by linear, log, exponential or bi-log (log x log). The mathematical pattern that better describes the relation CBR X DCP is the one of log x log, with the CBR being the dependent variable and the DCP the independent variable, as given by:

$$\log(\mathrm{CBR}) = a + b.\log(\mathrm{DCP}) \tag{2}$$

where CBR = California Support Index (% in percentage), DCP = Penetration Index of the DCP (mm/hit); and a and b = constants that can vary according to the author of the research.

Table 1 presents some equations of correlation between DCP and CBR.

3. Materials and Methods

3.1. Choice of the test locations

Several locations of different districts of Campina Grande were chosen and studied, located in the state of Paraíba, Brazil, encoded as shown in Table 2.

Table 1 - Correlation DCP X CBR.

Correlations DCP X CBR		
Author	Region of the studied soil	Equation of correlation
Trichês & Cardoso (1999)	Duplication of the BR-101/SC	log(CBR) = 2.710-1.250.log(CPD) log(CBR) = 2.181-1.030.log(CPD)
Lima (2000)	Maringá/PR, Taubaté/SP, Palmas/To & São Carlos/SP	log(CBR) = 2.809-1.288.log(CPD)
	Estado do Paraná	log(CBR) = 2.647-1.300.log(CPD)
Silva Junior (2005)	Airport of Parnaiba/PI - BR	log(CBR) = 2.717-1.247.log(CPD)
Harison (1987)	Indonésia cohesive and graned	log(CBR) = 2.810-1.320.log(CPD) log(CBR) = 2.550-1.140.log(CPD)

Two inspection wells were dug in opposite sides to the axes of the streets, aiming this way, a more representative character to the procedure of data acquisition. The wells for physic and mechanic characteristics analysis of the subgrade soil were dug in a depth where it found the natural soil, therefore the depths of the inspection wells varied.

All tests *in situ* were carried out in the month of July of 2009. July is in the rainy period to this region, becoming the best period for the study of the behavior of the soils of the subgrade because it is more unfavorable for the pavement.

3.2. Procedures

The sequence of the works carried out during the experimental phase is illustrated in Fig. 2.

The tests carried out in laboratory and *in situ*, and its respective Standards (Table 3).

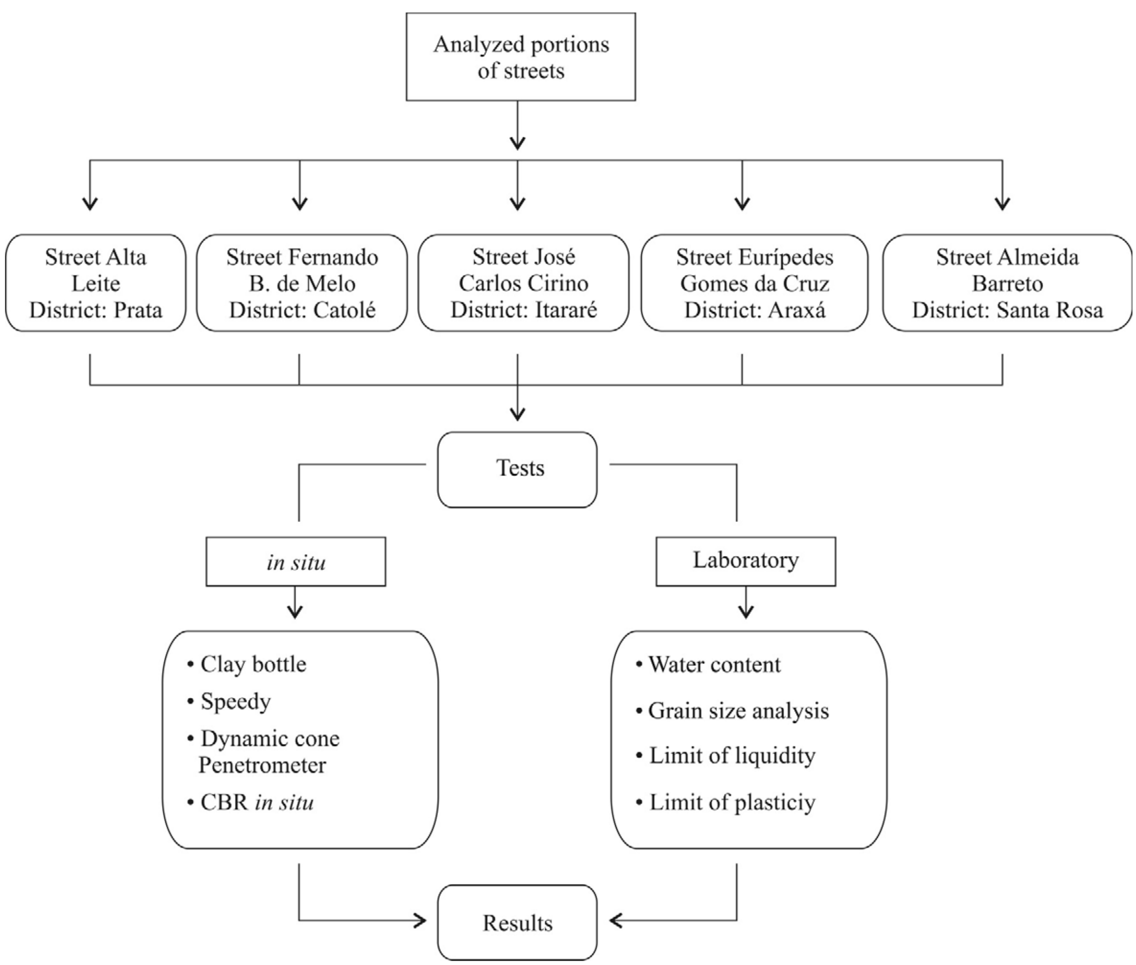

Figure 2 - Sequence of activities carried out during the experimental phase of the work.

Table 2 - Name of the streets and localization.

Inspection well	Street Name	District
AL- 01	Alta Leite - PI-01	Prata
AL- 02	Alta Leite - PI-02	Prata
FBM - 01	Fernando Barbosa de Melo - PI-01	Catolé
FBM - 02	Fernando Barbosa de Melo - PI-02	Catolé
JCC	José Carlos Cirino	Itararé
EGC - 01	Eurípedes Gomes da Cruz - PI-01	Araxá
EGC - 02	Eurípedes Gomes da Cruz - PI-02	Araxá
AB - 01	Almeida Barreto - PI-01	Santa Rosa
AB - 02	Almeida Barreto - PI-02	Santa Rosa

The tests carried out *in situ* and its respective Standards are shown in Tables 3 and 4.

4. Presentation and Results Analysis

4.1. Tests in laboratory

The classification and characterization tests of the collected samples were carried out for each inspection well.

The classifications of the samples obtained from the subgrade soils were made according to the methods HBR (Highway Research Board) and USCS (Unified System of Classification of Soil) since these systems are more commonly used. The results are found in Table 5.

The results of the carried out test indicates that the soils of the subgrade are predominantly a silty clay classified as A-2-4 and SM. The soil of the inspection well FBM-01 fits as A-6 and CL, which characterizes sandy soils, the soil of the well FBM-02 is A-4 and SC therefore a sandy clay and the well EGC-02 characterizes as A-1-b and SW that means gravel soil or well stuck clay.

Therefore, it is important to mention that the majority of the analysed soils are classified as of good quality to be used as subgrade in the pavement of streets, due to its behavior and for the possibility of stabilization with ligands.

4.2. Dynamic cone penetrometer

For each inspection well four penetrations were carried out with the DCP aiming to obtain a average index for each one of these wells. In the execution of the test it was considered the first hit of the hammer.

Table 3 - Laboratory tests.

Test	Standard
Preparation of the samples	NBR-6457 (ABNT, 1996)
Water content	ME-213 (DNER, 1994)
Grain size analysis	ME-080 (DNER, 1994)
Limit of liquidity	ME-122 (DNER, 1994)
Limit of plasticity	ME-082 (DNER, 1994)

Table 4 - *In situ* tests.

Test	Standard
Clay Bottle	ME-092 (DNER, 1994)
Speedy	ME-052 (DNER, 1994)
DCP	ASTM D 6951-03
CBR *in situ*	ME-47 (City Hall of Sao Paulo, 1999)

Table 6 presents the results of the average penetration index obtained from the tests of the Dynamic Cone Penetrometer (DCP).

The results of the penetration indexes indicate a higher resistance to the penetration of the tested soils in the FBM-02 and AB-01, which are classified as sandy clay and silty clay.

4.3. CBR *in situ*

The tests of CBR *in situ* were carried out in inspection wells until it reached the depth necessary to find the natural soil. The results are presented in Table 7.

It is possible to note that the higher values of CBR were obtained in the inspection wells EGC - 02 and AB - 01 which have soils SW and SM.

4.4. Analysis of the results: CPD *vs.* CBR *in situ*

The results of the Penetration Index (DN) obtained with the Dynamic Cone Penetrometer were correlated with the values of the CBR *in situ* for each inspection well. Table 8 presents the values of DCP and the respective CBRs *in situ*.

The CBR in situ values are outlier because the locations, type of soils and confinement conditions are different.

Table 5 - Results of soil classification.

Classification method	Inspection wells								
	AL-01	AL-02	FBM-01	FBM-02	JCC-01	EGC-01	EGC-02	AB-01	AB-02
HRB	A-2-4	A-2-4	A-6	A-4	A-2-4	A-2-4	A-1-b	A-2-4	A-2-4
SUCS	SM	SM	CL	SC	SM	SM	SW	SM	SM

Table 6 - Results of the tests of the Dynamic Cone de Penetrometer.

	Penetration index - DN - (mm/hit)								
Inspection well	AL- 01	AL- 02	FBM - 01	FBM - 02	JCC	EGC - 01	EGC - 02	AB-01	AB - 02
DCP	18.40	15.00	6.40	18.60	17.30	11.70	12.50	9.50	13.50

Table 7 - Results of the test of CBR *in situ*.

	CBR *in situ*								
Inspection well	AL- 01	AL- 02	FBM - 01	FBM - 02	JCC	EGC - 01	EGC - 02	AB - 01	AB - 02
CBR (%)	24.83	38.9	16.58	14.62	24.27	38.14	53.27	59.1	40.71

Table 8 - Results of the CPD to the respective CBR *in situ*.

Inspection well	DN (mm/hit)	CBR *in situ* (%)
AL- 1	18.40	24.83
AL- 2	15.00	38.90
FBM - 1	6.40	16.58
FBM - 2	18.60	14.62
EGC - 1	11.70	38.14
EGC - 2	12.50	53.27
AB - 1	9.50	59.10
AB - 2	13.50	40.71
JCC	17.30	24.27

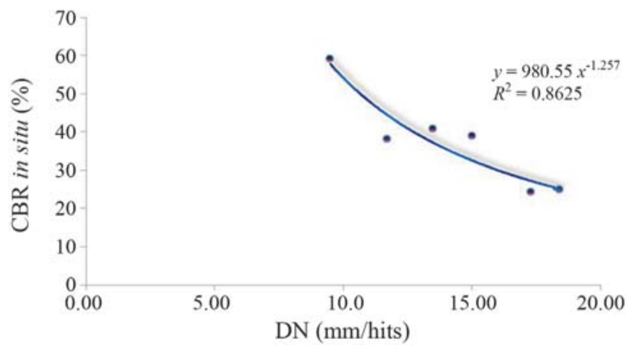

Figure 3 - Correlation between DCP x CBR *in situ*.

As shown in Table 5, the found soils were in its majority, A-2-4 kind, because it is a silty clay. Therefore, the results of the DCP and CBR *in situ* were correlated to the soils A-2-4 kind.

Figure 3 shows the correlation graphic of the DCP x CBR *in situ* to the materials classified according to the HRB as A-2-4 that are silty clays.

The regression equation correlating the CBR *in situ* and DCP indexes, relating the curve of the graphic, from the adopted model will be (Eq. 3):

$$\log(\mathrm{CBR}) = 2.98 - 1.257.\log(\mathrm{DCP})$$

or

$$\mathrm{CBR} = 950.55.\mathrm{CPD}^{-1,257} \tag{3}$$

Table 9 presents, in a detailed form, the results of the CBR obtained by means of the equations determined by the correlations in function of the penetration indexes of the DCP to the soils A-2-4.

Analysing the values of the calculated CBRs by the proposed equation the values are quite closer to the ones found in field, except by the wells FBM - 01, FBM - 02 and EGC - 02 where it is found soils silty and gravel types.

It is also observed, that the founded equation is equivalent to the known values in the bibliography, presented in Table 1.

4.5. Proposed urban pavements design method

The method suggests the design of urban pavements based in the following characteristics:

- with two tracks of traffic variation: very light and light traffic;
- in the structural characteristics of the subgrade, obtained in the field, in case of this research the acquired results with the test of the DCP, expressed in penetration index (mm/hit);
- in the thicknesses recommended by U.S. Corps of Engineers for urban pavements with low volume traffic;
- and in designed cross sections of urban pavements types suggested by the City Hall of São Paulo (PMSP), what allows a quick convergence to a determinate kind of pavement.

The presentation of the design method proposed obeys to the following sequence: subgrade, traffic and the layers of the pavement.

4.5.1. Subgrade

The subgrade soil will be presented by its capacity of support that is given from the results of the test with DCP considering, to the calculation of the penetration index with the first hit of the hammer.

This procedure is not applied to the calculation of the total thickness of the pavement in case of subgrades with

Table 9 - Values of CBR, obtained from the equation of correlation to the soils A-2-4, in function of the penetration indexes obtained with the CPD.

Well	DN (mm/hit) cons. o 1° hit	CBR (%)
AL- 01	18.40	24.44
AL- 02	15.00	32.69
FBM - 01	6.40	92.17
FBM - 02	18.60	24.11
EGC -01	11.70	43.19
EGC - 02	12.50	39.73
AB - 01	9.50	56.10
AB - 02	13.50	36.06
JCC	17.30	26.41

penetration indexes superior to 134.75 mm/hit, because, with these results it is obtained subgrades with low capacity of support (CBR ≤ 2%). In this case the subgrade soil must be substituted by soil with CBR ≥ 5% and expansion ≤ 2%.

4.5.2. Traffic

The traffic in the urban-road design was classified in two kinds to essentially residential streets:

- Very Light Traffic - essentially residential streets, with no forecast of bus traffic, and can occasionally exist, passages of trucks in a number not superior to three (03) per day, per traffic lane, characterized by a typical number N of 10000 (10^4) requests of the pattern simple axis to the life time of 10 years (Senço, 1997).
- Light Traffic - streets of essentially residential characteristics, forecasting the bus traffic, and can occasionally exist, passages of trucks or buses in number not superior to fifty per day, per traffic lane, characterized by a number N - operations equivalence, typical of 100000 (10^5) requests of the pattern simple axis (8.2 ton), to the life time of 10 years (Senço, 1997).

4.5.3. Pavements layers

The pavements layers are considered in function of the structural equivalence coefficient, which is a number that relates the thickness of the layer, constituted of pattern material, with the equivalent thickness of the material that will effectively compose this layer.

According to Senço (1997), the pavement layers have an effective thickness (ER) equal to the sum of the layer thicknesses and an equivalent thickness (Eq), calculated by the sum of the product of the effective thicknesses of the layers by the respective structural equivalence coefficients of the materials that compose them.

The proposed coefficients of structural equivalence (k) are based and exposed by the method of the DNIT (former DNER) and by the design method of the City Hall of São Paulo (PMSP). The values are presented in Table 10. It is recommended to adopt k = 1 to the sub-base or reinforcement of the subgrade, when necessary.

4.5.4. Pavements thicknes design

The value of the CBR is obtained from Eq. 3 of the correlation with the DCP.

$$\log(\mathrm{CBR}) = 2.98 - 1.257\log(\mathrm{DCP}) \rightarrow \mathrm{DCP} = \left(\frac{\mathrm{CBR}}{950.55}\right)^{-1/1.257} \qquad (3)$$

With the established correlation, it is predicted the value of the DN correspondent to each CBR and then it is obtained the thicknesses to each penetration index.

The total thicknesses of the pavement to this method were obtained based in the abacus of the U.S. Corps of Engineers. By means of the proposed equation (Eq. 3), it is found the penetration index (mm/hit) of the DCP, in function to the values of CBR (%) and the values of the thicknesses to each traffic presented in Table 11 or in the abacus of Fig. 3.

With the total thickness necessary for the pavement (ETOTAL), according to the traffic (T), the option was made for one of the design alternatives, where it is obtained the thickness of the covering + base thickness (ERB or Eq). The thickness of the sub-base corresponds to the difference between the total thickness and the equivalent thickness (ESUB = ETOTAL - Eq). The equivalent thickness is the sum of the layers thicknesses multiplied by the

Table 10 - Structural equivalence coefficient (k) to various materials (Source: Silva Júnior, 2005).

Type of material	Symbol	Coefficient - k
Revestment of the asphaltic concrete	CA	2.0
Revestment of the thin concrete	CM	2.0
“Binder” or Pre-mixtured by heat	BI	1.8
Base of soil-cement	SC	1.7
Base or revestment pre-mixtured by cold, of dense graduation	PMF	1.4
Asphaltic revestment of penetration	PI	1.2
Articulate Pavement of concrete	PA	1.2
Base of bituminous macadame	MB	1.2
Granular Base	BG	1.0
Base of hydraulic macadame	MH	1.0
Revestment cobblestone type in pavement stone	P	1.0
Selected Running Gravel	BCS	0.9
Clay	A	1.0

Obs: Old pavements of pavement stone, when recovered with bitumen mixtures, the value of k can vary from 1.2 to 1.8 in function of the behavior, bulging and sealing of the pavement stones.

Table 11 - Total thicknesses of the pavement in function of the values of CBR, obtained based in the abacus of U.S. Corps of Engineers.

CBR (%)	DN (mm/ hit)	Total thickness of pavement (cm)	
		Traffic	
		Very light	Light
2	134.78	60	70
3	97.62	46	57
4	77.65	39	48
5	65.02	34	42
6	56.24	30	37
7	49.75	27	33
8	44.74	24	30
9	40.74	22	27
10	37.46	20	25
12	32.40	17	22
15	27.13	15	18
17	24.56	13	16
20	21.58	11	14
25	18.07	9	12
30	15.63	8	10
Comercials vehicles by day in a direction			
	Máx. 3	Máx. 50	

respective structural equivalence coefficients of the same type project.

It is important to mention that for the proposed abacus that all the materials of layers of the pavement have structural equivalence coefficient equal to one ($k = 1$).

Figure 4 presents the abacus for the design of the total thickness of the pavement.

With the value of the penetration index (axis X) obtained with the Dynamic Cone Penetrometer and in function of the kind of traffic (Very Light or Light), one finds the total thickness of the pavement in cm (axis Y).

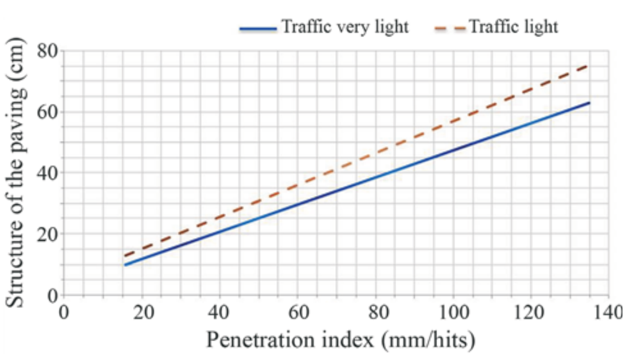

Figure 4 - Abacus of design of the total thickness of the structure of the pavement in function of the penetration index of the DCP, and of the traffic (T), to the proposed method Very Light Traffic.

By this proposed design method for urban pavements it becomes possible from the Dynamic Cone Penetrometer, as a tool to evaluate the support capacity of subgrade soils, to design streets pavements of low volume traffic.

5. Conclusions

The DCP, unlike the CBR *in situ*, is a practical test, quick and more economical due to its easy execution and semi-destructive nature, with no great movement of soil.

When the tests of DCP and CBR *in situ* correlate each other to all kind of soils found in the inspection wells, there is no practical correlation between them. This is due to the fact that the conditions found in field, to each kind of soil, are diverse enough because they present countless variables (variation of the water content, density, grain size, kind of soil, confinement state, etc.).

The correlations found in this work serve only to the penetration indexes obtained with the DCP and the values of CBR *in situ* to the soils A-2-4 and SM. Therefore, these correlations do not necessarily serve to other kind of soils.

The creation of an abacus in the urban pavement design method aims to simplify the design practice, leaving little margin to the variant studies, converging quickly to a project-type economically recommended.

The result of the proposed method suggests smaller thicknesses to the pavement when compared to the ones obtained by the DNIT method. This results in lower costs when talking about the execution.

References

NBR-6457 (1986) Amostras de Solo - Preparação para Ensaios de Compactação e Ensaios de Caracterização. ABNT - Associação Brasileira de Normas Técnicas, Rio de Janeiro, Brazil, 8 pp.

Alves, A.B.C. (2002) Avaliação da Capacidade de Suporte e Controle Tecnológico de Execução da Camada Final de Terraplenagem Utilizando o Penetrômetro Dinâmico de Cone. Dissertação de Mestrado em Engenharia Civil, Universidade Federal de Santa Catarina, Florianópolis, 185 pp.

Amaral, F.C.F. (2005) Previsão da Capacidade de Suporte de Areias Médias e Finas Uniformes em Obras Viárias com o Emprego do Ensaio DCP. Mestrado em Engenharia de Infra-Estrutura Aeronáutica, Instituto Tecnológico de Aeronáutica, São José dos Campos, São Paulo, 136 pp.

ASTM (2004) Standard Test Method for Nonrepetitive Static Plate Load Tests of Soils and Flexible Pavement Components, for Use in Evaluation and Design of Airport and Highway Pavements - D 1196. ASTM International, West Conshohocken, Pennsylvania, EUA, 3 pp.

ASTM (2003) Standard Test Method for Use of the Dynamic Cone Penetrometer in Shallow Pavement Applications – D 6951. ASTM International, West Conshohocken, Pennsylvania, EUA, 7 pp.

Berti, C. (2005) Avaliação da Capacidade de Suporte de Solos in situ em Obras Viárias Através do Cone de Penetração Dinâmica - Estudo Experimental. Dissertação de Mestrado em Engenharia Civil, Universidade Estadual de Campinas, Campinas, São Paulo, 142 pp.

DNER (1994) Solos - Determinação do Índice de Suporte Califórnia - ME 049. Departamento Nacional de Estradas de Rodagem. Rio de Janeiro, Brazil, 14 pp.

DNER (1994) Solos e Aregados Miúdos - Determinação da Umidade com o Emprego do "Speedy" - ME 052. Departamento Nacional de Estradas de Rodagem. Rio de Janeiro, Brazil, 4 pp.

DNER (1994) Solos - Análise Granulométrica por Peneiramento - ME 080. Departamento Nacional de Estradas de Rodagem. Rio de Janeiro, Brazil, 4 pp.

DNER (1994) Solos - Determinação do Limite de Plasticidade - ME 082. Departamento Nacional de Estradas de Rodagem. Rio de Janeiro, Brazil, 3 pp.

DNER (1994) Solos - Determinação da Massa Específica Aparente Seca com o Emprego do Frasco de Areia - ME 092. Departamento Nacional de Estradas de Rodagem. Rio de Janeiro, Brazil, 5 pp.

DNER (1994) Solos - Determinação do Limite de Liquidez - Método de Referência e Método Expedito - ME 0122. Departamento Nacional de Estradas de Rodagem. Rio de Janeiro, Brazil, 7 pp.

Guedes, S.B. (2008) Estudo da Viabilidade Técnica do Cone de Penetração Dinâmica (CPD), do Cone de Penetração Estática (CPE) e do Penetrômetro Panda no Dimensionamento de Pavimentos Urbanos. Dissertação de Mestrado em Engenharia Civi e Ambiental, Departamento de Engenharia Civil, Universidade Federal de Campina Grande, Campina Grande, Paraíba, 311 pp.

Harison, J.A. (1987) Correlation between California bearing ratio and dynamic cone penetrometer strength measurement of soil. Australian Road Research, v. 16:2, p. 130-136.

Herrick, J.E.; Jones, T. L. (2001) A Dynamic Cone Penetrometer for Measuring Soil Penetration Resistance. Soil Science Society of America Journal, v. 66, p. 1323-1324.

Karunaprema, K.A.K.; Edirisinghe, A.G.H.J. (2002) A laboratory study to establish some udeful relationships for the use of dynamic cone. The Electronic Journal of Geotechnical Engineering, v. 7, Bundle B. Disponível em:
http://www.ejge.com/2002/Ppr0228/Abs0228.htm.

Lima, L.C. (2000) O Ensaio DCP aplicado no Controle de Qualidade de Compactação de Obras Viárias Executadas com Solos Lateríticos de Textura Fina. Tese de Mestrado, Instituto Tecnológico de Aeronáutica. São José dos Campos, São Paulo, 164 pp.

PATTROL. Ensaio Califórnia. Disponível em: http://www.pattrol.com.br/equipamentos/califo.html. Acesso em March 5, 2009.

PMSP (1999) Determinação do Índice de Suporte do Subleito in situ. PMSP/SP-ME 47. Prefeitura do Município de São Paulo - SVP. São Paulo, Brazil, 37 pp.

Senço, W (1997) Manual de Técnicas de Pavimentação. Volume 1, 2a ed. Editora Pini, São Paulo, 779 pp.

Silva Júnior, F.A. (2005) Cone de Penetração Dinâmica (DCP): Uma Alternativa ao Dimensionamento de Pavimentos Urbanos. Dissertação de Mestrado em Engenharia Civil, Departamento de Engenharia Civil, Universidade Federal de Campina Grande, Campina Grande, Paraíba, 109 pp.

Trichês, G. & Cardoso, A.B. (1999) Avaliação da capacidade de aterros e subleito de rodovias utilizando o penetrômetro dinâmico de cone e a viga Benkelman. In: Transporte em Transformação, IV. Trabalhos Vencedores do Prêmio CNT, Produção Acadêmica. Anais Makron Books, pp. 35-49.

Yoder, E.J. (1959) Principles of Pavement Design. Second Edition, John Wiley & Sons, New Jersey, 585 pp.

Engineering Geological Mapping in the Basaltic Cuestas, São Paulo State, Brazil

A.E.S. de Abreu, O. Augusto Filho

Abstract. Some difficulties of performing an engineering geological mapping task in sites where residual and transported sandy soils are widespread are discussed in this paper. The study area is located in the municipality of Analândia in the southeast of Brazil. In this region landscape evolution is dominated by scarp retreat and relief inversion processes. As transported and residual soils have very similar grain size distributions, the results of geotechnical tests performed on both kinds of soils are very similar. Understanding the regional landscape evolution was essential for performing the mapping task. The method used combined aspects of engineering geological mapping based on synthetic and analytical approaches and it is strongly supported by field observations. The expected engineering behaviors of the mapped units are presented. Some of the units correspond to colluviums that occupy hilltops, a geomorphological position were they would not be expected. Moreover, the "stone lines" are common features in the area and their identification clearly defines the unconsolidated material as allochtonous. However, they are not always located at the bottom of the colluvial deposits, and sometimes they are not present at all or show lateral discontinuity. Some other characteristics are distinctive of these widespread deposits.

Keywords: residual and transported sandy soils, "stone line", relief inversion, "Basaltic Cuestas".

1. Introduction

The purpose of engineering geology is to provide basic information for the planning of land-use and for the design, construction and maintenance of civil engineering works. A map provides the best impression of a geological environment, including the character and variety of engineering geological conditions, their individual components and their interrelationships (UNESCO, 1976).

Maps are primarily instruments for arranging, storing, transmitting and analyzing information about the spatial distribution of attributes. Spatial extrapolation or the assertion that place B has the same set of attributes known at place A, even though not all the attributes were measured or observed at B, is one of the transformations to be made by the specialist, when constructing a map (Varnes, 1974). Interpreting the units genetically is essential to allow reliable extrapolation of data.

This paper outlines the engineering geology of an area in the "Basaltic Cuestas", a typical landscape in São Paulo State, in the southeast of Brazil, and it presents the expected geotechnical behavior of each mapped unit.

Emphasis is placed on the experiences and specific difficulties of performing an engineering geological mapping task of the residual and transported sandy soils in a subtropical area where several different sandstone formations outcrop and which is affected by cliff retreat and relief inversion processes.

The experience gained in this research should prove useful in other areas with similar engineering geological conditions and weathering profiles of the "Basaltic Cuestas" geomorphologic province, which occurs in three different countries in South America (Paraguay, Uruguay and Brazil).

Mapping the area also aimed at gathering information about the physical environment to support land use planning. The use of the engineering geological data gathered in this case study for land use planning is discussed in Abreu & Augusto Filho (2012).

2. Study Area

The study area is located in the southeast region of Brazil, in São Paulo state (Fig. 1) and comprises the municipality of Analândia with a total area of 327 km^2. It is situated in a phanerozoic sedimentary basin called Paraná Basin. The Pirambóia, Serra Geral, Botucatu and Itaqueri geological formations outcrop in the area (Table 1).

Most of the study area is located in the geomorphological province called "Basaltic Cuestas", with altitudes ranging from 760 to 1020 m a.s.l. Only the south and central areas along the Corumbatai river are located in the "Peripheral Depression", with altitudes ranging from 560 to 760 m a.s.l. (Fig. 2).

The Basaltic Cuestas are an erosive feature of the Paraná basin border and are considered to have been formed in the Tertiary in the São Paulo state area (Fulfaro,

Ana Elisa S. de Abreu, MSc, Phd Student, Departamento de Geotecnia, Escola de Engenharia de São Carlos, Universidade de São Paulo, Av. Trabalhador São-Carlense 400, 13560-970 São Carlos, SP, Brazil, e-mail: aesabreu@usp.br.
Oswaldo Augusto Filho, DSc, Associate Professor, Departamento de Geotecnia, Escola de Engenharia de São Carlos, Universidade de São Paulo, Av. Trabalhador São-Carlense 400, 13560-970 São Carlos, SP, Brazil, e-mail: oafilho@sc.usp.br.
Submitted on November 6, 2011; Final Acceptance on August 6, 2012; Discussion open until December 29, 2012.

Figure 1 - Location of the study area.

1975). In Analândia, this geomorphological province corresponds to two cliff systems, sometimes separated from one another: the lowest one is supported by the diabases of the Serra Geral Formation and ranges from 760 to 800 m. The upper one is supported by the Botucatu sandstone, with altitudes ranging from 800 to 900 m.

Melo *et al.* (1998, apud Melo & Cuchierato, 2004) recognized five planation surfaces having regional extent in the region, which can be interpreted as pediplains formed during Paleogene, Neogene and Quaternary in arid or semi-arid climates. Only three of them occur in the study area. Planation surfaces "A" and "I" were formed during the Paleogene and are located in the Basaltic Cuestas geomorphological province. Their altitudes range from 800 to 880 m (surface "I") and above 1,000 m (surface "A"). Planation surface "B" was formed during Neogene and is situated in the Peripheral Depression geomorphological province. Its altitude ranges from 700 to 780 m.

According to the Koeppen classification, the predominant climate is type Cwa (humid mesotermic subtropical), with hot and rainy summers, as well as mild dry winters. The average precipitation is 1,350 mm/yr. Most of the study area was assigned as a protected area in 1983 due to its scenic beauty, as well as the remnants of local flora and fauna.

3. Method

The method used in this research combined characteristics of different existing methods of engineering geological mapping and it was presented in details by Abreu & Augusto Filho (2009). Basically, this method joined aspects of the synthetic approach, which is used by several researchers, such as Culshaw *et al.* (1990), Schalkwyk & Price (1990) and Nakazawa (1995), and aspects of the analytical approach, used by UNESCO (1976), Zuquette *et al.* (2004, 2009) and others. A Geographical Information System – GIS (Arcview) was used to combine information on surface and subsurface investigations and laboratory tests.

Table 1 - Simplified stratigraphic column of the study area

Formation	Age	Lithology
Itaqueri	Tertiary	Siltstone, sandstone, claystone
Serra Geral	Jurassic-Cretaceous	Basalt and diabase
Botucatu	Jurassic-Cretaceous	Sandstone
Pirambóia	Triassic	Sandstone

The mapping task was done on two different scales: a regional scale (1:50,000), covering the whole municipality, and a local scale (1:10,000), covering the urban area where geological hazards proved to be more intense. This progressive elaboration and zooming in of the mapping task was performed by other authors, such as Cerri *et al.* (1996) and the ZERMOS program by the French Laboratoire de Ponts et Chausse's, Paris (Antoine, 1977).

The engineering geological mapping was carried out in three stages: the first stage comprised desk work and aimed at gathering the information already available for the area (government agencies, private consulting firms and research institutes), interpreting the aerial photographs and producing the digital elevation model. Field activities were undertaken, aiming at understanding the most significant geological processes occurring in the area (synthetic approach). This first stage determined the relevant attributes for the engineering geological mapping.

The second stage consisted of field activities and desk work needed to map these attributes (bedrock, unconsolidated materials and slope), as well as drawing the preliminary engineering geological map (analytical approach). Special attention was drawn in this stage to defining the typical weathering profile for each engineering geological unit and to deciding which soil samples could be regarded as representative of the respective profile.

The third stage comprised sampling and testing the materials representative of each typical weathering profile. Transfering geological data into geotechnical behavior involved an analysis of the test results and of the geological processes observed in the area, and relied on previous experience of the mapping team. This stage led to reviewing the unit division proposed on the second stage and drawing the final engineering geological map of the area (regional scale).

At this point, the urban area had already been identified as an area where unit detailing was necessary and the second and third stage activities were undertaken for mapping the urban area on a local scale. Data processing and final map preparation were carried out digitally using GIS tools.

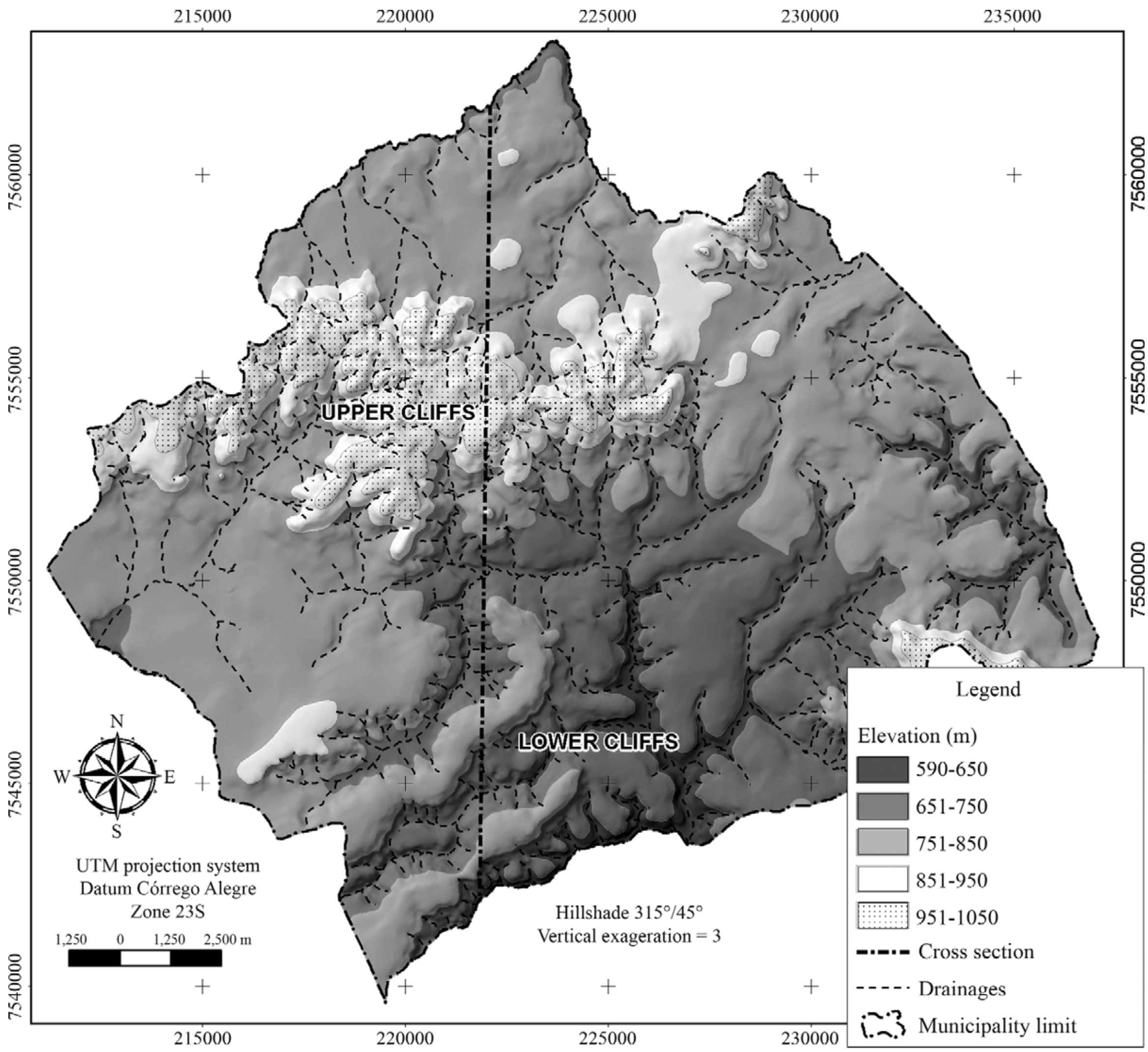

Figure 2 - Regional relief of the study area.

The approach proposed by Vaz (1996) was used to describe the weathering profiles. It comprises tropical soils and is based on a life-long experience in dealing with engineering geology in building and repairing dams, roads and tunnels in all kinds of rocks. This classification is based on the origin of the materials and encompasses transported and residual soils. In the study area, the transported soils consisted of alluviums, colluviums and talus.

For the *in situ* materials, the weathering profiles were divided into two significant horizons: residual soil, which corresponds to diggable material, and rock, which corresponds to rippable and blastable materials. The residual soil was subdivided into eluvial soil, which is homogeneous and shows no more traces of the original rock, and saprolite, which is heterogeneous and shows properties inherited from the parent rock.

The rock horizon was subdivided into weak weathered rock (WWR), hard weathered rock (HWR) and fresh rock (FR). WWR corresponds to a rippable, considerably weakened material, in which discoloration is penetrative. HWR and FR correspond to blastable material. FR is the material unchanged from the original state and HWR is the material that shows slight discoloration and weakening, especially along fractures. A description of a weathering profile does not necessarily include all these five subdivisions. Weak rocks typically show only the more weathered horizons, while hard rocks usually develop a complete weathering profile.

A total of 151 outcrops were described. Twenty disturbed and 20 undisturbed samples were collected. Samples were taken from slide planes, excavations, quarries and road cuts. Bearing in mind that it is crucial to transfer geological data into mechanical parameters, and to work with a minimum budget at the same time, few samples were taken for each unit, after considering which outcrops could be regarded as representative of the weathering profile for each unit.

The Atterberg limits, grain size distribution, unit weight, specific gravity and void ratio were determined in accordance with ASTM standards. The "activity" of the soils, as defined by Skempton (1953), was calculated.

The results of 115 m of boreholes with Standard Penetration Tests (SPT) performed in the urban area and 122 m performed in a nearby quarry were also considered for the characterization of the units.

4. Mapped Engineering Geological Units

Twelve individual engineering geological units were defined in the study area based on their origin, composition and expected geotechnical behavior. As expected for a subtropical climate, most of these units correspond to unconsolidated materials. Only two of them are characterized as fresh rock domains. The main characteristics of these engineering geological units are described as follows:

4.1. Unit 1- Recent alluvium

This includes loose soil deposits which occupy the river floodplains. They consist of clayey sands with light to dark grayish colors, sandy dark gray organic clays and brownish clayey gravels. These layers tend to be discontinuous and saturated. The engineering difficulties expected for this unit are low bearing capacity and differential settlements, as well as flooding prone areas.

4.2. Unit 2 - Recent talus

These deposits occupy the cliff footslopes in the present landscape. They consist of sandstone blocks, basalt-core gravels and a sandy or clayey sandy matrix, in variable proportions. The watertable forms at the bottom of the deposits. The geological processes associated with this unit are rotational landslides, especially in the rainy season, and creep.

4.3. Unit 3 - Sandy colluvium

These are terrestrial deposits, 5 to 15 m thick. They are composed of non plastic brownish or orange sands, with massive porous fabric, classified as SP-SM or SW-SM in the Unified Soil Classification System (USC).

They occur at the hilltops and slopes of broad hills with slopes ranging from 0 to 20% and elevations ranging from 680 to 880 m (Fig. 2). Melo & Cuchierato (2004) wrote about the origin and characterization of these deposits, which are regarded as quaternary colluvial-eluvial covers, and assigned them to the Santa Rita do Passa Quatro Formation.

"Stone lines" can usually be identified in these deposits. They should indeed be called "stone layers", as proposed by Morrás *et al.* (2009), because they are a three-dimensional body. In the study area these "stone lines" are flat or undulating sub-horizontal surfaces, which parallel the slope surface only when the slope is gentle. The gravel in the "stone lines" is formed of basalt, silica cemented sandstone, iron oxides cemented sandstone, ferricrete angular fragments and rounded quartz cobbles. The matrix is sandy, showing the same characteristic of the layers above and underneath the "stone line". Its thickness varies from 0.1 to 0.6 m and it can either show large lateral continuity (over a hundred meters) or it can be discontinuous. It may appear at the bottom of the deposit, but it is also often observed in the middle of it (Fig. 3) and sometimes there are various "stone line" levels in the same deposit.

These deposits have low bearing capacities and high compressibility, as stated by the SPT N values, which range from 0 to 9. They are prone to linear erosion and shallow translational slides. They are mined for the foundry and construction industries. Moreover, circular slides are common in road cuts.

4.4 Unit 4 - Clayey-sandy colluvium

These are tertiary-quaternary terrestrial deposits, which are over 7 m thick. They are composed of red brownish clayey sands, with massive porous fabric, classified as SC or SC-SM in the USC. They often present a "stone line", with the same characteristics of the "stone lines" described

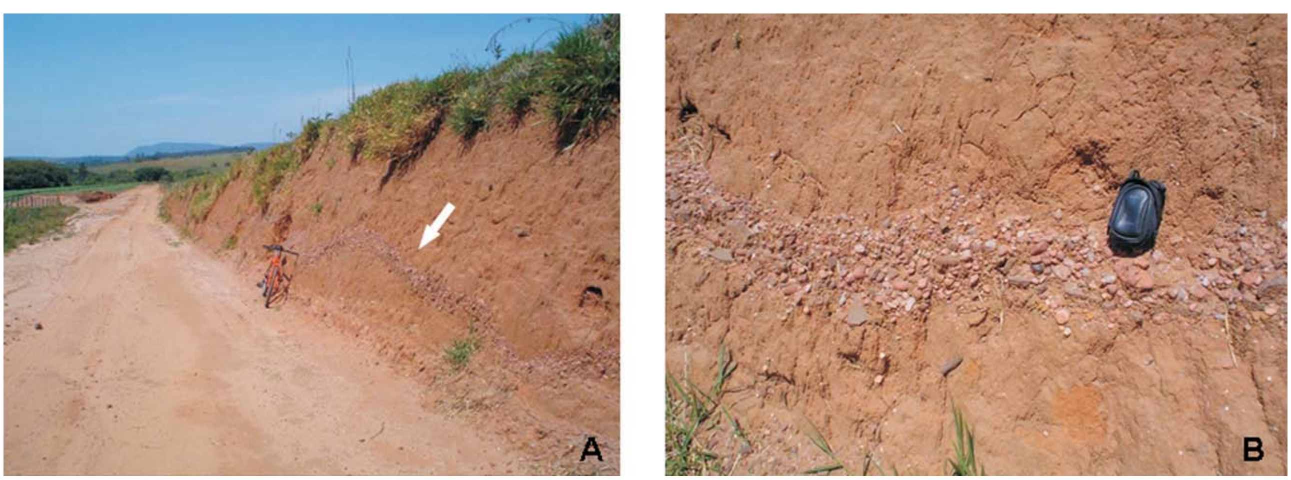

Figure 3 - Stone line in the middle of the sandy colluvium. A: Outcrop general aspect. B: Close view.

for the sandy colluviums (unit 3), except that the matrix is of clayey-sandy material.

This unit occupies the hilltops at the southwest of the study area, with elevations ranging from 780 to 870 m a.s.l. (Fig. 2). A colluvial origin is not expected for this geomorphological position, but the presence of the "stone lines" suggests an allochthonous origin for these covers.

These deposits are expected to have low bearing capacities and to behave as collapsible soils. They show little tendency to linear erosion and shallow translational slides are common in road cuts. This material is very adequate for fills, especially when impermeability is desirable.

4.5. Unit 5 - Sandy-gravelly colluvium

This unit comprises various layers of transported soils with different grain sizes and thicknesses (0.05 to 3 m) that are interpreted as remnants of old talus or alluvial fan deposits, formed at the footslope of ancient (eroded) cliffs. The most common layers are sands, gravelly sands, sandy gravels or clayey sandy gravels, with gravels composed of basalt, silica cemented sandstone, iron oxides cemented sandstone and ferricrete angular fragments and rounded quartz cobbles. Coal grains are also common and sandstone blocks occur rarely.

Where the gravel layers are thick, this material is extracted to be used for dirt road conservation, and the exposed layers are now prone to accelerated erosion. It is not always possible to determine the lateral extent of these deposits, unless large excavations are made, and this was not the aim of the present study. Nonetheless, site specific investigations in correlated areas must be aware of the possibility of its occurrence.

Engineering difficulties expected when handling these deposits are heterogeneities for excavation and for foundations (rock blocks immersed in a clayey-sandy matrix).

4.6. Unit 6 - Duricrusts of the Itaqueri Formation

The duricrusts correspond to tertiary nodular ferricretes that occupy the highest elevations of the study area, at the top of angular narrow hills. They comprise a 3 m thick layer formed in a more arid climate which is now being weathered under present climatic conditions. The ferricrete is a rippable material and it has been used by local farmers for dirty road conservation. The residual soil developed over this layer is eluvial homogenous brown silty clayey sand (SM) only 0.5 m thick. Coal grains are common in this soil. This unit is expected to have a high bearing capacity for shallow foundations and very low susceptibility to linear erosion.

4.7. Unit 7 - Residual soils of the Itaqueri Formation (non duricrusts)

This unit occupies the moderate to very steep slopes of the angular narrow hills, which occur in the study area in altitudes ranging from 940 to 1050 m. It corresponds to the weathering profiles developed over the conglomerates and conglomerate sandstones of the Itaqueri Formation. These profiles are uniformly weathered, and can be over 4 m deep in moderate and moderately steep slopes and only 2 m deep in steep to very steep slopes. In fact, no fresh rock has been identified in the outcrops. Only eluvial soils and saprolites were described.

The saprolite developed over the conglomerates shows inherited fabric: the matrix corresponds to a white and red silty sand (SM – sampled material), where the weathered gravel of the original conglomerate can be clearly identified. This horizon shows higher activity than all the other soils in the area and swells with moisture variations. The eluvial soil developed from the conglomerates is red clayey silty sand (SC-SM – sampled material).

The conglomerate sandstones showed no eluvial soil, and the saprolite showed clear inherited interbedded layers: sandy clays (CL-ML – sampled material) and sandy-gravels.

These soils can be excavated, but there are cobbles of ferricrete and quartz on the surface, so mechanized agriculture has to be done carefully. They are moderately prone to linear erosion. Swelling in the silty sands of the saprolite horizons and creep in the steep and very steep slopes have been observed in this unit. These soils are expected to have low bearing capacity and moderate compressibility. Pearched watertables occur.

4.8. Unit 8 - Residual soils of the Botucatu sandstones

They are composed of brownish non plastic sands, with massive fabric, classified as SP-SM. The weathering profile can be up to 20 m deep and is very permeable and homogenous. These soils occupy the tops and slopes of broad hills, with slope angles ranging from 0 to 20% and elevations ranging from 840 to 890 m a.s.l. They are expected to have low bearing capacities and high compressibility. They are prone to linear erosion and shallow translational slides are common in road cuts.

4.9. Unit 9 - Botucatu sandstone cliffs

This unit corresponds to the outcrops of silica cemented sandstone in the cliffs that surround the hills in the study area. They correspond to the upper cliff described previously. Residual soil up to 1 m thick may be present and corresponds to clean sand. Slab and block failures are common geological processes. The fresh Botucatu sandstone is used in neighboring areas as dimension stone.

4.10. Unit 10 - Residual soils of basalts and diabases (Serra Geral Formation)

The basalts and diabases which occur in moderate to moderately steep slopes in the area (angles ranging from 6 to 20%) show thin weathering profiles (2 to 5 m deep). The rock mass is typically corestone weathered and the eluvial soil is clayey, classified as MH, with a high void ratio. This material is used to maintain dirt roads. Linear erosion and creep are the most frequent processes in this unit.

4.11. Unit 11 - Diabase cliffs and steep slopes (Serra Geral Formation)

The diabases hold the lower scarp and neighboring steep slopes in the study area. The weathering profiles are corestone, usually less than 1 m deep, or the fresh rock is covered by recent colluvial soil. Slab and block failures and shallow translational slides are typical.

4.12. Unit 12 - Residual soils of the Pirambóia Formation

This unit is mainly composed of non plastic sands (classified as SM-SW soils), gravelly sands and clayey sands. These soils occupy the tops and the slopes of broad hills in altitudes ranging from 560 to 840 m.

The unit can be subdivided into three subunits, according to slope angles and corresponding erosion susceptibility (0%-12% - low tendency to erosion; 12%-20% - moderate tendency to erosion and 20%-40% - high tendency to erosion). This subdivision was based on a statistical analysis of the distribution of the existing linear erosions lengths in the various slope angle ranges.

The weathering profile can be over 30 m deep, showing only eluvial soil, saprolite and WWR horizons up to this depth. WWR is of interest as raw material for the glass industry. Saprolite and eluvial soil are of interest for the foundry industry. Eluvial soils give SPT N values of 3 to 9 and are up to 6 m thick. Saprolites give SPT N values of 7 to 13 in the first three meters and 28 to impenetrable to the SPT for another 3 to 4 meters, where they reach the WWR layer.

These soils are moderately permeable and develop pearched watertables over the clayey layers. Piping is a common process. They are diggable materials expected to have low bearing capacity for shallow foundations and to show high compressibility. Natural slopes with positive breaks show rotational landslides.

Table 2 presents the area distribution of the engineering geological units in the study area and summarizes their expected geotechnical behavior. Tables 3 and 4 present the results of the laboratory tests for the soils considered to stand for units 3, 4, 6, 7, 8, 10 and 12.

Units 1, 2 and 5 were not sampled, because they correspond to naturally discontinuous and heterogeneous materials and a few samples would not be representative of their variability. Units 9 and 11 were not sampled either, because no tests were performed on fresh rocks. Units 7 and 12 show significant variability in terms of grain size and only the most significant (or widespread) layers have been sampled.

Figure 4 illustrates the spatial relationships between the engineering geological units mapped using a south to north cross section of the study area.

Unit 3, which corresponds to sandy colluviums, stands out for covering over 50% of the land area. Residual soils of the Pirambóia Formation (Unit 12) also cover a significant municipal land area.

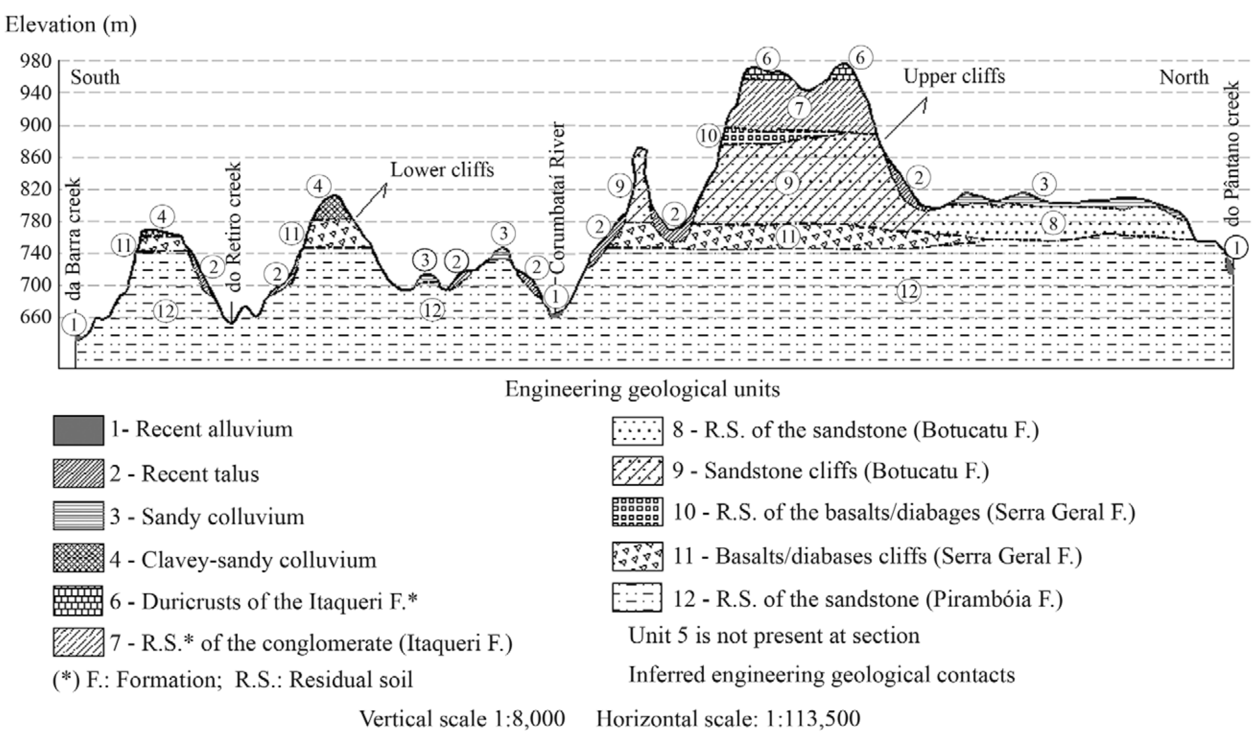

Figure 4 - Cross section of the study area with the mapped engineering geological units.

Table 2 - Engineering geological units and their expected geotechnical behavior.

Engineering geological units	Expected geotechnical behavior	Municipal land area (%)
1-Recent alluvium	Low bearing capacity for shallow foundations and differential settlements. Diggable material. Areas subjected to annual flooding.	2.3
2-Recent talus	Rotational landslides, especially in the rainy season, and creep. Heterogeneities for excavation and for foundations.	1.9
3-Sandy colluviums	Low bearing capacity for shallow foundations and high compressibility. Diggable material. High tendency to linear erosion. Shallow translational slides and circular slides in road cuts.	50.5
4-Clayey-sandy colluviums	Low bearing capacity for shallow foundations and collapse. Shallow translational slides in road cuts. Material is diggable and very adequate for fills, especially when impermeability is desirable.	5.6
5-Sandy-gravelly colluviums	Heterogeneities for excavation and for foundations. This material is exploited for dirt road conservation. Accelerated linear and laminar erosion takes place in exposed areas.	0.2
6-Duricrusts of the Itaqueri Formation	Rippable material, which has been used for dirt road conservation. High bearing capacity for shallow foundations and low susceptibility to linear erosion.	1.5
7-Residual soils of the Itaqueri Formation	Swelling in the silty sands of the saprolite horizons. Creep in the steep and very steep slopes. Low bearing capacity for shallow foundations and moderate compressibility. Perched water tables occur. Moderately prone to linear erosion. Diggable material, but there are cobbles of ferricrete and quartz on the surface, so mechanized agriculture must be done carefully.	7.4
8-Residual soils of the Botucatu Formation	Low bearing capacity for shallow foundations and high compressibility. Prone to linear erosion. Shallow translational slides in road cuts.	2.0
9-Botucatu Formation cliffs	Slab and block failures. Fresh Botucatu sandstone is quarried as dimension stone.	5.0
10-Residual soils of basalts and diabases (Serra Geral Formation)	Linear erosion and creep are the most frequent processes in this unit. Heterogeneities for excavation and for foundations. Typically corestone weathered material used to maintain dirt tracks.	1.8
11-Diabase cliffs and steep slopes (Serra Geral Formation)	Slab and block failures. Shallow translational slides.	2.6
12-Residual soils of the Pirambóia Formation	Perched water tables over the clayey layers are common. Piping is expected. Diggable material. Low bearing capacity for shallow foundations and high compressibility. Natural and man-made slopes show rotational landslides. Erosion susceptibility varies from low to high, depending on slope angle. Weak weathered rock horizons are of interest for the glass industry. Eluvial soils and saprolites are of interest for the foundry industry.	19.2

Table 3 - Engineering geological units, grain size distribution and Unified Soil Classification (USC).

Engineering geological units	Grain size distribution (%) (according to ASTM D422-63)				USC
	Gravel	Sand	Silt	Clay	
3-Sandy colluviums	0-2	88-90	3	5-9	SP-SM (SW-SM)
4-Clayey sandy colluviums	0-1	67-77	6-8	16-25	SC (SC-SM)
6-Itaqueri Formation – Duricrusts	2	49	20	29	SM
7- RS* Itaqueri Formation	0-9	39-67	10-20	10-44	CL-ML; SC-SM;
8- RS Botucatu Formation	0	65-91	4-20	5-15	SP-SM
10-RS Serra Geral Formation	0	3	24	73	MH
12-RS Pirambóia Formation	0-2	77-90	4-13	4-10	SW-SM

(*)RS = residual soil.

Table 4 - Engineering geological units, field density (ρ_{nat}), field dry density ($\rho_{d\,nat}$), specific gravity (ρ_s), field void ratio (e_{nat}), liquid limit (w_L), plastic limit (w_P) and activity of the clay fraction (A).

Engineering geological units	ρ_{nat} (g/cm^3)	$\rho_{d\,nat}$ (g/cm^3)	ρ_s (g/cm^3)	e_{nat}	w_L (%)	w_P (%)	A
3-Sandy colluviums	1.573-1.675	1.505-1.618	2.791-2.833	0.729-0.854	-	NP	-
4-Clayey sandy colluviums	1.427-1.676	1.322-1.587	2.722-2.849	0.775-1.145	21-32	15-18	0.28-0.67
6-Itaqueri Formation – Duricrusts	1.627	1.445	2.780	0.924	37	29	0.33
7- RS* Itaqueri Formation	1.455-1.775	1.300-1.588	2.848-2.986	0.880-1.191	39-64	25-44	0.36-2.86
8- RS Botucatu Formation	*	2.625	*	*	-	NP	-
10-RS Serra Geral Formation	1.668	1.217	3.156	1.593	98	46	0.80
12-RS Pirambóia Formation	1.636	1.544-2.780	2.786	0.804	-	NP	-

(*)RS = residual soil; * = sample was damaged during transportation.

Some of the units have economic or scenic importance, even though they account for a small land area. For instance, Unit 9 (Botucatu sandstone cliffs) accounts for the scenic beauty of the area and for the income from tourism. Unconsolidated materials of units 5 (sandy-gravelly colluviums), 6 (duricrusts of the Itaqueri Formation) and 10 (residual soils of the Serra Geral Formation) are used for dirt road conservation in the rural areas.

5. Discussion

One of the most challenging aspects of the performed mapping task was to identify the origin of the various sandy unconsolidated materials which occur in the area and to map their continuity. As described previously, units 3, 4, 8 and 12 are composed mainly of sandy materials (over 65% of their grain size distribution).

As weathering profiles developed over sandstones are relatively simple, when compared to those developed over igneous and metamorphic rocks (Price, 1995), one would at first expect that mapping the engineering geological units in the study area would be an easy task.

The fact that the landscape in the area is marked by cliff retreats implies that transported soils are widespread in the study area and mapping their distribution makes the mapping task much more complicated.

Moreover, there are two separated cliff systems in the study area, which are locally joined in one escarpment. This implies that the terrestrial transported unconsolidated materials (talus and colluviums) derived from the retreat of the upper cliff system may occupy the hill tops of the lower cliff system, and that characterizes a process of relief inversion. Figure 5 is an interpretation of how the landscape evolved in the area during Paleogene and Neogene adapted from Vaz (1997).

This is typical of Unit 4 in part of the study area (Fig. 4). Materials classified as Unit 4 can be easily distinguished from the other sandy materials, both in field work and when comparing laboratory test results, because their clay content (minimum 16%) is sufficient to give them plasticity and this alters their geotechnical behavior significantly. Moreover, the material shows a distinctive red brownish color, when compared to the other yellowish sandy materials which characterize units 3, 5, 8 and 12. However, as they occupy hill tops and show this particular color, they have been mapped as residual soils derived from diabases in some of the previous work done in the area. Identifying "stone lines" has proved that they are terrestrial transported soils derived from the weathering of basalts and sandstones in the upper cliff retreat process. As the area is undergoing relief inversion, "stone lines" occupy hilltops nowadays.

Units 3, 8 and 12 are all composed mostly of non-plastic unconsolidated materials classified as SW-SM-SP soils. Figure 6 shows a comparison of their grain size distribution, highlighting the difficulty in distinguishing one from the other, considering the test results only. This situation could even be expected, as the sandy colluviums are basically transported soils formed by sandstone cliff retreats. In other words, Unit 3 is a transported soil derived from materials of Unit 8, which explains their similarities. Unit 12, although not directly related to the origin of Unit 3 (except locally), is composed of sandy soil profiles, which can mistakenly be interpreted as belonging to Unit 3, if their origin is not properly identified.

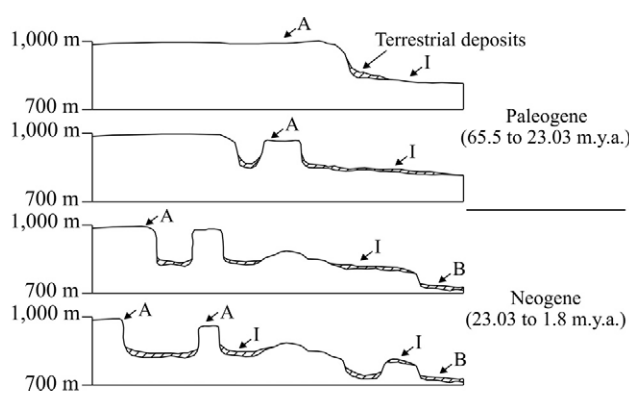

Figure 5 - Schematics of landscape evolution in the study area (m.y.a. = million years ago).

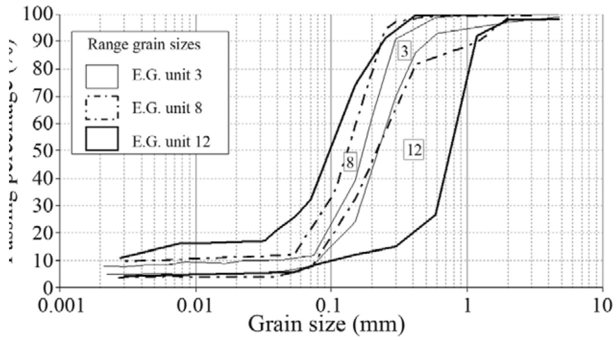

Figure 6 - Range grain sizes of the engineering geological units: sandy colluviums (3); residual soils of Botucatu formation (8) and residual soils of Pirambóia formation (12).

Although their expected geotechnical behavior is similar, especially for units 3 and 8, it is important to map these materials as separate units. Understanding their genesis is essential to defining their spatial distribution and extrapolating expected behaviors for land-use planning and engineering design purposes. Field work is essential to distinguish between these two units. The sandy colluviums (Unit 3) show a distinctive porous massive fabric with scattered quartz pebbles (4-64 mm). In the residual soils of the Botucatu Formation (Unit 8) the fabric is massive, but less porous, and the quartz pebbles are not common.

Identifying a “stone line” is a decisive factor in considering the sandy material as transported, but unfortunately this is not always possible. On one hand, because the “stone line” is not always present in the deposit and on the other hand, because sometimes the outcrop is not high enough to show the “stone line”. “Stone lines” covered by 1.5 up to 10 meters of sandy material were identified in the study area.

There is much controversy in the literature about the origin of “stone lines” and results obtained so far suggest that there may exist allochthonous and autochthonous “stone lines” (Braucher *et al.*, 1998; Lichte & Behling, 1999; Brown *et al.*, 2004; Morrás *et al.*, 2009). The characteristics of the “stone lines” in the study area suggest that they are allochthonous, in accordance with Melo & Cuchierato (2004). The cobbles in the “stone lines” are clearly transported material, because they include siliceous and iron cemented sandstone and laterite fragments, similar to those that occur in Unit 6 on hilltops of the upper cliff system (highest elevations of the area).

Moreover, in many outcrops more than one “stone line” was identified, which proves that they are not necessarily located at the bottom of the transported material layer and belies common sense that their identification characterizes the end of the deposit (*e.g.* Landim *et al.*, 1974; Giacheti *et al.*, 1993).

Mapping Unit 12 and separating it from the other sandy materials is relatively easy and clear, because it shows greater variability in grain size distribution (Fig. 6) and has occasionally an interbedded clayey-sandy layer or a sandy-clayey layer, and thus it can be identified in the field and in comparing test results.

6. Conclusion

The method used for this mapping task combines the characteristics of other different methods presented in the technical literature and is able to gather sufficient information about the geological setting of a region, while working with a minimum budget. It combines field and laboratory work, as well as data from superficial and subsurface investigations.

Twelve engineering geological units have been mapped in Analândia. The expected engineering properties of these units, as well as the geotechnical problems which occur in the area were presented. Because the study area is part of a larger, geologically and geomorphologically similar terrain, the anticipated problems here are relevant to other similar areas.

As the area is almost entirely covered by sandy soils, one could first expect that there would be no significant differences in their response to the various engineering tasks. However, this study has shown that, although these soils have similar behavior, they also show distinctive characteristics. Understanding their origin is the only way of reliably extrapolating their characteristics and mapping their lateral continuity and spatial distribution.

In the Analândia municipality, some of these sandy soils are colluviums and occupy geomorphological positions were they would not be expected (hilltops). Their position in the present landscape is explained by the fact that the area is undergoing relief inversion. Understanding the evolution of the regional landscape is essential for mapping these units.

These tertiary-quaternary colluviums are widespread in the border of the Paraná Basin in the southeast of Brazil and play an important role in engineering. On one hand, it has been determined that there are three different kinds of colluviums in the area: sandy colluvium, clayey sandy colluvium and sandy gravelly colluvium. On the other hand, it has been shown that it is impossible to distinguish between residual soils developed over the sandstones and the sandy colluvium, based only on currently used geotechnical tests (grain size distribution and Atterberg limits). Understanding the occurrence of these deposits in the present landscape and observing their undisturbed characteristic in natural or artificial cuts is essential for mapping their spatial distribution.

Moreover, it has become clear that “stone lines” are not always located at the bottom of the colluvial deposits, and sometimes they are not present at all or show lateral discontinuity. Identifying a “stone line” clearly defines the unconsolidated material as allochtonous, but this is not the only distinctive characteristic of these deposits. Their massive porous fabric is also an important characteristic, which must be observed in field work.

Acknowledgments

The authors gratefully acknowledge the financial support of the Brazilian research funding agency National Council for Scientific and Technological Development (CNPq).

References

Abreu, A.E.S. & Augusto Filho, O. (2009) Engineering geological mapping for municipality land use planning. Geotecnia, v. 115, p. 45-80 (in Portuguese).

Abreu, A.E.S. & Augusto Filho, O. (2012) Engineering geological data in support of municipal land use planning – A case study in Analândia, southeast Brazil. Environmental Earth Sciences, v. 65. p. 277-289, DOI 10.1007/s12665-011-1089-6.

Antoine, P. (1977) Reflections about the ZERMOS cartography and evaluation of the ongoing experiences. Bull Bur Rech Geol Min Sec. v. III:1-2, p. 9-20 (in French).

Braucher, R.; Bourles, D.L.; Colin, F.; Brown, E.T. & Boulange, B. (1998) Brazilian laterite dynamics using in situ-produced ^{10}Be. Earth and Planetary Science Letters, v. 163:1-4, p. 197-205.

Brown, D.J.; McSweeney, K. & Helmke, P.A. (2004) Statistical, geochemical, and morphological analyses of stone line formation in Uganda. Geomorphology, v. 62:3-4, p. 217-237.

Cerri, L.E.S.; Akiossi, A.; Augusto Filho, O. & Zaine, J.E. (1996) Geotechnical maps and cartograms of urban areas: considerations about the mapping scale and a proposal for their preparation using the Progressive Detailing Method. Anais do 8º Congresso Brasileiro de Geologia de Engenharia, Rio de Janeiro, Associação Brasileira de Geologia de Engenharia, v. 2, pp. 537-547 (in Portuguese).

Culshaw, M.G.; Forster, A.; Cripps, J.C. & Bell, F.G. (1990) Applied geology maps for land-use planning in Great Britain. Proc. 6th International Congress of International Association of Engineering Geology, Amsterdam, v. 1, pp. 85-93.

Fulfaro, V.J. (1975) Mesozoic-cenozoic tectonic and paleogeographic evolution of southeastern Brazil. Proc. IX International Congress of Sedimentology, Nice, Theme IX, pp. 125-133.

Giacheti, H.L.; Rohm, S.A.; Nogueira, J.B. & Cintra, J.C.A. (1993) Cenozoic sediments geotechnical properties. In: Cintra, J.C.A. & Albiero, J.H. (eds) Soils of the Country Area of São Paulo State. Associação Brasileira de Mecânica dos Solos, São Carlos, pp. 143-175 (in Portuguese).

Landim, P.M.B.; Soares, P.C. & Fúlfaro, V.J. (1974) Cenozoic deposits in south-central Brazil and the engineering geology. Proc. 2nd International Congress of International Association of Engineering Geology, São Paulo, v. 1, Theme III-11, 7 pp.

Lichte, M. & Behling, H. (1999) Dry and cold climatic conditions in the formation of the present landscape in Southeastern Brazil. An interdisciplinary approach to a controversially discussed topic. Zeitschrift fur Geomorphologie, v. 43:3, p. 341-358.

Melo, M.S. & Cuchierato, G. (2004) Quaternary colluvial-eluvial covers of the Eastern Paraná Basin, Southeastern Brazil. Quaternary International, v. 114:1, p. 45-53.

Morrás, H.; Moretti, L.; Píccolo, G. & Zech, W. (2009) Genesis of subtropical soils with stony horizons in NE Argentina: Autochthony and polygenesis. Quaternary International, v. 196:2, p. 137-159.

Nakazawa, V.A. (1995) Geotechnical mapping. In: Repetto, F.L. & Karez, C.S. (eds) Geological Aspects of Environmental Protection. UNESCO Press, Montevideo, pp. 65-69 (in Spanish).

Price, D.G. (1995) Weathering and weathering processes. Quarterly Journal of Engineering Geology, v. 28:3, p. 243-252.

Schalkwyk, A. & Price, G.V. (1990) Engineering Geological Mapping for urban planning in developing countries. Proc. 6th International Congress of International Association of Engineering Geology, Amsterdam, v. 1, pp. 257-264.

Skempton, A.W. (1953) The colloidal activity of clays. Proc. 3rd International Conference on Soil Mechanics and Foundation Engineering, London, v. 1, pp. 47-61.

UNESCO (1976) Engineering Geological Maps. A Guide to their Preparation. The Unesco Press, Paris, 79 pp.

Vaz, L.F. (1996) Genetic classification of soils and rock weathering layers in tropical regions. Soils and Rocks, v. 19:2, p. 117-136 (in Portuguese).

Vaz, L.F. (1997) Scarp retreat colluviums. Proc. 6th Conference of the Brazilian Quaternary Studies Association, Curitiba, pp. 274-277 (in Portuguese).

Zuquette, L.V.; Pejon, O.J. & Collares, J.Q.S. (2004) Engineering geological mapping developed in the Fortaleza Metropolitan Region, State of Ceará, Brazil. Engineering Geology, v. 71:3-4, p. 227-253, DOI 10.1016/S0013-7952(03)00136-4.

Zuquette, L.V.; Palma, J.B. & Pejon, O.J. (2009) Methodology to assess groundwater pollution conditions (current and pre-disposition) in the São Carlos and Ribeirão Preto regions, Brazil. Bull Eng Geol Environ, v. 68:1, p. 117-136, DOI 10.1007/s10064-008-0173-y.

Technical Note

Simulation of the Mechanical Behavior of Fiber Reinforced Sand using the Discrete Element Method

R.Q. Velloso, M.D.T. Casagrande, E.A. Vargas Junior, N.C. Consoli

Abstract. The general characteristics of granular soils reinforced with fibres have been reported in previous studies and have shown that fibre inclusion provides an increase in material strength and ductility and that the composite behaviour is governed by fibre content, as well as the mechanical and geometrical properties of the fibre. The present work presents a numerical procedure to incorporate fiber elements into an existing discrete element code (GeoDEM). The fiber elements are represented by linear elastic-plastic segments that connect two neighbor contacts where the fiber is located. These elements are characterized by an axial stiffness, tensile strength and length. The effect of the addition of fibers was evaluated numerically by comparing the stress-strain behavior of a pure sand with and without fibers. These simulations showed that the addition of fibers provides a significant increase in strength for the mixture in comparison with strength of the pure sand.

Keywords: DEM, fiber-reinforced soils, biaxial tests.

1. Introduction

Past research has demonstrated that inclusion of fibers significantly improves the engineering response of soils. Gray & Ohashi (1983) studied the mechanics of fiber-reinforcement in cohesionless soils and showed that inclusion of fibers increased peak shear strength and ductility of soils under static loads. A number of factors such as fiber content, orientation of fibers with respect to the shear surface, and the elastic modulus of the fiber were each found to influence the contribution of fibers to the shear strength. Later work (*e.g.* Maher & Gray, 1990; Maher & Ho, 1993; Morel & Gourc, 1997; Consoli *et al.*, 1998, 1999, 2002, 2004, 2005, 2007a, 2007b, 2009; Zornberg, 2002; Vendruscolo, 2003; Michalowski & Cermák, 2003; Heineck *et al.*, 2005; Casagrande, 2005 and Casagrande *et al.*, 2006) has improved understanding of the mechanisms involved and the parameters affecting the behavior of fiber reinforced soils under static loading conditions.

Within this context, the Discrete Element Method (DEM) was used in the present work, as a modeling tool for analysis of micro-scale reinforced soil, to understand how these materials interact. In particular evaluation was made of the behavior of soil-polypropylene fibers mixtures, when compared to a non-reinforced soil.

DEM was introduced by Cundall (1971) for the analysis of rock mechanics problems and later specialized to granular media by Cundall & Strack (1979). Since then, the DEM has been utilized to represent the mechanical behavior of pure sands subjected to different loading conditions (Belheine *et al.*, 2009; Plassiard *et al.*, 2009 and Zhao & Evans, 2009). However, little work has been reported on the behavior of sand mixed with fibers using DEM. One of these studies, Maeda & Ibraim (2008) used DEM for the study of granular soils reinforced with fibers. In the approach adopted by these authors, fibers were modeled as particles themselves connected by contact bonds possessing tensile and shear strength but no restriction to rotation, behaving as hinge connections.

A two dimensional DEM simulation of the mixture of granular soil and fibers was carried out by implementing a special procedure to take into account the fiber-soil interaction. This implementation was carried out in the numerical code GeoDEM (Velloso, 2010) which is a general purpose discrete element code. Numerical results under biaxial compression are presented and discussed.

DEM is a method that carries relatively high computational costs. Simulation times for a fair sized problem may take hours or even days to process. However, the proposed formulation for inclusion of fibers inside the granular mass does not alter in a significant way the demands in computing power.

The main objective of the present work is to describe and to evaluate the proposed procedure for the inclusion of fibers into the DEM.

Raquel Quadros Velloso, DSc, Pontifícia Universidade Católica do Rio de Janeiro, Rio de Janeiro, RJ, Brazil, e-mail: raquelvelloso@puc-rio.br.
Michéle Dal Toé Casagrande, DSc, Pontifícia Universidade Católica do Rio de Janeiro, Rio de Janeiro, RJ, Brazil, e-mail: michele_casagrande@puc-rio.br.
Eurípedes do Amaral Vargas Junior, PhD, Pontifícia Universidade Católica do Rio de Janeiro, Rio de Janeiro, RJ, Brazil, e-mail: vargas@puc-rio.br.
Nilo Cesar Consoli, PhD, Universidade Federal do Rio Grande do Sul, Porto Alegre, RS, Brazil, e-mail: consoli@ufrgs.br.
Submitted on April 30, 2012; Final Acceptance on July 10, 2012; Discussion open until December 29, 2012.

2. Fiber Modeling Inside the Discrete Element Method

2.1. The discrete element method

Motion of particles and their interaction are modeled in the present work by the Discrete Element Method (DEM) implemented in the GeoDEM code (Velloso, 2010). DEM was introduced by Cundall (1971) for the analysis of rock mechanics problems and later specialized to granular media by Cundall & Strack (1979). In this method, Newton's second law is used to describe the motion of an individual particle. The equation that governs the translation motion of an individual particle i is:

$$m_i = \frac{d\mathbf{v}_i}{dt} = \sum_{j=1}^{nc_i} \mathbf{F}_{cij} + \mathbf{F}_{gi} + \mathbf{F}_{fi} \tag{1}$$

where m_i e $\mathbf{v}_i$ are respectively mass and velocity of particle i, nc_i is the number of contacts of particle i. Forces acting on particle are gravitational force ($\mathbf{F}_{gi}$), contact forces between particles i and j ($\mathbf{F}_{cij}$), forces due to fibers ($\mathbf{F}_{fi}$).

The equation that governs the rotational motion of particle i is:

$$I_i = \frac{d\omega_i}{dt} = \sum_{j=1}^{nc_i} \mathbf{T}_{ij} \tag{2}$$

where ω_i is the angular velocity of particle i, I_i is the moment of inertia of particle i, and $\mathbf{T}_{ij}$ is the torque generated by the contact forces between particles i and j. Motion Eqs. 1 and 2 are integrated using a central difference scheme. Details of expressions for accelerations, velocities and displacements can be found in Cundall & Strack (1979).

The mechanical (macroscopic) behavior of a particular material is simulated in DEM through constitutive models associated to each contact (through the force-displacement relationship). By using the adopted constitutive model, the contact forces between two particles can be determined. In the present work, a linear elastic-perfectly plastic (sliding) behavior, whose graphical representation is shown in Fig. 1, was adopted.

The contact force $\mathbf{F}_c$ can be decomposed in normal $\mathbf{F}_c^N$ and shear forces $\mathbf{F}_c^S$:

$$\mathbf{F}_c = \mathbf{F}_c^N + \mathbf{F}_c^S \tag{3}$$

Normal force is given by:

$$\mathbf{F}_c^N = K_N U_N \mathbf{n} \tag{4}$$

where K_N is contact normal stiffness, $\mathbf{n}$ is the normal vector to the contact plane and U_N is the superposition between particles.

$$U_N = R_1 + R_2 - d \tag{5}$$

being R_1 e R_2 particle radii in contact and d the distance between particles centroid.

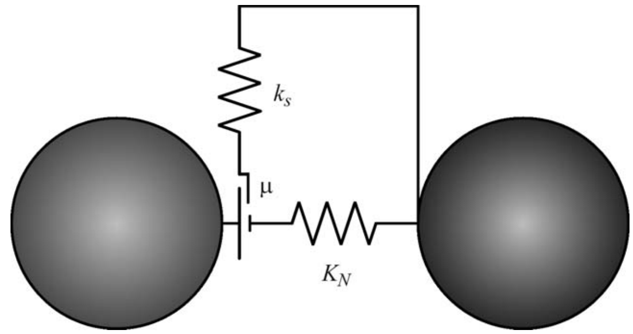

Figure 1 - Linear elastic-perfectly plastic (sliding) model at particle contact.

The shear force is determined in an incremental form. When a contact is formed, the shear force is initially zero and the subsequent shear displacements result in increments of this force:

$$\Delta\mathbf{F}_c^S = k_s \mathbf{v}_c^s \Delta t \tag{6}$$

being $\mathbf{v}_c^s$ the relative velocity in the shear direction at the contact, k_s the contact shear stiffness and Δt the time interval. In DEM application to sands, tensile forces at the contact are not allowed and therefore:

$$\text{if } U_N < 0 \text{ then } \mathbf{F}_c^N = \mathbf{F}_c^S = \mathbf{0} \tag{7}$$

The sliding model between particles is defined by the friction coefficient (μ) that limits the shear force to a maximum value given by:

$$F_{c\max}^S = \mu \left| \mathbf{F}_c^N \right| \tag{8}$$

If $\left|\mathbf{F}_c^S\right| \geq F_{c\max}^s$, sliding occurs making:

$$F_c^S = F_c^S \frac{F_{c\max}^S}{\left|\mathbf{F}_c^S\right|} \tag{9}$$

After calculations of the contact forces, these are transferred to the particles and used in Eqs. 1 and 2. Equations 1 and 2 correspond to dynamic conditions. Natural dynamic systems contain some degree of damping otherwise the system would oscillate indefinitely. Various types of damping have been proposed in the solution of problems using the DEM. For the quasi-static problems, such as the ones included in the present work, local, non-viscous damping is indicated. Details of characteristics of different forms of damping can be found in Figueiredo (1991) and in the user's manual of the code PFC2D (Itasca, 2002).

2.2. The fiber element

In this work, it is proposed the addition of fiber elements in the code GeoDEM (Velloso, 2010). The implementation is carried out by the addition of fiber elements in GeoDEM through the use of linear elastic- plastic segments connecting two neighboring contacts as shown in Fig. 2

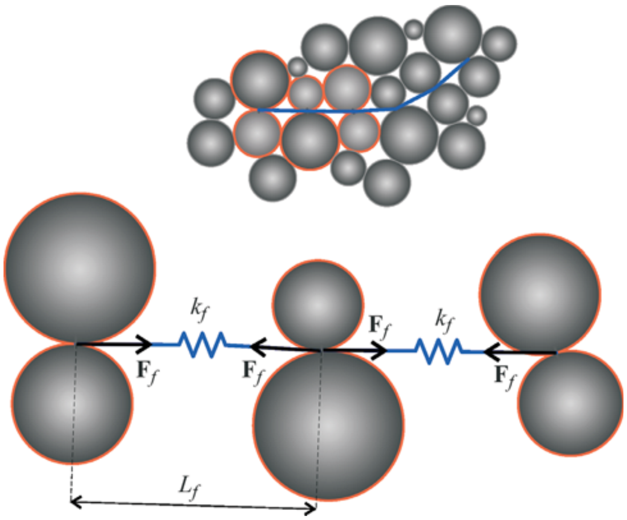

Figure 2 - Graphical representation of fibers between contacts.

(Ferreira, 2010). These fiber elements are characterized by axial stiffness, tensile strength and fiber length.

The relative displacement of these contacts generates a force that is transmitted to each pair of particles that forms the contact. The force due to the fiber is calculated as:

$$F_f = K_f (L_f - L_{f0}) \mathbf{n}_f \tag{10}$$

where $\mathbf{F}_f$ is the fiber related force to be transmitted to the particles, K_f is the fiber stiffness, L_f is the present length of the fiber segment, L_{f0} is the initial length (at the moment the fiber was generated) of the fiber segment and $\mathbf{n}_f$ is the unit vector in the direction that connects the two neighboring contacts. If the fiber segment shortens, ($L_f < L_{f0}$), the fiber force is zero, that is, the fiber only transfers forces to the particles when subjected to tensile forces. If the force calculated by Eq. 10 in a fiber segment is larger than the tensile strength of the fiber, the fiber force becomes zero, this fiber segment is disabled, indicating failure of the fiber at this point. With the addition of the fiber elements, the calculation cycle of DEM is shown in Fig. 3.

The generation of fibers is carried out after the granular medium reaches an equilibrium configuration. Fibers

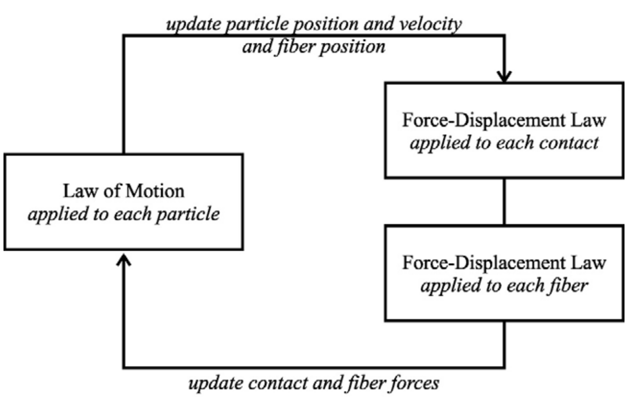

Figure 3 - Calculation cycle in the DEM.

can be generated stochastically, whose distribution are described by average and standard deviation values for length and direction. Fibers can be generated in the whole domain or in specific and prescribe regions.

3. Results

A granular sample 5 mm wide and 10 mm high formed by circular particles having an average diameter of 0.25 mm and a 20% porosity was generated and is shown in Fig. 4. The micromechanical parameters, shown in Table 1, were calibrated in a way to obtain the stress strain behavior of a sand having an effective friction angle of 30°, and Young's modulus of approximately 10 MPa for a confining stress of 100 kPa. One hundred fiber elements having a length equal to five times the average diameter of the particles were generated in random directions of the sample.

Figure 4 - Granular sample containing fibers (in green, see electronic version).

Table 1 - Micromechanical parameters of particle contacts.

Normal stiffness (K_N)	50 MN/m
Shear stiffness (k_s)	25 MN/m
Friction coefficient (μ)	0.45

The axial stiffness of the fibers is 100 MN/m and their tensile strength is 10 kN.

Figure 5 shows the stress-strain curves obtained from the numerical simulations of a sample of pure sand and one of pure sand with the inclusion of fibers. One is able to observe a significant increase in strength with the addition of fibers. This increase in strength is also reflected in in the strength envelope represented in Fig. 6. Figure 7 shows the influence of the fiber stiffness in the mechanical behavior of the tested samples. One is able to note that an increase in stiffness of the fibers, as implemented in the present work, has the effect of increasing both strength and stiffness of samples (reflected by their Young's modulus).

Experimental work (Casagrande, 2005) has shown that the addition of fibers increase both strength and ductility of sandy soils. The increase in ductility was not observed in the numerical simulations carried out. A possible reason for this discrepancy is related to the elasto-plastic model adopted for the fibers. This model incorporates softening, that is, fibers fail completely when reaching their tensile strength.

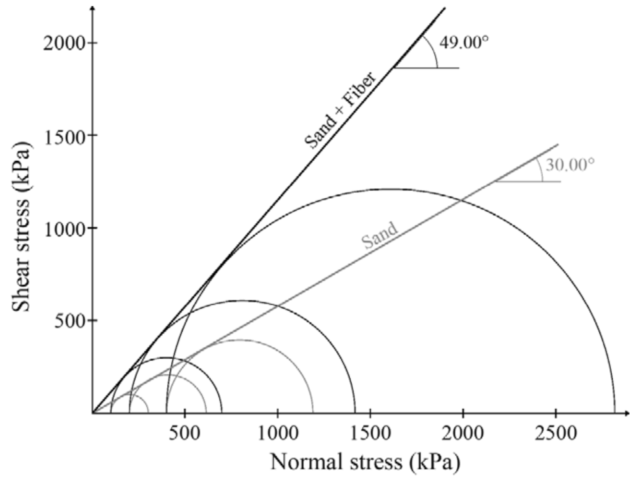

Figure 6 - Strength envelopes obtained in the numerical simulation of pure sand and sand with fibers.

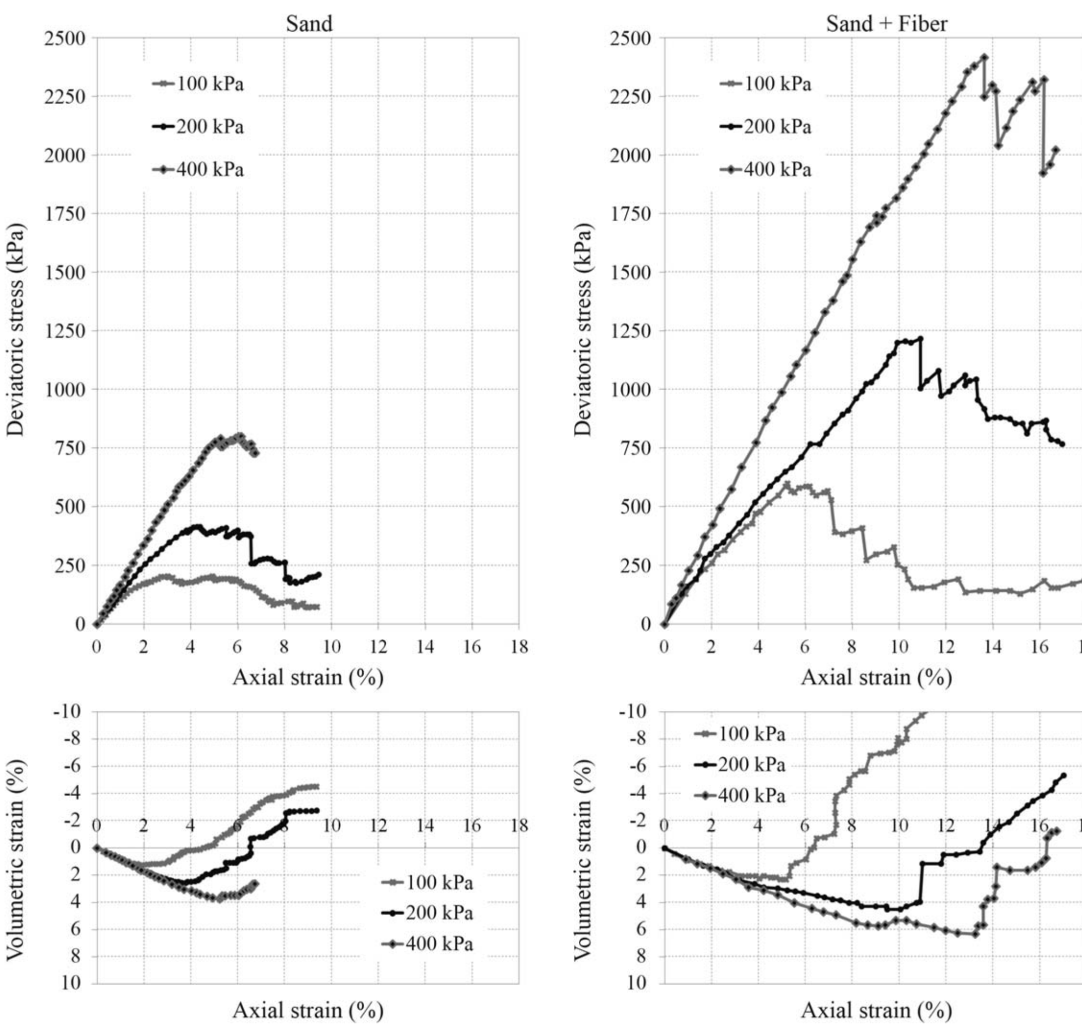

Figure 5 - Stress-strain curves obtained in the numerical simulation of pure sand (left hand side) and san with fibers (right hand side).

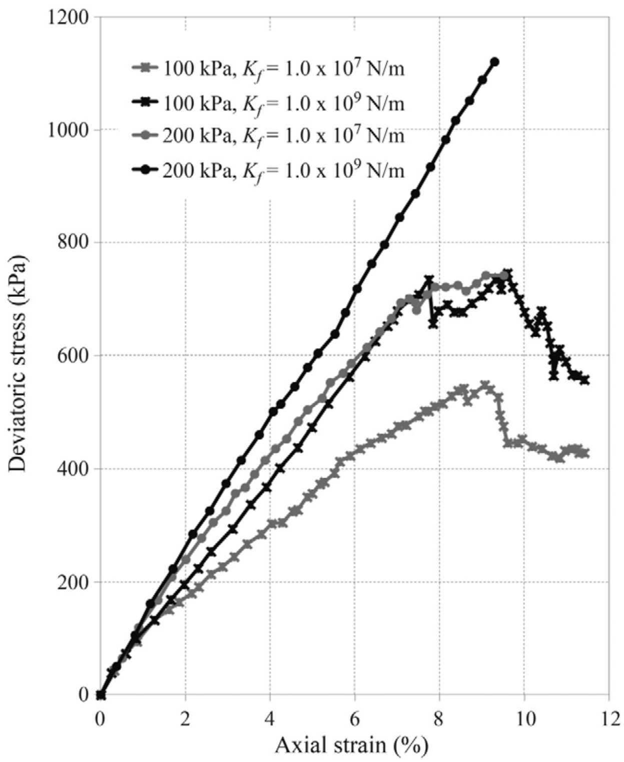

Figure 7 - Stress-strain curves obtained in the numerical simulation of sand with fibers having different axial stiffnesses.

4. Conclusions

This work presented a simple procedure for the inclusion of fiber elements in the discrete element formulation. In the proposed procedure, the fiber element is represented by a virtual segment connecting particles.

Numerical simulations of biaxial compression tests were carried out in samples of sand and sand mixed with fibers. These simulations showed that the addition of fibers provides a significant increase in strength for the mixture in comparison with strength of the pure sand.

However, the increase in ductility due to the addition of fibers as reported in the literature was not fully observed in the numerical simulations, indicating that the constitutive model adopted for the fibers has to be improved in order to reproduce all features observed in the experimental work

A 2D simulation has some limitations to the system, such as simulating the actual interaction between the granular material and the fibers and their continuity. All phenomena implemented for the 2D case can be extended to 3D case; however, the 2D model has shown, in a satisfactory case, the increase in soil strength with fibers insertion.

References

Belheine, N.; Plassiard, J.P.; Donzé, F.V.; Darve, F. & Seridi, A. (2009) Numerical simulation of drained triaxial test using 3D discrete element modeling. Computers and Geotechnics, v. 36:1-2, p. 320-331.

Casagrande, M.D.T. (2005) Behavior of Fiber-Reinforced Soils Under Large Strains. PhD Thesis, Universidade Federal do Rio Grande do Sul, Porto Alegre (in Portuguese).

Casagrande, M.D.T.; Coop, M.R. & Consoli, N.C. (2006) Behavior of a fiber-reinforced bentonite. Journal of Geotechnical and Geoenvironmental Engineering, v. 132:11, p. 1505-1508.

Consoli, N.C.; Casagrande, M.D.T. & Coop, M.R. (2007a) Performance of a fiber reinforced sand at large shear strains. Géotechnique, v. 57:9, p. 751-756.

Consoli, N.C.; Heineck, K.S.; Casagrande, M.D.T. & Coop, M.R. (2007b) Shear strength behavior of fiber-reinforced sand considering triaxial tests under distinct stress paths. Journal of Geotechnical and Geoenvironmental Engineering, ASCE, v.133:11, p. 1466-1469.

Consoli, N.C.; Prietto, P.D.M. & Ulbrich, L.A. (1999) The behaviour of a fibre-reinforced cemented soil. Ground Improvement, ICE, Thomas Telford, v. 3:1, p. 21-30.

Consoli, N.C.; Casagrande, M.D.T.; Thome, A.; Rosa, F.D. & Fahey, M. (2009) Effect of relative density on plate tests on fibre-reinforced sand. Géotechnique, v. 59:5, p. 471-476.

Consoli, N.C.; Montardo, J.P.; Prietto, P.D.M. & Donato, M. (2004) Effect of material properties on the behaviour of sand-cement-fibre composites. Ground Improvement, ICE, Thomas Telford, v. 8:2, p. 77-90.

Consoli, N.C.; Casagrande, M.D.T. & Coop, M.R. (2005) Effect of fiber reinforcement on the isotropic compression behaviour of sand. Journal of Geotechnical and Geoenvironmental Engineering, v. 131:11, p. 1434-1436.

Consoli, N.C.; Montardo, J.; Prietto, P.D.M. & Pasa, G. (2002) Engineering behavior of a sand reinforced with plastic waste. Journal of Geotechnical and Geoenvironmental Engineering, ASCE, v. 128:6, p. 462-472.

Consoli, N.C.; Prietto, P.D.M. & Ulbrich, L.A. (1998) The influence of fiber and cement addition on behavior of a sandy soil. Journal of Geotechnical and Geoenvironmental Engineering, v. 124:12, p. 1211-1214.

Cundall, P.A. & Strack, O.D. (1979) A discrete numerical model for granular assemblies. Géotechnique, v. 21:1, p. 47-65.

Cundall, P.A. (1971) A computer model for simulating progressive, large scale movements in blocky rock systems. In: Proc. Symp. Int. Soc. Rock Mech., Nancy 2, pp. 129-136.

Ferreira, C.A. (2010) Study of Mechanical Behaviour of Fiber Reinforced Soil by Discrete Element Method. MSc Dissertation, Departamento de Engenharia Civil, Universidade Católica do Rio de Janeiro, Rio de Janeiro (In Portuguese).

Figueiredo, R.P. (1991) Application of Dynamic Relaxation Procedures for the Solution of Geotechnical Problems. MSc Dissertation, Departamento de Engenharia Civil, Universidade Católica do Rio de Janeiro, Rio de Janeiro (In Portuguese).

Gray, D.H. & Ohashi, H. (1983) Mechanics of fiber reinforcement in sand. Journal of Geotechnical Engineering, ASCE, v. 109:3, p. 335-353.

Heineck, K.S.; Coop, M.R. & Consoli, N.C. (2005) The effect of micro-reinforcement of soils from very small to large shear strains, Journal of Geotechnical and Geoenvironmental Engineering, ASCE, v. 131:8, p. 1024-1033.

Itasca Consulting Group (2002) PFC2D Particle Flow Code in 2 Dimensions Theory and Background.

Maeda, K. & Ibraim, E. (2008) DEM analysis of 2D fibre-reinforced granular soils. Proc. 4th Int. Symp. on Deformation Characteristics of Geomaterials, Atlanta, pp. 623-628.

Maher, M.H. & Gray, D.H. (1990) Static response of sands reinforced with randomly distributed fibers. Journal of Geotechnical Engineering, ASCE, v. 116:11, p. 1661-1677.

Maher, M.H. & Ho, Y.C. (1993) Behavior of fiber-reinforced cemented sand under static and cyclic loads. Geotechnical Testing Journal, ASTM, v. 16:3, p. 330-338.

Michalowski, R.L. & Cermák, J. (2003) Triaxial compression of sand reinforced with fibers. Journal of Geotechnical and Geoenvironmental Engineering, ASCE, v. 129:2, p. 125-136.

Morel, J.C. & Gourc, J.P. (1997) Mechanical behavior of sand reinforced with mesh elements. Geosynthetics International, v. 4:5, p. 481-508.

Plassiard, J.P.; Belheine, N. & Donzé, F.V. (2009) A spherical discrete element model: calibration procedure and incremental response. Granular Matter, v. 11:5, p. 293-306.

Velloso, R.Q. (2010) Numerical Analysis of Fluid Mechanical Coupling in Porous Media Using the Discrete Element Method. DSc. Thesis, Departamento de Engenharia Civil, Universidade Católica do Rio de Janeiro, Rio de Janeiro (In Portuguese).

Vendruscolo, M.A. (2003) Behavior of Plate Load Tests on Soil Layers Improved with Cement and Polypropylene Fiber. PhD Thesis, Universidade Federal do Rio Grande do Sul, Porto Alegre (in Portuguese).

Zhao, X. & Evans, M. (2009) Discrete simulations of laboratory loading conditions. International Journal of Geomechanics, v. 9:4, p. 169-178.

Zornberg, J.G. (2002) Discrete frame work for limit equilibrium analysis of fiber-reinforced soil. Géotechnique, v. 52:8, p. 593-604.

List of Symbols

m: mass of particle
$\mathbf{v}$: velocity of particle
$\mathbf{F}_g$: gravitational force
$\mathbf{F}_c$: contact force
$\mathbf{F}_f$: fiber force
ω : angular velocity of particle
I: moment of inertia of particle
$\mathbf{T}$: torque
$\mathbf{F}_c^N$: contact normal force
$\mathbf{F}_c^S$: contact shear force
K_N: contact normal stiffness
$\mathbf{n}$: normal vector to the contact plane
U_N: superposition displacement
R: particle radius
d: distance between particles centroid
$\mathbf{v}_c^s$: relative velocity in the shear direction at the contact
k_s: contact shear stiffness
Δt: time interval
μ : friction coefficient
K_f: fiber stiffness
L_f: length of the fiber segment
L_{f0}: initial length of the fiber segment
$\mathbf{n}_f$: unit vector in the direction that connects the two neighboring contacts

SOILS and ROCKS
An International Journal of Geotechnical and Geoenvironmental Engineering
Publication of
ABMS - Brazilian Association for Soil Mechanics and Geotechnical Engineering
SPG - Portuguese Geotechnical Society
Volume 35, N. 2, May-August 2012

Author index

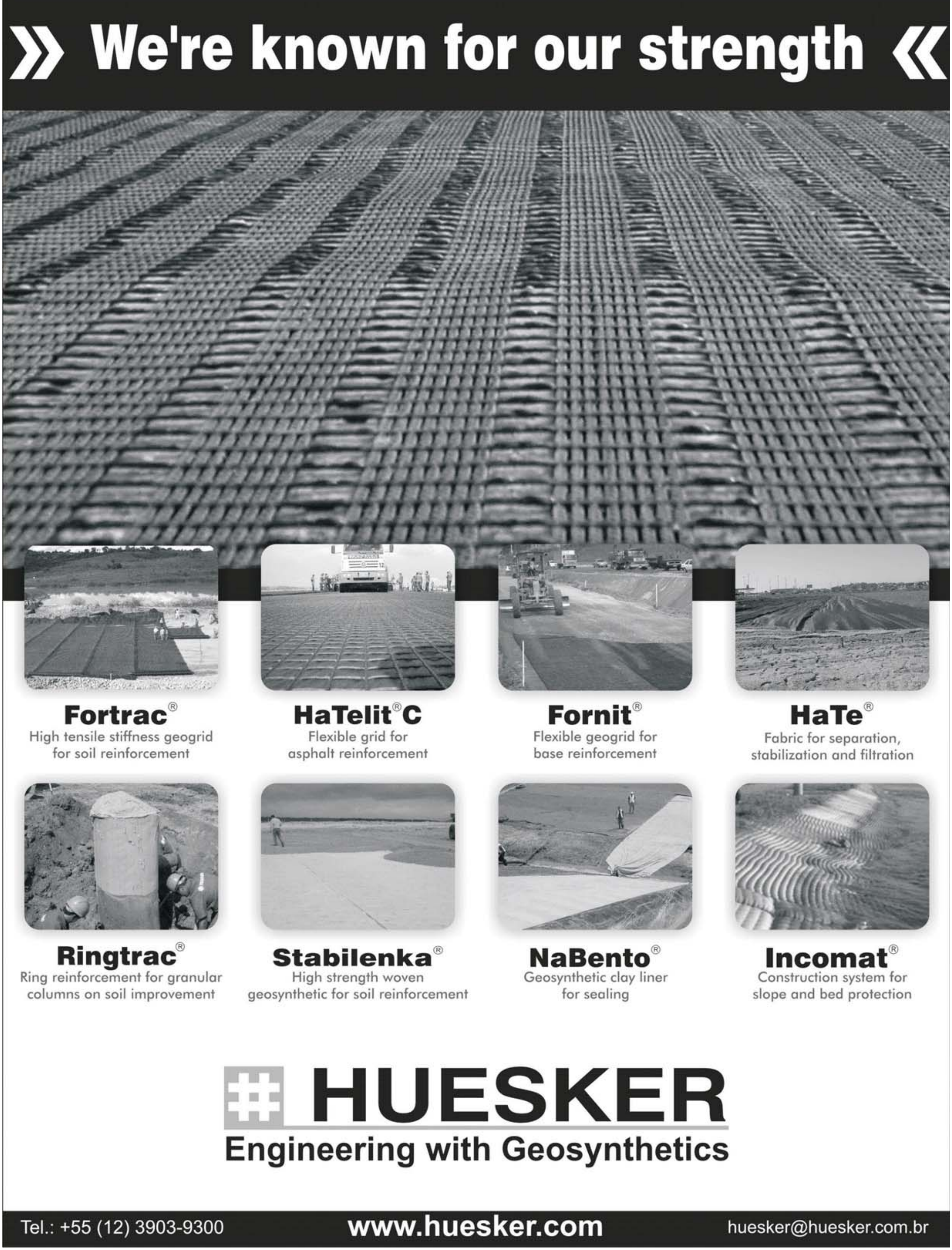

We're known for our strength
Fortrac®
High tensile stiffness geogrid for soil reinforcement
HaTelit®C
Flexible grid for asphalt reinforcement
Fornit®
Flexible geogrid for base reinforcement
HaTe®
Fabric for separation, stabilization and filtration
Ringtrac®
Ring reinforcement for granular columns on soil improvement
Stabilenka®
High strength woven geosynthetic for soil reinforcement
NaBento®
Geosynthetic clay liner for sealing
Incomat®
Construction system for slope and bed protection
HUESKER
Engineering with Geosynthetics
Tel.: +55 (12) 3903-9300
www.huesker.com
huesker@huesker.com.br


SOLOS MOLES?
ENGEGRAUT
www.engegraut.com.br
CPR®
CONSOLIDAÇÃO PROFUNDA RADIAL
O MAIS RÁPIDO E EFETIVO TRATAMENTO PARA SOLOS MOLES
Processo de adensamento de solo mole, eficientemente controlado, monitorando-se o grau de consolidação desejado.
TÉCNICA DE TRATAMENTO DE SOLO MOLE POR CONSOLIDAÇÃO
METODOLOGIA PREMIADA PARA TRATAMENTO DE
SOLO MOLE
Vantagens do CPR
• 100% específico para solos moles;
• Mobilização rápida;
• Ausência de transtornos à obra;
• Ampla gama de aplicações;
• Ausência de aterros, refugos e lama;
• Técnica não destrutiva;
• Alternativa super econômica, além de prazos extremamente curtos em relação à substituição de solos, aterros temporários, colunas granulares e estaqueamentos;
• Alcança profundidades de tratamento onde técnicas clássicas são limitadas;
• Acesso a locais restritos, limitados e difíceis, sem interferência com a rotina do cliente;
• Melhor custo benefício;
• Perfeito para reforço de fundação.
www.engegraut.com.br
Para maiores informações, entre em contato com nosso departamento de geotecnia. A marca CPR® e a tecnologia Consolidação Profunda Radial são patentes da ENGEGRAUT.

ROCKFALL PROTECTION SYSTEMS

Rockfall protection systems have become a key element in the design and maintenance of infrastructure networks impacting directly on safety and necessitating thus, a new approach that encompasses the overall analysis of the rockfall structural system and not the individual components alone. The word ''system'', best describes the different structural components that interact with one another.

MACCAFERRI

www.maccaferri.com.br

BRASIL
Phone: 55 (11) 4525-5000
Fax: 55 (11) 4599-4275
maccaferri@maccaferri.com.br
www.maccaferri.com.br

PORTUGAL
Phone: (351) 263 858 030
Fax: (351) 263 858 036
maccaferri@mail.telepac.pt
www.maccaferri.pt

SPECIALISTS IN GEOTECHNICAL IN-SITU TESTS AND INSTRUMENTATION

GEOTECHNICAL SERVICES (onshore and offshore)

- **IN-SITU TESTS**
  Seismic CPT
  Cone Penetration Testing Undrained-CPTu (cordless system)
  Vane Shear Testing (electrical apparatus)
  Pressuremeter Testing (Menard)
  Flat Dilatometer Test-DMT (Machetti)
  Standard Penetration Test-SPT-T

- **INSTRUMENTATION**
  Instrumentation, installation and direct import
  Routine Monitoring
  Operation and Maintenance
  Engineering analyses
  Consultancy, design & geotechnical engineering services

- **SAMPLING**
  Soil sampling and monitoring
  Groundwater sampling and monitoring
  Field and laboratory testing

- **ENVIRONMENTAL**
  Environmental Services
  Soil and groundwater sampling and monitoring
  Field and laboratory testing

0800 979 3436
São Paulo: +55 11 8133 6030
Minas Gerais: +55 31 8563 2520 / 8619 6469
www.deltageo.com.br deltageo@deltageo.com.br

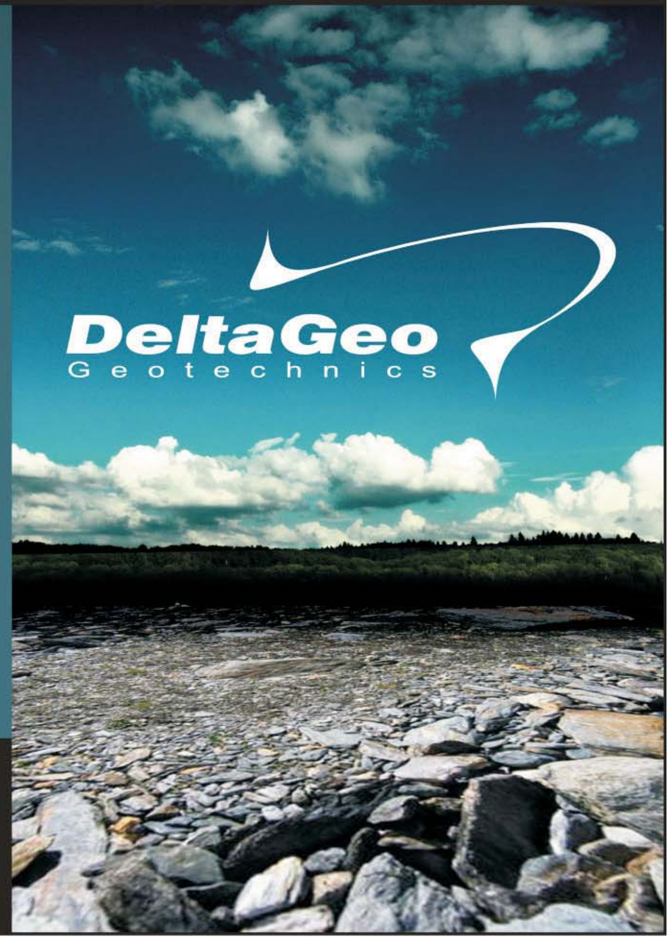

TEIXEIRA DUARTE
ENGENHARIA E CONSTRUÇÕES, S.A.

- Head Office
  Lagoas Park – Edifício 2
  2740-265 Porto Salvo - Portugal
  Tel.:(+351) 217 912 300
  Fax: (+351) 217 941 120/21/26

- Angola
  Alameda Manuel Van Dunen 316/320 - A
  Caixa Postal 2857 - Luanda
  Tel.:(+34) 915 550 903
  Fax: (+34) 915 972 834

- Algeria
  Parc Miremont – Rua A, Nº136 - Bouzareah
  16000 Alger
  Tel.:(+213) 219 362 83
  Fax: (+213) 219 365 66

- Brazil
  Rua Iguatemi, nº488 – 14º - Conj. 1401
  CEP 01451 - 010 - Itaim Bibi - São Paulo
  Tel.: (+55) 112 144 5700
  Fax: (+55) 112 144 5704

- Spain
  Avenida Alberto Alcocer, nº24 – 7º C
  28036 Madrid
  Tel.:(+34) 915 550 903
  Fax: (+34) 915 972 834

- Mozambique
  Avenida Julyus Nyerere, 130 – R/C
  Maputo
  Tel.:(+258) 214 914 01
  Fax: (+258) 214 914 00

www.teixeiraduarte.pt

CENOR®
Consulting Engineers

www.cenor.pt



GEOLOGY - GEOTECHNICS - SUPERVISION OF GEOTECHNICAL WORKS



EMBANKMENT DAMS - UNDERGROUND WORKS - RETAINING STRUCTURES



SPECIAL FOUNDATIONS - SOIL IMPROVEMENT - GEOMATERIALS

CENOR GROUP
PORTUGAL, ANGOLA, ALGERIA, MOROCCO, ROMANIA, TIMOR

CENORGEO - Engenharia Geotécnica, Lda.
Rua das Vigias, 2 . Piso 1 Parque das Nações 1990-506 LISBOA . PORTUGAL
T. +351.218 437 300 **F.** +351.218 437 301 cenorgeo@**cenor.pt**

ISO 9001
BUREAU VERITAS
Certification


> Prospecção Geotécnica
Site Investigation
> Consultoria Geotécnica
Geotechnical Consultancy
> Obras Geotécnicas
Ground Treatment-Construction Services
> Controlo e Observação
Field Instrumentation Services and Monitoring Services
> Laboratório de Mecânica de Solos
Soil and Rock Mechanics Laboratory

Certificada ISO 9001 por BVQi







Parque Oriente, Bloco 4, EN10
2699-501 Bobadela LRS
Tel. 21 995 80 00
Fax. 21 995 80 01
e.mail: mail@geocontrole.pt
www.geocontrole.pt

Geocontrole
Geotecnia e Estruturas de Fundação SA

ENGINEERING AND ENVIRONMENTAL CONSULTANTS


COBA


GEOLOGY AND GEOTECHNICS

Hydrogeology • Engineering Geology • Rock Mechanics • Soil Mechanics • Foundations and Retaining Structures • Underground Works • Embankments and Slope Stability Environmental Geotechnics • Geotechnical Mapping

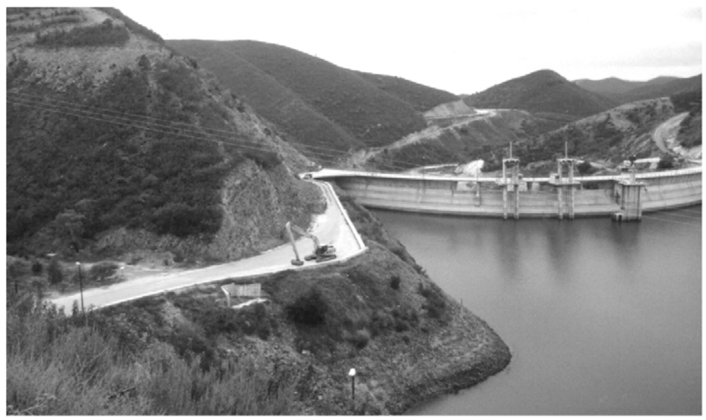

Water Resources Planning and Management
Hydraulic Undertakings
Electrical Power Generation and Transmission
Water Supply Systems and Pluvial and Wastewater Systems
Agriculture and Rural Development
Road, Railway and Airway Infrastructures
Environment
Geotechnical Structures
Cartography and Cadastre
Safety Control and Work Rehabilitation
Project Management and Construction Supervision

EMPRESA CERTIFICADA apcer ISO 9001

CERTIFIED IQNet MANAGEMENT SYSTEM

PORTUGAL
CENTER AND SOUTH REGION
Av. 5 de Outubro, 323
1649-011 LISBOA
Tel.: (351) 210125000, (351) 217925000
Fax: (351) 217970348
E-mail: coba@coba.pt
www.coba.pt

Av. Marquês de Tomar, 9, 6°.
1050-152 LISBOA
Tel.:(351) 217925000
Fax:(351) 213537492

NORTH REGION
Rua Mouzinho de Albuquerque, 744, 1°.
4450-203 MATOSINHOS
Tel:(351) 229380421
Fax:(351) 229373648
E-mail: engico@engico.pt

ANGOLA
Praceta Farinha Leitão, edifício nº 27, 27-A - 2º Dto
Bairro do Maculusso, LUANDA
Tel./Fax: (244) 222338 513
Cell: (244) 923317541
E-mail: coba-angola@netcabo.co.ao

MOZAMBIQUE
Pestana Rovuma Hotel. Centro de Escritórios.
Rua da Sé nº114. Piso 3, MAPUTO
Tel./Fax: (258) 21 328 813
Cell:(258) 82 409 9605
E-mail: coba.mz@tdm.co.mz

ALGERIA
09, Rue des Frères Hocine
El Biar - 16606, ARGEL
Tel.: (213) 21 922802
Fax: (213) 21 922802
E-mail: coba.alger@gmail.com

BRAZIL
Rio de Janeiro
COBA Ltd. - Rua Bela 1128
São Cristóvão
20930-380 Rio de Janeiro RJ
Tel.: (55 21) 351 50 101
Fax: (55 21) 258 01 026

Fortaleza
Av. Senador Virgílio Távora 1701, Sala 403
Aldeota - Fortaleza CEP 60170 - 251
Tel.: (55 85) 3261 17 38
Fax: (55 85) 3261 50 83
E-mail: coba@esc-te.com.br

UNITED ARAB EMIRATES
Corniche Road – Corniche Tower - 5th Floor - 5B
P. O. Box 38360 ABU DHABI
Tel.: (971) 2 627 0088
Fax: (971) 2 627 0087

tgeotecnia
in the origin
of construction

dstgroup

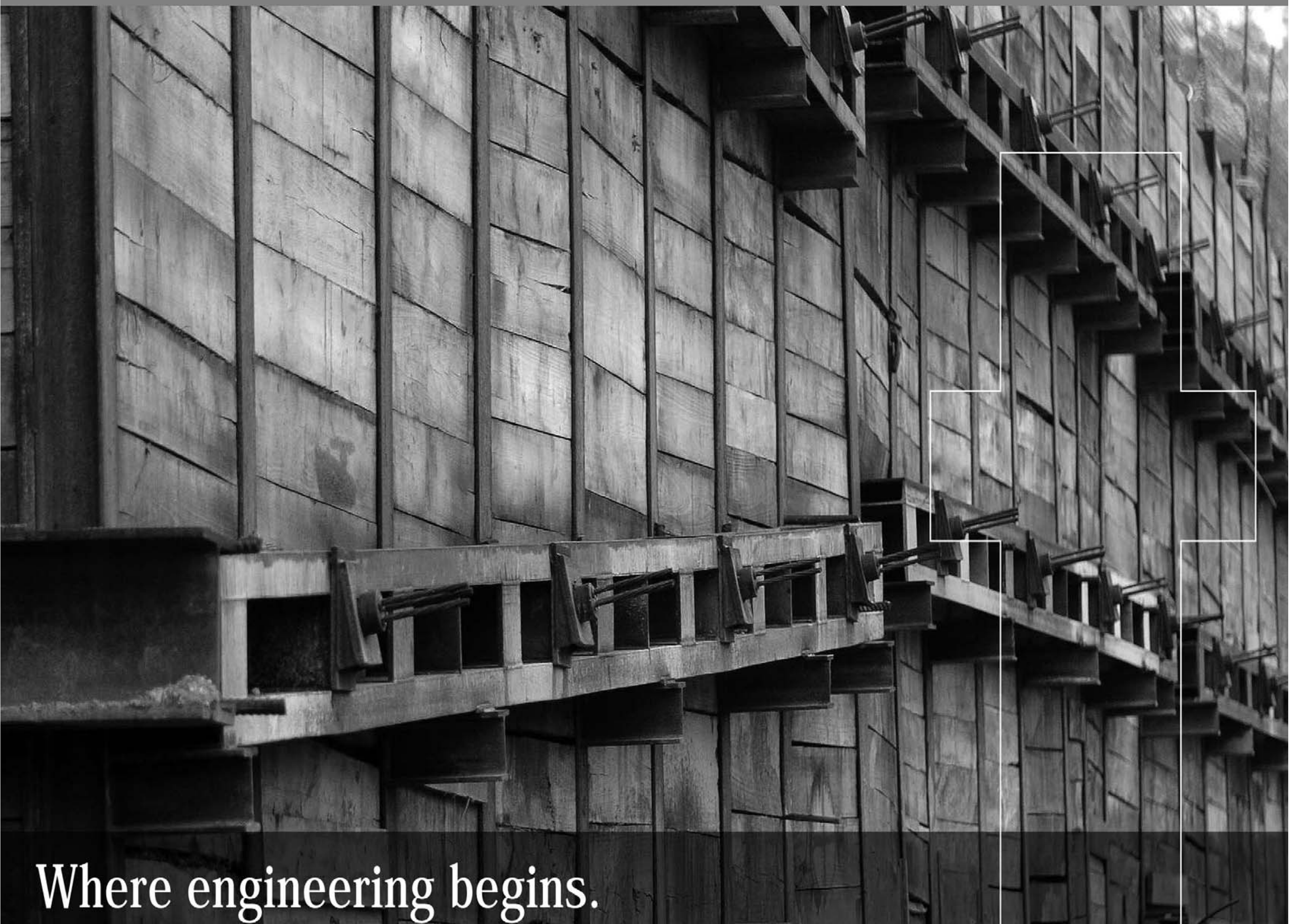

Behind a great work there's always a great company.
tgeotecnia enters in national and Spanish market with a wide range of solutions, with state of the art technology and qualified means necessaries to engage geotechnical studies, projects and works.
Currently, tgeotecnia is specialised in all kinds of work, from geologic-geotechnical studies and project development to slope stabilisation, reinforcement, soil treatment and special foundations.
The works carried out and client satisfaction, as well as the growing number of projects, are the proof that it is worth making innovation the lever of development.

tgeotecnia
In the origin of construction

a dst group company

ph + 351 253 307 285 | geral@tgeotecnia.pt | www.dstsgps.com

Tecnasol

Geotechnics and Foundation Engineering

Diaphragm Walls

Piles

Micropiles

Retaining Walls

Anchors

Soil nails

Monitoring

Repair Stuctures

Post tensioning

Grouting

Jet Grouting

Compensation Grouting

Tunnelling and

Underground Works

Sealing and

Waterproofing Systems

Site Investigations

Slope Stabilization

HEAD OFFICE
Edifício Edifer
Estrada do Seminário , 4 - Alfragide
2610 - 171 Amadora - PORTUGAL
Tel. 00 351 21 475 90 00 / Fax 00 351 21 475 95 00

Madrid
Calle Rodríguez Marín, Nº 88 1º Dcha
28016 Madrid – ESPANHA
Tel. 00 34 91 745 03 64 / Fax 00 34 91 411 31 87

Porto
Rua Eng. Ferreira Dias, nº 161 2º Andar
4100-247 Porto – PORTUGAL
Tel. 00 351 22 616 74 60 / Fax 00 351 22 616 74 69

Madeira
Rampa dos Piornais, n.º 5 - Sala 1
9000-248 Funchal – PORTUGAL
Tel. 00 351 291 22 10 33 / Fax 00351 291 22 10 34

Angola
Rua Alameda Van-Dúnem, n.º 265 R/c
Luanda - ANGOLA
Tel. 00 244 222 443 559 / Fax 00 244 222 448 843

Barcelona
Calle Comte d' Urgell, 204-208 6.º A
08036 Barcelona – ESPANHA
Tel. 00 34 93 419 04 52 / Fax 00 34 93 419 04 16

Sevilha
Polígono Industrial de Guadalquivir, C/ Artesania, 3
41120 Gelves (Sevilla) - ESPANHA
Tel. 00 34 955 762 833 / Fax 00 34 955 76 11 75

www.tecnasolfge.com

Instructions to Authors

Category of the Papers

Soils and Rocks is the scientific journal edited by the Brazilian Association for Soil Mechanics and Geotechnical Engineering (ABMS) and the Portuguese Geotechnical Society (SPG). The journal is intended to the divulgation of original research works from all geotechnical branches.

The accepted papers are classified either as an Article paper, a Technical Note, a Case Study, or a Discussion according to its content. An article paper is an extensive and conclusive dissertation about a geotechnical topic. A paper is considered as a technical note if it gives a short description of ongoing studies, comprising partial results and/or particular aspects of the investigation. A case study is a report of unusual problems found during the design, construction or the performance of geotechnical projects. A case study is also considered as the report of an unusual solution given to an ordinary problem. The discussions about published papers, case studies and technical notes are made in the Discussions Section.

When submitting a manuscript for review, the authors should indicate the category of the manuscript, and is also understood that they:

a) assume full responsibility for the contents and accuracy of the information in the paper;

b) assure that the paper has not been previously published, and is not being submitted to any other periodical for publication.

Manuscript Instructions

Manuscripts must be written in English. The text is to be typed in a word processor (MS Word or equivalent), using ISO A4 page size, left, right, top, and bottom margins of 25 mm, Times New Roman 12 font, and line spacing of 1.5. All lines and pages should be numbered. The text should be written in the third person.

The fist page of the manuscript is to include the title of the paper in English, followed by the names of the authors with the abbreviation of the most relevant academic title. The affiliation, address and e-mail is to be indicated below each author's name. An abstract of 200 words is to be written in English after the author's names. A list with up to six keywords at the end of the abstract is required.

Although alteration of the sequence and the title of each section may be required, it is suggested that the text contains the following sections: Introduction, Material and Methods, Results, Discussions, Conclusion, Acknowledgements, References and List of Symbols. A brief description of each section is given next.

Introduction: This section should indicate the state of the art of the problem under evaluation, a description of the problem and the methods undertaken. The objective of the work is to be clearly presented at the end of the section.

Materials and Methods: This section should include all information needed to the reproduction of the presented work by other researchers.

Results: In this section the data of the investigation should be presented in a clear and concise way. Figures and tables should not repeat the same information.

Discussion: The analyses of the results should be described in this section. **Conclusions**: The text of this section should be based on the presented data and in the discussions.

Acknowledgenments: If necessary, concise acknowledgements should be written in this section.

References: References to other published sources are to be made in the text by the last name(s) of the author(s), followed by the year of publication, similarly to one of the two possibilities below:

"*while Silva & Pereira (1987) observed that resistance depended on soil density*" or "*It was observed that resistance depended on soil density (Silva & Pereira, 1987).*"

In the case of three or more authors, the reduced format must be used, *e.g.*: Silva *et al.* (1982) or (Silva *et al.*, 1982). Two or more citations belonging to the same author(s) and published in the same year are to be distinguished with small letters, *e.g.*: (Silva, 1975a, b, c.). Standards must be cited in the text by the initials of the entity and the year of publication, *e.g.*: ABNT (1996), ASTM (2003).

Full references shall be listed alphabetically at the end of the text by the first author's last name. Several references belonging to the same author shall be cited chronologically. Some examples are listed next:

Papers: Bishop, A.W. & Blight, G.E. (1963) Some aspects of effective stress in saturated and unsaturated soils. Géotechnique, v. 13:2, p. 177-197.

Books: Lambe, T.W & Whitman, R.V. (1979) Soil Mechanics, SI Version, 2nd ed. John Wiley & Sons, New York, p. 553.

Book with editors: Sharma, H.D.; Dukes, M.T. & Olsen, D.M. (1990) Field measurements of dynamic moduli and Poisson's ratios of refuse and underlying soils at a landfill site. Landva A. & Knowles, G.D. (eds) Geotechnics of Waste Fills - Theory and Practice, American Society for Testing and Materials - STP 1070, Philadelphia, p. 57-70.

Proceedings (printed matter or CD-ROM): Jamiolkowski, M.; Ladd, C.C.; Germaine, J.T & Lancellotta, R. (1985) New developments in field and laboratory testing of soils. Proc. 11th Int. Conf. on Soil Mech. and Found. Engn., ISSMFE, San Francisco, v. 1, pp. 57-153.(specify if CD – ROM)

Thesis and dissertations: Lee, K.L. (1965) Triaxial Compressive Strength of Saturated Sands Under Seismic Loading Conditions. PhD Dissertation, Department of Civil Engineering, University of California, Berkeley, 521 p.

Standards: ASTM (2003) Standard Test Method for Particle Size Analysis of Soils - D 422-63. ASTM International, West Conshohocken, Pennsylvania, USA, 8 p.

Internet references: Soils and Rocks available at http://www.abms.com.br.

On line first publications must also bring the digital object identifier (DOI) at the end.

Figures shall be either computer generated or drawn with India ink on tracing paper. Computer generated figures must be accompanied by the corresponding digital file (.tif, .jpg, .pcx, etc.). All figures (graphs, line drawings, photographs, etc.) shall be numbered consecutively and have a caption consisting of the figure number and a brief title or description of the figure. This number should be used when referring to the figure in text. Photographs should be black and white, sharp, high contrasted and printed on glossy paper.

Tables shall be numbered consecutively in Arabic and have a caption consisting of the table number and a brief title. This number should be used when referring to the table in text. Units should be indicated in the first line of the table, below the title of each column. Abbreviations should be avoided. Column headings should not be abbreviated. When applicable, the units should come right below the corresponding column heading. Any necessary explanation can be placed as footnotes.

Equations shall appear isolated in a single line of the text. Numbers identifying equations must be flush with the right margin. International System (SI) units are to be used. The symbols used in the equations shall be listed in the List of Symbols. It is recommended that the used symbols be in accordance with Lexicon in 8 Languages, ISSMFE (1981) and the ISRM List of Symbols.

The text of the submitted manuscript (including figures, tables and references) intended to be published as an article paper or a case history should not contain more than 30 pages formatted according to the instructions mentioned above. Technical notes and discussions should have no more than 15 and 8 pages, respectively. Longer manuscripts may be exceptionally accepted if the authors provide proper explanation for the need of the required extra space in the cover letter.

Discussion

Discussions must be written in English. The first page of a discussion paper should contain:

• The title of the paper under discussion in the language chosen for publication;

• Name of the author(s) of the discussion, followed by the position, affiliation, address and e-mail. The discusser(s) should refer himself (herself, themselves) as "the discusser(s)" and to the author(s) of the paper as "the author(s)".

Figures, tables and equations should be numbered following the same sequence of the original paper. All instructions previously mentioned for the preparation of article papers, case studies and technical notes also apply to the preparation of discussions.

Editorial Review

Each paper will be evaluated by reviewers selected by the editors according to the subject of the paper. The authors will be informed about the results of the review process. If the paper is accepted, the authors will be required to submit a version of the revised manuscript with the suggested modifications. If the manuscript is refused for publication, the authors will be informed about the reasons for rejection. In any situation comprising modification of the original text, classification of the manuscript in a category different from that proposed by the authors, or refusal for publication, the authors can reply presenting their reasons for disagreeing with the reviewers' comments

Submission

The author(s) must submit for review:

1. A hard copy of the manuscript to Editors - Soils and Rocks, Av. Prof. Almeida Prado, 532 – IPT, Prédio 54 – DEC/ABMS, 05508-901 - São Paulo, SP, Brazil. The first page of the manuscript should contain the identification of the author(s), or

2. The digital file of the manuscript, omitting the authors' name and any information that eventually could identify them, should be sent to **abms@ipt.br**. The following must be written in the subject of the e-mail message: "*Paper submitted to Soils and Rocks*". The authors' names, academic degrees and affiliations should be mentioned in the e-mail message. The e-mail address from which the digital file of the paper was sent will be the only one used by the editors for communication with the corresponding author.

Follow Up

Authors of manuscripts can assess the status of the review process at the journal website (www.soilsandrocks.com.br) or by contacting the ABMS secretariat.

Volume 35, N. 2, May-August 2012

Table of Contents